

## INFORMATION TO USERS

This was produced from a copy of a document sent to us for microfilming. While the most advanced technological means to photograph and reproduce this document have been used, the quality is heavily dependent upon the quality of the material submitted.

The following explanation of techniques is provided to help you understand markings or notations which may appear on this reproduction.

1. The sign or "target" for pages apparently lacking from the document photographed is "Missing Page(s)". If it was possible to obtain the missing page(s) or section, they are spliced into the film along with adjacent pages. This may have necessitated cutting through an image and duplicating adjacent pages to assure you of complete continuity.
2. When an image on the film is obliterated with a round black mark it is an indication that the film inspector noticed either blurred copy because of movement during exposure, or duplicate copy. Unless we meant to delete copyrighted materials that should not have been filmed, you will find a good image of the page in the adjacent frame. If copyrighted materials were deleted you will find a target note listing the pages in the adjacent frame.
3. When a map, drawing or chart, etc., is part of the material being photographed the photographer has followed a definite method in "sectioning" the material. It is customary to begin filming at the upper left hand corner of a large sheet and to continue from left to right in equal sections with small overlaps. If necessary, sectioning is continued again—beginning below the first row and continuing on until complete.
4. For any illustrations that cannot be reproduced satisfactorily by xerography, photographic prints can be purchased at additional cost and tipped into your xerographic copy. Requests can be made to our Dissertations Customer Services Department.
5. Some pages in any document may have indistinct print. In all cases we have filmed the best available copy.

University  
Microfilms  
International

300 N. ZEEB RD., ANN ARBOR, MI 48106



Merrill, Connie Lange

BIOMIMICRY OF THE DIOXYGEN ACTIVE SITE IN THE COPPER  
PROTEINS HEMOCYANIN AND CYTOCHROME OXIDASE: PART I:  
COPPER(I) COMPLEXES WHICH REACT REVERSIBLY WITH DIOXYGEN  
AND SERVE TO MIMIC THE ACTIVE SITE FUNCTION OF HEMOCYANIN.  
PART II: MU-IMIDAZOLATO BINUCLEAR METALLOPORPHYRIN  
COMPLEXES OF IRON AND COPPER AS MODELS FOR THE ACTIVE  
SITE STRUCTURE IN CYTOCHROME OXIDASE

*Rice University*

PH.D. 1982

University  
Microfilms  
International

300 N. Zeeb Road, Ann Arbor, MI 48106



RICE UNIVERSITY

BIOMIMICRY OF THE DIOXYGEN ACTIVE SITE IN THE COPPER PROTEINS

HEMOCYANIN AND CYTOCHROME OXIDASE

PART I: COPPER(I) COMPLEXES WHICH REACT REVERSIBLY WITH DIOXYGEN  
AND SERVE TO MIMIC THE ACTIVE SITE FUNCTION OF HEMOCYANIN

PART II:  $\mu$ -IMIDAZOLATO BINUCLEAR METALLOPORPHYRIN COMPLEXES  
OF IRON AND COPPER AS MODELS FOR THE ACTIVE SITE  
STRUCTURE IN CYTOCHROME OXIDASE


by

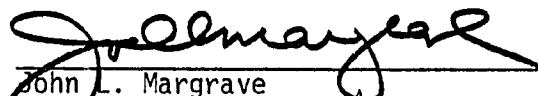
CONNIE LANGE MERRILL

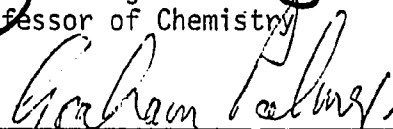
A THESIS SUBMITTED  
IN PARTIAL FULFILLMENT OF THE  
REQUIREMENTS FOR THE DEGREE

DOCTOR OF PHILOSOPHY

APPROVED, THESIS COMMITTEE:

  
Lon J. Wilson, Associate Professor  
of Chemistry, Chairman

  
John L. Margrave  
Professor of Chemistry

  
Graham A. Palmer  
Professor of Biochemistry

HOUSTON, TEXAS

MARCH 1982

## ABSTRACT

### BIOMIMICRY OF THE DIOXYGEN ACTIVE SITE IN THE COPPER PROTEINS HEMOCYANIN AND CYTOCHROME OXIDASE

PART I: COPPER(I) COMPLEXES WHICH REACT REVERSIBLY WITH DIOXYGEN  
AND SERVE TO MIMIC THE ACTIVE SITE FUNCTION OF HEMOCYANIN

PART II:  $\mu$ -IMIDAZOLATO BINUCLEAR METALLOPORPHYRIN COMPLEXES  
OF IRON AND COPPER AS MODELS FOR THE ACTIVE SITE  
STRUCTURE IN CYTOCHROME OXIDASE

by Connie Lange Merrill

PART I: Previously the {bis-2,6[1-(2-imidazol-4-ylethylimino)-ethyl]pyridine}copper(I) cation,  $[\text{Cu}^{\text{I}}(\text{imidH})_2\text{DAP}]^+$ , was found to reversibly bind dioxygen, whereas the {bis-2,6-[1-(2-pyridin-2-ylethylimino)ethyl]pyridine}copper(I) cation,  $[\text{Cu}^{\text{I}}(\text{py})_2\text{DAP}]^+$ , was unreactive toward  $\text{O}_2$ . Magnetochemical and resonance Raman experiments were conducted to characterize the  $[\text{Cu}^{\text{I}}(\text{imidH})_2\text{DAP}]^+$ -dioxygen interaction.  $[\text{Cu}^{\text{I}}(\text{imidR})(\text{py})\text{DAP}]^+$ ,  $[\text{Cu}^{\text{I}}(\text{imidH})(\text{py})\text{DAP}]^+$ ,  $[\text{Cu}^{\text{I}}(\text{imidR})_2\text{DAP}]^+$ , and  $[\text{Cu}^{\text{I}}(\text{imidR})(\text{imidH})\text{DAP}]^+$  where  $\text{R} = -\text{CH}_2(\text{C}_6\text{H}_4)\text{CH}_3$ , were synthesized to examine the role of the acidic imidazole proton of  $[\text{Cu}^{\text{I}}(\text{imidH})_2\text{DAP}]^+$  in the reversible oxygenation process. While  $[\text{Cu}^{\text{I}}(\text{imidR})(\text{py})\text{DAP}]^+$  was dioxygen-inactive,  $[\text{Cu}^{\text{I}}(\text{imidH})(\text{py})\text{DAP}]^+$  reacted irreversibly with dioxygen.  $[\text{Cu}^{\text{I}}(\text{imidR})_2\text{DAP}]^+$  and  $[\text{Cu}^{\text{I}}(\text{imidR})(\text{imidH})\text{DAP}]^+$  reacted reversibly with dioxygen (1 mole  $\text{O}_2$ :2 moles Cu), paralleling the dioxygen reactivity for  $[\text{Cu}^{\text{I}}(\text{imidH})_2\text{DAP}]^+$ . Correlation between the redox potential of the  $\text{Cu(II)} \rightleftharpoons \text{Cu(I)}$  couple and the reaction of the Cu(I)

center toward  $O_2$  was proposed. Analogous Cu(II) and Zn(II) complexes of all the Cu(I) species were characterized. The relevance of these copper(I) compounds as the first synthetic copper(I) dioxygen carriers to model the active site function of hemocyanin was discussed.

PART II:  $\mu$ -Imidazolato mixed-metal complexes were synthesized to model the proposed imidazolate-bridged  $[Cyt.a_3^{3+}(imid)Cu^{2+}]$  active site structure of cytochrome oxidase where  $-J_{(Fe^{III}-Cu^{II})} \gtrsim 200 \text{ cm}^{-1}$ . The compounds were derived from  $[Fe^{III}(TPP)X]$  ( $TPP^{2-}$  = tetraphenylporphyrinato and  $X = Cl^-$  or  $OSO_2CF_3^-$ ) and  $[M^{II}(imidH)_2DAP]^{2+}$  or  $[M^{II}(imidH)(py)DAP]^{2+}$  ( $M = Zn$  or  $Cu$ ) to yield species containing the following  $\mu$ -imidazolato cationic cores:  $[ClFe^{III}(imid)Zn^{II}]^+$  [compound (1)],  $[ClFe^{III}(imid)Cu^{II}]^+$  [compound (2)],  $[(OSO_2CF_3)Fe^{III}(imid)Zn^{II}]^+$  [compound (3)],  $[(OSO_2CF_3)Fe^{III}(imid)Cu^{II}]^+$  [compound (4)],  $[ClFe^{III}(imid)Zn^{II}(py)]^+$  [compound (5)], and  $[ClFe^{III}(imid)Cu^{II}(py)]^+$  [compound (6)]. The variable-temperature magnetochemical and EPR data obtained on the solid state samples indicated that the iron(III) and copper(II) centers of the (2) and (6) complexes are electronically isolated with  $-J_{(Fe^{III}-Cu^{II})} \lesssim 15 \text{ cm}^{-1}$ . Studies of  $[(OSO_2CF_3)Fe^{III}(imid)Cu^{II}]^+$  were complicated by what appears to be two distinct molecular species of spin = 5/2 and spin = 1/2 coexisting in the same crystalline sample. The magnetic properties and EPR silent behavior of (4) were rationalized in terms of a ( $S=0,2$ ) mixture arising from strong antiferromagnetic coupling between  $Fe^{III}(S=1/2,5/2)$  and  $Cu^{II}(S=1/2)$  where  $-J_{(Fe^{III}-Cu^{II})} \gtrsim 200 \text{ cm}^{-1}$ . Compound (4) is the first synthetic  $\mu$ -imidazolato iron(II)-copper(II) metalloporphyrin complex where strong

antiferromagnetic exchange interaction between metal centers has been observed. Reinvestigation of the magnetic properties of the "2Co<sup>II</sup>2Cu<sup>II</sup>" superoxide dismutase derivative confirmed that strong antiferromagnetic coupling [ $-J_{(\text{Co}^{\text{II}}-\text{Cu}^{\text{II}})} \gtrsim 300 \text{ cm}^{-1}$ ], mediated by a bridging imidazolate moiety, exists between the Co(II) and Cu(II) centers. These results provided evidence supporting the possibility of an imidazolate bridge at the active site of cytochrome oxidase.



DEDICATION

To my parents:

Doris, an oasis of love and support, and Lange, in spirit with me always.

## ACKNOWLEDGMENTS

The author (CLM) acknowledges Lon Wilson, her graduate research director, for his chemical knowledge, intuition, and curiosity. Through his guidance, CLM learned to define a chemical problem, work toward its solution, and communicate these results to others. Lon graciously provided the opportunity to establish meaningful collaborations with several scientists. CLM thanks these men, W. H. Woodruff, T. M. Loehr, and G. Palmer, for sharing their expertise and laboratories so that resonance Raman and EPR data could be obtained and included in this thesis.

CLM greatly appreciates the efforts of Kevin Carter in recording EPR spectra and protein sample preparation. Many thanks go to Nancy Ferris and Tom Thamann for collecting the Raman data.

While at Rice University CLM developed many friendships with fellow students. In particular, Bob Saxton's timely humor and intellectual debate are acknowledged. The drawings constructed by Rick Ashcraft are appreciated but it is his caring heart that will remain most endearing. Miriam Simmons provided a challenging thesis topic by her initial synthesis. For this and our continued friendship, CLM will always be grateful.

CLM wishes to acknowledge her son, Adam, who, with the wisdom of a sensitive child, afforded his mom the opportunity to be herself.

Finally, immeasurable appreciation goes to Jim, a loving and understanding spouse, who opened up the world so that the author may experience all things.

## TABLE OF CONTENTS

|   | <u>Page</u> |
|---|-------------|
| <u>PART I:</u> COPPER(I) COMPLEXES WHICH REACT REVERSIBLY<br>WITH DIOXYGEN AND SERVE TO MIMIC THE ACTIVE<br>SITE FUNCTION OF HEMOCYANIN . . . . . | 1           |
| INTRODUCTION . . . . .  | 2           |
| EXPERIMENTAL SECTION . . . . .  | 17          |
| Materials . . . . .   | 17          |
| Syntheses . . . . .   | 17          |
| Physical and Spectroscopic Measurements . . . . .   | 28          |
| RESULTS AND DISCUSSION . . . . .  | 34          |
| Synthesis and Characterization of the Complexes . . . . .   | 34          |
| Reactivity of the Copper(I) Complexes with Dioxygen . . . . .   | 58          |
| Electrochemical Experiments . . . . .   | 80          |
| EPR Results . . . . .   | 105         |
| Magnetochemical Studies . . . . .   | 111         |
| Resonance Raman Results . . . . .   | 117         |
| Conclusions . . . . .   | 136         |
| REFERENCES . . . . .  | 138         |

|  | <u>Page</u> |
|--|-------------|
| <u>PART II:</u> $\mu$ -IMIDAZOLATO BINUCLEAR METALLOPORPHYRIN COMPLEXES<br>OF IRON AND COPPER AS MODELS FOR THE ACTIVE SITE<br>STRUCTURE IN CYTOCHROME OXIDASE . . . . . | 144         |
| INTRODUCTION . . . . .   | 145         |
| EXPERIMENTAL SECTION . . . . .   | 155         |
| Materials . . . . .  | 155         |
| Syntheses . . . . .  | 155         |
| Physical and Spectroscopic Measurements . . . . .  | 161         |
| RESULTS AND DISCUSSION . . . . .   | 163         |
| Synthesis and Characterization of the Complexes . . . . .  | 163         |
| Mössbauer Spectroscopic Measurements . . . . .   | 165         |
| Magnetochemical and EPR Studies . . . . .  | 178         |
| A Reinvestigation of the Magnetic Properties of the<br>"2Co2Cu" Superoxide Dismutase (SOD) Derivative . . . . .  | 192         |
| Conclusions . . . . .  | 197         |
| REFERENCES AND NOTES . . . . .   | 200         |

## LIST OF FIGURES

| <u>PART I</u>   | <u>Page</u> |
|---|-------------|
| FIGURE 1. Proposed Active Site Structures for Oxyhemocyanin .   | 6           |
| FIGURE 2. Flow Diagram for the Hemocyanin Derivatives . . . . .   | 7           |
| FIGURE 3. The Bosnich Model for the Active Site<br>Structure of Oxyhemocyanin . . . . .   | 11          |
| FIGURE 4. The Copper(I) Model Compounds . . . . .   | 13          |
| FIGURE 5. The Synthetic Scheme for {Bis-2,6[1-(2-(N <sub>1</sub> -p-methyl-<br>benzyl)imidazol-4-ylethyl]pyridine}copper(I)tetra-<br>fluoroborate . . . . . | 35          |
| FIGURE 6. <sup>1</sup> H N.M.R. Spectrum for Free Base Histamine<br>in DCCl <sub>3</sub> Relative to Internal TMS . . . . .                                 | 36          |
| FIGURE 7. <sup>1</sup> H N.M.R. Spectrum for R-substituted Histamine<br>Hydrochloride in D <sub>2</sub> O Relative to TMS . . . . .                         | 38          |
| FIGURE 8. <sup>1</sup> H N.M.R. Spectrum for Free Base R-substituted<br>Histamine in DCCl <sub>3</sub> Relative to Internal TMS . . . . .                   | 40          |
| FIGURE 9. Synthetic Scheme for the Copper(II) and<br>Zinc(II) Tetrafluoroborate Complexes . . . . .   | 44          |
| FIGURE 10. <sup>1</sup> H N.M.R. Spectrum and Assignments<br>for [Zn(imidH)(py)DAP] <sup>2+</sup> . . . . .   | 48          |
| FIGURE 11. <sup>1</sup> H N.M.R. Spectrum and Assignments<br>for [Zn(imidR) <sub>2</sub> DAP] <sup>2+</sup> . . . . .                                       | 50          |
| FIGURE 12. <sup>1</sup> H N.M.R. Spectrum and Assignments<br>for [Zn(imidR)(py)DAP] <sup>2+</sup> . . . . .   | 52          |
| FIGURE 13. <sup>1</sup> H N.M.R. Spectrum and Assignments<br>for [Zn(imidR)(imidH)DAP] <sup>2+</sup> . . . . .  | 54          |

|  | <u>Page</u> |
|--|-------------|
| FIGURE 14. Electronic Absorption Spectrum<br>of $[\text{Cu}(\text{imidH})(\text{py})\text{DAP}]^{2+}$ . . . . .                      | 59          |
| FIGURE 15. Electronic Absorption Spectrum<br>of $[\text{Cu}(\text{imidR})_2\text{DAP}]^{2+}$ . . . . .                               | 61          |
| FIGURE 16. Electronic Absorption Spectrum<br>of $[\text{Cu}(\text{imidR})(\text{py})\text{DAP}]^{2+}$ . . . . .                      | 63          |
| FIGURE 17. Electronic Absorption Spectrum<br>of $[\text{Cu}(\text{imidR})(\text{imidH})\text{DAP}]^{2+}$ . . . . .                   | 65          |
| FIGURE 18. Electronic Absorption Spectrum<br>of $[\text{Cu}(\text{imidR})(\text{py})\text{DAP}]^+$ . . . . .                         | 70          |
| FIGURE 19. Electronic Absorption Spectrum<br>of $[\text{Cu}(\text{imidH})(\text{py})\text{DAP}]^+$ . . . . .                         | 72          |
| FIGURE 20. Electronic Absorption Spectrum of $[\text{Cu}(\text{imidR})_2\text{DAP}]^+$ .   | 74          |
| FIGURE 21. Electronic Absorption Spectrum<br>of $[\text{Cu}(\text{imidR})(\text{imidH})\text{DAP}]^+$ . . . . .                      | 76          |
| FIGURE 22. Cyclic Voltammograms and Differential Pulse<br>Polarograms for the Copper(II) Complexes . . . . .                         | 82          |
| FIGURE 23. Cyclic Voltammograms for the Zinc(II) Complexes . .   | 85          |
| FIGURE 24. Cyclic Voltammograms of $[\text{Cu}(\text{imidH})(\text{py})\text{DAP}]^{2+}$<br>Under Nitrogen and Dioxygen . . . . .    | 88          |
| FIGURE 25. Cyclic Voltammograms of $[\text{Cu}(\text{imidR})_2\text{DAP}]^{2+}$<br>Under Nitrogen and Dioxygen . . . . .             | 90          |
| FIGURE 26. Cyclic Voltammograms of $[\text{Cu}(\text{imidR})(\text{imidH})\text{DAP}]^{2+}$<br>Under Nitrogen and Dioxygen . . . . . | 92          |

|  | <u>Page</u> |
|--|-------------|
| FIGURE 27. Cyclic Voltammograms of $[\text{Cu}(\text{imidR})(\text{py})\text{DAP}]^{2+}$<br>Under Nitrogen and Dioxygen . . . . .  | 95          |
| FIGURE 28. A Proposed Proton Involvement Mechanism . . . . .   | 102         |
| FIGURE 29. EPR Spectra for the Copper(II) Complexes at 100 K . .   | 106         |
| FIGURE 30. EPR Spectra for $[\text{Cu}(\text{imidR})(\text{imidH})\text{DAP}]^{2+}$ and the Deoxy,<br>Oxy, and Redeoxy Forms of $[\text{Cu}(\text{imidR})(\text{imidH})\text{DAP}]^+$ . . .  | 108         |
| FIGURE 31. $\chi_M$ vs. Temperature <sup>-1</sup> "Difference" Plot for the<br>Oxygenated- $[\text{Cu}(\text{imidH})_2\text{DAP}](\text{BF}_4)$ Solution in $\text{Me}_2\text{SO}$ . .   | 116         |
| FIGURE 32. Electronic Absorption Spectra for the<br>$[\text{Cu}(\text{imidH})_2\text{DAP}]^{2+}$ , $[\text{Cu}(\text{py})_2\text{DAP}]^{2+}$ , and<br>$[\text{Cu}(\text{imidH})_2\text{DAP}]^+$ Complexes . . . . .  | 120         |
| FIGURE 33. Raman Spectra of $[\text{Cu}(\text{imidH})_2\text{DAP}]^+$ and $[\text{Cu}(\text{py})_2\text{DAP}]^+$<br>Taken at 77 K with 0.1 M Copper in $\text{CH}_3\text{CN}$ Using<br>a 514.5 nm Excitation Wavelength . . . . .                                  | 122         |
| FIGURE 34. Raman Spectra of the Deoxy, Oxy, and Redeoxy Forms<br>of $[\text{Cu}(\text{imidH})_2\text{DAP}]^+$ Taken at 77 K with 0.1 M<br>Copper in $\text{CH}_3\text{CN}$ Using 514.5 nm and 457.9 nm<br>Excitation Wavelengths . . . . .                         | 125         |
| FIGURE 35. Raman Spectra of $[\text{Cu}(\text{imidH})_2\text{DAP}]^{2+}$ and<br>Oxygenated- $[\text{Cu}(\text{imidH})_2\text{DAP}]^+$ Taken at 77 K with<br>0.1 M Copper in $\text{CH}_3\text{CN}$ Using 514.5 nm and 457.9 nm<br>Excitation Wavelengths . . . . . | 128         |
| FIGURE 36. Potential Energy Well Diagrams . . . . .  | 135         |

|   | <u>Page</u> |
|---|-------------|
| <u>PART II</u>  |             |
| FIGURE 1. Proposed Models for the Active Site Structure<br>in Cytochrome Oxidase . . . . .  | 147         |
| FIGURE 2. Proposed Catalytic Cycle Involving the $\mu$ -Oxo Model<br>for the Active Site Structure in Resting Cytochrome<br>Oxidase . . . . . | 149         |
| FIGURE 3. A Proposed Cyclic Mechanism of Oxygen Reduction<br>Involving the $\mu$ -Mercapto Model . . . . .                                    | 150         |
| FIGURE 4. The New $\mu$ -Imidazolato Mixed-Metal Complexes . . . . .  | 153         |
| FIGURE 5. Synthetic Scheme for the $\mu$ -Imidazolato<br>Mixed-Metal Complexes . . . . .  | 164         |
| FIGURE 6. Nujol Mull Infrared Spectra of the<br>Metalloporphyrin Complexes . . . . .  | 166         |
| FIGURE 7. Mössbauer Spectra at 100 K of the<br>Metalloporphyrin Complexes . . . . .   | 172         |
| FIGURE 8. $\mu_{\text{eff}}$ vs. Temperature Plots for the<br>$\mu$ -Imidazolato Complexes . . . . .  | 185         |
| FIGURE 9. EPR Spectra at 10 K for the $\mu$ -Imidazolato<br>Complexes in the Polycrystalline State . . . . .                                  | 187         |
| FIGURE 10. Schematic Drawing of the Active Site of<br>Bovine Superoxide Dismutase . . . . .   | 193         |
| FIGURE 11. $\chi_M'$ vs. Temperature <sup>-1</sup> Plot for the "2Co2Cu"<br>Superoxide Dismutase Derivative . . . . .                         | 195         |



## LIST OF TABLES

| <u>PART I</u>  | <u>Page</u> |
|--|-------------|
| TABLE 1. $^1\text{H}$ N.M.R. Spectral Data for Various Histamine Compounds . . . . .   | 42          |
| TABLE 2. Infrared Spectral Data for the Zinc(II), Copper(II), and Copper(I) Tetrafluoroborate Complexes as Solid State Nujol Mulls . . . . .                             | 46          |
| TABLE 3. $^1\text{H}$ N.M.R. Spectral Data for the Zinc(II) Complexes as Tetrafluoroborate Salts in $\text{CD}_3\text{CN}$ at Room Temperature Relative to TMS . . . . . | 56          |
| TABLE 4. Electronic Spectral Data for the Copper Complexes at Room Temperature . . . . .   | 67          |
| TABLE 5. Manometric Measurements and Dioxygen Uptake Results for Copper(I) Complexes in $\text{Me}_2\text{SO}$ at $23^\circ\text{C}$ and 1 Atm Dioxygen . . . . .        | 79          |
| TABLE 6. Cyclic Voltammetric Data for the Tetrafluoroborate Salts in $\text{CH}_3\text{CN}$ at $10^{-3}$ M Copper and 0.1 M in TBAP . . . . .                            | 81          |
| TABLE 7. Cyclic Voltammetric Data for the Zinc(II) Tetrafluoroborate Complexes in $\text{CH}_3\text{CN}$ at $10^{-3}$ M Zinc and 0.1 M in TBAP . . . . .                 | 87          |
| TABLE 8. EPR Data for the Copper Complexes as $\text{Me}_2\text{SO}$ Glasses at 100 K, $10^{-3}$ M Copper . . . . .  | 110         |
| TABLE 9. Magnetochemical Data on Deoxygenated- $[\text{Cu}(\text{imidH})_2\text{DAP}]^+$ at 0.1 M Copper in $\text{Me}_2\text{SO}$ . . . . .                             | 112         |
| TABLE 10. Magnetochemical Data on Oxygenated- $[\text{Cu}(\text{imidH})_2\text{DAP}]^{n+}$ at 0.1 M Copper in $\text{Me}_2\text{SO}$ . . . . .                           | 113         |

|   | <u>Page</u> |
|---|-------------|
| TABLE 11. Magnetochemical "Difference" Data on<br>Oxygenated-[Cu(imidH) <sub>2</sub> DAP] <sup>n+</sup> at 0.1 M<br>Copper in Me <sub>2</sub> SO . . . . .                                  | 114         |
| TABLE 12. Raman Spectral Data for the Cu(I) Complexes<br>Using 514.5 nm Excitation Wavelength . . . . .   | 123         |
| TABLE 13. Raman Spectral Data for the Deoxy, Oxy, and<br>Redeoxy Forms of [Cu(imidH) <sub>2</sub> DAP] <sup>+</sup> Complex Using<br>514.5 nm and 457.9 nm Excitation Wavelengths . . . . . | 126         |
| TABLE 14. Raman Spectral Data for the Oxidized and<br>Oxygenated Forms of [Cu(imidH) <sub>2</sub> DAP](BF <sub>4</sub> ) Using<br>514.5 nm and 457.9 nm Excitation Wavelengths . . . . .    | 129         |
| TABLE 15. Resonance Raman Spectral Data of the Copper<br>Complexes Taken at 295 K Using 413.1 nm, 406.7 nm,<br>and 363.8 nm Excitation Wavelengths . . . . .                                | 131         |
| TABLE 16. Resonance Raman Spectral Data Taken at 295 K<br>for [Cu(imidH)(py)DAP] <sup>2+</sup> Using 406.7 nm<br>Excitation Wavelength . . . . .  | 132         |
| <br><u>PART II</u>  |             |
| TABLE 1. Mössbauer Parameters for the μ-Imidazolato<br>Complexes at 100 K . . . . .   | 176         |
| TABLE 2. Variable-Temperature (15-300 K) Magnetochemical<br>Data for the μ-Imidazolato Complexes . . . . .  | 179         |

|  | <u>Page</u> |
|--|-------------|
| TABLE 3. EPR Parameters at 10 K for the $\mu$ -Imidazolato<br>Complexes in the Polycrystalline State . . . . . | 188         |
| TABLE 4. Magnetic Susceptibility Data for the "2Co2Cu"<br>Superoxide Dismutase Sample . . . . .                | 196         |

PART I

COPPER(I) COMPLEXES WHICH REACT REVERSIBLY WITH DIOXYGEN  
AND SERVE TO MIMIC THE ACTIVE SITE FUNCTION OF HEMOCYANIN

## INTRODUCTION

In Nature there exist certain copper metalloproteins which utilize dioxygen as a central theme in their functionality. These copper proteins fall into three major categories based on their reactivity with dioxygen.<sup>1</sup> The oxidation of certain organic substrates by dioxygen is catalyzed by type III copper centers in the copper proteins (e.g., laccase, tyrosinases, and oxidases). Cytochrome c oxidase, containing iron and copper active site centers, represents another type of dioxygen-active metalloprotein. Here the iron and copper active site centers form intermediates with dioxygen to catalyze the "ADP  $\rightarrow$  ATP, energy" reaction, where dioxygen is reduced to form water and energy is released for the production of ATP. The hemocyanins, a third class of copper proteins reacting with dioxygen, transport dioxygen through the respiratory cycle of molluscs and arthropods. The first two types of copper proteins discussed above incorporate the oxygen atom into substrate reactions, yielding oxygen-containing products. However, the hemocyanins are best described as dioxygen carriers and no substrate-enzyme interaction is involved.<sup>2</sup>

The hemocyanin proteins reversibly bind one dioxygen molecule per two copper atoms present at the active site unit.<sup>2</sup> The proteins are also known to react with NO and CO.<sup>3,4</sup> Magnus and Love<sup>5</sup> have successfully grown blue crystals of Limulus polyphemus hemocyanin (oxygenated form) whose total molecular weight is about  $3 \times 10^6$  daltons. The molecule has approximately 50 spherical subunits, each with a molecular weight of 70,000 daltons and a radius of about 27.2 Å. In order to

determine the location of the dioxygen binding site within the copper protein, Daniel et al.,<sup>6</sup> have detailed the effect of iodide on the fluorescence of Levantina hierosolima hemocyanin. These results indicate that the copper active site in hemocyanin is located by the solvent-accessible tryptophan amino acid residues, near the exterior of the molecule. In apparent contrast, infrared<sup>7</sup> and resonance Raman<sup>8</sup> spectral data offer evidence that the copper ions in hemocyanin are situated in a hydrophobic environment. However, both hydrophobicity and solvent accessibility represent structural features essential for reversible dioxygen binding. While the binding site has to be accessible to dissolved dioxygen, it has to be located in a nonpolar environment to prevent oxidation of the monovalent copper.

Since deoxyhemocyanin (deoxy-Hcyn) is colorless and diamagnetic,<sup>9</sup> the coppers in this dioxygen-active form are considered 'Cu(I)'s and the EPR silent behavior for deoxy-Hcyn is expected.<sup>10</sup> On the other hand, the oxyhemocyanins (oxy-Hcyn) are deep blue with electronic spectral parameters indicating the copper centers to be Cu(II)'s, yet oxy-Hcyn is also EPR silent.<sup>10</sup> Allowing that the copper(I) ions in deoxy-Hcyn react with dioxygen in a stoichiometry of two moles of copper per one mole of dioxygen, it has been proposed that the oxy-Hcyn contains two copper(II) centers antiferromagnetically coupled by a  $\mu$ -peroxo bridging ligand. The variable temperature magnetic susceptibility study of Limulus polyphemus oxy-Hcyn by Gray and workers<sup>11</sup> supports this premise and establishes the lower limit of  $550\text{ cm}^{-1}$  for the  $-J$  value (anti-ferromagnetic coupling constant) for this system.

Identification of the nature of the copper-dioxygen bonding scheme in the oxygenated form of hemocyanin has been achieved by Loehr et al.,<sup>12</sup> using resonance Raman (RR) spectroscopic techniques. Employing either 530.9 nm or 457.9 nm laser wavelengths for excitation within the 570 nm absorption band of oxy-Hcyn, RR spectra have been recorded and  $\mu$ -peroxo stretches at  $744\text{ cm}^{-1}$  for Cancer magister (arthropod) and at  $749\text{ cm}^{-1}$  for Busycon canaliculatum (mollusc) obtained. Isotopic labeling studies<sup>13</sup> have been performed where substitution of  $^{18}\text{O}_2$  for  $^{16}\text{O}_2$  in oxy-Hcyn has caused the peroxo peaks to shift to  $704\text{ cm}^{-1}$  and  $708\text{ cm}^{-1}$ , respectively. Thus dioxygen is seemingly bound as a peroxide-like anion and this bonding mode can be described as an oxidative addition process in which dioxygen is reduced and two Cu(I) atoms of deoxy-Hcyn are oxidized to Cu(II) during the oxygenation procedure.

Additional resonance Raman experiments by Spiro et al.,<sup>14</sup> have been conducted using ultraviolet excitation wavelengths (351.1 nm and 363.8 nm). The RR spectra of oxy-Hcyn depict enhanced low-frequency modes in the range of  $119\text{--}360\text{ cm}^{-1}$ , characteristic of metal-ligand vibrations. These data, combined with no detectable enhancement of imidazole ligand modes, point to the assignment of the 345 nm absorption band to a "simultaneous pair excitation,"<sup>14</sup> not a charge-transfer transition. An SPE transition involves the simultaneous excitation of a "d-d" transition on each of the Cu(II) ions by a photon of about twice the energy. In another isotopic labeling study by Larrabee and Spiro,<sup>15</sup>  $^{63}\text{Cu}/^{65}\text{Cu}$  and  $\text{H}_2\text{O}/\text{D}_2\text{O}$  frequency shifts confirm the assignment of  $226\text{--}267\text{ cm}^{-1}$  RR bands to copper-imidazole modes. The  $^{63}\text{Cu}/^{65}\text{Cu}$  isotope shifts for these bands as well as the  $287\text{ cm}^{-1}$  peak depict an

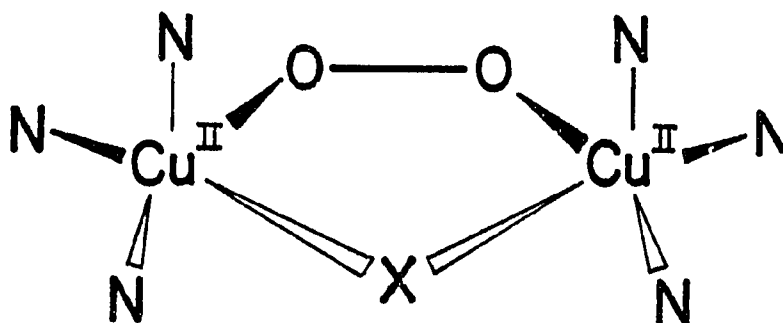
asymmetric disposition of imidazole ligands, consistent with a square-pyramidal model, with an apical imidazole. According to Spiro, the broad RR band at  $1075\text{ cm}^{-1}$  could indicate the singlet  $\rightarrow$  triplet transition of coupled Cu(II) ions. This proposal supports the 345 nm absorption band being an SPE transition.

Employing synchrotron radiation techniques, x-ray absorption spectra near the Cu K edge have been recorded for Busycon canaliculatum deoxy- and oxy-Hcyn.<sup>16</sup> Comparison of these data with EXAFS spectra of known copper complexes indicates that imidazoles are coordinated to both the Cu(I) and Cu(II) centers. Also in deoxy-Hcyn, some copper-copper interaction is observed. Based on these EXAFS results, and in combination with the aforementioned resonance Raman data, Spiro and workers<sup>15</sup> have proposed a model for the hemocyanin copper-dioxygen binding site (Figure 1-A). In the deoxygenated form of the protein, two Cu(I) atoms are bound to the protein backbone by three histidine (imidazole) ligands per copper center. Upon oxygenation, the hemocyanin has the Cu(II) ions bridged by a  $\mu$ -peroxo linkage and by an additional atom (or atoms) from a protein ligand, possibly tyrosine.

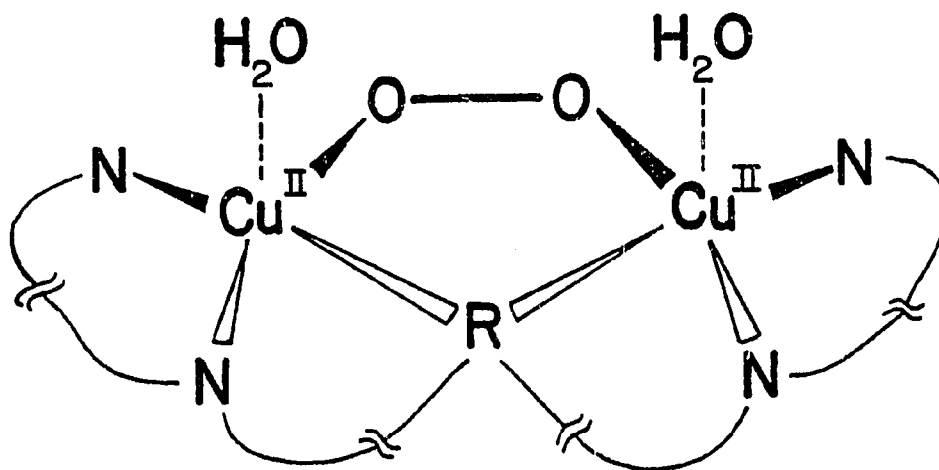
Solomon and workers<sup>17,18</sup> have systematically studied the chemical and spectral properties of several derivatives of various hemocyanins. While some spectral differences were observed for the various species, overwhelmingly the spectral parameters for the hemocyanins were quite similar. Relying on substantial electronic and EPR spectral data, Solomon has formulated active site structures for a family of hemocyanin derivatives (Figure 2).<sup>19</sup> Several conclusions can be drawn from the work of Spiro and Solomon:



Figure 1

Proposed Active Site Structures for Oxyhemocyanin

(A) THE SPIRO MODEL

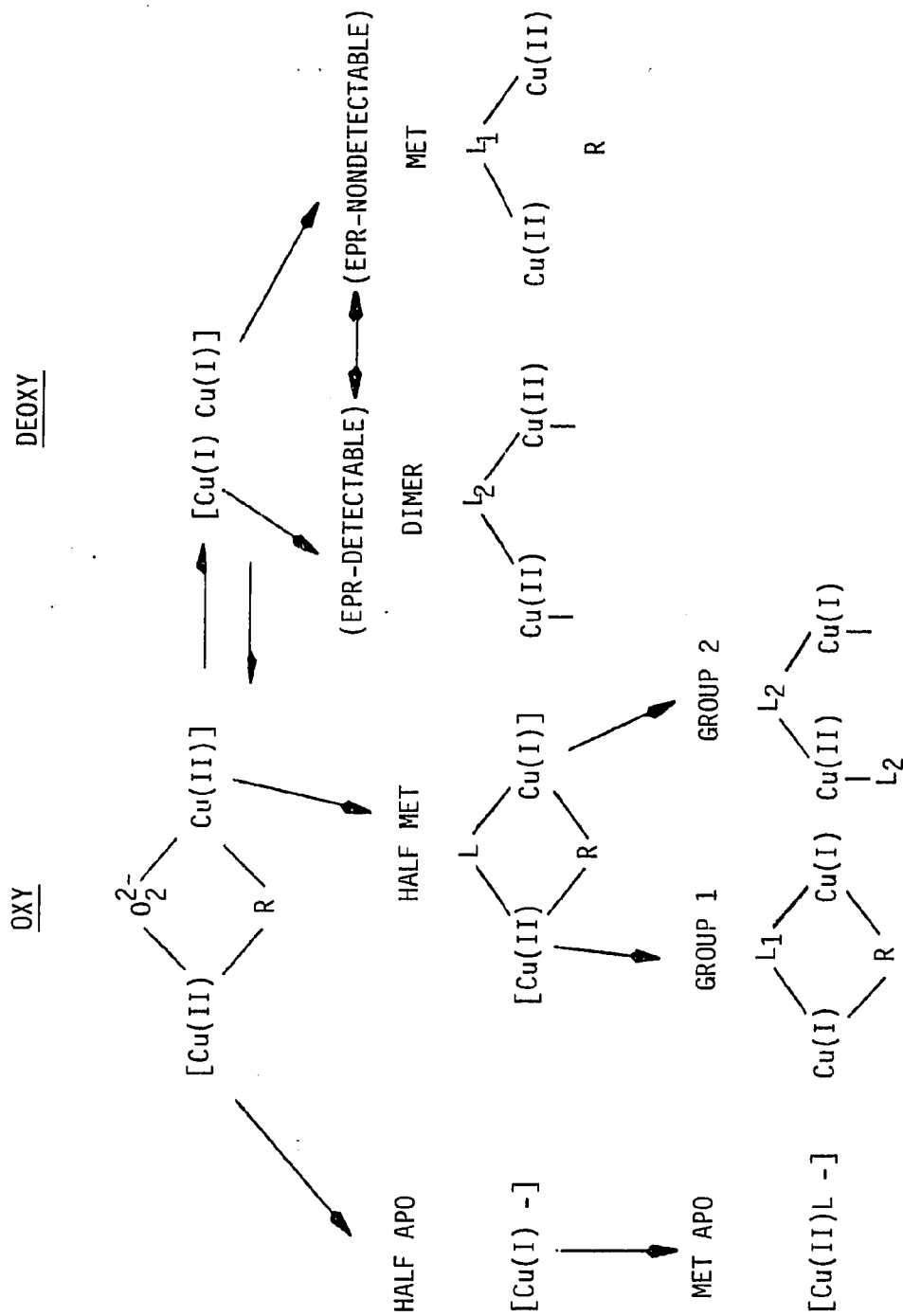
 $\text{X}$  = Tyrosine (phenol)

(B) THE SOLOMON MODEL

 $\text{R}$  = Tyrosine (phenol) $\text{N}$  = Histidine (imidazole)

Figure 2

Flow Diagram for the Hemocyanin Derivatives



- (1) A comparison of the met apo[Cu(II) - ] and half met [Cu(II)Cu(I)] forms indicates that both the exogenous ligand and a protein ligand bridge the two copper ions.
- (2) Both the met and dimer derivatives contain two tetragonal Cu(II) atoms [Cu(II)Cu(II)], yet the copper in the dimer is EPR-detectable and in the met form of hemocyanins is EPR-silent. This lack of EPR signal must be due to the antiferromagnetic coupling between the coppers, mediated by an endogenous bridge which is broken in the dimer. Similarly, the oxy-Hcyn derivative is EPR-silent, and has a geometry and electronic structure similar to that of met-Hcyn.
- (3) Contrary to Spiro's SPE theory explaining the RR data, Solomon proposes that the 346 nm absorption band in oxy-Hcyn is not an SPE transition. Rather, the 345 nm and 570 nm bands are associated with the peroxide to copper charge transfer transitions. This "transition dipole-vector coupling model" supports the conclusion that the oxy-Hcyn derivative has an end-to-end peroxide bridging geometry. Regardless of this discrepancy in explanations for the observed spectral data, one consistent active site structure for oxy-Hcyn is presented (Figure 1-B). The binuclear Cu(II) active site contains both an endogenous and exogenous ligand bridge with the peroxide binding in a  $\mu$ -peroxo manner between equatorial planes of both tetragonal coppers.<sup>19</sup>

In addition to direct studies of proteins, information concerning the active site structure in large proteins may also be gathered by the

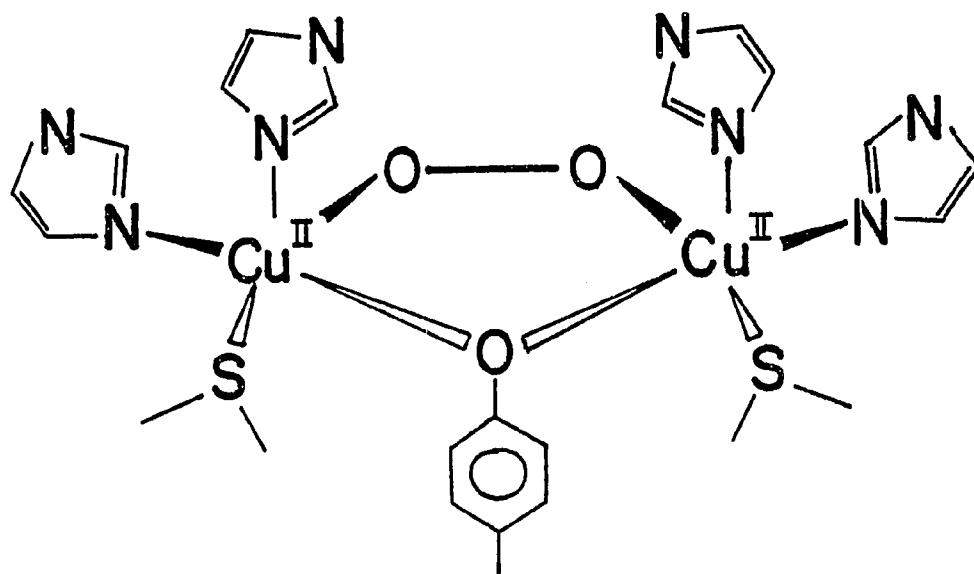
synthesis and study of small model compounds which serve to mimic a protein's functionality. While certain aspects of a metalloprotein's activity, such as cooperativity and physiological conditions, cannot be addressed by the study of synthetic compounds, these low molecular weight models can be structurally varied in a systematic manner in order to establish structure/function relationships in the protein's active site unit. This modeling approach has been applied to several metalloproteins. For example, the heme  $O_2$ -transport proteins myoglobin and hemoglobin (molecular weights of 17,800 and 64,500 daltons, respectively) have been characterized by x-ray structural analysis.<sup>20</sup> Collman,<sup>21</sup> among others,<sup>22</sup> has subsequently modeled hemoglobin's active site structure with synthetic iron complexes, the "picket fence porphyrins," which reversibly bind dioxygen. By contrast, the non-heme  $O_2$ -carrying proteins like hemerythrin and hemocyanin are not as well defined. While low resolution structural data have been obtained for the hemerythrin protein,<sup>23</sup> the lack of a definitive active site structure has greatly impeded the modeling efforts concerning this iron metalloprotein. With molecular weights of several million daltons for the hemocyanins, the growth of a single crystal for high resolution x-ray structural analysis is not forthcoming. Thus, with no explicit structural data from which to draw analogies, the modeling of hemocyanin's active site structure represents quite a challenging endeavor.

Synthetic model complexes containing copper(I) with nitrogen and/or oxygen donor atoms would serve to mimic the active site structure of hemocyanin if reversible dioxygen reactivity by these compounds is observed. However, copper(I) model complexes for the  $O_2$ -Hcyn inter-

action have for the most part evaded chemists for ca. 40 years, due largely to the lack of information concerning Cu(I) chemistry involving nitrogenous ligands. Also the preparation of analytically pure copper(I) complexes is complicated by the problems of the air sensitivity, kinetic lability, and tendency for disproportionation of Cu(I).<sup>24</sup> Several investigators have reported the synthesis of Cu(II) and Cu(I) complexes having nitrogen, oxygen, or sulfur donor atoms coordinating to the metal center.<sup>25-28</sup> These compounds have import in the study of certain copper proteins (Types I, II, and III copper) but they are not dioxygen carriers like the hemocyanins. One example is the work of Bosnich et al.,<sup>29</sup> where Cu(II) complexes having sulfur ligands have been prepared and studied spectroscopically in order to propose active site structures for the copper proteins. While these results provide valuable information about types I and II copper, there is evidence refuting the proposed ligand environment of the copper-dioxygen binding site in oxy-Hcyn (Figure 3), namely, that resonance Raman<sup>15</sup> and EXAFS<sup>16,30</sup> results emphatically state that no sulfur donor atom is present in the primary coordination sphere around copper. More recently, Gagne' and workers<sup>31</sup> have synthesized noteworthy Cu(I) complexes which form CO adducts and have provided insight into the understanding of copper(I) chemistry through the model compound approach. In particular, one of these Cu(I)-CO compounds, (carbonyl){1,3-bis-[2-(4-methylpyridyl)imino]isoindoline}copper(I), reacted stoichiometrically in solution with dioxygen (1 mole O<sub>2</sub>:2 moles Cu). However, this oxygenation reaction was irreversible and a mixture of ( $\mu$ -CO<sub>3</sub>) and ( $\mu$ -OH) bridged Cu(II) dimers was produced. As this reaction was not

Figure 3

The Bosnich Model for the Active Site Structure of  
Oxyhemocyanin



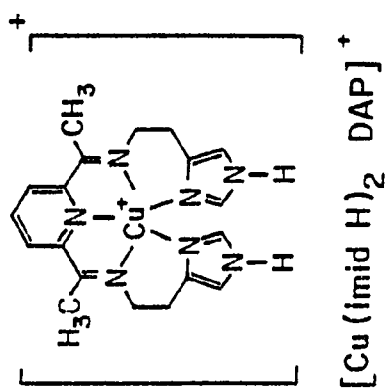
reversible and no isolatable copper-dioxygen adduct formed (except possibly as an intermediate), this complex cannot be viewed as a viable hemocyanin model compound. The first claim of a reversible Cu-O<sub>2</sub> interaction has been reported<sup>32</sup> where an NOS<sub>2</sub> donor set was chosen as a model for the copper environment in hemocyanin. However, only solid-state reactivity with dioxygen was documented and the oxygenated product was identified only by EPR spectroscopy with no information given about the O<sub>2</sub>:Cu reaction stoichiometry; furthermore, reactivity with dioxygen in solution was reported to proceed irreversibly.

The synthesis of the first reversible dioxygen-binding copper(I) system has been achieved by Dr. Miriam Simmons,<sup>33,34,37</sup> formerly of our research group. This complex, [Cu<sup>I</sup>(imidH)<sub>2</sub>DAP]<sup>+</sup> (Figure 4-A), has been found to react reversibly at room temperature in solution with dioxygen in a stoichiometry of one mole dioxygen for two moles Cu(I) present. The EPR spectral data taken at 100 K for the red deoxy and green oxy forms of this compound indicate essentially diamagnetic material in both cases. These results, combined with the dioxygen uptake stoichiometry, suggest that the oxygenated copper complex may contain two Cu(II) centers antiferromagnetically coupled through a  $\mu$ -peroxo bridge similar to that proposed for oxyhemocyanin. On the other hand, the [Cu<sup>I</sup>(py)<sub>2</sub>DAP]<sup>+</sup> (Figure 4-C) species was found to undergo a much slower, nonstoichiometric dioxygen uptake, indicating some irreversible oxidation reaction of the Cu(I) center or perhaps the ligand framework itself. Thus by varying the nature of the ligand environment, one can fine tune the degree of reversible oxygenation in this family

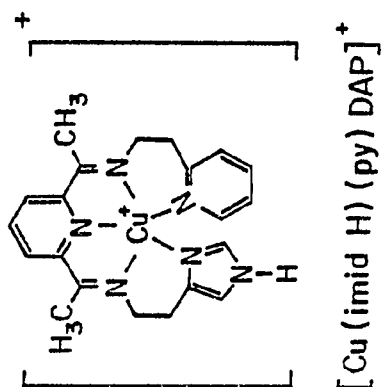
Figure 4The Copper(I) Model Compounds

- (A) The {Bis-2,6-[1-(2-imidazol-4-ylethylimino)ethyl]pyridine}-copper(I) Cation.
- (B) The {2-[1-(2-Imidazol-4-ylethylimino)ethyl],6-[1-(2-pyridin-2-ylethylimino)ethyl]pyridine}copper(I) Cation.
- (C) The {Bis-2,6-[1-(pyridin-2-ylethylimino)ethyl]pyridine}copper(I) Cation.
- (D) The {Bis-2,6-[1-(2-(N<sub>1</sub>-p-methylbenzyl)imidazol-4-ylethylimino)-ethyl]pyridine}copper(I) Cation.
- (E) The {2-[1-(2-(N<sub>1</sub>-p-methylbenzyl)imidazol-4-ylethylimino)ethyl],-6-[1-(2-pyridin-2-ylethylimino)ethyl]pyridine}copper(I) Cation.
- (F) The {2-[1-(2-(N<sub>1</sub>-p-methylbenzyl)imidazol-4-ylethylimino)ethyl],-6-[1-(2-imidazol-4-ylethylimino)ethyl]pyridine}copper(I) Cation.

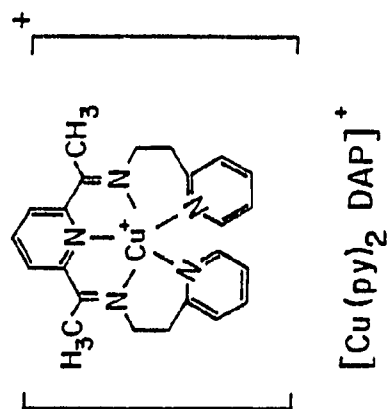




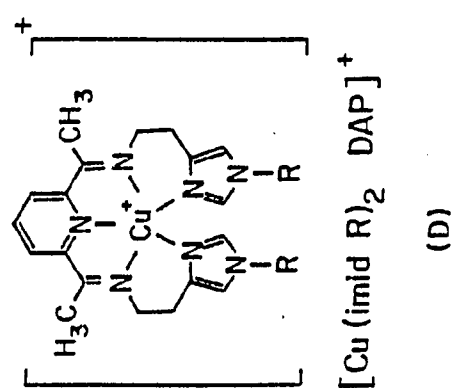
(A)



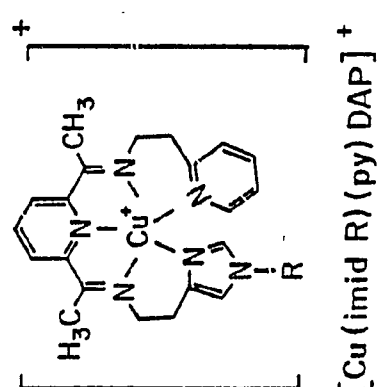
(B)



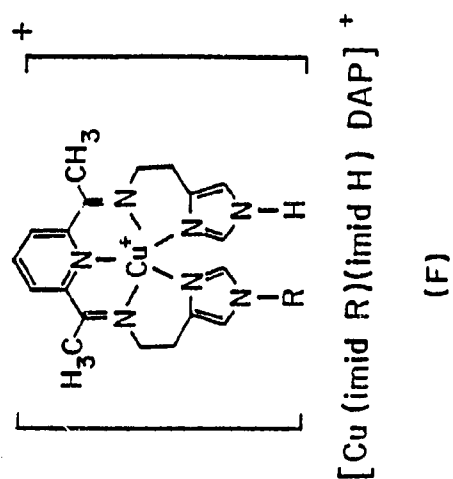
(C)



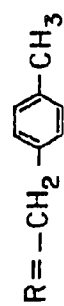
(D)



(E)



(F)



of Cu(I) complexes. Several structural aspects of the  $[\text{Cu}^{\text{I}}(\text{imidH})_2\text{DAP}]^+$  species make this type of complex novel in bioinorganic chemistry as a successful, reversible dioxygen carrier. As discussed previously,<sup>34</sup> the oxygenation process for a Cu(I) center most probably concerns an oxidative addition reaction where, upon binding with  $\text{O}_2$  the Cu(I) is oxidized to Cu(II) and the dioxygen is reduced to the anion ( $\text{O}_2^-$ ). For this reaction to be reversible, the Cu(II) oxidation state must be facile to reduction. Thus an appropriate ligand environment must be employed to stabilize the copper in both +1 and +2 oxidation, as well as allow for any geometrical changes in the coordination sphere that may occur during the oxygenation procedure. The imine nitrogen donor atoms present in the ligating system of the  $[\text{Cu}^{\text{I}}(\text{imidH})_2\text{DAP}]^+$  species are known to provide strong  $\pi$  back-bonding toward the Cu(I) center and thus help to stabilize the +1 oxidation state.<sup>35</sup> Also, the ability of the imine moiety to stabilize Cu(II) is well documented.<sup>36</sup> In addition, the imine-containing macrocycle around the copper center provides flexibility for geometrical changes during the oxygenation reaction; furthermore, the enclosed coordination sphere serves to eliminate ligand exchange problems.<sup>34</sup> Thus, while other Cu(I) complexes (which do not bind dioxygen) have not been synthesized to possess such characteristics, the  $[\text{Cu}^{\text{I}}(\text{imidH})_2\text{DAP}]^+$  species and related derivatives discussed below do incorporate into their ligand environment these apparently necessary structural requirements for reversible dioxygen binding.

In a continuing study of these intriguing copper(I) compounds, magnetochemical and resonance Raman experiments have been conducted in

order to more fully characterize the nature of this copper-dioxygen interaction. Also, the synthesis of additional copper(I) derivatives, i.e.,  $[\text{Cu}^{\text{I}}(\text{imidH})(\text{py})\text{DAP}]^+$ ,  $[\text{Cu}^{\text{I}}(\text{imidR})_2\text{DAP}]^+$ ,  $[\text{Cu}^{\text{I}}(\text{imidR})(\text{py})\text{DAP}]^+$ , and  $[\text{Cu}^{\text{I}}(\text{imidR})(\text{imidH})\text{DAP}]^+$  (see Figure 4), has been achieved in order to examine the role, if any, of the acidic imidazole proton of the  $[\text{Cu}^{\text{I}}(\text{imidH})_2\text{DAP}]^+$  species in the reversible oxygenation process. While the  $[\text{Cu}^{\text{I}}(\text{imidR})(\text{py})\text{DAP}]^+$  species has been found to be dioxygen-inactive, the  $[\text{Cu}^{\text{I}}(\text{imidH})(\text{py})\text{DAP}]^+$  compound reacted stoichiometrically (1 mole  $\text{O}_2$ :2 moles Cu) yet irreversibly toward dioxygen. The  $[\text{Cu}^{\text{I}}(\text{imidR})_2\text{DAP}]^+$  and  $[\text{Cu}^{\text{I}}(\text{imidR})(\text{imidH})\text{DAP}]^+$  cations reacted reversibly toward dioxygen in a stoichiometric manner (1  $\text{O}_2$ : 2 Cu), paralleling the dioxygen reactivity observed for the parent  $[\text{Cu}^{\text{I}}(\text{imidH})_2\text{DAP}]^+$  species. The possible correlation of redox potential for the  $\text{Cu}(\text{II}) \rightleftharpoons \text{Cu}(\text{I})$  couple and the reaction of the Cu(I) center toward dioxygen has been explored. The analogous Cu(II) and Zn(II) complexes have also been prepared and fully characterized. In summary, a systematic and comprehensive study of this family of compounds employing spectroscopic (notably resonance Raman, EPR, and electronic), electrochemical, and magnetochemical techniques has been undertaken to further elucidate the nature of Cu(I)- $\text{O}_2$  interactions. The relevance of these complexes as the first, and to date only, synthetic copper(I) dioxygen carriers to the modeling of the active site function of hemocyanin has been addressed.

## EXPERIMENTAL SECTION

### Materials

All solvents were reagent grade, distilled before use, and stored over molecular sieves: methanol (MeOH) from sodium metal, dimethyl sulfoxide (Me<sub>2</sub>SO) from BaO in vacuo, acetonitrile (CH<sub>3</sub>CN) from KMnO<sub>4</sub> and Na<sub>2</sub>CO<sub>3</sub>, and methylene chloride (CH<sub>2</sub>Cl<sub>2</sub>) from P<sub>2</sub>O<sub>5</sub>. Degassing was accomplished by the standard freeze-thaw method using argon gas. Histamine, free base, was procured from Sigma Chemical Company; 2,6-diacetylpyridine (DAP), 2-(2-aminoethyl)pyridine,  $\alpha$ -chloro-p-xylene, and histamine dihydrochloride salt from Aldrich Chemicals; and Cu(BF<sub>4</sub>)<sub>2</sub>·6H<sub>2</sub>O, Zn(BF<sub>4</sub>)<sub>2</sub>·6H<sub>2</sub>O, Cu<sub>2</sub>O, and NaBF<sub>4</sub> from Alfa Products. The electrochemical grade tetrabutylammonium perchlorate (TBAP) was purchased from G. Frederick Smith. Industrial grade nitrogen, argon, and dioxygen gases were obtained from Big Three Industries and streamed through H<sub>2</sub>SO<sub>4</sub>, KOH<sub>(s)</sub>, a heated copper catalyst, and a P<sub>2</sub>O<sub>5</sub> scrub train to insure dry, oxygen-free gases (with the exception of dioxygen gas, which was purified and dried by a H<sub>2</sub>SO<sub>4</sub>, KOH<sub>(s)</sub>, and drierite scrub train).

### Syntheses

The copper(I) complexes were prepared under an argon atmosphere using Schlenk techniques or under nitrogen gas in a Vacuum/Atmospheres dry box.<sup>39</sup> The air stable copper(II) and zinc(II) compounds were prepared on the open lab bench, but taking great care to eliminate moisture from the solvents and glassware since their tetrafluoroborate

salts were found to be fairly hygroscopic. Chemical analyses were obtained commercially from Schwarzkopf Microanalytical Laboratory, Inc.

[N<sub>1</sub>-(p-methylbenzyl)]histamine, free base. The compound was prepared by the modified method of Averill.<sup>40</sup> Substitution of the p-methylbenzyl group for the acidic proton on the imidazole ring of histamine was achieved in two steps. First, histamine·dihydrochloride salt (20.0 g) was dissolved in distilled liquid ammonia (400 ml), to which metallic sodium was slowly added. This step was completed when the addition of sodium resulted in a persistent blue solution. A solution of  $\alpha$ -Cl-p-xylene in absolute ethyl ether (2 ml solute/5 ml solvent) was then added dropwise until the blue color just disappeared. In the second step of the reaction, neat  $\alpha$ -Cl-p-xylene (10 ml) was added stoichiometrically and dropwise. Next the liquid ammonia was allowed to evaporate overnight at room temperature. The yellow-white oily crude product was dissolved in 400 ml 1M HCl and this slightly acidic solution extracted with three 50 ml portions of CH<sub>2</sub>Cl<sub>2</sub>. The aqueous layer was basified to pH = 10-11 with NaOH pellets and then reduced to dryness. The crude R-substituted free base histamine was dissolved in CH<sub>2</sub>Cl<sub>2</sub> (20 ml) and filtered away from the insoluble inorganic by-products. This filtered solution was then evaporated to dryness. The remaining oil, which contained a mixture of the geometric isomers N<sub>1</sub>-R and N<sub>3</sub>-R, was weighed, dissolved in a minimum amount of dry absolute ethanol (20 ml), and acidified with a stoichiometric amount of conc. HCl to yield the monohydrochloride salt. The desired N<sub>1</sub>-R-substituted histamine·HCl was separated from the N<sub>3</sub>-R isomer by re-

crystallization from absolute ethanol and dried in vacuo at room temperature for 24 h. The HCl salt was then dissolved in a minimum amount of H<sub>2</sub>O (10 ml), basified with NaOH<sub>(s)</sub> to pH = 11, and the solution was reduced to dryness. The oily solids were washed with CH<sub>2</sub>Cl<sub>2</sub>, and the solution filtered and reduced to dryness. The remaining solid was the hygroscopic, yellow [N<sub>1</sub>-(p-methylbenzyl)]histamine in its free base form.

{Tetra(acetonitrile)}copper(I)tetrafluoroborate, [Cu<sup>I</sup>(CH<sub>3</sub>CN)<sub>4</sub>](BF<sub>4</sub>).

The compound was prepared by the method of Hemmerich and Sigwart.<sup>41</sup> Cu<sub>2</sub>O (2.2 g) was added to a degassed mixture of H<sub>2</sub>O (40 ml) and CH<sub>3</sub>CN (30 ml). Upon the dropwise addition of OEt<sub>2</sub>·BF<sub>3</sub> (60 ml), white needles formed. The reaction mixture was then refluxed under argon gas for 1 h. Upon cooling, the white needles were collected by filtration, dried in vacuo, and recrystallized from hot degassed CH<sub>3</sub>CN. The purified product was collected, dried in vacuo, and stored under nitrogen.

{Bis-2,6-[1-(2-imidazol-4-ylethylimino)ethyl]pyridine}zinc(II)tetrafluoroborate, [Zn<sup>II</sup>(imidH)<sub>2</sub>DAP](BF<sub>4</sub>)<sub>2</sub>.

The ligand solution was prepared by refluxing a methanolic solution (25 ml) of 2,6-diacetylpyridine (1 mmol) and histamine, free base (2 mmol) for 1 h. This yellow solution, cooled to room temperature, was combined with solid Zn(BF<sub>4</sub>)<sub>2</sub>·6H<sub>2</sub>O (1 mmol), and stirred at room temperature for 5 min. The resulting bright yellow solution was filtered and evaporated to dryness. The collected solids were recrystallized from a hot

methanol/ethyl ether mixture. Anal. calcd. for  $\text{ZnC}_{19}\text{H}_{23}\text{N}_7\text{B}_2\text{F}_8$ :  
C, 38.78%; H, 3.94%; N, 16.66%. Found: C, 38.36%; H, 3.96%;  
N, 16.66%.

{Bis-2,6-[1-(2-pyridin-2-ylethylimino)ethyl]pyridine}zinc(II)tetra-  
fluoroborate,  $[\text{Zn}^{\text{II}}(\text{py})_2\text{DAP}](\text{BF}_4)_2$ . A ligand solution was prepared by  
dissolving 2,6-diacetylpyridine (1 mmol) and [2-(2-aminoethyl)]-  
pyridine (2 mmol) in 25 ml MeOH. This solution was refluxed for about  
1 h, after which it was cooled. One mmol of solid  $\text{Zn}(\text{BF}_4)_2 \cdot 6\text{H}_2\text{O}$  was  
added. The resulting orange solution was stirred for approximately  
5 min, filtered, and reduced to dryness in vacuo. The orange solid  
was recrystallized from hot MeOH. Anal. calcd. for  $\text{ZnC}_{23}\text{H}_{25}\text{N}_5\text{B}_2\text{F}_8$ :  
C, 45.25%; H, 4.13%; N, 11.47%. Found: C, 45.03%; H, 4.01%; N,  
11.52%.

{Bis-2,6-[1-(2-(N<sub>1</sub>-p-methylbenzyl)imidazol-4-ylethylimino)ethyl]-  
pyridine zinc(II)tetrafluoroborate,  $[\text{Zn}^{\text{II}}(\text{imidR})_2\text{DAP}](\text{BF}_4)_2$ . The  
ligand solution was prepared by dissolving 1 mmol 2,6-diacetylpyridine  
and 2 mmol [N<sub>1</sub>-(p-methylbenzyl)]histamine, free base in 25 ml MeOH.  
This reaction mixture was refluxed for 1 h to yield a yellow solution.  
Upon cooling, this solution was combined with 1 mmol solid  
 $\text{Zn}(\text{BF}_4)_2 \cdot 6\text{H}_2\text{O}$  and stirred for about 5 min. The bright yellow-orange  
solution was filtered and reduced to dryness under vacuum. The result-  
ing orange solid was recrystallized from a minimum amount of hot MeOH  
and a small amount of absolute ethyl ether. The final product was a  
cream colored solid. Anal. calcd. for  $\text{ZnC}_{35}\text{H}_{39}\text{N}_7\text{B}_2\text{F}_8$ : C, 52.76%;  
H, 4.93%; N, 12.31%. Found: C, 52.79%; H, 5.18%; N, 12.35%.

{2-[1-(2-imidazol-4-ylethylimino)ethyl],6-[1-(2-pyridin-2-ylethylimino)ethyl]pyridine}zinc(II)tetrafluoroborate·monohydrate, [Zn<sup>II</sup>(imidH)(py)DAP](BF<sub>4</sub>)<sub>2</sub>·H<sub>2</sub>O. A ligand solution was prepared by dissolving 2,6-diacetylpyridine (1 mmol) in 50 ml dry MeOH and dropwise adding a solution of 2-(2-aminoethyl)pyridine (1 mmol) and free base histamine (1 mmol) in 75 ml MeOH. During this procedure (about 3/4 h), the reaction mixture was stirred and heated at 60°C. Following the addition of the two bases, the ligand solution was allowed to reflux for another 3/4 h and then cooled to room temperature. To this yellow solution was added solid Zn(BF<sub>4</sub>)<sub>2</sub>·6H<sub>2</sub>O (1 mmol), and, upon stirring at room temperature, the solution became deep orange in color. The solvent was removed under vacuum and the resulting orange solid recrystallized from hot MeOH yielding a slightly hygroscopic cream powder. Anal. calcd. for ZnC<sub>21</sub>H<sub>26</sub>N<sub>6</sub>B<sub>2</sub>F<sub>8</sub>O: C, 40.84%; H, 4.25%; N, 13.61%. Found: C, 40.90%; H, 4.08%; N, 13.66%.

{2-[1-(2-(N<sub>1</sub>-p-methylbenzyl)imidazol-4-ylethylimino)ethyl],6-[1-(2-pyridin-2-ylethylimino)ethyl]pyridine}zinc(II)tetrafluoroborate·monohydrate, [Zn<sup>II</sup>(imidR)(py)DAP](BF<sub>4</sub>)<sub>2</sub>·H<sub>2</sub>O. The ligand was prepared by dissolving 2,6-diacetylpyridine (1 mmol) in 50 ml dry MeOH and adding dropwise a solution of 2-(2-aminoethyl)pyridine (1 mmol) and [N<sub>1</sub>-(p-methylbenzyl)]histamine, free base (1 mmol) in 75 ml MeOH. During this addition, over a period of about 3/4 h, the reaction mixture was stirred and heated at 60°C. Upon completion of this step, the yellow ligand solution was refluxed 3/4 h and then cooled to room temperature. Next solid Zn(BF<sub>4</sub>)<sub>2</sub>·6H<sub>2</sub>O (1 mmol) was added and the



solution became bright yellow orange in color. This product solution was filtered and reduced to dryness under vacuum. Recrystallization of the resulting solid from a hot MeOH/Et<sub>2</sub>O mixture produced a hygroscopic yellow powder. Anal. calcd. for ZnC<sub>29</sub>H<sub>36</sub>N<sub>6</sub>B<sub>2</sub>F<sub>8</sub>O: C, 48.27%; H, 4.75%; N, 11.65%. Found: C, 48.08%; H, 4.84%; N, 11.74%.

{2-[1-(2-(N<sub>1</sub>-p-methylbenzyl)imidazol-4-ylethylimino)ethyl],6-[1-(2-imidazol-4-ylethylimino)ethyl]pyridine}zinc(II)tetrafluoroborate·dihydrate, [Zn<sup>II</sup>(imidR)(imidH)DAP](BF<sub>4</sub>)<sub>2</sub>·2H<sub>2</sub>O. This ligand was prepared by reacting 2,6-diacetylpyridine (1 mmol) with a methanolic solution of free base histamine (1 mmol) and [N<sub>1</sub>-(p-methylbenzyl)]-histamine, free base (1 mmol), in the manner identical to the procedure employed in the syntheses of the other zinc(II) hybrids (see above). Due to the high degree of hygroscopicity exhibited by this complex, normal recrystallization techniques were not successful. Rather, a hot, dry MeOH/Et<sub>2</sub>O mixture was used to dissolve the yellow solid product. Addition of more absolute ethyl ether caused a deep orange oil to separate, leaving behind a yellow-orange mother liquor. This solution was decanted from the oil, filtered, and reduced to dryness under vacuum. The resulting light orange solid was quite hygroscopic. Anal. calcd. for ZnC<sub>27</sub>H<sub>35</sub>N<sub>7</sub>B<sub>2</sub>F<sub>8</sub>O<sub>2</sub>: C, 44.51%; H, 4.84%; N, 13.46%. Found: C, 45.10%; H, 4.64%; N, 13.35%.

{Bis-2,6-[1-(2-imidazol-4-ylethylimino)ethyl]pyridine}copper(II)tetrafluoroborate, [Cu<sup>II</sup>(imidH)<sub>2</sub>DAP](BF<sub>4</sub>)<sub>2</sub>. The compound was prepared, using Cu(BF<sub>4</sub>)<sub>2</sub>·6H<sub>2</sub>O instead of Zn(BF<sub>4</sub>)<sub>2</sub>·6H<sub>2</sub>O, and treated identically

to the analogous zinc(II) complex. The recrystallized light green solid gave a  $\mu_{\text{eff}}(\text{solid}, 298 \text{ K}) = 2.0 \mu_{\text{B}}$ . Anal. calcd. for  $\text{CuC}_{19}\text{H}_{23}\text{N}_7\text{B}_2\text{F}_8$ : C, 38.90%; H, 3.95%; N, 16.72%. Found: C, 39.30%; H, 3.96%; N, 16.61%.

{Bis-2,6-[1-(2-pyridin-2-ylethylimino)ethyl]pyridine}copper(II)tetrafluoroborate,  $[\text{Cu}^{\text{II}}(\text{py})_2\text{DAP}](\text{BF}_4)_2$ . The compound was synthesized, using  $\text{Cu}(\text{BF}_4)_2 \cdot 6\text{H}_2\text{O}$  instead of  $\text{Zn}(\text{BF}_4)_2 \cdot 6\text{H}_2\text{O}$ , and treated identically to the analogous zinc(II) complex. The recrystallized blue-green solid gave a  $\mu_{\text{eff}}(\text{solid}, 298 \text{ K}) = 2.1 \mu_{\text{B}}$ . Anal. calcd. for  $\text{CuC}_{23}\text{H}_{25}\text{N}_5\text{B}_2\text{F}_8$ : C, 45.39%; H, 4.14%; N, 11.51%. Found: C, 44.93%; H, 4.33%; N, 11.98%.

{Bis-2,6-[1-(2-(N<sub>1</sub>-p-methylbenzyl)imidazol-4-ylethylimino)ethyl]pyridine}copper(II)tetrafluoroborate dihydrate,  $[\text{Cu}^{\text{II}}(\text{imidR})_2\text{DAP}](\text{BF}_4)_2 \cdot 2\text{H}_2\text{O}$ . The compound was prepared, using  $\text{Cu}(\text{BF}_4)_2 \cdot 6\text{H}_2\text{O}$  instead of  $\text{Zn}(\text{BF}_4)_2 \cdot 6\text{H}_2\text{O}$ , and treated identically to the analogous zinc(II) compound. The recrystallized lime green powder was fairly hygroscopic.  $\mu_{\text{eff}}(\text{solid}, 298 \text{ K}) = 2.2 \mu_{\text{B}}$ . Anal. calcd. for  $\text{CuC}_{35}\text{H}_{43}\text{N}_7\text{B}_2\text{F}_8\text{O}_2$ : C, 50.59%; H, 5.22%; N, 11.80%. Found: C, 50.45%; H, 4.92%; N, 11.36%.

{2-[1-(2-imidazol-4-ylethylimino)ethyl],6-[1-(2-pyridin-2-ylethylimino)ethyl]pyridine}copper(II)tetrafluoroborate,  $[\text{Cu}^{\text{II}}(\text{imidH})(\text{py})\text{DAP}](\text{BF}_4)_2$ . The compound was prepared, using  $\text{Cu}(\text{BF}_4)_2 \cdot 6\text{H}_2\text{O}$  instead of  $\text{Zn}(\text{BF}_4)_2 \cdot 6\text{H}_2\text{O}$ , and treated identically to the analogous zinc(II) compound. The recrystallized aquamarine powder gave a  $\mu_{\text{eff}}(\text{solid}, 298 \text{ K}) = 2.0 \mu_{\text{B}}$ .

Anal. calcd. for  $\text{CuC}_{21}\text{H}_{24}\text{N}_6\text{B}_2\text{F}_8$ : C, 42.20%; H, 4.06%; N, 14.06%.

Found: C, 42.36%; H, 4.14%; N, 13.82%.

{2-[1-(2-(N<sub>1</sub>-p-methylbenzyl)imidazol-4-ylethylimino)ethyl], 6-[1-(2-pyridin-2-ylethylimino)ethyl]pyridine}copper(II)tetrafluoroborate·monohydrate,  $[\text{Cu}^{\text{II}}(\text{imidR})(\text{py})\text{DAP}](\text{BF}_4)_2 \cdot \text{H}_2\text{O}$ . The compound was synthesized, using  $\text{Cu}(\text{BF}_4)_2 \cdot 6\text{H}_2\text{O}$  instead of  $\text{Zn}(\text{BF}_4)_2 \cdot 6\text{H}_2\text{O}$ , and treated identically to the analogous zinc(II) complex. Recrystallization of the product produced a blue-green powder.  $\mu_{\text{eff}}(\text{solid}, 298 \text{ K}) = 1.9 \mu_{\text{B}}$ . Anal. calcd. for  $\text{CuC}_{29}\text{H}_{36}\text{N}_6\text{B}_2\text{F}_8\text{O}$ : C, 48.39%; H, 4.76%; N, 11.68%. Found: C, 48.78%; H, 4.82%; N, 11.92%.

{2-[1-(2-(N<sub>1</sub>-p-methylbenzyl)imidazol-4-ylethylimino)ethyl], 6-[1-(2-imidazol-4-ylethylimino)ethyl]pyridine}copper(II)tetrafluoroborate·dihydrate,  $[\text{Cu}^{\text{II}}(\text{imidR})(\text{imidH})\text{DAP}](\text{BF}_4)_2 \cdot 2\text{H}_2\text{O}$ . The compound was prepared, using  $\text{Cu}(\text{BF}_4)_2 \cdot 6\text{H}_2\text{O}$  instead of  $\text{Zn}(\text{BF}_4)_2 \cdot 6\text{H}_2\text{O}$ , and treated identically to the analogous zinc(II) compound. The resulting green solid product was quite hygroscopic.  $\mu_{\text{eff}}(\text{solid}, 298 \text{ K}) = 1.8 \mu_{\text{B}}$ . Anal. calcd. for  $\text{CuC}_{27}\text{H}_{35}\text{N}_7\text{B}_2\text{F}_8\text{O}_2$ : C, 44.62%; H, 4.85%; N, 13.49%. Found: C, 44.03%; H, 4.59%; N, 13.35%.

{Bis-2,6-[1-(2-imidazol-4-ylethylimino)ethyl]pyridine}copper(I)tetrafluoroborate·1.5H<sub>2</sub>O,  $[\text{Cu}^{\text{I}}(\text{imidH})_2\text{DAP}](\text{BF}_4) \cdot 1.5\text{H}_2\text{O}$ . The compound was prepared according to the method of Simmons *et al.*<sup>37</sup> The ligand solution was prepared by dissolving 2,6-diacetylpyridine (1 mmol) and histamine, free base (1 mmol), in degassed methanol (25 ml). This reaction mixture was refluxed for 1 h to yield a yellow solution.

$[\text{Cu}^{\text{I}}(\text{CH}_3\text{CN})_4](\text{BF}_4)$  (1 mmol in 20 ml of degassed  $\text{CH}_3\text{CN}$ ) was syringed into the ligand solution, immediately producing a deep red solution. This solution was evaporated to dryness in vacuo to yield a shiny dark red solid, which was slightly hygroscopic.  $\mu_{\text{eff}}(\text{solid}, 298 \text{ K}) = 0.8 \mu_{\text{B}}$ . Anal. calcd. for  $\text{CuC}_{19}\text{H}_{26}\text{N}_7\text{BF}_4\text{O}_{1.5}$ : C, 43.32%; H, 4.97%; N, 18.61%. Found: C, 43.16%; H, 4.46%; N, 18.66%.

{Bis-2,6-[1-(2-pyridin-2-ylethylimino)ethyl]pyridin}copper(I)tetrafluoroborate·0.5H<sub>2</sub>O,  $[\text{Cu}^{\text{I}}(\text{py})_2\text{DAP}](\text{BF}_4)·0.5\text{H}_2\text{O}$ . The complex was synthesized by the method of Simmons.<sup>34</sup> A ligand solution was prepared by dissolving 1 mmol 2,6-diacetylpyridine in 25 ml MeOH and dropwise adding 2 mmol of 2-(2-aminoethyl)pyridine. This solution was stirred and refluxed for about 1 h, after which it appeared yellow in color. One mmol of  $[\text{Cu}^{\text{I}}(\text{CH}_3\text{CN})_4](\text{BF}_4)$  was added to 20 ml deoxygenated  $\text{CH}_3\text{CN}$ , allowed to dissolve, and then syringed into the ligand solution. The cherry red colored solution was reduced to dryness under vacuum. The resulting solid was recrystallized from hot, dry MeOH, producing a cherry red powder.  $\mu_{\text{eff}}(\text{solid}, 298 \text{ K}) = 0.2 \mu_{\text{B}}$ . Anal. calcd. for  $\text{CuC}_{23}\text{H}_{26}\text{N}_5\text{BF}_4\text{O}_{0.5}$ : C, 52.04%; H, 4.94%; N, 13.19%. Found: C, 52.35%; H, 4.77%; N, 13.26%.

{Bis-2,6-[1-(2-(N<sub>1</sub>-p-methylbenzyl)imidazol-4-ylethylimino)ethyl]-pyridine}copper(I)tetrafluoroborate,  $[\text{Cu}^{\text{I}}(\text{imidR})_2\text{DAP}](\text{BF}_4)$ . A ligand solution was prepared by dissolving 2,6-diacetylpyridine (1 mmol) and [N<sub>1</sub>-(p-methylbenzyl)]histamine, free base (2 mmol), in degassed methanol (25 ml). This reaction mixture was refluxed for 1 h to yield

a yellow solution.  $[\text{Cu}^{\text{I}}(\text{CH}_3\text{CN})_4](\text{BF}_4)$  (1 mmol in 20 ml of degassed  $\text{CH}_3\text{CN}$ ) was syringed into the ligand solution, immediately producing an intense purple solution. This solution was evaporated to dryness in vacuo to yield a bright purple-red solid, which was slightly hygroscopic.  $\mu_{\text{eff}}(\text{solid}, 298 \text{ K}) = 0.8 \mu_{\text{B}}$ . Anal. calcd. for  $\text{CuC}_{35}\text{H}_{39}\text{N}_7\text{BF}_4$ : C, 59.37%; H, 5.55%; N, 13.85%. Found: C, 58.82%; H, 5.67%; N, 14.09%.

{2-[1-(2-imidazol-4-ylethylimino)ethyl],6-[1-(2-pyridin-2-ylethylimino)ethyl]pyridine}copper(I)tetrafluoroborate·monohydrate,  
 $[\text{Cu}^{\text{I}}(\text{imidH})(\text{py})\text{DAP}](\text{BF}_4) \cdot \text{H}_2\text{O}$ . The compound was prepared by controlled potential electrolysis<sup>42</sup> of the analogous copper(II) compound. Typically 0.20 of a gram of the copper(II) complex was electrolyzed under nitrogen gas, in a supporting electrolyte solution 0.01 M  $\text{NaBF}_4$  in acetonitrile, at a potential of -0.55 volts (versus S.C.E.) for 2-3 h. The end point of the electrolysis was noted by little or no current flow. The resulting red solution, containing the desired copper(I) compound, was transferred to a Schlenkline apparatus and the solution reduced to dryness under vacuum. Separation of the copper(I) compound from supporting electrolyte was accomplished using methylene chloride as a solvent for the copper(I) complex. The  $\text{CH}_2\text{Cl}_2$  filtrates were then reduced to dryness in vacuo and yielded an analytically pure, hygroscopic dark red product.  $\mu_{\text{eff}}(\text{solid}, 298 \text{ K}) = 0.5 \mu_{\text{B}}$ . Anal. calcd. for  $\text{CuC}_{21}\text{H}_{26}\text{N}_6\text{BF}_4\text{O}$ : C, 47.69%; H, 4.96%; N, 15.89%. Found: C, 47.43%; H, 4.80%; N, 15.34%.

{2-[1-(2-(N<sub>1</sub>-p-methylbenzyl)imidazol-4-ylethylimino)ethyl],6-[1-(2-pyridin-2-ylethylimino)ethyl]pyridine}copper(I)tetrafluoroborate·trihydrate, [Cu<sup>I</sup>(imidR)(py)DAP](BF<sub>4</sub>)·3H<sub>2</sub>O. The complex was prepared by the controlled potential electrolysis of the corresponding copper(II) compound. Typically 0.1-0.2 g of the copper(II) compound was electrolyzed at a potential of -0.55 volts (S.C.E.) for about 3 h. During this electrochemical synthesis the acetonitrile solution, containing 0.01 M NaBF<sub>4</sub> supporting electrolyte, was stirred under nitrogen gas. The deep red product solution was transferred to Schlenk glassware and evaporated to dryness in vacuo. The solid, containing NaBF<sub>4</sub> and the desired copper(I) product, was extracted with degassed, dry CH<sub>2</sub>Cl<sub>2</sub>, and the filtrate dried in vacuo to yield the dark red copper(I) compound.  $\mu_{\text{eff}}(\text{solid}, 298 \text{ K}) = 0.8 \mu_{\text{B}}$ . Anal. calcd. for CuC<sub>29</sub>H<sub>40</sub>N<sub>6</sub>BF<sub>4</sub>O<sub>3</sub>: C, 52.07%; H, 5.72%; N, 12.56%. Found: C, 51.93%; H, 5.36%; N, 12.18%.

{2-[1-(2-(N<sub>1</sub>-p-methylbenzyl)imidazol-4-ylethylimino)ethyl],6-[1-(2-imidazol-4-ylethylimino)ethyl]pyridine}copper(I)tetrafluoroborate·dihydrate, [Cu<sup>I</sup>(imidR)(imidH)DAP](BF<sub>4</sub>)·2H<sub>2</sub>O. The compound was prepared by controlled potential electrolysis of the analogous copper(II) complex. The details of the synthesis and recovery of the pure copper(I) species were as above for the [Cu<sup>I</sup>(imidH)(py)DAP]<sup>+</sup> and [Cu<sup>I</sup>(imidR)(py)DAP]<sup>+</sup> species. The potential used was -0.575 volts (S.C.E.) and the time of completion for the reaction was approximately 3 h. The final red-purple solid was quite hygroscopic.  $\mu_{\text{eff}}(\text{solid},$

298 K) =  $0.7 \mu_B$ . Anal. calcd. for  $\text{CuC}_{27}\text{H}_{35}\text{N}_7\text{BF}_4\text{O}_2$ : C, 44.62%; H, 4.85%; N, 13.49%. Found: C, 44.05%; H, 4.95%; N, 13.10%.

### Physical and Spectroscopic Measurements

Solid state infrared spectra were recorded as Nujol mulls using NaCl plates and a Beckman IR-4230 spectrophotometer. The copper(II) and zinc(II) samples were prepared in air, while the copper(I) samples were mulled under nitrogen gas. UV-VIS spectra were obtained on a Cary 17 Recording Spectrophotometer, using matched quartz cells of 1 cm path length. The oxygen sensitive copper(I) samples were prepared on an argon gas Schlenk line, using degassed  $\text{CH}_3\text{CN}$  and  $\text{Me}_2\text{SO}$  solvents, and sealed under an argon atmosphere in the quartz cells for study. Proton nmr spectra were recorded at 90 MHz on a Varian EM390 Spectrometer.  $\text{D}_3$ -acetonitrile, obtained from Aldrich Chemical Company, Inc., was used as a solvent for the zinc(II) and copper(I) complexes with tetramethylsilane (TMS) as the internal standard. For  $^1\text{H}$  nmr studies of the hydrochloride salt and free base  $[\text{N}_1-(p\text{-methylbenzyl})]$ -histamine derivatives, either  $\text{D}_2\text{O}$  or  $\text{CDCl}_3$  were used as solvents.

Warburg manometry was employed to measure dioxygen uptake by the copper(I) complexes in solution at  $23^\circ\text{C}$ .<sup>43,44</sup> The Warburg manometers were procured from Precision Scientific (model #66662). The manometer flask volumes were determined with mercury. In order to study  $3\text{--}5 \times 10^{-3} \text{ M}$  solutions, 30-40 mg of the copper(I) solid was carefully weighed into the side arm of the manometer flask and exactly 3 ml of degassed, distilled  $\text{Me}_2\text{SO}$  was syringed into the flask bottom. After a constant temperature equilibration under flowing dry nitrogen gas, the

manometer was flushed with dry dioxygen for 1 min, adjusted to atmospheric pressure, and the manometer was tilted so as to dissolve the red copper(I) solid in the  $\text{Me}_2\text{SO}$  solvent. Complete dioxygen uptake required about 15 min. A  $\text{Me}_2\text{SO}$  solvent blank was treated exactly as stated above and its dioxygen uptake volume subtracted from the uptake volumes of the copper(I) sample solutions. A complete description of the Warburg manometry techniques and apparatus was recorded in Appendix I of M. G. Simmons's Ph.D. dissertation.<sup>34</sup>

X-band EPR spectra were recorded at 100 K on a Varian E-line spectrometer. The magnetic field positions were referenced relative to diphenylpicrylhydrazyl (dpph) and the detectable ( $S=1/2$ ) copper(II) was measured quantitatively employing  $\text{Cu}(\text{SO}_4)$  of known concentration as the calibrant. The cycling procedure between deoxy/oxy/redeoxy states of the dioxygen-active copper(I) complexes involved the cycling of the parent  $\text{Me}_2\text{SO}$  solution and taking of aliquots from this solution at each phase of the experiment. These aliquots were syringed into EPR tubes and frozen at liquid nitrogen temperature (77 K) until the EPR spectra were recorded.

Magnetic susceptibilities of the solids were measured by the Faraday technique using a Cahn model 6600-1 research magnetic susceptibility system and  $\text{Hg}[\text{Co}(\text{NCS})_4]$  as the calibrant.<sup>45</sup> All measurements were recorded at room temperature under 1 atmosphere helium. Corrections for ligand and anion diamagnetism in all the copper complexes were made using the molar susceptibilities measured for the corresponding zinc(II) complexes:



|  |  |
|--|--|
| $[\text{Zn}(\text{imidH})_2\text{DAP}](\text{BF}_4)_2$ :             | $\chi_M^I = -2.980 \times 10^{-4} \text{ cgsu mol}^{-1}$ |
| $[\text{Zn}(\text{py})_2\text{DAP}](\text{BF}_4)_2$ :                | $\chi_M^I = -1.702 \times 10^{-4} \text{ cgsu mol}^{-1}$ |
| $[\text{Zn}(\text{imidR})_2\text{DAP}](\text{BF}_4)_2$ :             | $\chi_M^I = -1.084 \times 10^{-3} \text{ cgsu mol}^{-1}$ |
| $[\text{Zn}(\text{imidH})(\text{py})\text{DAP}](\text{BF}_4)_2$ :    | $\chi_M^I = -3.539 \times 10^{-4} \text{ cgsu mol}^{-1}$ |
| $[\text{Zn}(\text{imidR})(\text{py})\text{DAP}](\text{BF}_4)_2$ :    | $\chi_M^I = -5.386 \times 10^{-4} \text{ cgsu mol}^{-1}$ |
| $[\text{Zn}(\text{imidR})(\text{imidH})\text{DAP}](\text{BF}_4)_2$ : | $\chi_M^I = -1.355 \times 10^{-4} \text{ cgsu mol}^{-1}$ |

The solution state magnetochemical studies were also performed on the Cahn 6600-1 Faraday balance.<sup>46</sup> Using a quartz boat with a gas-tight cap,<sup>47</sup> samples were sealed under controlled gaseous environment to avoid contamination of the solution by the intrusion of moist air. The cryogenic apparatus consisted of an Air Products Interface model DMX-19 vacuum shroud, an LT-3-110 B Heli-tran system, and an APD-TL digital temperature readout monitoring an iron-doped gold versus chromel thermocouple. The deoxy- $[\text{Cu}^{\text{I}}(\text{imidH})_2\text{DAP}](\text{BF}_4)$  samples were dissolved in purified, degassed  $\text{Me}_2\text{SO}$  and sealed for study under an argon atmosphere. The oxy- $[\text{Cu}(\text{imidH})_2\text{DAP}]$  samples were prepared in  $\text{Me}_2\text{SO}$ , degassed with argon, oxygenated with dry dioxygen, placed in a quartz boat, and sealed under dioxygen. All the samples were slowly cooled to liquid nitrogen temperature so as to freeze without "cracking" the solvent glass. Solutions of  $[\text{Zn}^{\text{II}}(\text{imidH})_2\text{DAP}](\text{BF}_4)_2$  in  $\text{Me}_2\text{SO}$  were studied under argon and dioxygen gases and used as blanks for the diamagnetic correction factors. The full temperature (80-250 K) magnetochemical data were reported as a "difference" ( $\chi_M$  vs.  $T^{-1}$ ) plot depicting the "net" magnetic behavior of the oxygenated  $[\text{Cu}(\text{imidH})_2\text{DAP}]$  species in frozen  $\text{Me}_2\text{SO}$  solution.

Cyclic voltammetric measurements were recorded in  $\text{CH}_3\text{CN}$  under a constant flow of dry nitrogen or dioxygen gas using a PAR model 174 polarographic analyzer. Electrolyses were carried out using a PAR polarographic model K62 cell. A three-electrode geometry with platinum buttons as the working and counter electrodes and a Fisher Scientific saturated calomel electrode (S.C.E.) as the reference electrode was employed. The reference electrode was separated from the bulk solution by a fritted-glass bridge containing supporting electrolyte solution, preventing aqueous contamination of the cell solution. Current-voltage curves were recorded on a Houston Instruments Omnigraphic 2000 X-Y recorder at scan rates of 200 and 500 mV/s. Differential pulse polarograms were obtained at a scan rate of 10 mV/s and a 0.5 s drop time. For the cyclic voltammetric and controlled potential electrolytic experiments, the copper(II) samples were dissolved in distilled, dry  $\text{CH}_3\text{CN}$  and were  $10^{-3}$  M in copper(II), with 0.1 M in tetrabutylammonium perchlorate, supporting electrolyte. Controlled potential electrolytic syntheses were performed in a glass cell equipped with adapters for interfacing the cell with Schlenk line apparatus. A platinum gauze electrode served as the working electrode with a platinum wire and saturated calomel electrode being the counter and reference electrodes, respectively. The bulk solution was stirred with bubbling solvent-saturated nitrogen gas during the electrolysis. Electronic integration of the current vs. time curves was achieved by a PAR model 179 coulometer and displayed as coulombs vs. time by an Omniscribe strip chart recorder. All redox potentials were reported versus S.C.E. and were uncorrected for junction potentials.

Resonance Raman spectra, obtained using visible wavelengths for excitation, were recorded on a computerized Jarrell-Ash 25-300 Raman spectrophotometer as previously described.<sup>48</sup> The 457.9 nm and 514.5 nm wavelengths for excitation were provided by a Coherent Radiation (CR) model 52MG Ar<sup>+</sup>/Kr<sup>+</sup> laser. Plasma lines were eliminated by spike filters. An ITT FW-130 (S-20) photomultiplier served as the scattered light detector and the output was processed in an ORTEC model 9302 Amplified/Discriminator. Standard melting point capillaries containing about 10  $\mu$ l of sample were inserted into a copper rod cold finger immersed in liquid nitrogen and irradiated in 180° backscattering geometry.<sup>49</sup> Laser power at the sample ranged from 10-50 mW, depending on the sample concentrations of 0.01-0.1 M.

Resonance Raman spectra, obtained using ultraviolet wavelengths for excitation, were recorded using a SPEX Ramlog EU spectrometer with a cooled RCA C31034A photomultiplier and an ORTEC 9300 series photon counting system. Laser excitation at 413.1 nm and 406.7 nm was provided by a Spectra-Physics 171-01 krypton laser, and at 363.8 nm by a S-P171-18 argon laser. Samples for room temperature RR study were contained in a spinning cell employing the Shriver design.<sup>50</sup> The low temperature experiments were conducted on frozen solution samples cooled in a liquid nitrogen dewar, designed by Loehr.<sup>49</sup> Raman scattering was observed in a 135° backscattering geometry in a plane perpendicular to the polarization of the laser beam. The following spectral acquisition conditions were the same for all samples and all excitation lines:

scan speed,  $0.5\text{ cm}^{-1}/\text{s}$  (except for oxygenated- $[\text{Cu}(\text{imidH})_2\text{DAP}](\text{BF}_4)$ ,  $0.2\text{ cm}^{-1}/\text{s}$ ); laser power at the sample, between 100 and 190 mW.

## RESULTS AND DISCUSSION

### Synthesis and Characterization of the Complexes

The reactions involved in the synthesis of the  $[\text{Cu}^{\text{I}}(\text{imidR})_2\text{DAP}](\text{BF}_4)$  complex are depicted in Figure 5. In the first step, a Schiff Base condensation of 2,6-diacetylpyridine and R-substituted histamine, free base, occurs under argon atmosphere as the methanolic solution is refluxed. The  $[\text{Cu}^{\text{I}}(\text{CH}_3\text{CN})_4](\text{BF}_4)$  is added to the pale yellow ligand solution and a bright purple-red solution results, from which the  $[\text{Cu}^{\text{I}}(\text{imidR})_2\text{DAP}](\text{BF}_4)$  compound is isolated as a deep purple-red solid. In order to prepare the ligand, the synthesis of the free base R-substituted histamine must be performed. In this procedure, the hydrochloride salt of histamine is reacted with  $\alpha\text{-Cl-p-xylene}$  in a  $\text{NH}_3(1)^-$  sodium metal solution to add an  $\text{R} = \text{-p-methylbenzyl}$  functionality to the  $\text{N}_7$  nitrogen atom of the imidazolate anion of the histamine. The  $^1\text{H}$  n.m.r. spectra for the R-substituted histamine hydrochloride salt and free base species provide proof of structure and indication of purity for the new histamine derivatives. Figures 6-8 show comparative  $^1\text{H}$  n.m.r. spectra for the parent histamine and the hydrochloride salt and free base R-substituted histamine compounds; spectral assignments are documented in Table 1.

While the analytically pure copper(I) species A, C, and D are prepared by the direct chemical synthetic scheme shown in Figure 5, the hybrid Cu(I) compounds B, E, and F are best prepared by the electrochemical reduction of their Cu(II) analogs under nitrogen or argon atmosphere.<sup>51</sup> In addition to the three hybrid Cu(I) complexes,

The Synthetic Scheme for {Bis-2,6[1-(2-(N<sub>1</sub>-p-methylbenzyl)-  
imidazol-4-ylethyl]pyridine}copper(I)tetrafluoroborate

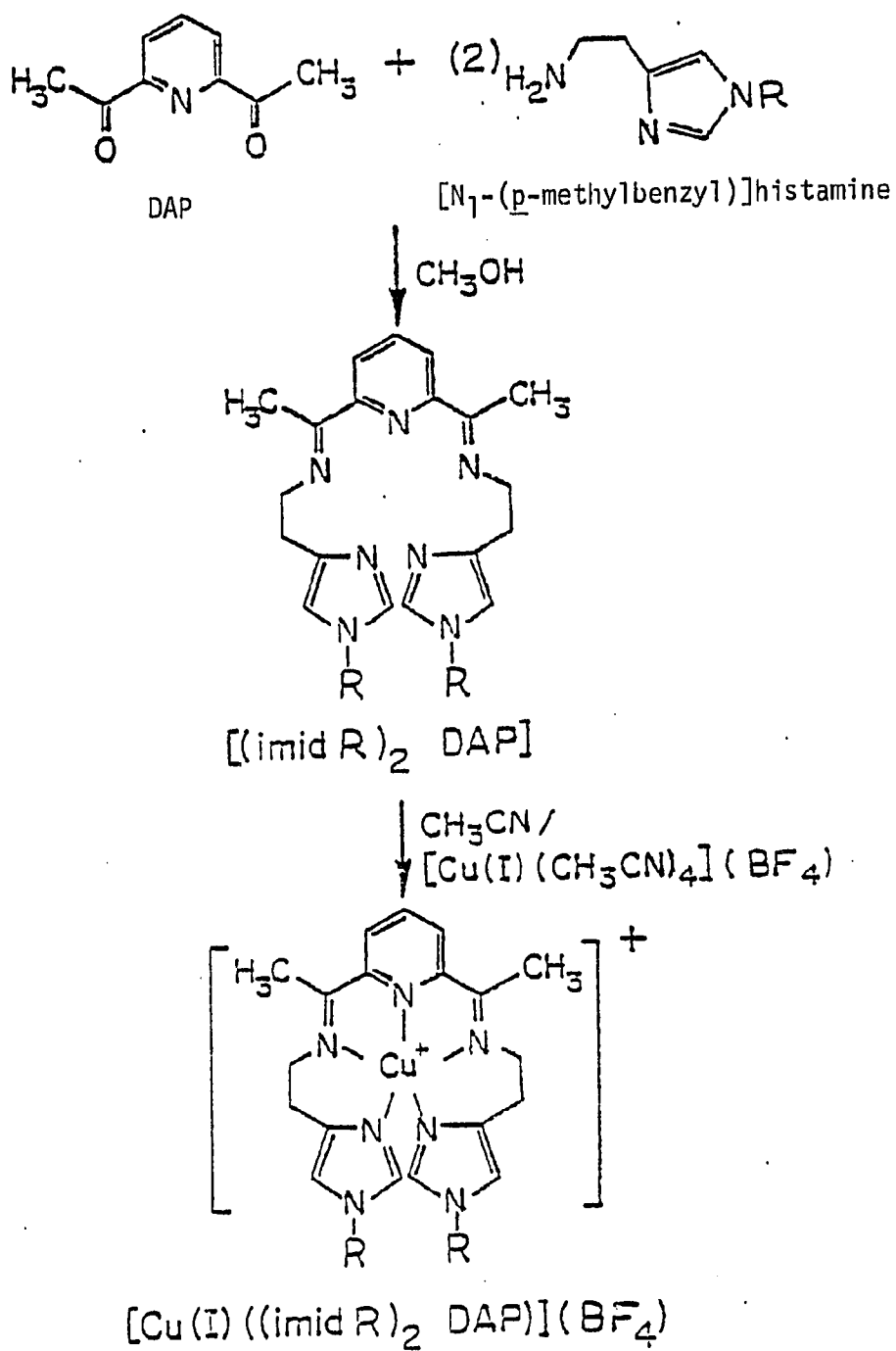


Figure 6

$^1\text{H}$  N.M.R. Spectrum for Free Base Histamine  
in  $\text{DCCl}_3$  Relative to Internal TMS

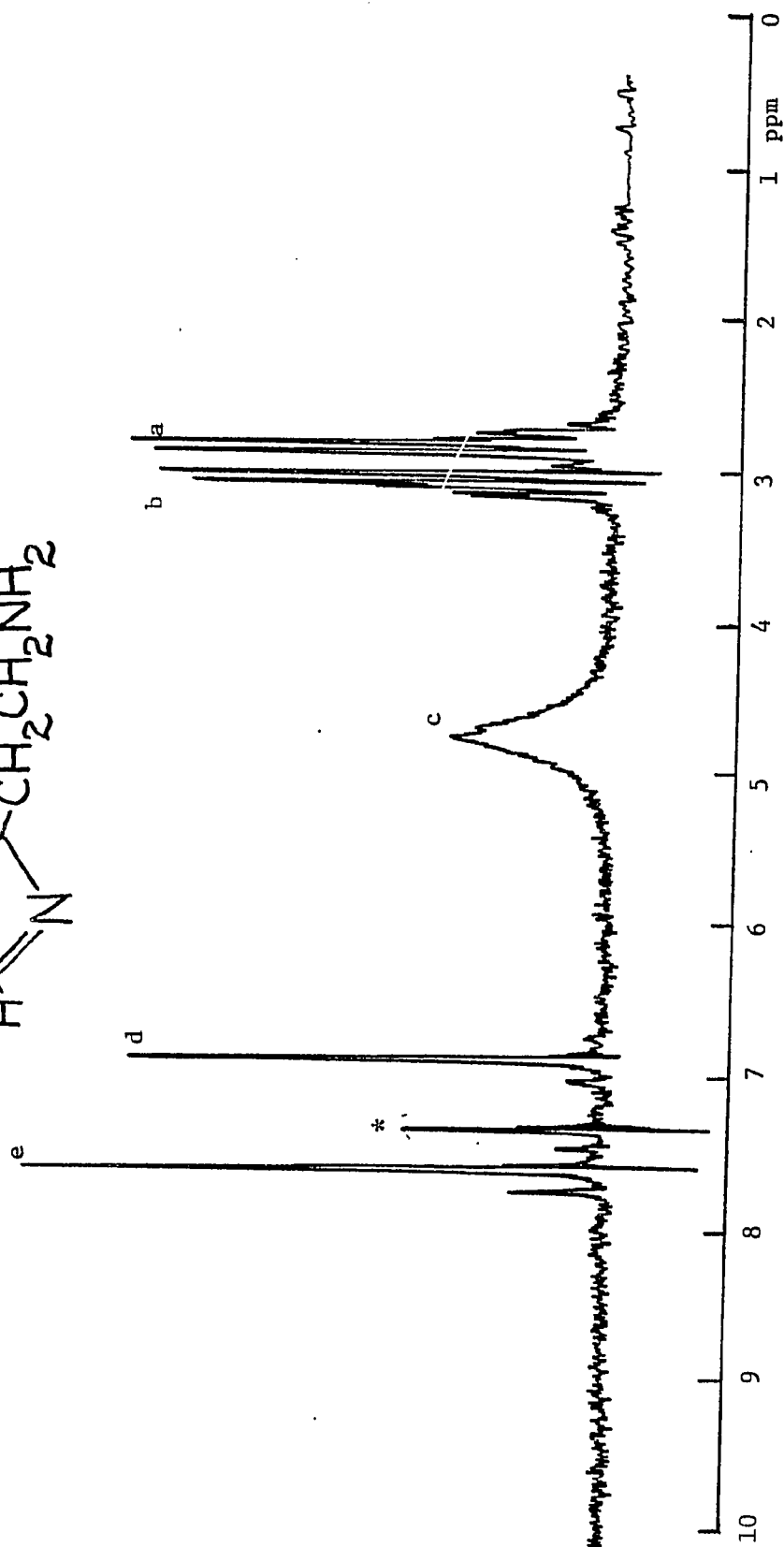
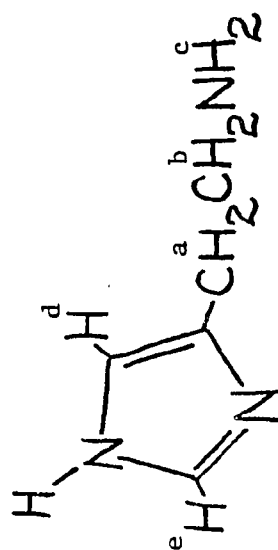




Figure 7

$^1\text{H}$  N.M.R. Spectrum for R-substituted  
Histamine Hydrochloride in  $\text{D}_2\text{O}$  Relative to TMS

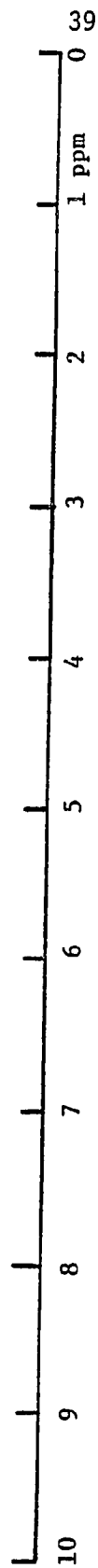
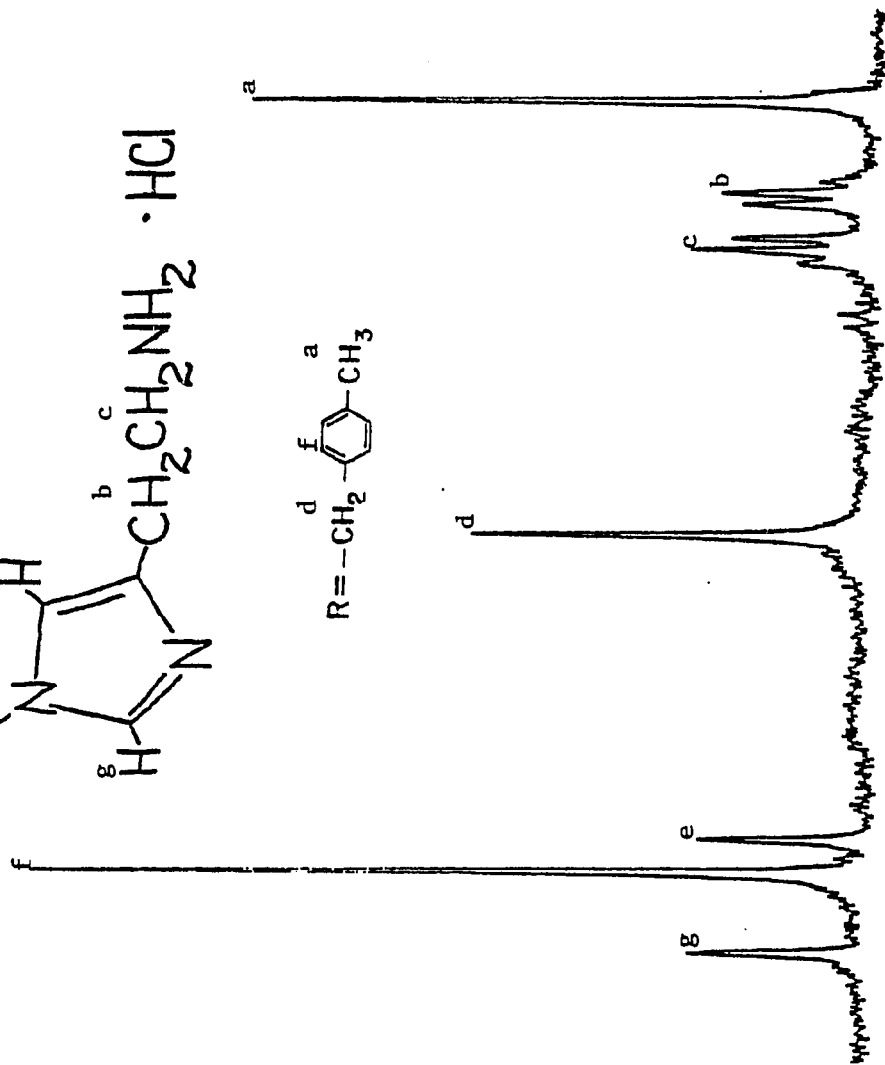
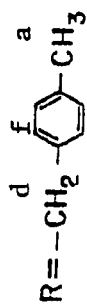
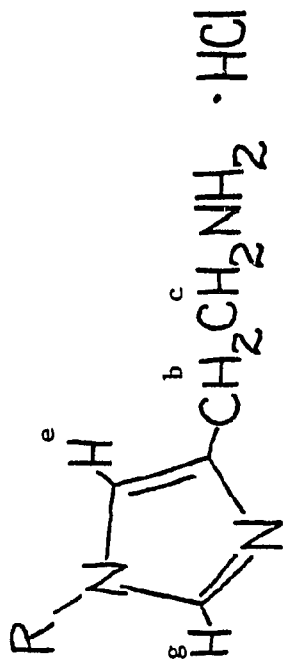


Figure 8

$^1\text{H}$  N.M.R. Spectrum for Free Base R-substituted  
Histamine in  $\text{DCCl}_3$  Relative to Internal TMS

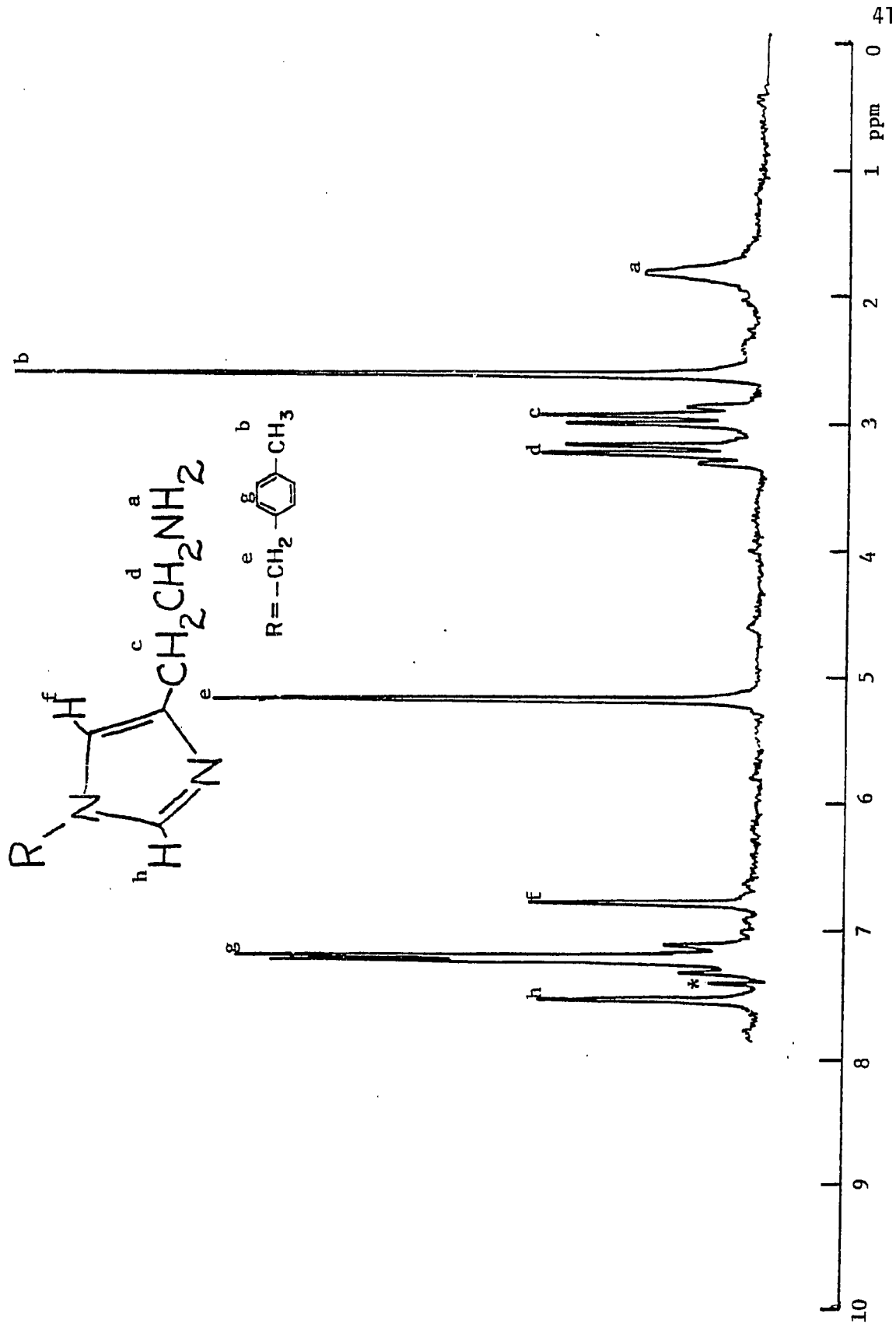


Table 1

<sup>1</sup>H N.M.R. Spectral Data for Various Histamine Compounds

| Compound  | Solvent           | Proton Assignment <sup>a)</sup> | Chemical Shift, p.p.m. <sup>b)</sup> |
|---|-------------------|---------------------------------|--------------------------------------|
| Histamine, free base                                    | DCCl <sub>3</sub> | a                               | 2.80 (multiplet)                     |
|   |                   | b                               | 3.00 (m)                             |
|   |                   | c                               | 4.70 (broad singlet)                 |
|   |                   | d                               | 6.82 (s)                             |
|   |                   | e                               | 7.54 (s)                             |
| [N <sub>1</sub> -(p-methylbenzyl)]-histamine·HCl        | D <sub>2</sub> O  | a                               | 2.20 (s)                             |
|   |                   | b                               | 2.78 (triplet)                       |
|   |                   | c                               | 3.15 (t)                             |
|   |                   | d                               | 4.85 (s)                             |
|   |                   | e                               | 6.83 (s)                             |
|   |                   | f                               | 7.05 (s)                             |
|   |                   | g                               | 7.55 (s)                             |
| [N <sub>1</sub> -(p-methylbenzyl)]-histamine, free base | DCCl <sub>3</sub> | a                               | 1.78 (broad s)                       |
|   |                   | b                               | 2.60 (s)                             |
|   |                   | c                               | 2.87 (t)                             |
|   |                   | d                               | 3.15 (t)                             |
|   |                   | e                               | 5.15 (s)                             |
|   |                   | f                               | 6.80 (s)                             |
|   |                   | g                               | 7.12 (m)                             |
|   |                   | h                               | 7.55 (s)                             |

a) Refers to Figures 6-8.

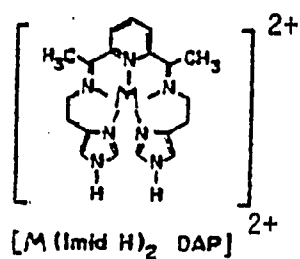
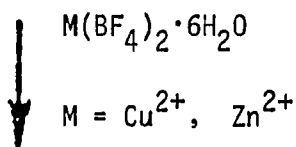
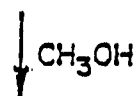
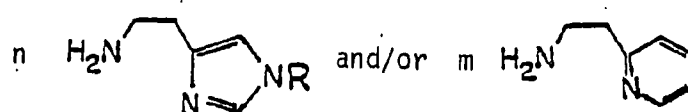
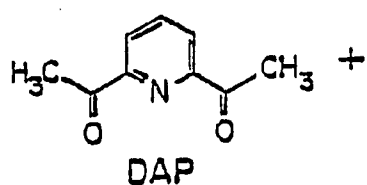
b) Relative to internal TMS for DCCl<sub>3</sub> and for D<sub>2</sub>O solutions.

the other Cu(I) species A, C, and D are successfully prepared by electrochemical synthetic techniques as a "check" on the validity of this preparative procedure. The analogous Zn(II) and Cu(II) compounds are also prepared by the standard Schiff Base condensation reaction and subsequent addition of  $\text{Zn}(\text{BF}_4)_2 \cdot 6\text{H}_2\text{O}$ , or  $\text{Cu}(\text{BF}_4)_2 \cdot 6\text{H}_2\text{O}$ , to the ligand solution. Figure 9 represents the total synthetic scheme for the twelve Zn(II) and Cu(II) complexes examined in this work.

Evidence for the success of the Schiff Base condensation reaction between 2,6-diacetylpyridine and the various free base amine moieties is indicated in the infrared spectroscopic data presented in Table 2. The C=N stretching frequency for the newly formed imine linkage is depicted in the  $1580\text{--}1600\text{ cm}^{-1}$  region of the IR spectrum.<sup>52</sup> Clearly the infrared spectra of all the copper and zinc compounds exhibit this characteristic absorption peak. Also the hybrid complexes,  $[\text{M}(\text{imidH})(\text{py})\text{DAP}]^{n+}$  and  $[\text{M}(\text{imidR})(\text{py})\text{DAP}]^{n+}$ , possess two distinct imine stretching frequencies, one in the  $1580\text{ cm}^{-1}$  range found for the  $[\text{M}(\text{imidH})_2\text{DAP}]^{n+}$  and  $[\text{M}(\text{imidR})_2\text{DAP}]^{n+}$  species and one in the  $1600\text{ cm}^{-1}$  region for the  $[\text{M}(\text{py})_2\text{DAP}]^{n+}$  complex. Another region of interest in the IR spectrum is the  $3300\text{--}3600\text{ cm}^{-1}$  range. For the compounds possessing the (imidH) moiety, the N-H stretching vibrational frequency is observed around  $3320\text{ cm}^{-1}$ , yet the complexes containing the (imidR) group, i.e., no N-H linkage, are devoid of absorption at  $3300\text{ cm}^{-1}$ . In general, the complexes which are hygroscopic in behavior (as evidenced by the hydrated water included in their elemental analysis data), exhibit an O-H stretch at ca.  $3620\text{ cm}^{-1}$ . The B-F stretching frequency is found to

Figure 9

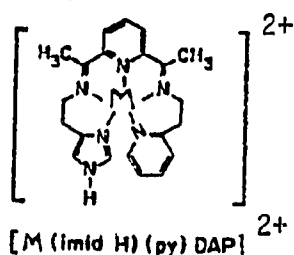
Synthetic Scheme for the Copper(II) and Zinc(II)  
Tetrafluoroborate Complexes



(A)

$$n = 2, R = H$$

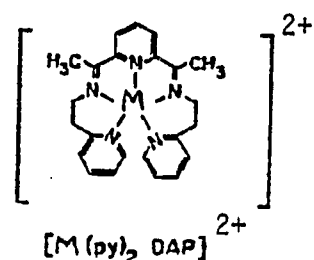
$$m = 0$$



(B)

$$n = 1, R = H$$

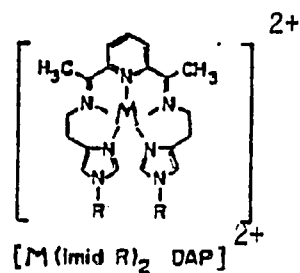
$$m = 1$$



(C)

$$n = 0, R = N.A.$$

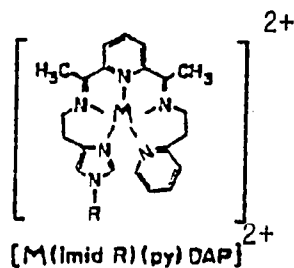
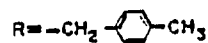
$$m = 2$$



(D)

$$n = 2$$

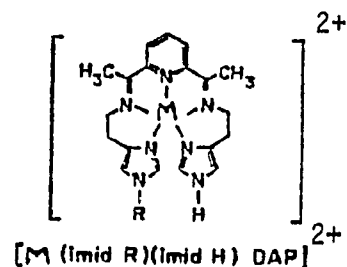
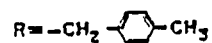
$$m = 0$$



(E)

$$n = 1$$

$$m = 1$$



(F)

$$n = 2$$

$$m = 0$$

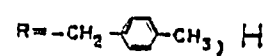




Table 2

Infrared Spectral Data for the Zinc(II), Copper(II),  
and Copper(I) Tetrafluoroborate Complexes as Solid State Nujol Mulls<sup>a)</sup>

| Complex   | Lattice                            |                           |                           | Anion <sup>b)</sup>                             |
|---|------------------------------------|---------------------------|---------------------------|---|
|   | H <sub>2</sub> O, cm <sup>-1</sup> | N-H(st), cm <sup>-1</sup> | C=N(st), cm <sup>-1</sup> | BF <sub>4</sub> <sup>-</sup> , cm <sup>-1</sup> |
| [Zn <sup>II</sup> (imidH)(py)DAP] <sup>2+</sup>           | 3620(m)                            | 3350(s)                   | 1610(s)<br>1590(s)        | 1070(s)   |
| [Cu <sup>II</sup> (imidH)(py)DAP] <sup>2+</sup>           |                                    | 3320(s)                   | 1610(s)<br>1590(s)        | 1080(s)   |
| [Cu <sup>I</sup> (imidH)(py)DAP] <sup>+</sup>             | 3610(m)                            | 3320(s)                   | 1595(s)<br>1580(s)        | 1070(s)   |
| [Zn <sup>II</sup> (imidR) <sub>2</sub> DAP] <sup>2+</sup> |                                    |                           | 1585(s)                   | 1050(s)   |
| [Cu <sup>II</sup> (imidR) <sub>2</sub> DAP] <sup>2+</sup> |                                    |                           | 1585(s)                   | 1040(s)   |
| [Cu <sup>I</sup> (imidR) <sub>2</sub> DAP] <sup>+</sup>   |                                    |                           | 1580(s)                   | 1050(s)   |
| [Zn <sup>II</sup> (imidR)(py)DAP] <sup>2+</sup>           | 3610(m)                            |                           | 1610(s)<br>1580(s)        | 1055(s)   |
| [Cu <sup>II</sup> (imidR)(py)DAP] <sup>2+</sup>           | 3620(w)                            |                           | 1605(s)<br>1585(s)        | 1055(s)   |
| [Cu <sup>I</sup> (imidR)(py)DAP] <sup>+</sup>             | 3620(m)                            |                           | 1600(s)<br>1580(s)        | 1055(s)   |
| [Zn <sup>II</sup> (imidR)(imidH)DAP] <sup>2+</sup>        | 3600(m)                            | 3320(s)                   | 1580(s)                   | 1050(s)   |
| [Cu <sup>II</sup> (imidR)(imidH)DAP] <sup>2+</sup>        | 3620(m)                            | 3315(s)                   | 1585(s)                   | 1040(s)   |
| [Cu <sup>I</sup> (imidR)(imidH)DAP] <sup>+</sup>          | 3610(m)                            | 3320(s)                   | 1580(s)                   | 1050(s)   |

a) s = strong; m = medium; w = weak intensity.

b) Center of broad (ca. 200 cm<sup>-1</sup>) absorption envelope.

be quite broad, centering around  $1050\text{ cm}^{-1}$ , and is typical of compounds having  $\text{BF}_4^-$  counterions.<sup>52</sup>

The  $^1\text{H}$  n.m.r. spectra for the  $[\text{Zn}^{\text{II}}(\text{imidH})(\text{py})\text{DAP}]^{2+}$ ,  $[\text{Zn}^{\text{II}}(\text{imidR})_2\text{DAP}]^{2+}$ ,  $[\text{Zn}^{\text{II}}(\text{imidR})(\text{py})\text{DAP}]^{2+}$ , and  $[\text{Zn}^{\text{II}}(\text{imidR})(\text{imidH})\text{DAP}]^{2+}$  species in  $\text{CD}_3\text{CN}$  are presented in Figures 10-13, with the proton resonance assignments and signal positions documented in Table 3. As in the cases of the  $[\text{Zn}^{\text{II}}(\text{imidH})_2\text{DAP}]^{2+}$  and  $[\text{Zn}^{\text{II}}(\text{py})_2\text{DAP}]^{2+}$  cations studied previously,<sup>37</sup> there is no additional multiplicity of signals, which would indicate the presence of uncoordinated ligand arms. Thus, these spectra support the proposal that all of these complexes exist as five coordinate species in solution, as is the case in the solid state for  $[\text{Zn}^{\text{II}}(\text{imidH})_2\text{DAP}]^{2+}$ .<sup>53</sup> The  $^1\text{H}$  n.m.r. spectra for the three hybrid Zn(II) compounds essentially represent the overlaying of the appropriate "bis" species' spectra and no significant changes in chemical shift are noted. In the Zn(II) compounds containing the  $\text{R} = \text{-p-methylbenzyl}$  group, the phenyl ring is a sharp singlet, a change from the multiplet observed in the  $^1\text{H}$  n.m.r. spectrum of the free base R-substituted histamine. This evidence serves as a marker for the successful incorporation into the ligand of the R-substituted histamine moiety. Attempts to prepare thoroughly deoxygenated, purely diamagnetic Cu(I) complex solutions for  $^1\text{H}$  n.m.r. study result only in spectra having severely broadened absorption peaks. Since these Cu(I) species are very oxygen-sensitive, even slight contamination of the solutions apparently causes the production of some paramagnetic Cu(II) materials, which produce the broadened spectra.<sup>25</sup> Thus,  $^1\text{H}$  n.m.r. spectra are not

Figure 10

$^1\text{H}$  N.M.R. Spectrum and Assignments for  
 $[\text{Zn}(\text{imidH})(\text{py})\text{DAP}]^{2+}$

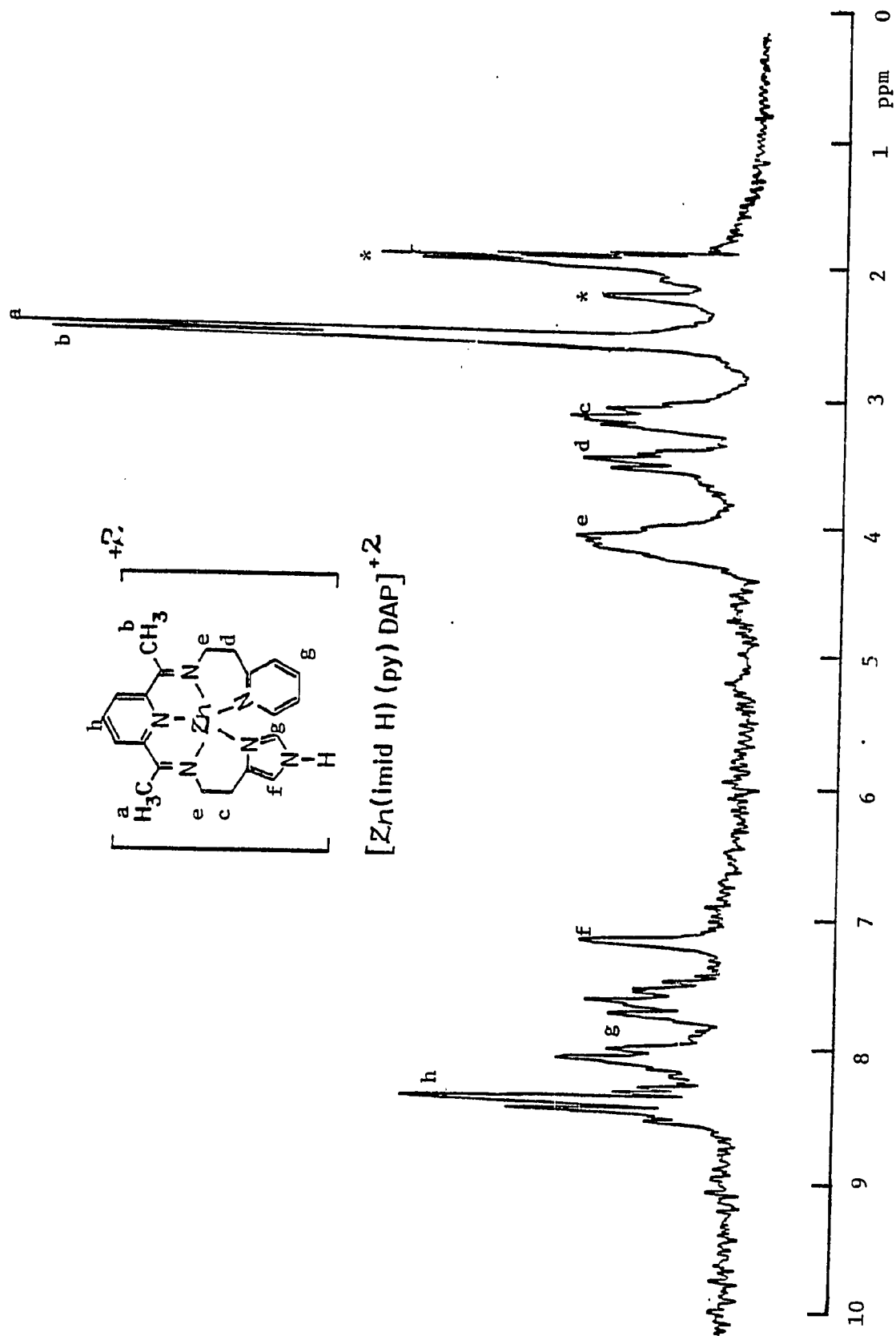


Figure 11

<sup>1</sup>H N.M.R. Spectrum and Assignments for  

---

[Zn(imidR)<sub>2</sub>DAP]<sup>2+</sup>

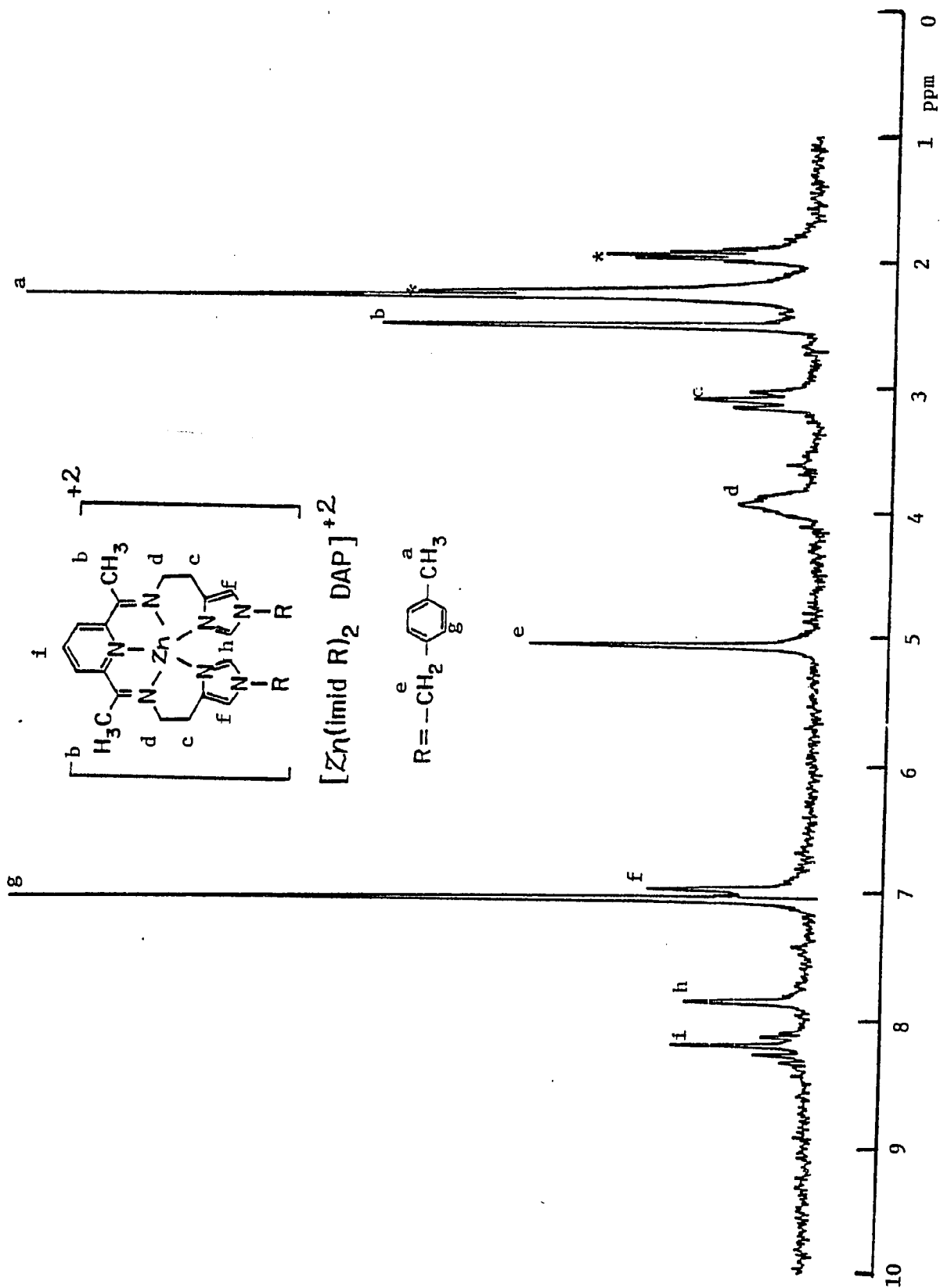


Figure 12

$^1\text{H}$  N.M.R. Spectrum and Assignments for  
 $[\text{Zn}(\text{imidR})(\text{py})\text{DAP}]^{2+}$

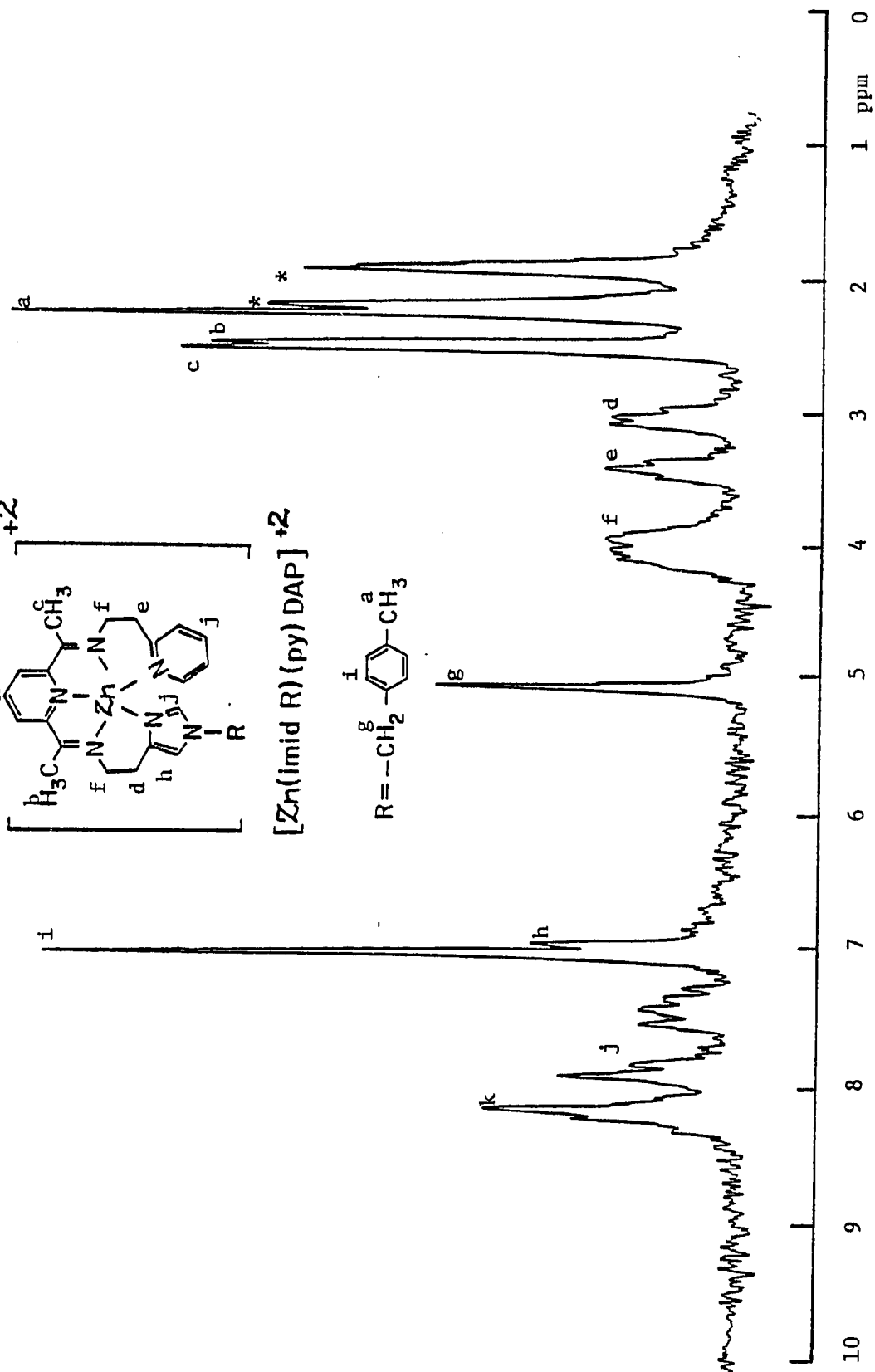
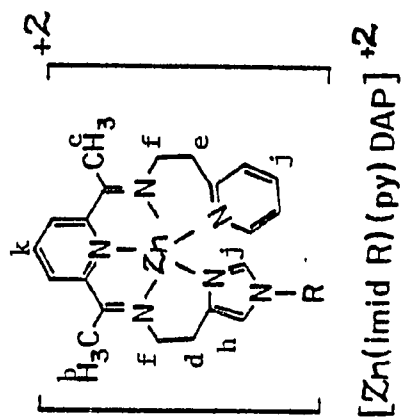




Figure 13

$^1\text{H}$  N.M.R. Spectrum and Assignments for  
 $[\text{Zn}(\text{imidR})(\text{imidH})\text{DAP}]^{2+}$

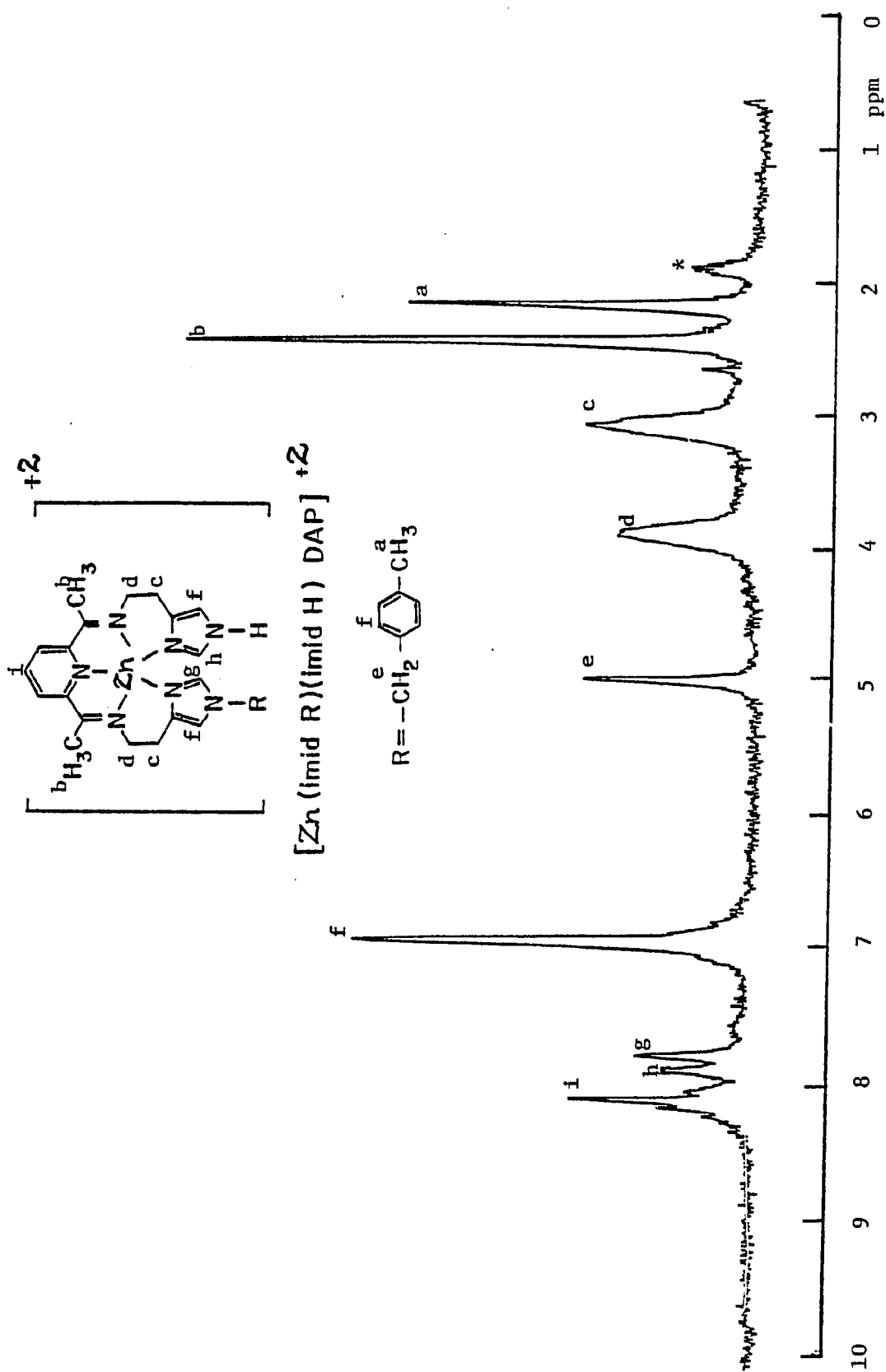


Table 3

<sup>1</sup>H N.M.R. Spectral Data for the Zinc(II) Complexes as  
Tetrafluoroborate Salts in CD<sub>3</sub>DN at Room Temperature Relative to TMS

| Complex   | Proton<br>Assignment <sup>a)</sup> | Chemical<br>Shift, p.p.m. |
|---|------------------------------------|---------------------------|
| [Zn <sup>II</sup> (imidH)(py)DAP] <sup>2+</sup>           | a                                  | 2.50 (singlet)            |
|   | b                                  | 2.61 (s)                  |
|   | c                                  | 3.10 (triplet)            |
|   | d                                  | 3.44 (t)                  |
|   | e                                  | 4.08 (multiplet)          |
|   | f                                  | 6.98 (s)                  |
|   | g                                  | 7.3-8.0 (m)               |
|   | h                                  | 8.25 (m)                  |
| [Zn <sup>II</sup> (imidR) <sub>2</sub> DAP] <sup>2+</sup> | a                                  | 2.30 (s)                  |
|   | b                                  | 2.55 (s)                  |
|   | c                                  | 3.16 (t)                  |
|   | d                                  | 3.94 (t)                  |
|   | e                                  | 5.04 (s)                  |
|   | f                                  | 6.95 (s)                  |
|   | g                                  | 7.02 (s)                  |
|   | h                                  | 7.85 (s)                  |
|   | i                                  | 8.23 (m)                  |

(Table 3 Continued)

(Table 3 Continued)

| Complex  | Proton<br>Assignment <sup>a)</sup> | Chemical<br>Shift, p.p.m. |
|--|------------------------------------|---------------------------|
| $[\text{Zn}^{\text{II}}(\text{imidR})(\text{py})\text{DAP}]^{2+}$    | a                                  | 2.28 (s)                  |
|  | b                                  | 2.50 (s)                  |
|  | c                                  | 2.56 (s)                  |
|  | d                                  | 3.07 (t)                  |
|  | e                                  | 3.43 (t)                  |
|  | f                                  | 4.13 (m)                  |
|  | g                                  | 5.16 (s)                  |
|  | h                                  | 7.10 (s)                  |
|  | i                                  | 7.15 (s)                  |
|  | j                                  | 7.5-8.1 (m)               |
|  | k                                  | 8.25 (m)                  |
| $[\text{Zn}^{\text{II}}(\text{imidR})(\text{imidH})\text{DAP}]^{2+}$ | a                                  | 2.21 (s)                  |
|  | b                                  | 2.48 (s)                  |
|  | c                                  | 3.08 (t)                  |
|  | d                                  | 3.85 (t)                  |
|  | e                                  | 5.04 (s)                  |
|  | f                                  | 7.08 (broad s)            |
|  | g                                  | 7.87 (s)                  |
|  | h                                  | 8.02 (s)                  |
|  | i                                  | 8.25 (m)                  |

a) Refers to Figures 10-13.

obtained for any of the Cu(I) complexes, except for the  $[\text{Cu}^{\text{I}}(\text{py})_2\text{DAP}]^+$  cation which was reported earlier.<sup>37</sup>

While the Zn(II) complexes have been studied by  $^1\text{H}$  n.m.r. spectroscopy to substantiate their solution state structure, the analogous Cu(II) species have been examined by UV-VIS spectroscopy to determine the electronic structure of these compounds. The UV-VIS spectra, Figures 14-17, and the spectral parameters, Table 4, obtained indicate that the  $d^9$  Cu(II) species exhibit at least two d-d transitions in the range of 670-800 nm. The molar extinction coefficients for these compounds are typical for Cu(II) coordination complexes.<sup>54</sup> Using the Schlenk line apparatus and gas tight seals for the quartz sample cells, the deoxygenated Cu(I) samples have also been prepared in an argon atmosphere and their UV-VIS electronic spectra recorded as shown in Figures 18-21; the final results are tabulated in Table 4. In the absence of dioxygen, these Cu(I) species exhibit electronic spectra having charge transfer bands (presumably metal $\rightarrow$ ligand) around 480-520 nm, as well as more intense charge transfer bands in the 290-340 nm region.<sup>54</sup>

#### Reactivity of the Copper(I) Complexes with Dioxygen

It is the oxygenation of the oxygen-active Cu(I) complexes that is so vividly evidenced in the accompanying electronic spectral changes. While the red  $[\text{Cu}^{\text{I}}(\text{imidR})(\text{py})\text{DAP}]^+$  species does not undergo a color change in the presence of dioxygen, the red or purple-red solutions of the  $[\text{Cu}^{\text{I}}(\text{imidH})(\text{py})\text{DAP}]^+$ ,  $[\text{Cu}^{\text{I}}(\text{imidR})_2\text{DAP}]^+$ , and  $[\text{Cu}^{\text{I}}(\text{imidR})(\text{imidH})\text{DAP}]^+$  cations turn green upon bubbling the deoxy solutions with dry dioxygen.

Figure 14

Electronic Absorption Spectrum of  $[\text{Cu}(\text{imidH})(\text{py})\text{DAP}]^{2+}$

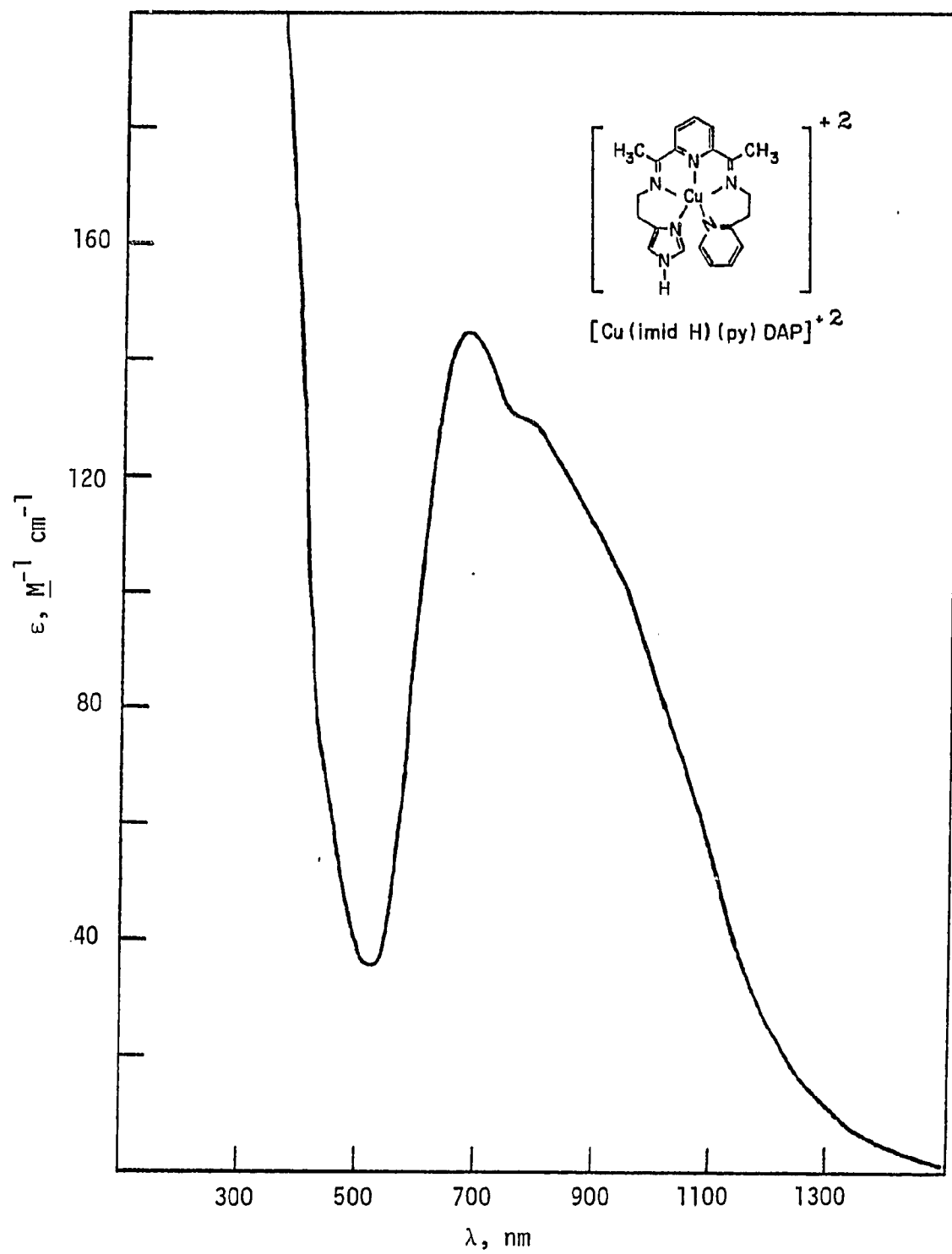


Figure 15

Electronic Absorption Spectrum of  $[\text{Cu}(\text{imidR})_2\text{DAP}]^{2+}$



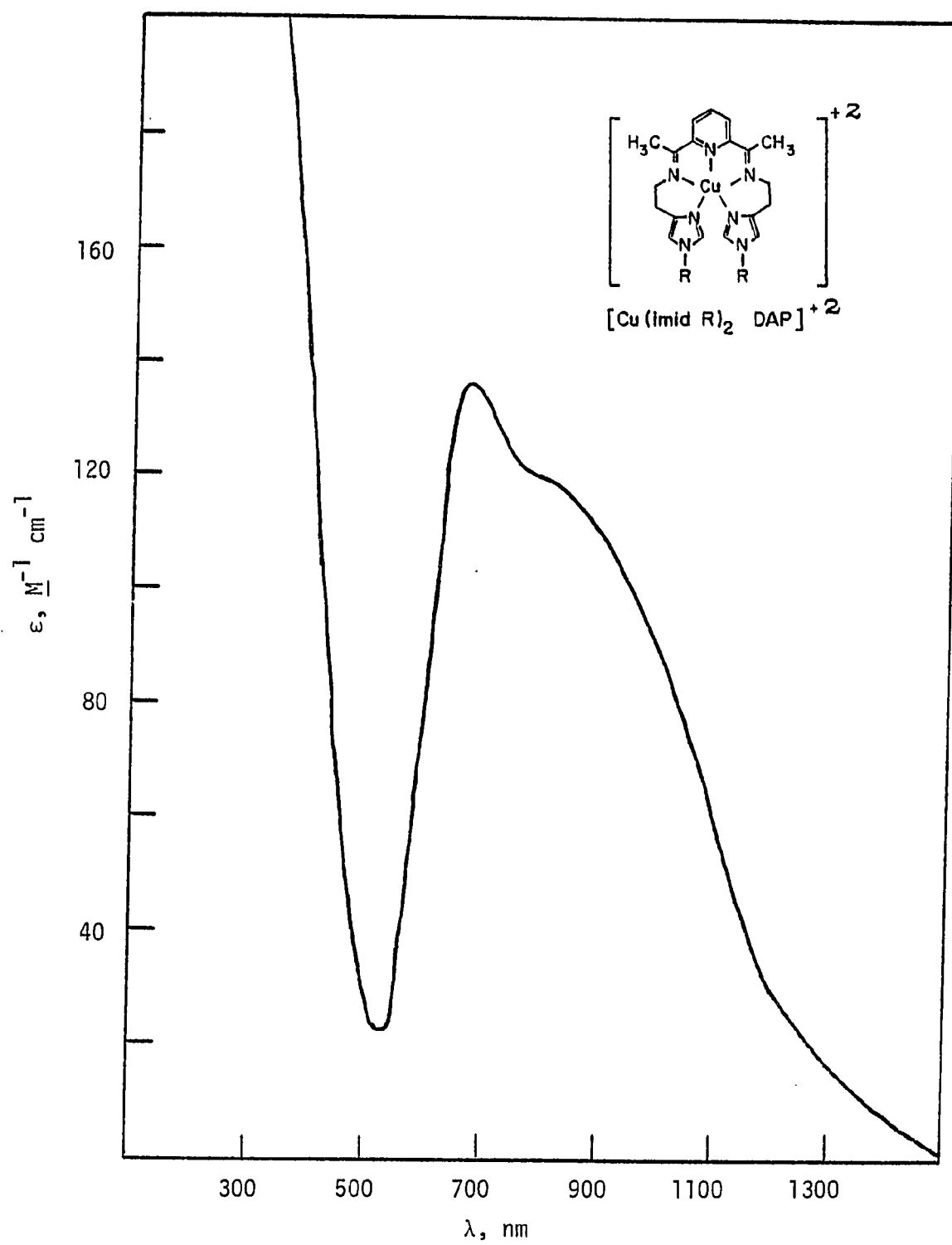


Figure 16

Electronic Absorption Spectrum of  $[\text{Cu}(\text{imidR})(\text{py})\text{DAP}]^{2+}$

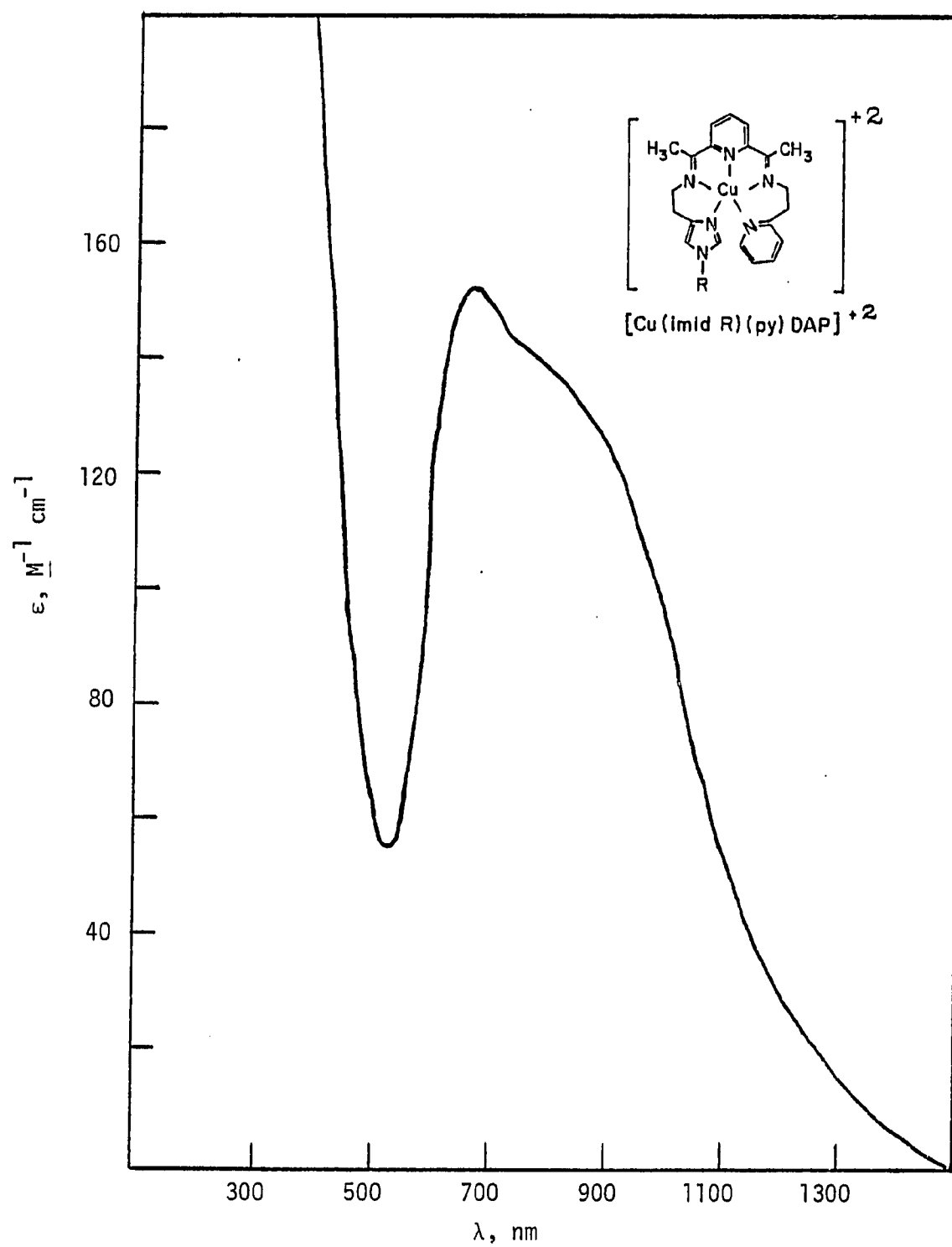


Figure 17

Electronic Absorption Spectrum of  $[\text{Cu}(\text{imidR})(\text{imidH})\text{DAP}]^{2+}$

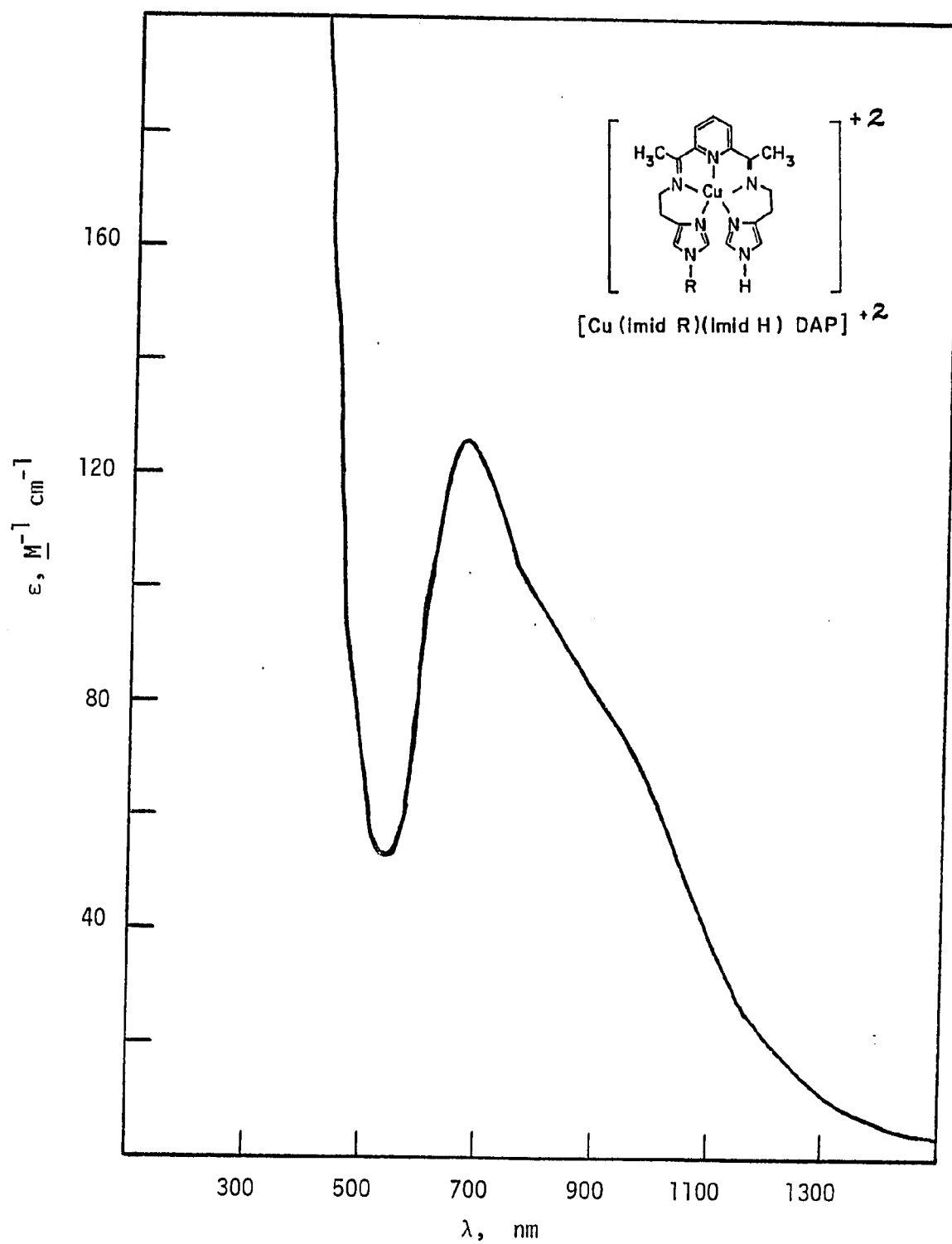


Table 4

Electronic Spectral Data for the Copper Complexes at Room Temperature

| Complex  | Solvent                | $\lambda_{\max}$ , nm | $\epsilon_{\max}$ , $\text{M}^{-1}\text{cm}^{-1}$ |
|--|------------------------|-----------------------|---|
| $[\text{Cu}^{\text{II}}(\text{imidH})(\text{py})\text{DAP}]^{2+}$    | $\text{CH}_3\text{CN}$ | 780                   | 130   |
|  |                        | 675                   | 145   |
|  |                        | 300 (broad)           | 3,350   |
|  |                        | 215                   | 31,500  |
| $[\text{Cu}^{\text{II}}(\text{imidR})_2\text{DAP}]^{2+}$             | $\text{CH}_3\text{CN}$ | 800                   | 120   |
|  |                        | 670                   | 136   |
|  |                        | 300 (broad)           | 3,600   |
|  |                        | 215                   | 35,000  |
| $[\text{Cu}^{\text{II}}(\text{imidR})(\text{py})\text{DAP}]^{2+}$    | $\text{CH}_3\text{CN}$ | 800                   | 139   |
|  |                        | 675                   | 154   |
|  |                        | 300 (broad)           | 3,500   |
|  |                        | 215                   | 35,000  |
| $[\text{Cu}^{\text{II}}(\text{imidR})(\text{imidH})\text{DAP}]^{2+}$ | $\text{CH}_3\text{CN}$ | 800                   | 98  |
|  |                        | 670                   | 126   |
|  |                        | 300 (broad)           | 3,200   |
|  |                        | 215                   | 34,000  |
| $[\text{Cu}^{\text{I}}(\text{imidH})(\text{py})\text{DAP}]^{+}$      | $\text{Me}_2\text{SO}$ | 485                   | 2,000   |
|  |                        | 340                   | 3,550   |
|  |                        | 290                   | 6,150   |

(Table 4 Continued)

| Complex  | Solvent                | $\lambda_{\text{max}}$ , nm | $\epsilon_{\text{max}}$ , $\text{M}^{-1}\text{cm}^{-1}$ |
|--|------------------------|-----------------------------|---|
| $[\text{Cu}^{\text{I}}(\text{imidR})_2\text{DAP}]^+$             | $\text{Me}_2\text{SO}$ | 515                         | 1,800   |
|  |                        | 420                         | 1,760   |
|  |                        | 310 (sh)                    | 3,300   |
| $[\text{Cu}^{\text{I}}(\text{imidR})(\text{py})\text{DAP}]^+$    | $\text{Me}_2\text{SO}$ | 480                         | 1,240   |
|  |                        | 320 (sh)                    | 3,000   |
| $[\text{Cu}^{\text{I}}(\text{imidR})(\text{imidH})\text{DAP}]^+$ | $\text{Me}_2\text{SO}$ | 520                         | 2,250   |

Due to this dramatic color change, the visible spectra of the deoxy and oxy solutions are quite informative. The  $[\text{Cu}^{\text{I}}(\text{imidH})(\text{py})\text{DAP}]^+$  cation clearly reacts with dioxygen, yet even with slight heating and prolonged nitrogen gas purge, the khaki green oxygenated solution remains green with no change in electronic spectrum, indicating the oxygenation process is not reversible for this Cu(I) hybrid complex (see Figure 19). This result is in contrast to that of the  $[\text{Cu}^{\text{I}}(\text{imidH})_2\text{DAP}]^+$  parent compound<sup>34</sup> where the red deoxy solution turns green in the presence of dioxygen and turns back to red upon the heating and nitrogen purging step. As depicted in Figure 20, the red deoxy  $[\text{Cu}^{\text{I}}(\text{imidR})_2\text{DAP}]^+$  solution becomes light green upon bubbling with dioxygen and by a subsequent nitrogen purge returns to a pinkish orange color. While the degree of reversibility for the oxygenation process is quite diminished when compared to the  $[\text{Cu}^{\text{I}}(\text{imidH})_2\text{DAP}]^+$  species, some oxy material must convert back to the deoxy form. Finally, the oxygenation procedure for the  $[\text{Cu}^{\text{I}}(\text{imidR})(\text{imidH})\text{DAP}]^+$  complex is shown in Figure 21. Of all the Cu(I) complexes studied in this work, this hybrid's electronic spectral changes during the oxygenation/deoxygenation procedure most closely resembles that of the parent  $[\text{Cu}^{\text{I}}(\text{imidH})_2\text{DAP}]^+$  species. Based on examination of the deoxy-A and redeoxy-C spectra in the 520 nm region, the degree of reversible oxygenation is estimated at ca. 65%, compared to ca. 85% for the  $[\text{Cu}^{\text{I}}(\text{imidH})_2\text{DAP}]^+$  complex at room temperature.<sup>37</sup>

Warburg manometric techniques have been employed to determine the stoichiometry, or the  $\text{O}_2:\text{Cu}$  mole ratio, of the dioxygen uptake by these Cu(I) complexes in solution at room temperature. Paralleling the  $[\text{Cu}^{\text{I}}(\text{py})_2\text{DAP}]^+$  species, the  $[\text{Cu}^{\text{I}}(\text{imidR})(\text{py})\text{DAP}]^+$  is found not to react



Figure 18

Electronic Absorption Spectrum of  $[\text{Cu}(\text{imidR})(\text{py})\text{DAP}]^+$

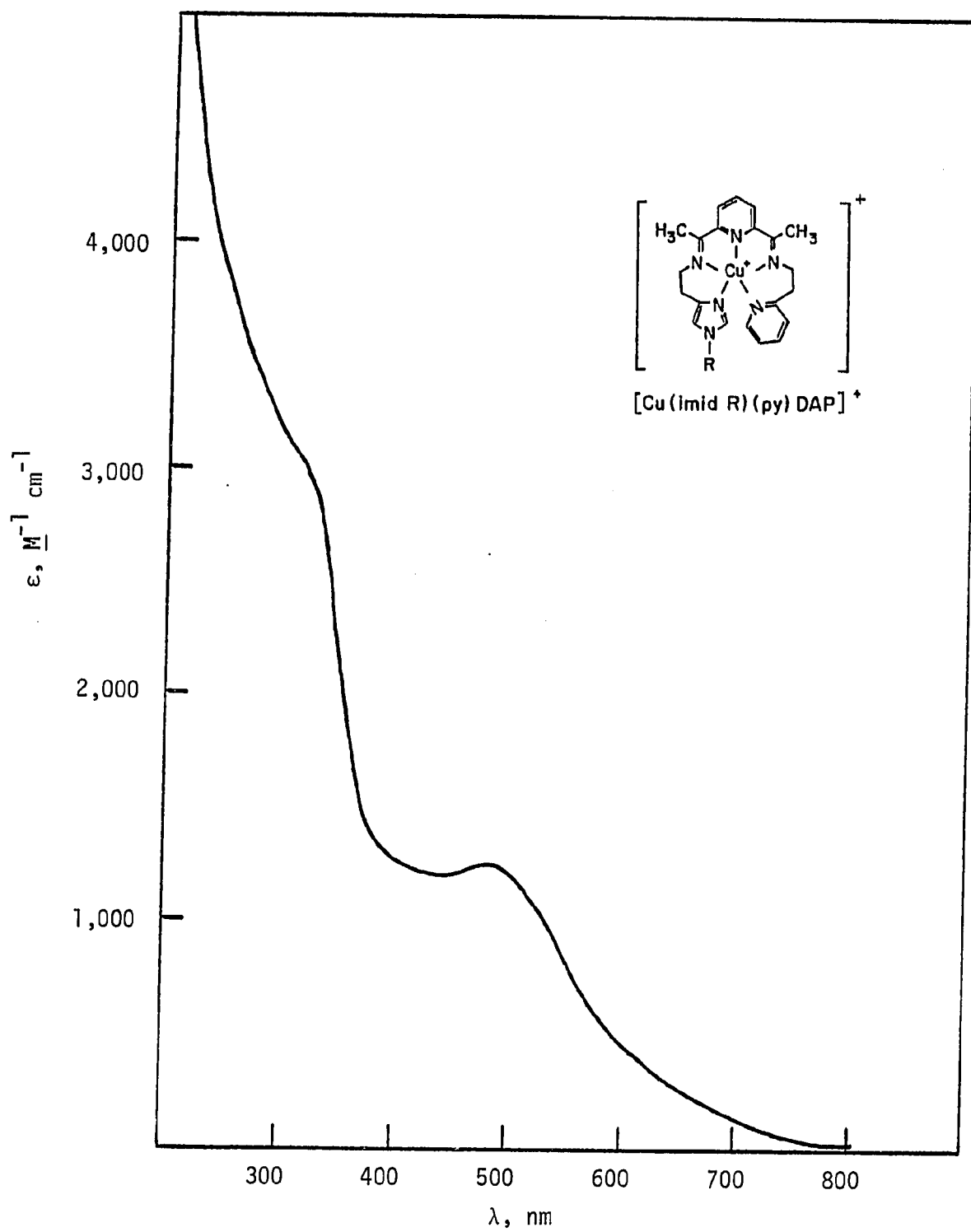


Figure 19

Electronic Absorption Spectrum of

- A -  $[\text{Cu}(\text{imidH})(\text{py})\text{DAP}]^+$  in deoxygenated  $\text{Me}_2\text{SO}$  at  
0.5 mM copper.
- B - Solution A after oxygenation under 1 atm for 5 min  
with uptake of 0.5 moles of  $\text{O}_2$  per Cu.  
(Same spectrum resulted after deoxygenation with  
nitrogen gas purge and slight heating.)

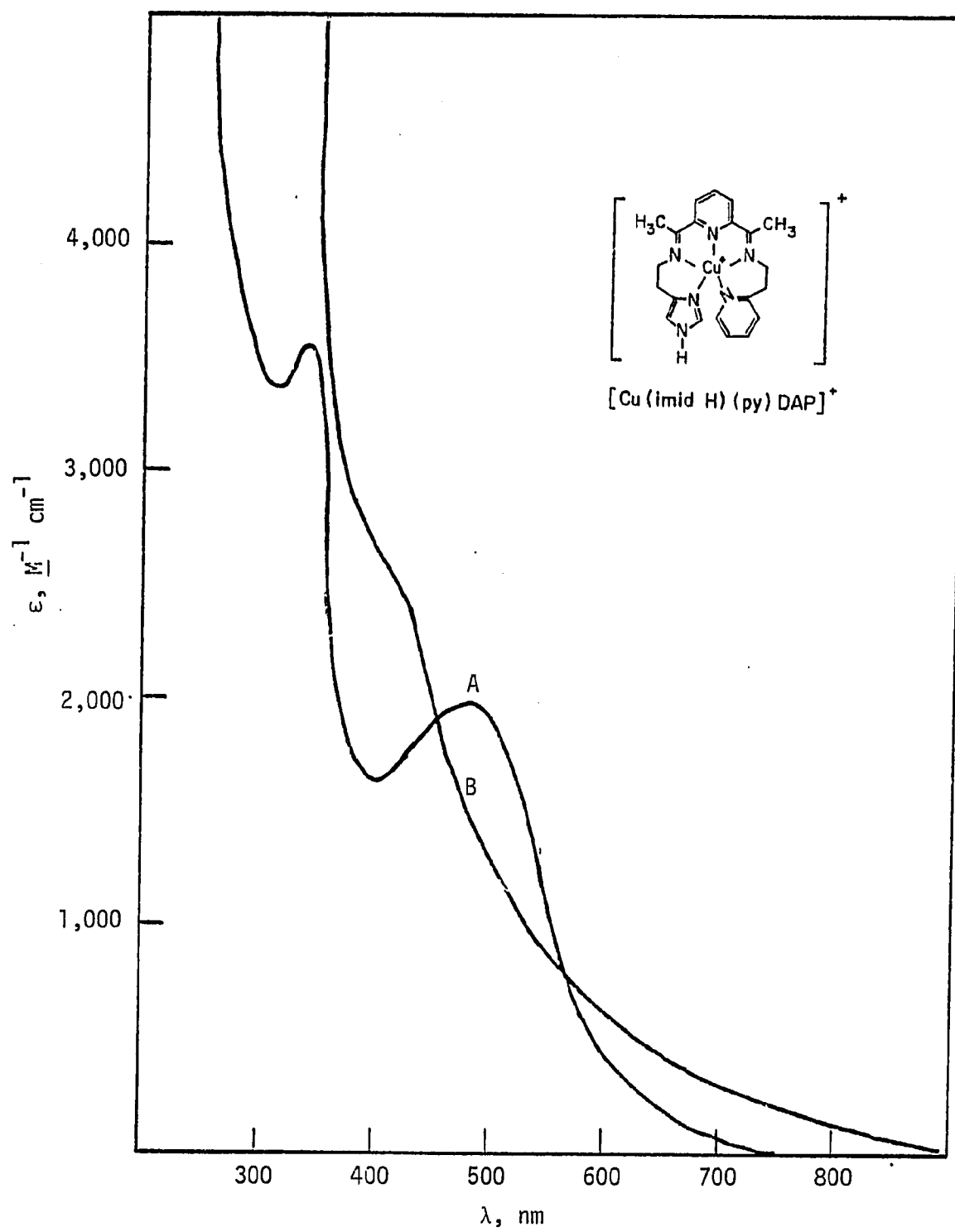


Figure 20

Electronic Absorption Spectrum of

- A -  $[\text{Cu}(\text{imidR})_2\text{DAP}]^+$  in deoxygenated  $\text{Me}_2\text{SO}$  at 0.5 mM copper.
- B - Solution A after oxygenation under 1 atm for 5 min with uptake of 0.5 moles of  $\text{O}_2$  per Cu.
- C - Solution B after deoxygenation with nitrogen gas purge and slight heating.

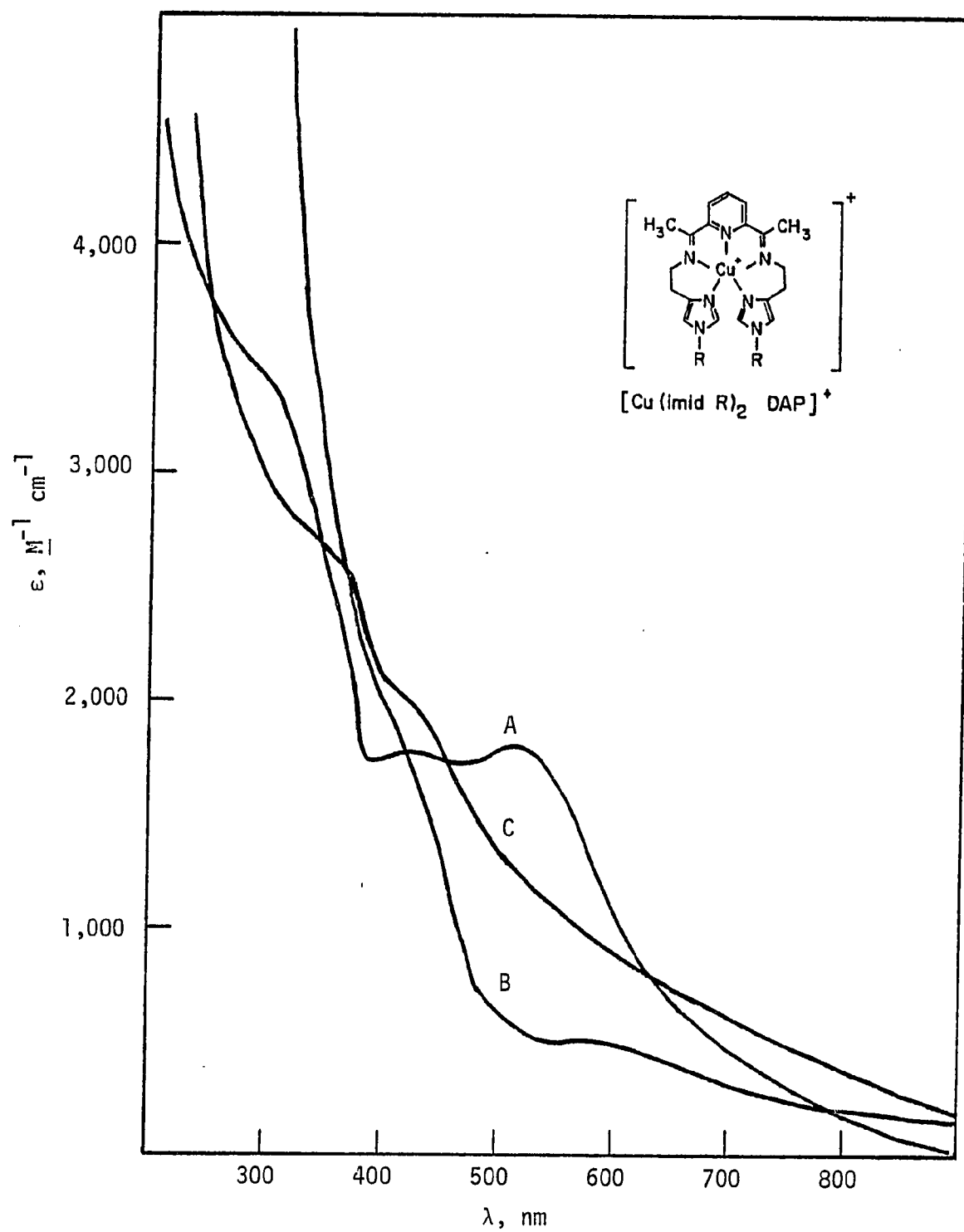
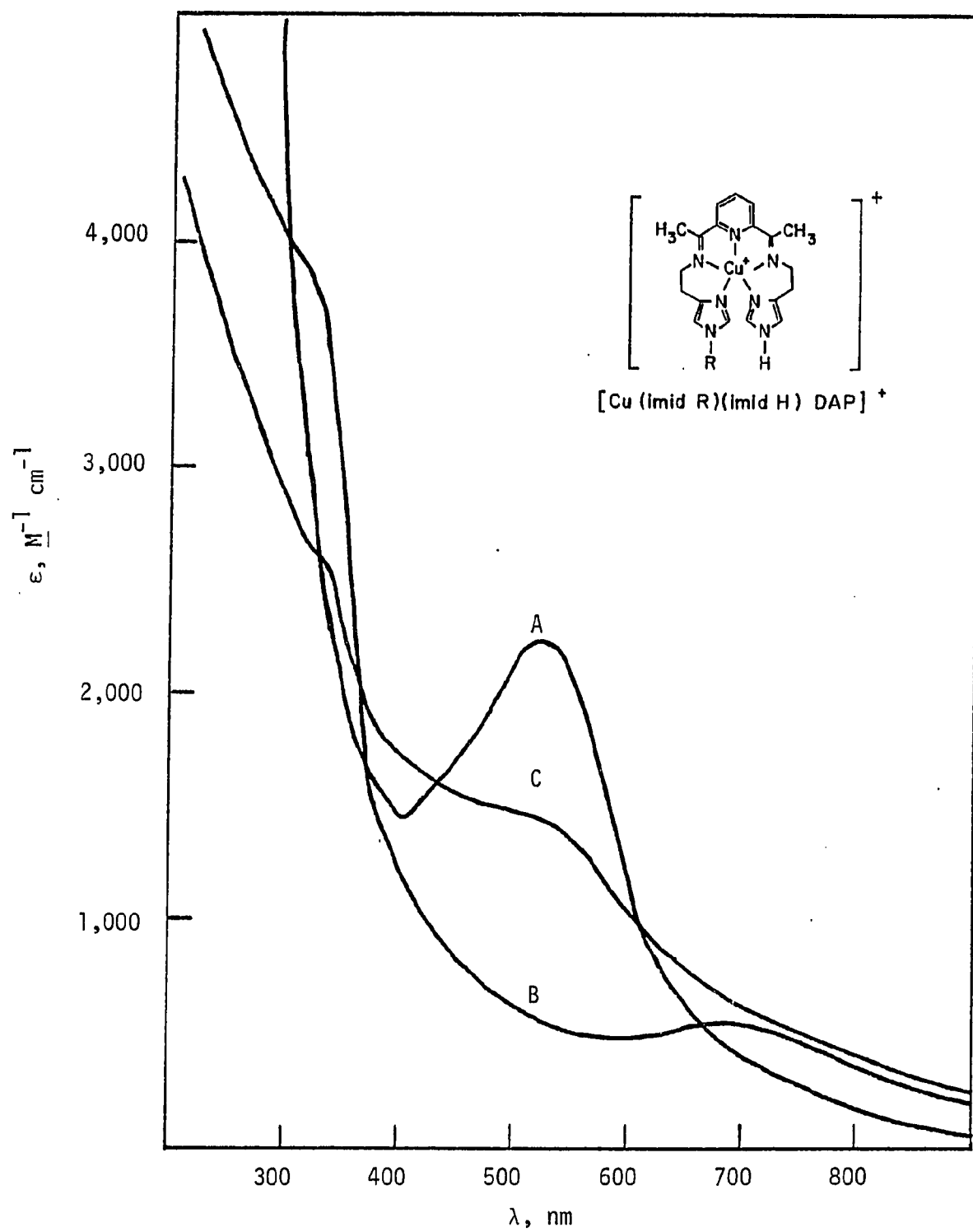


Figure 21

Electronic Absorption Spectrum of

- A -  $[\text{Cu}(\text{imidR})(\text{imidH})\text{DAP}]^+$  in deoxygenated  $\text{Me}_2\text{SO}$  at 0.5 mM copper.
- B - Solution A after oxygenation under 1 atm for 5 min with uptake of 0.5 moles  $\text{O}_2$  per Cu.
- C - Solution B after deoxygenation with nitrogen gas purge and slight heating.





immediately with dioxygen at 1 atm and 23°C. However, upon standing in air for an extended period (greater than 1 h), this red Cu(I) solution slowly becomes murky green-brown in color, indicative of a slow irreversible, chemical oxidation to Cu(II) products. A plausible explanation for the non-reactivity of the  $[\text{Cu}^{\text{I}}(\text{imidR})(\text{py})\text{DAP}]^+$  species toward dioxygen involves the stability of the Cu(I) oxidation state and is fully discussed below. On the other hand, the oxygenation of the Cu(I) centers in the  $[\text{Cu}^{\text{I}}(\text{imidH})(\text{py})\text{DAP}]^+$ ,  $[\text{Cu}^{\text{I}}(\text{imidR})_2\text{DAP}]^+$ , and  $[\text{Cu}^{\text{I}}(\text{imidR})(\text{imidH})\text{DAP}]^+$  species is accomplished much more rapidly (10-20 min). Typical manometric results in  $\text{Me}_2\text{SO}$  are presented in Table 5. It is noted that the rate of oxygenation is slower for the  $[\text{Cu}^{\text{I}}(\text{imidH})(\text{py})\text{DAP}]^+$  and  $[\text{Cu}^{\text{I}}(\text{imidR})_2\text{DAP}]^+$  compounds (time for complete oxygenation ca. 20 min) than for the  $[\text{Cu}^{\text{I}}(\text{imidH})_2\text{DAP}]^+$  and  $[\text{Cu}^{\text{I}}(\text{imidR})-(\text{imidH})\text{DAP}]^+$  species (ca. 10 min). Differences in the stability of the Cu(I) center toward oxidation and in the mechanism for this oxygenation process may account for this variation. As in the case of the parent  $[\text{Cu}^{\text{I}}(\text{imidH})_2\text{DAP}]^+$  complex, solutions of Cu(I) compounds B, D, and F at 23°C absorb 0.5 mole of dioxygen per 1 mole copper. Thus by varying the ligand environment, yet maintaining the presence of the (imidX) moiety around the Cu(I) center, the  $\text{O}_2:\text{Cu}$  stoichiometry is established to be 1:2 for the oxygenation process, indicating formation of a  $\mu$ -peroxo bridged copper species similar to that proposed for oxyhemocyanin.<sup>13</sup> While no reaction of the Cu(I) complexes in the solid state with dry dioxygen is observed, all sample preparations must be performed under an inert atmosphere to avoid moist air contamination which results in slow, irreversible oxidation of the compounds. As expected,

Table 5

## Manometric Measurements and Dioxygen Uptake

Results for Copper(I) Complexes in Me<sub>2</sub>SO at 23°C and 1 Atm Oxygen

| Complex Run                 | Moles Copper<br>$\times 10^{-6}$ | $h^*$ , in mm<br>$[(h_M - h_{TB}) - h_{Blank}]$ | Moles O <sub>2</sub><br>$\times 10^{-6}$ | O <sub>2</sub> /Cu |
|-----------------------------|----------------------------------|---|--|--------------------|
| $[Cu^I(imidH)(py)DAP]^+$    |                                  |   |  |                    |
| 1                           | 9.63                             | 74.0  | 4.11                                     | 0.43               |
| 2                           | 12.97                            | 120.0   | 7.13                                     | 0.55               |
| 3                           | 7.08                             | 55.5  | 2.88                                     | 0.41               |
| 4                           | 11.05                            | 110.0   | 7.29                                     | 0.66               |
| 5                           | 6.10                             | 58.0  | 2.88                                     | 0.47               |
| * $h_{Blank} = 22.7$ mm     |                                  |   |  |                    |
| $[Cu^I(imidR)_2DAP]^+$      |                                  |   |  |                    |
| 1                           | 13.70                            | 107.0   | 6.20                                     | 0.45               |
| 2                           | 14.69                            | 118.0   | 7.10                                     | 0.48               |
| * $h_{Blank} = 31.0$ mm     |                                  |   |  |                    |
| $[Cu^I(imidR)(imidH)DAP]^+$ |                                  |   |  |                    |
| 1                           | 6.62                             | 67.5  | 3.05                                     | 0.46               |
| 2                           | 2.98                             | 53.0  | 1.88                                     | 0.63               |
| 3                           | 4.14                             | 59.0  | 2.36                                     | 0.57               |
| 4                           | 6.62                             | 62.0  | 2.61                                     | 0.39               |
| * $h_{Blank} = 30.0$ mm     |                                  |   |  |                    |

the analogous Cu(II) and Zn(II) compounds are completely stable toward dioxygen, albeit fairly hygroscopic.

### Electrochemical Experiments

As the oxygenation procedure most probably involves an oxidative addition reaction between the Cu(I) centers and the dioxygen molecule,<sup>38</sup> the stability of this Cu(I) oxidation state has been examined electrochemically. Electrochemical assays, including cyclic voltammetry (c.v.) and differential pulse polarography (d.p.p.), have been performed to characterize the  $\text{Cu(II)} \rightleftharpoons \text{Cu(I)}$  redox couple in each of the copper(II) complexes. The cyclic voltammograms for the Cu(II) compounds have been recorded in the absence and presence of dissolved dioxygen. Under a nitrogen atmosphere, the Cu(II) species are characterized by reversible, one-electron processes (controlled potential electrolyses at potentials 250 mV cathodic of the  $\text{Cu(II)} \rightleftharpoons \text{Cu(I)}$   $E_{1/2}$  have confirmed this description) with half-wave reduction potentials in the range of -200 to -350 mV (vs. S.C.E.). The  $E_{1/2}$ 's have been determined by differential pulse polarography as documented in Table 6. Cyclic voltammetry has been used, in addition to elemental analysis, to determine the uniqueness and purity of the hybrid Cu(II) complexes. For example, the physical mixture of the  $[\text{Cu}^{\text{II}}(\text{imidH})_2\text{DAP}]^{2+}$  and  $[\text{Cu}^{\text{II}}(\text{py})_2\text{DAP}]^{2+}$  compounds yields two distinct differential pulse polarograms, whereas the hybrid  $[\text{Cu}^{\text{II}}(\text{imidH})(\text{py})\text{DAP}]^{2+}$  species has a sharp, single peak with a half-wave potential midway between that of the "bis"-(imidH) and "bis"-(py) complexes (Figure 22). Likewise the hybrid  $[\text{Cu}^{\text{II}}(\text{imidR})(\text{py})\text{DAP}]^{2+}$  complex exhibits a sharp  $E_{1/2}$  between that for the

Table 6  
Cyclic Voltammetric Data  
for the Copper(II) Tetrafluoroborate Salts in  
CH<sub>3</sub>CN at 10<sup>-3</sup> M in Copper and 0.1 M in TBAP

| Complex   | $E_{1/2}$ (Cu <sup>II</sup> $\rightleftharpoons$ Cu <sup>I</sup> ),<br>in Volts (vs. S.C.E.) |
|---|--|
| [Cu <sup>II</sup> (py) <sub>2</sub> DAP] <sup>2+</sup>    | -0.20  |
| [Cu <sup>II</sup> (imidR)(py)DAP] <sup>2+</sup>           | -0.25  |
| [Cu <sup>II</sup> (imidH)(py)DAP] <sup>2+</sup>           | -0.27  |
| [Cu <sup>II</sup> (imidR) <sub>2</sub> DAP] <sup>2+</sup> | -0.32  |
| [Cu <sup>II</sup> (imidR)(imidH)DAP] <sup>2+</sup>        | -0.33  |
| [Cu <sup>II</sup> (imidH) <sub>2</sub> DAP] <sup>2+</sup> | -0.35  |

Figure 22

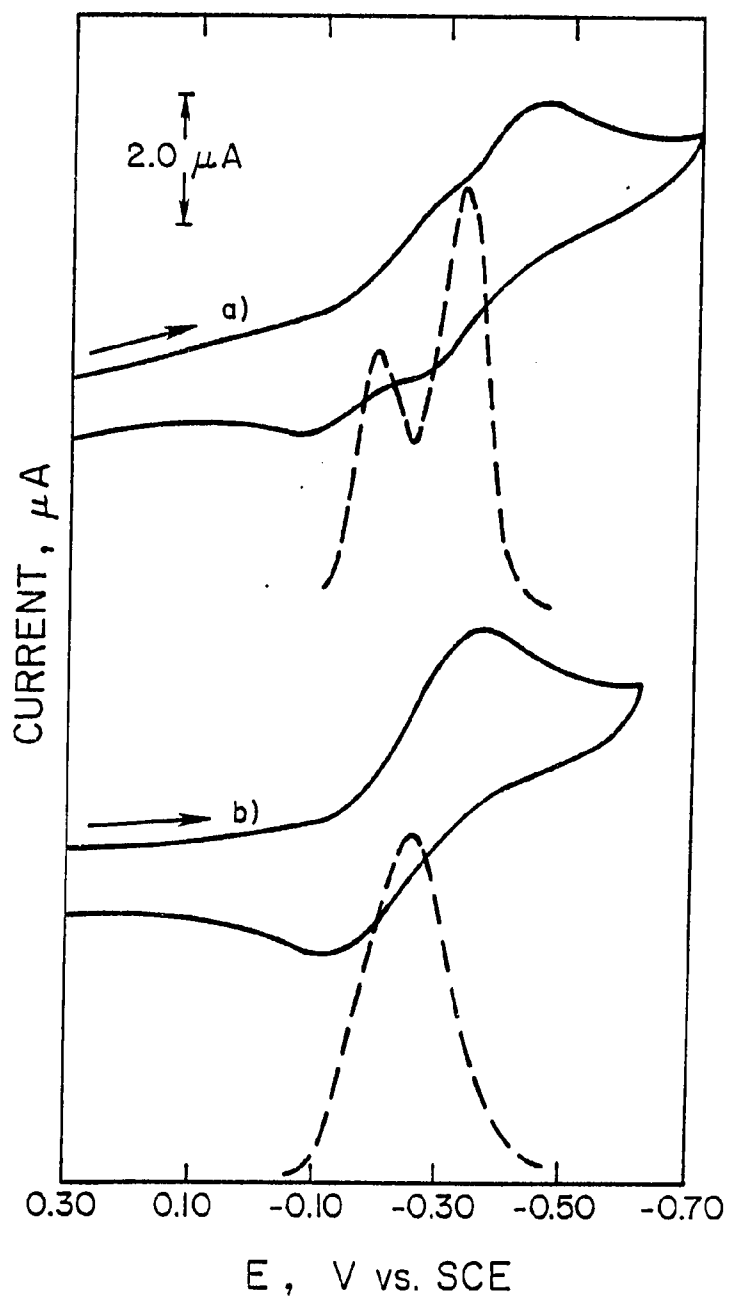
Cyclic Voltammograms and Differential Pulse Polarograms  
at Platinum Button Electrodes for the Copper(II) Complexes  
in Degassed CH<sub>3</sub>CN at 10<sup>-3</sup> M Copper and 0.1 M in TBAP

a) - A 1:1 mixture of [Cu<sup>II</sup>(imidH)<sub>2</sub>DAP]<sup>2+</sup> (E<sub>1/2</sub> = -0.35 V)  
and [Cu<sup>II</sup>(py)<sub>2</sub>DAP]<sup>2+</sup> (E<sub>1/2</sub> = -0.20 V).

b) - [Cu<sup>II</sup>(imidH)(py)DAP]<sup>2+</sup> (E<sub>1/2</sub> = -0.27 V).

Scan Rate = 200 mV/s

E<sub>1/2</sub> vs. S.C.E.



$[\text{Cu}^{\text{II}}(\text{imidR})_2\text{DAP}]^{2+}$  and  $[\text{Cu}^{\text{II}}(\text{py})_2\text{DAP}]^{2+}$  species. Since the redox potentials for the  $[\text{Cu}^{\text{II}}(\text{imidH})_2\text{DAP}]^{2+}$  and  $[\text{Cu}^{\text{II}}(\text{imidR})_2\text{DAP}]^{2+}$  compounds are so similar, this electrochemical test for the distinctness of the hybrid  $[\text{Cu}^{\text{II}}(\text{imidR})(\text{imidH})\text{DAP}]^{2+}$  is not valid. Nevertheless elemental analysis confirms the purity of this hybrid species.

In addition to the Cu(II) compounds, the analogous Zn(II) complexes have been studied electrochemically under a nitrogen atmosphere. The cyclic voltammograms for these Zn(II) species exhibit one-electron reductions at potentials ranging from -1.12 to -1.40 V (vs. S.C.E.) (see Figure 23 and Table 7 for the appropriate electrochemical data). Since the  $E_{1/2}$ 's for these c.v.'s are quite negative and owing to the inherent stability of the Zn(II) metal center with respect to reduction,<sup>42</sup> these reductions most probably correspond to ligand centered reductions yielding ligand-based radical anions. Since the potential range scanned during the c.v. study of the Cu(II) complexes shows no redox reaction for the Zn(II) complexes, the redox process observed in the Cu(II) study must be a metal-centered  $\text{Cu(II)} \rightleftharpoons \text{Cu(I)}$  electrochemical process.

Cyclic voltammetry has also been employed to examine the oxygenation process of the Cu(I) species as it is generated at the Pt electrode surface from its Cu(II) analog. Figures 24, 25, and 26 illustrate these c.v. experiments involving the  $[\text{Cu}^{\text{II}}(\text{imidH})(\text{py})\text{DAP}]^{2+}$ ,  $[\text{Cu}^{\text{II}}(\text{imidR})_2\text{DAP}]^{2+}$ , and  $[\text{Cu}^{\text{II}}(\text{imidR})(\text{imidH})\text{DAP}]^{2+}$  species. While all three species exhibit cyclic voltammograms unaffected by the presence of dissolved dioxygen when the potential scan is not interrupted with a holding procedure, definite changes to the appearance of the anodic wave do occur as the potential is held cathodic of the  $E_{1/2}$ . In the case of the

Figure 23

Cyclic Voltammograms for the  
Zinc(II) Tetrafluoroborate Complexes in  
CH<sub>3</sub>CN, 10<sup>-3</sup> M Zinc and 0.1 M in TBAP

- a)  $[\text{Zn}^{\text{II}}(\text{imidH})(\text{py})\text{DAP}]^{2+}$
- b)  $[\text{Zn}^{\text{II}}(\text{imidR})(\text{py})\text{DAP}]^{2+}$
- c)  $[\text{Zn}^{\text{II}}(\text{imidR})_2\text{DAP}]^{2+}$
- d)  $[\text{Zn}^{\text{II}}(\text{imidR})(\text{imidH})\text{DAP}]^{2+}$



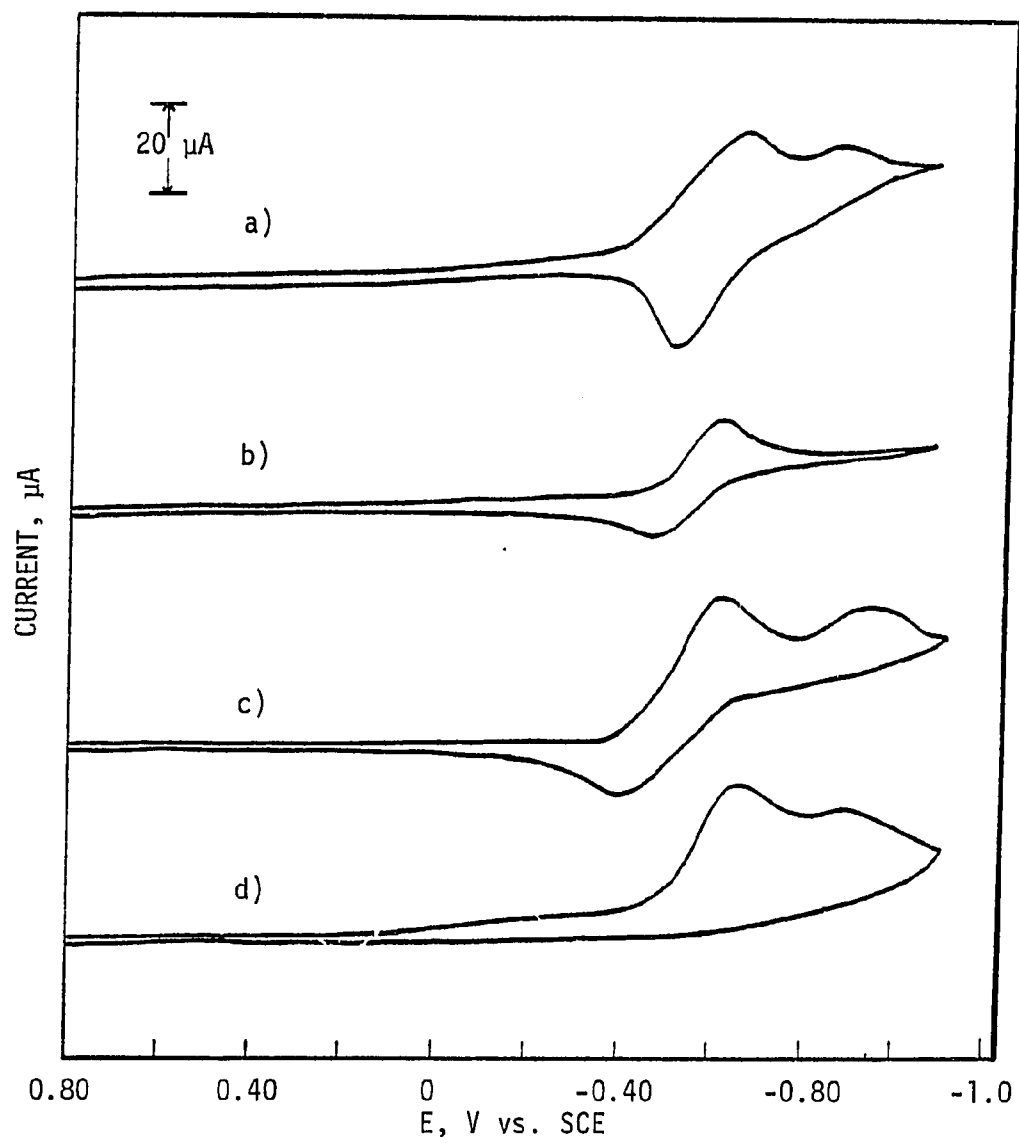


Table 7  
Cyclic Voltammetric Data  
for the Zinc(II) Tetrafluoroborate Complexes  
in CH<sub>3</sub>CN at 10<sup>-3</sup> M Zinc and 0.1 M in TBAP

| Complex  | Volts ( <u>vs.</u> S.C.E.) |
|--|----------------------------|
| [Zn <sup>II</sup> (imidH)(py)DAP] <sup>2+</sup>    | -1.14                      |
|  | -1.22                      |
|  | -1.36                      |
| [Zn <sup>II</sup> (imidR)DAP] <sup>2+</sup>        | -1.16                      |
| [Zn <sup>II</sup> (imidR)(py)DAP] <sup>2+</sup>    | -1.12                      |
|  | -1.40                      |
| [Zn <sup>II</sup> (imidR)(imidH)DAP] <sup>2+</sup> | -1.18                      |
|  | -1.39                      |

Scan Rate = 200 mV/s

Figure 24

Cyclic Voltammograms of  $[\text{Cu}^{\text{II}}(\text{imidH})(\text{py})\text{DAP}]^{2+}$   
in  $\text{CH}_3\text{CN}$  at 2.0 mM Copper and 0.1 M in TBAP

- a) - Under nitrogen.
- b) - Under dioxygen.
- c) - Under dioxygen, holding potential at -0.60 V  
for 9 s, then scanning anodically.
- d) - Under dioxygen, holding potential at -0.60 V  
for 25 s, then scanning anodically.
- e) - Under dioxygen.

Scan Rate = 200 mV/s

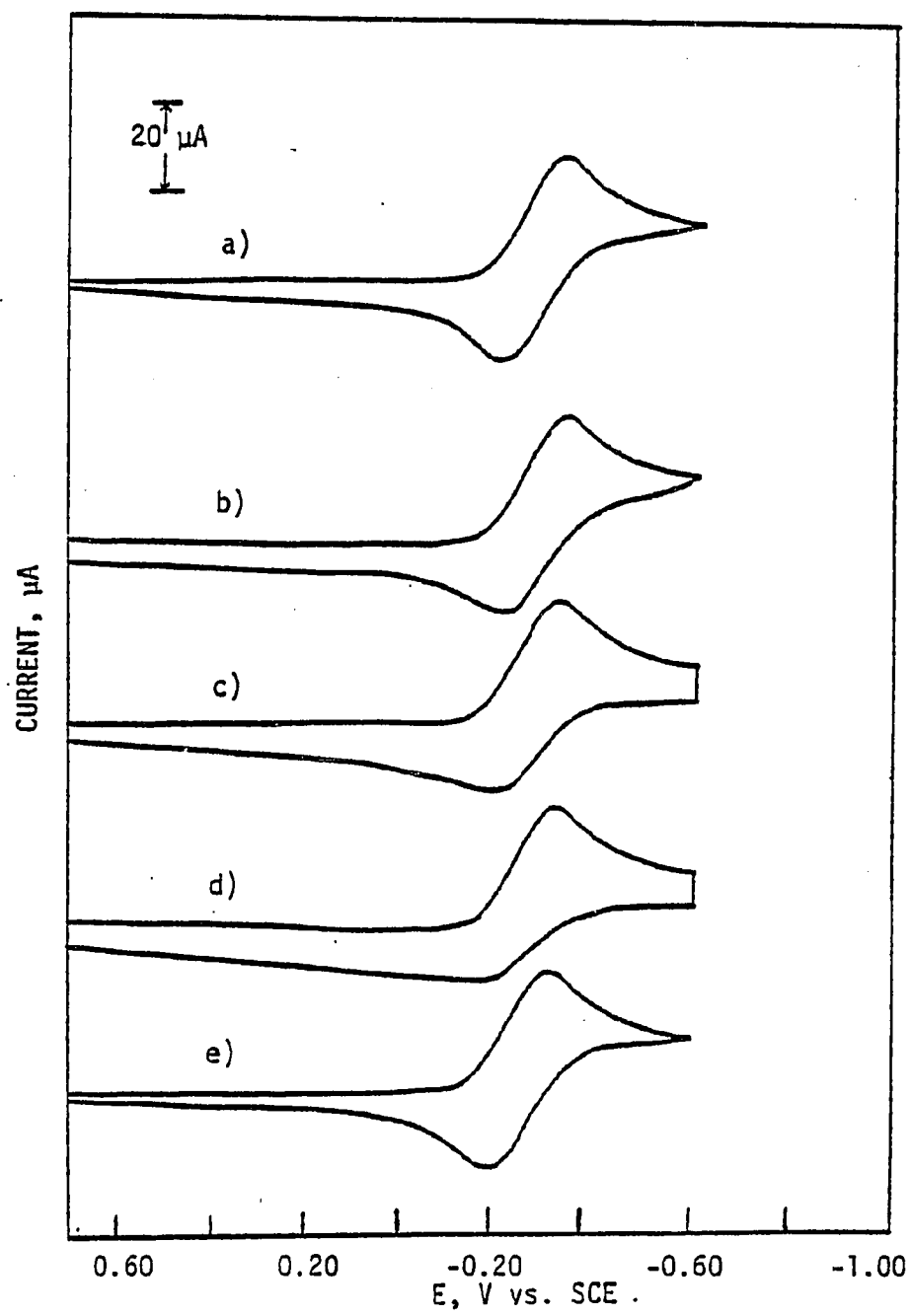


Figure 25

Cyclic Voltammograms of  $[\text{Cu}^{\text{II}}(\text{imidR})_2\text{DAP}]^{2+}$   
in  $\text{CH}_3\text{CN}$  at 2.0 mM Copper and 0.1 M in TBAP

- a) - Under nitrogen.
- b) - Under dioxygen.
- c) - Under dioxygen, holding potential at -0.60 V  
for 9 x, then scanning anodically.
- d) - Under dioxygen, holding potential at -0.60 V  
for 25 s, then scanning anodically.
- e) - Under dioxygen.

Scan Rate = 200 mV/s

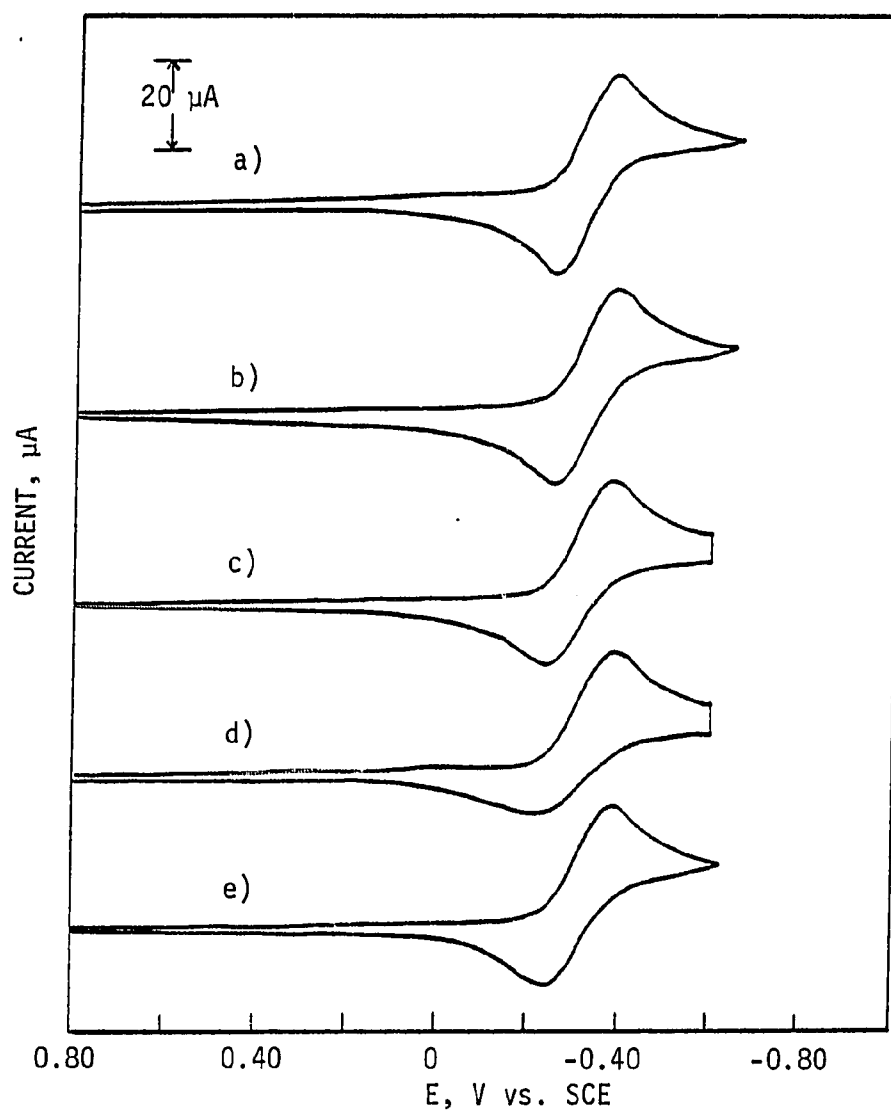
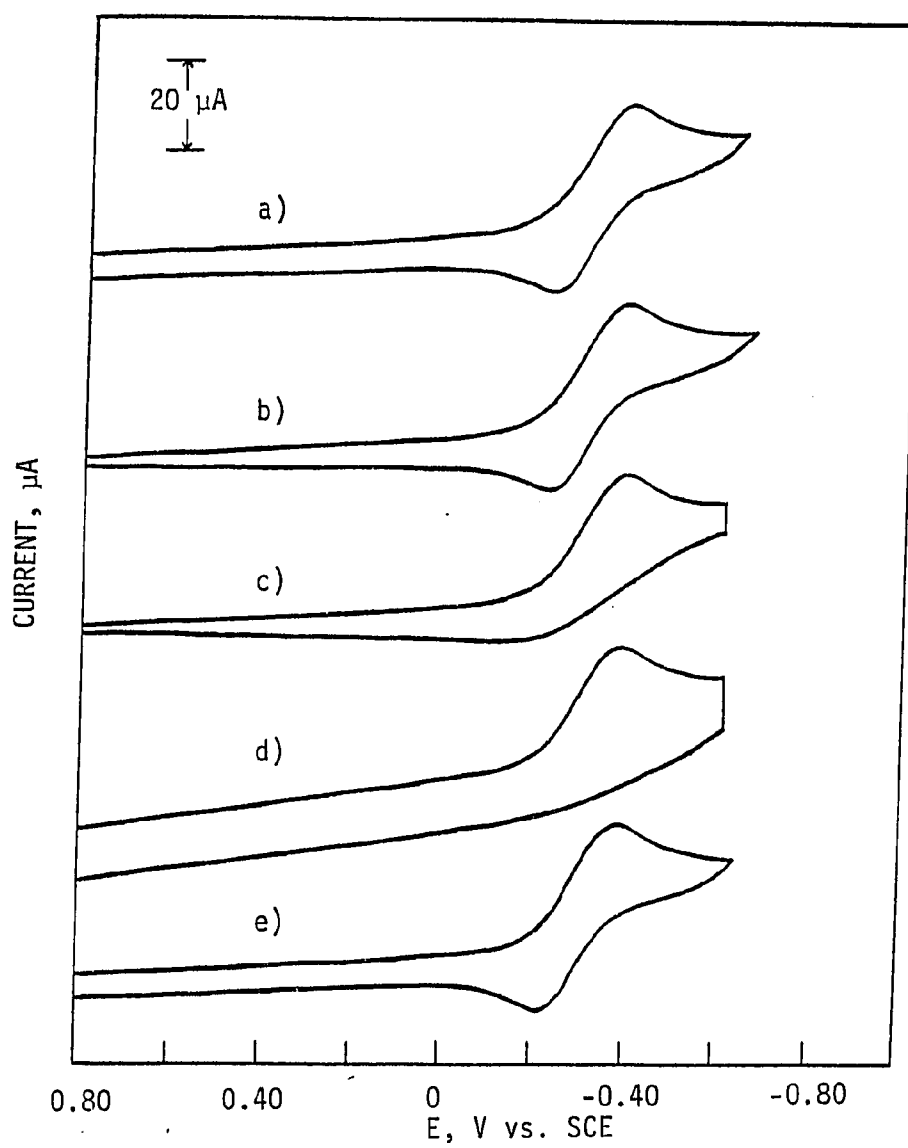


Figure 26

Cyclic Voltammograms of  $[\text{Cu}^{\text{II}}(\text{imidR})(\text{imidH})\text{DAP}]^{2+}$   
in  $\text{CH}_3\text{CN}$  at 2.0 mM Copper and 0.1 M in TBAP

- a) - Under nitrogen.
- b) - Under dioxygen.
- c) - Under dioxygen, holding potential at -0.60 V  
for 9 s, then scanning anodically.
- d) - Under dioxygen, holding potential at -0.60 V  
for 15 s, then scanning anodically.
- e) - Under dioxygen.

Scan Rate = 200 mV/s





$[\text{Cu}^{\text{II}}(\text{imidH})(\text{py})\text{DAP}]^{2+}$  and  $[\text{Cu}^{\text{II}}(\text{imidR})_2\text{DAP}]^{2+}$  compounds, the anodic wave is greatly diminished, but does not completely disappear, as the potential is held at  $-0.60$  V for 9, 15, and 25 seconds. This result supports the finding that the rate of dioxygen uptake by the Cu(I) complexes B and D is qualitatively less than for the parent  $[\text{Cu}^{\text{I}}(\text{imidH})_2\text{DAP}]^+$  species, where the anodic wave vanishes completely after a 9 second hold at  $-0.60$  V. A subsequent scan, with no hold, yields the reversible cathodic and anodic waves, just as when a nitrogen atmosphere is used. For the  $[\text{Cu}^{\text{II}}(\text{imidR})(\text{imidH})\text{DAP}]^{2+}$  complex, a similar result is obtained with the exception that a hold at  $-0.60$  V for 15 seconds causes the anodic wave to completely disappear. The rescan, with no hold under dioxygen, produces the same c.v. as that under nitrogen gas. The cyclic voltammogram of the  $[\text{Cu}^{\text{II}}(\text{imidR})(\text{py})\text{DAP}]^{2+}$  cation in the presence of dioxygen in  $\text{CH}_3\text{CN}$  (Figure 27) indicates no effect of dioxygen on the c.v. when the potential is scanned, with no hold, cathodic of the  $E_{1/2}$ . Similarly, when the potential is held at  $-0.60$  V for as long as 25 seconds, the cathodic and anodic waves appear as during scans under nitrogen or dioxygen with no hold. Thus, this hybrid Cu(II) compound is similar to the  $[\text{Cu}^{\text{II}}(\text{py})_2\text{DAP}]^{2+}$  species in that no reaction of the electrochemically generated Cu(I) and dissolved dioxygen is observed at all.

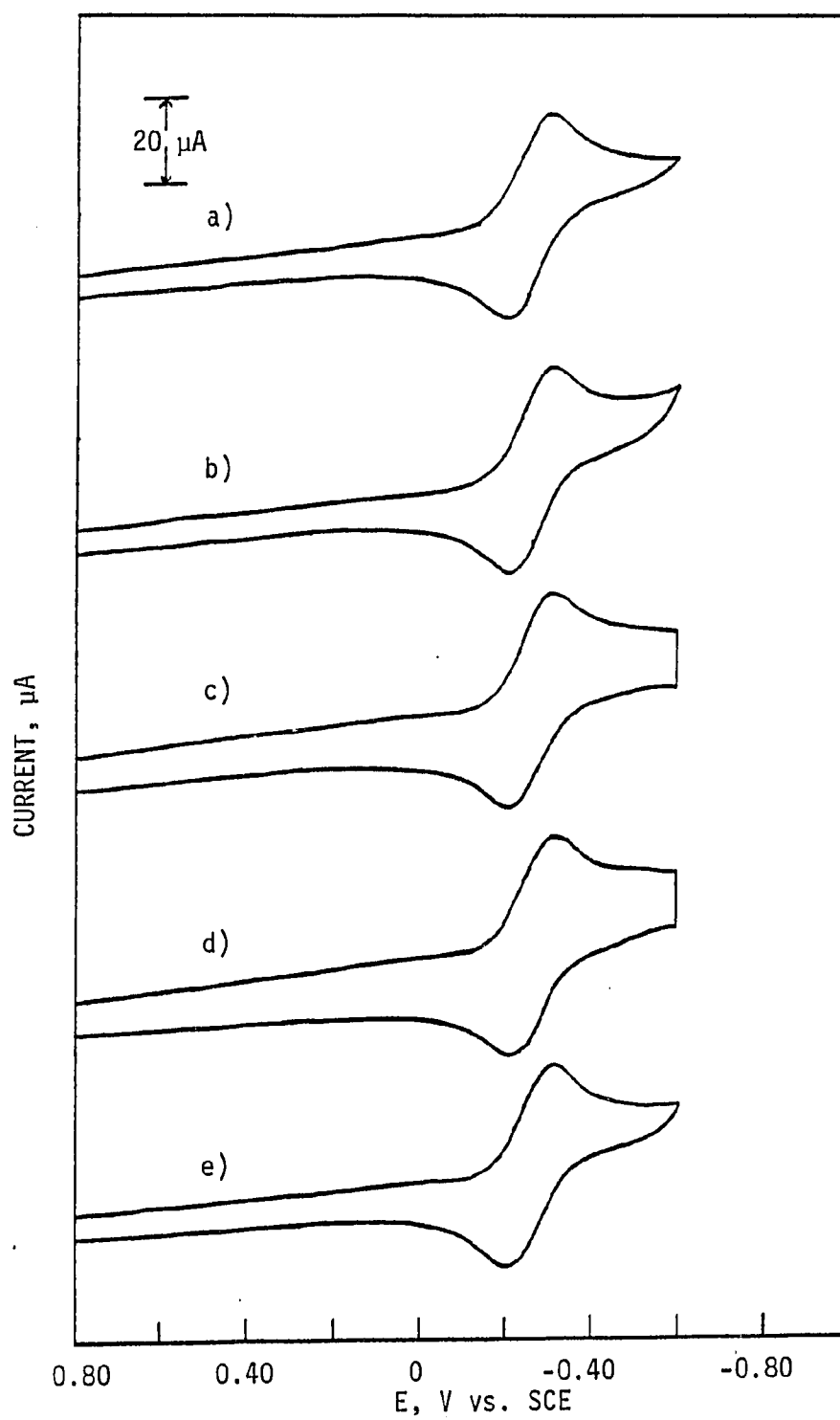
Upon examining the table of reduction potential data for the Cu(II) complexes and the observed behavior of the analogous Cu(I) derivatives under a dioxygen atmosphere, at least one conclusion can be made: the more positive the  $E_{1/2}$ , the greater the stability of the Cu(I) species, generated at the electrode surface, and the lower the reactivity of the

Figure 27

Cyclic Voltammograms of  $[\text{Cu}^{\text{II}}(\text{imidR})(\text{py})\text{DAP}]^{2+}$   
in  $\text{CH}_3\text{CN}$  at 2.0 mM Copper and 0.1 M in TBAP

- a) - Under nitrogen.
- b) - Under dioxygen.
- c) - Under dioxygen, holding potential at -0.60 V  
for 9 s, then scanning anodically.
- d) - Under dioxygen, holding potential at -0.60 V  
for 25 s, then scanning anodically.
- e) - Under dioxygen.

Scan Rate = 200 mV/s



Cu(I) center toward dioxygen, in a reversible manner. Slight variations in the structure of the ligand system alter the redox potential of the  $\text{Cu(II)} \rightleftharpoons \text{Cu(I)}$  couple, the stability of the copper(I) center, and thus the ability of the Cu(I) complex to react with dioxygen. The dioxygen-inactive  $[\text{Cu}^{\text{I}}(\text{py})_2\text{DAP}]^+$  and  $[\text{Cu}^{\text{I}}(\text{imidR})(\text{py})\text{DAP}]^+$  species exhibit  $E_{1/2}$ 's of -0.20 and -0.25 V, and the hybrid  $[\text{Cu}^{\text{I}}(\text{imidH})(\text{py})\text{DAP}]^+$ , which absorbs dioxygen irreversibly, has an  $E_{1/2}$  of -0.27 V. Yet the  $[\text{Cu}^{\text{I}}(\text{imidR})_2\text{DAP}]^+$ ,  $[\text{Cu}^{\text{I}}(\text{imidR})(\text{imidH})\text{DAP}]^+$ , and  $[\text{Cu}^{\text{I}}(\text{imidH})_2\text{DAP}]^+$  derivatives, reacting with a progressively greater degree of reversibility toward dioxygen, have  $E_{1/2}$ 's of -0.32, -0.33, and -0.35 V, only 50-80 mV negative of the hybrid  $[\text{Cu}^{\text{I}}(\text{imidH})(\text{py})\text{DAP}]^+$  species. It is also noteworthy that relatively small changes in  $E_{1/2}$  result in a substantial effect on the oxygenation of these Cu(I) complexes.

The correlation between Cu(I) stability, the redox properties of the  $\text{Cu(II)} \rightleftharpoons \text{Cu(I)}$  couple, and reactivity toward certain oxygenation, or oxidation, processes has been noted briefly in the literature.<sup>27,55</sup> Recently Gagné, *et al.*,<sup>31</sup> have synthesized some macrocyclic Cu(I) complexes and have characterized the redox properties of these complexes in non-aqueous (principally  $\text{CH}_3\text{CN}$ ) solution by cyclic voltammetry. These species exhibit  $E_{1/2}$ 's ranging from -0.46 to -0.80 V (*vs.* S.C.E.), far negative of the dioxygen-active Cu(I) complexes of this work, and thus are much less stable with respect to a metal-centered oxygenation or oxidation reaction. While Gagné's complexes react in solution with CO, the resulting Cu(I)-CO adducts, in the presence of dioxygen, undergo irreversible oxidation to form " $\mu\text{-CO}_3$ "

and " $\mu$ -OH" Cu(II) dimers.<sup>31</sup> On the other hand, the  $[\text{Cu}^{\text{I}}(\text{imidH})_2\text{DAP}]^+$  species, and related derivatives, react reversibly in solution with dioxygen, yet do not react with CO. From this admittedly brief comparative study, the reactivity of Cu(I) coordination compounds toward CO and  $\text{O}_2$  appears to be a mutually exclusive phenomenon. It is possible that copper(I) complexes, such as those prepared by Gagné, with  $E_{1/2}$ 's of such negative magnitude, are in effect too reactive toward oxidation by dioxygen to form any stable Cu- $\text{O}_2$  adducts. In addition, the geometrical changes that could occur during an oxidative addition reaction may be an important consideration<sup>25,56</sup> and the ligating structure of Gagné's compounds may be too rigid to allow any changes in coordination geometry that might be promoted by the oxygenation process.

Relevant to the dioxygen-active  $[\text{Cu}^{\text{I}}(\text{imidH})_2\text{DAP}]^+$  species, x-ray structural analysis is complete for the analogous Cu(II) and Zn(II) complexes. The five-coordinate  $[\text{M}(\text{imidH})_2\text{DAP}]^{2+}$  ( $\text{M} = \text{Cu}^{\text{II}}$  or  $\text{Zn}^{\text{II}}$ ) complexes are isomorphous and isostructural, with the coordination about Cu(II) and Zn(II) described as intermediate between an idealized trigonal bipyramid and a square pyramid.<sup>53</sup> On the basis of this structural study, it is possible to speculate on the structure of the  $[\text{Cu}^{\text{I}}(\text{imidH})_2\text{DAP}]^+$  dioxygen-carrier and on the mechanism for its reversible oxygenation. While pentacoordinate  $\text{Cu}^{\text{I}}$  species are still relatively rare, a few are now known,<sup>57</sup> and the predisposition of the five nitrogen donor atoms of the  $[(\text{imidH})_2\text{DAP}]$  ligand suggest that  $[\text{Cu}^{\text{I}}(\text{imidH})_2\text{DAP}]^+$  will ultimately prove to be five-coordinate as well.

Assuming this to be the case, the most reasonable site for initial  $O_2$  ligation appears to be trans to the pyridine nitrogen atom and between the two imidazole rings. However, due to steric hindrance with imidazole nitrogens, a bent  $O_2$  ligated at this site would produce a dioxygen adduct [probably more correctly written as  $[Cu^{II}-O_2^-]$ ] which could get no stabilization by intramolecular  $[Cu-O_2^- \cdots HN(imidazole)]$  hydrogen bonding interactions of the type proposed to exist between end-on bonded  $O_2$  in  $[Fe(heme)-O_2^-]$  and the distal histidine imidazole proton in oxymyoglobin and oxyhemoglobin.<sup>1</sup> On the other hand, the product of dioxygen addition could be a pentacoordinate species obtained by release of an imidazole ligand from the Cu coordination sphere at the time of attack by dioxygen. Such a species could then be stabilized by an  $NH \cdots O$  hydrogen bond between the end-on bonded dioxygen ligand and the hydrogen atom of the "free" imidazole. The resulting free space around the metal would be advantageous for dimer formation of the type discussed below. Finally, an end-on bonded configuration for  $O_2$  is also suggested by the fact that the stoichiometry of the reversible  $2[Cu^I(imidH)_2DAP]^+ + O_2 \rightleftharpoons (oxy\ product)$  reaction implies that the final oxygenated material is binuclear in copper and an end-on bonded  $\mu$ -peroxo bridge, i.e.,  $[Cu^{II}-O-O^{2-}-Cu^{II}]$ , would probably be necessary to span the distance (5-6 Å) required to bridge the two copper centers. Work is currently underway on the growth of single crystals of the deoxy and oxy forms of the  $[Cu^I(imidH)_2DAP]^+$  species for x-ray study to determine what, if any, geometrical changes occur during the oxygenation procedure.<sup>58</sup> Reversible oxygenation of a Cu(I) complex most probably depends upon two factors: the stability of the Cu(I) center

with respect to oxidation and the flexibility of the coordinating ligand toward geometrical changes which may occur during the oxidative addition reaction.

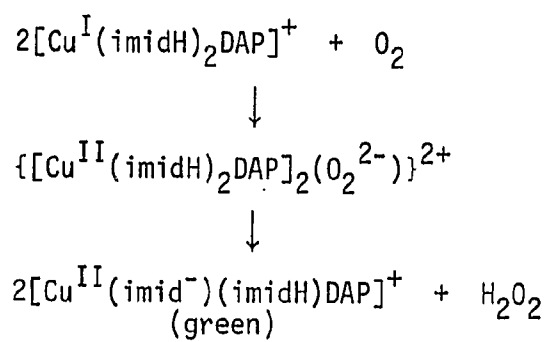
The  $\text{Cu(II)} \rightleftharpoons \text{Cu(I)}$  cyclic voltammograms in the absence and presence of dissolved dioxygen for compounds (A)-(F) provide valuable information concerning the nature of the copper(I)-dioxygen reaction. The disappearance of the anodic peak under a dioxygen atmosphere is undoubtedly due to the reaction of dioxygen with the electrochemically generated Cu(I) center. The reappearance of the anodic wave upon scanning with no hold indicates that the electrode surface is not contaminated with any oxidized products that would have prevented the observation of the anodic wave. With  $[\text{Cu}^{\text{II}}(\text{imidR})(\text{imidH})\text{DAP}]^{2+}$  behaving electrochemically most closely to the parent  $[\text{Cu}^{\text{II}}(\text{imidH})_2\text{DAP}]^{2+}$  compound, these results are quite consistent with the "electrode mechanism for the oxygen reaction" as proposed previously.<sup>37,38</sup> Essentially the Cu(II) complex is reduced under a dioxygen atmosphere, as the potential is scanned negative of the  $E_{1/2}$ . During the holding procedure, at -0.60 V, the electrochemically generated Cu(I) is allowed to react with a dissolved dioxygen molecule. The proposed oxidative addition reaction involves the chemical bonding of  $\text{O}_2$  with two Cu(I) centers, whereby these metal ions are "oxidized" to the Cu(II) state and the dioxygen is "reduced" to the peroxide anion. According to this mechanism, the oxy form of this complex has a binuclear structure  $[\text{LCu}^{\text{II}}-\text{O}_2^{2-}-\text{Cu}^{\text{II}}\text{L}]$ , where the two Cu(II) ions are linked by a  $\mu$ -peroxo bridge and L represents the unreacted ligand structure. Thus, as the potential scan is then reversed

toward the positive direction, there is no anodic wave because there is no available Cu(I) species to be oxidized.

An alternate discussion of the oxygenation process could involve some kind of "proton involvement" mechanism (Figure 28). In this proposal the  $\mu$ -dioxygen (or  $\mu$ -peroxo) species serves as only an intermediate from which proton abstraction can occur to give, for example,  $H_2O_2$  and a mono-deprotonated oxidized  $Cu^{II}$  product,  $[Cu^{II}(imid^-)(imidH)DAP]^+$ . In fact, a similar deprotonation scheme has recently been proposed for the reaction of  $O_2$  with  $[Fe^{II}(2,2'-bi-2-imidazoline)_3]^{2+}$ .<sup>59</sup> The final  $[Cu^{II}(imid^-)(imidH)DAP]^+$  product would need to be dimerized or polymerized to adequately explain the observed reduction in epr intensity of the oxy form.<sup>33,37</sup>

While both mechanisms have validity with respect to the  $[Cu^I(imidH)_2DAP]^+$  complex, the  $[Cu^I(imidR)_2DAP]^+$ ,  $[Cu^I(imidR)(py)DAP]^+$ ,  $[Cu^I(imidH)(py)DAP]^+$ , and  $[Cu^I(imidR)(imidH)DAP]^+$  compounds have been synthesized and examined toward elucidating the role of the proton in the oxygenation process. By the systematic elimination of the acidic ( $N_1$ -imidazole) proton from the ligand structure and subsequent study of reactivity of these Cu(I) complexes toward dioxygen, the proton involvement mechanism has been tested. The  $[Cu^I(imidR)(py)DAP]^+$  complex, containing no acidic imidazole protons, is found not to react with dioxygen in a stoichiometric reversible fashion. Yet the  $[Cu^I(imidR)_2DAP]^+$  and  $[Cu^I(imidR)(imidH)DAP]^+$  species do absorb  $O_2$  (1  $O_2$ :2 Cu), each at a rate similar to that of the parent  $[Cu^I(imidH)_2DAP]^+$  compound. Since the oxygenation of these Cu(I) solutions is partially reversed

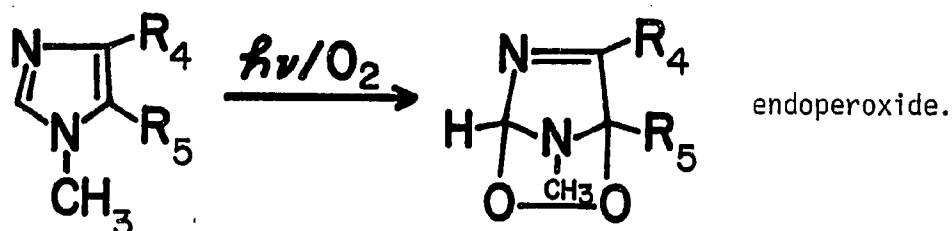


Figure 28A Proposed Proton Involvement Mechanism

by a nitrogen gas purge, the  $[\text{Cu}^{\text{I}}(\text{imidR})_2\text{DAP}]^+$  and  $[\text{Cu}^{\text{I}}(\text{imidR})-(\text{imidH})\text{DAP}]^+$  derivatives parallel the dioxygen reactivity profile of the  $[\text{Cu}^{\text{I}}(\text{imidH})_2\text{DAP}]^+$  complex. The hybrid  $[\text{Cu}^{\text{I}}(\text{imidH})(\text{py})\text{DAP}]^+$  species seems to be a "borderline" case between reversible oxygenation and irreversible oxidation of the Cu(I) center. This Cu(I) complex reacts stoichiometrically with dioxygen (1  $\text{O}_2$ :2 Cu), but at a much slower rate than the other dioxygen-active Cu(I) species A, D, and F, and the oxygenation process appears to be irreversible. Clearly, the oxygenation process for the  $[\text{Cu}^{\text{I}}(\text{imidR})_2\text{DAP}]^+$  complex cannot follow the proton involvement mechanism. Possibly the mechanism for the  $[\text{Cu}^{\text{I}}(\text{imidH})_2\text{DAP}]^+$  and  $[\text{Cu}^{\text{I}}(\text{imidR})_2\text{DAP}]^+$  complexes' reactivity toward dioxygen differ, but it is unlikely given the available experimental data.

The reactivity of these copper(I) compounds toward dioxygen could involve complex ligand oxidation reactions, rather than a simple ligation (oxidative addition reaction) of  $\text{O}_2$  to two Cu(I) centers. The most likely site for some kind of ligand oxidation would be the imidazole (imidX) moiety. While imidazoles are quite difficult to oxidize, "drastic" oxidation of the methylbenzimidazoles by concentrated potassium permanganate solution removes the benzene portion of the compound with the formation of 4,5-imidazoledicarboxylic acid.<sup>60</sup> Subsequent decarboxylation, with heating, yields the unsubstituted imidazole compound. A well-documented mechanism involving the oxidation of the imidazole ring structure,<sup>61-64</sup> using dioxygen as an oxidant, might be invoked to explain the observed reactivity of these Cu(I) complexes toward dioxygen. When in the presence of dyes, such as rose bengal or methylene blue, and visible light, triplet oxygen is photosensitized

to singlet oxygen, which then reacts with imidazoles to yield several photooxidized products, including the endoperoxide intermediate:<sup>61</sup>



While some substituted endoperoxides undergo a reverse Diels-Alder reaction at low temperature to regenerate a portion of singlet oxygen and the starting material, the majority of substituted endoperoxides do not regenerate starting imidazoles but form a complex mixture of products.<sup>62</sup> Unsubstituted imidazole undergoes a very slow photooxidation (requiring about two weeks), and the irradiation usually causes irreversible degradation of the heteromolecule. In addition, the oxygenation of histidine requires greater than one mole dioxygen per mole substrate destroyed and yields several complicated products.<sup>63,64</sup> This photooxidation procedure has also been employed to elucidate structure-function relationships in the hemocyanins.<sup>65,66</sup> In the photochemical irradiation of *octopus vulgaris* hemocyanin, using various external photosensitizers, tryptophanyl and histidyl side chain residues are selectively photooxidized, forming endoperoxide-like intermediates; fluorescence emission spectra of the photooxidized protein indicate that in addition to histidine, a tryptophanyl residue may be located near the copper-dioxygen binding site in hemocyanin.<sup>65</sup> To examine the possibility of endoperoxide formation [perhaps catalyzed by Cu(I)] in the present oxygenation reaction, the oxygenation of the

$[\text{Cu}^{\text{I}}(\text{imidH})_2\text{DAP}]^+$ ,  $[\text{Cu}^{\text{I}}(\text{imidR})_2\text{DAP}]^+$ ,  $[\text{Cu}^{\text{I}}(\text{imidR})(\text{imidH})\text{DAP}]^+$ , and  $[\text{Cu}^{\text{I}}(\text{imidH})(\text{py})\text{DAP}]^+$  species has been examined in the dark, but no noticeable difference in the red  $\rightleftharpoons$  green oxygenation cycle is observed. Thus, the lack of light has no qualitative effect on the oxygenation procedure. These results clearly indicate that an imidazole photo-oxidation reaction mechanism is at best a remote possibility. After discussing the proton involvement and imidazole photooxidation mechanisms, the oxidative addition reaction mechanism is still the most feasible explanation for the observed reversible reactivity of these copper(I) complexes toward dioxygen.

#### EPR Results

The oxygenated Cu(I) species, described above as  $[\text{LCu}^{\text{II}}-\text{O}_2^{2-}-\text{Cu}^{\text{II}}\text{L}]$ , may be diamagnetic via strong antiferromagnetic coupling between the two Cu(II)  $S = 1/2$  centers, mediated by the  $\mu$ -peroxo bridge. Such diamagnetic systems would be EPR silent, as is oxyhemocyanin. Thus, much information can be elucidated through an EPR spectroscopic study of these deoxy and oxy Cu(I) species, as well as the analogous Cu(II) complexes. The EPR spectral data obtained at 100 K for the Cu(II)  $S = 1/2$  systems depict spectral characteristics typical for electronically isolated Cu(II) centers in a four- or five-coordinate geometry (Figures 29 and 30).<sup>67</sup> In fact, the  $g_{||}$ ,  $g_{\perp}$ , and  $a_{||}$  parameters presented in Table 8 are strikingly similar to those obtained for two square pyramidal species,  $[\text{Cutrien}(\text{CH}_2\text{CH}_3)_6\text{Cl}_2]$  ( $g_{||} = 2.22$ ,  $g_{\perp} = 2.06$ ,  $a_{||} = 158$  G) and  $[\text{Cutrien}(\text{CH}_2\text{CH}_3)_6\text{Br}_2]$  ( $g_{||} = 2.22$ ,  $g_{\perp} = 2.05$ ,  $a_{||} = 158$  G) where trien = 1,4,7,10-tetraazadecane.<sup>68</sup> Signals obtained for the

Figure 29

EPR Spectra for the Copper Complexes as  
Me<sub>2</sub>SO Glasses at 100 K, 10<sup>-3</sup> M Copper

- A)  $[\text{Cu}^{\text{II}}(\text{imidH})(\text{py})\text{DAP}]^{2+}$
- B)  $[\text{Cu}^{\text{II}}(\text{imidR})_2\text{DAP}]^{2+}$
- C)  $[\text{Cu}^{\text{II}}(\text{imidR})(\text{py})\text{DAP}]^{2+}$

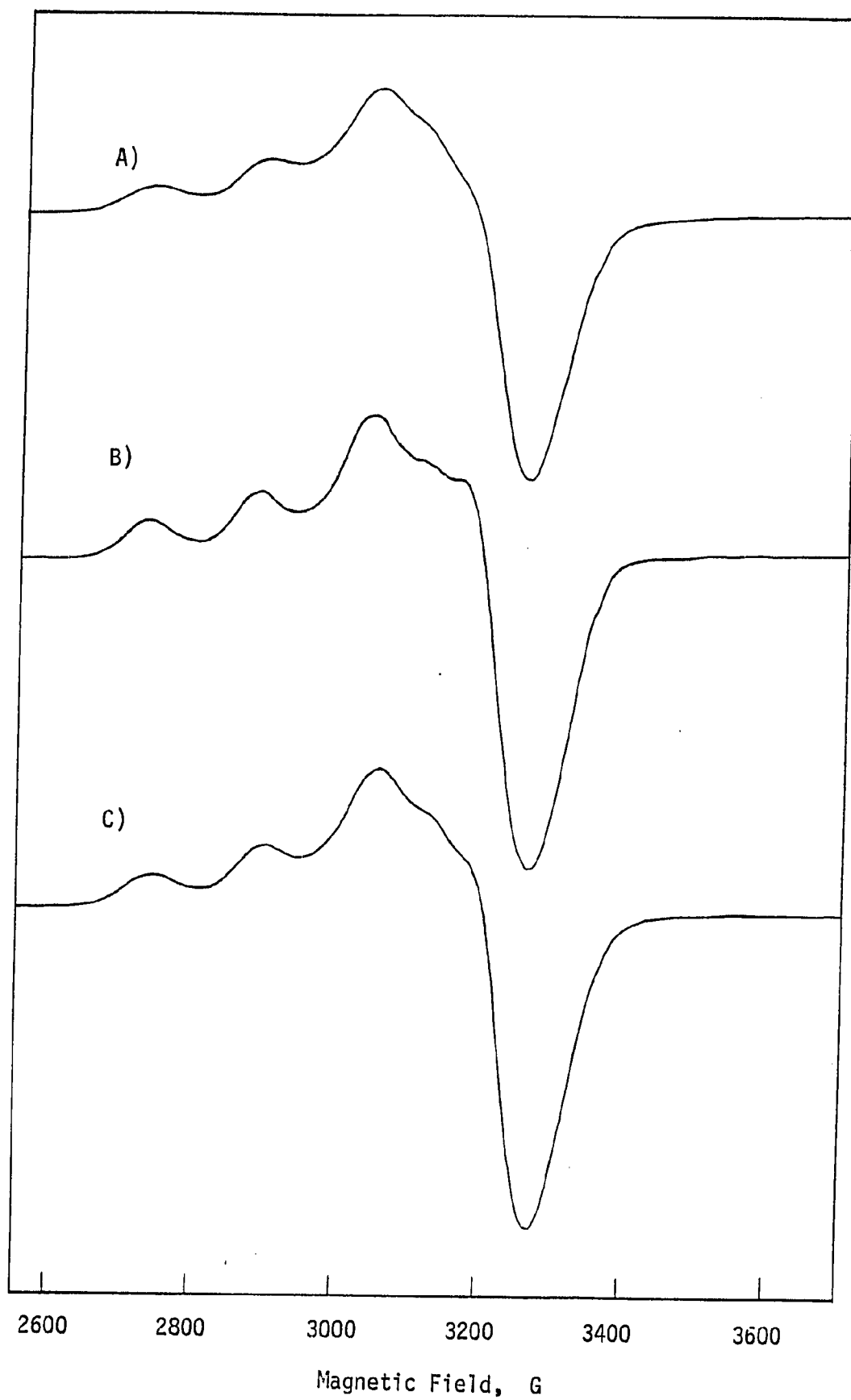


Figure 30

EPR Spectra for the Copper Complexes as  
Me<sub>2</sub>SO Glasses at 100 K, 10<sup>-3</sup> M Copper

- a)  $[\text{Cu}^{\text{II}}(\text{imidR})(\text{imidH})\text{DAP}]^{2+}$
- b)  $[\text{Cu}^{\text{I}}(\text{imidR})(\text{imidH})\text{DAP}]^{+}$  (2X actual intensity)
- c) Solution b) after absorption of 0.5:1 mole O<sub>2</sub>:Cu  
(oxygenated solution; 2X actual intensity)
- d) Solution c) degassed with nitrogen  
(redeoxygenated solution; 2X actual intensity)

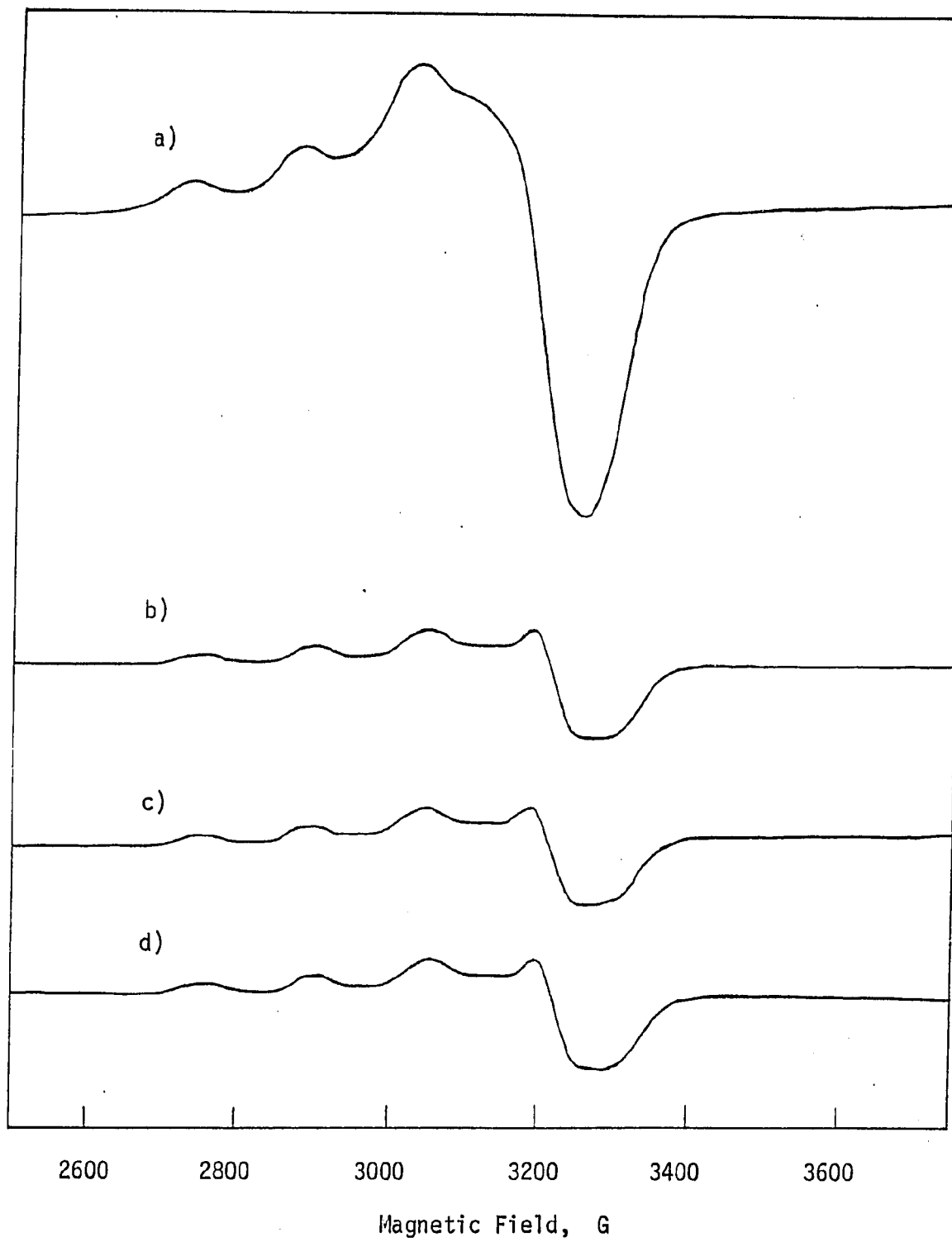




Table 8  
 EPR Data for the Copper Complexes as  
Me<sub>2</sub>SO Glasses at 100 K, 10<sup>-3</sup> M Copper

| Compound  | $g_{  }$ | $g_{\perp}$ | $a_{  }^a$ (Gauss) |
|---|----------|-------------|--------------------|
| [Cu <sup>II</sup> (imidH)(py)DAP] <sup>2+</sup>           | 2.21     | 2.07        | 155                |
| [Cu <sup>II</sup> (imidR) <sub>2</sub> DAP] <sup>2+</sup> | 2.22     | 2.06        | 150                |
| [Cu <sup>II</sup> (imidR)(py)DAP] <sup>2+</sup>           | 2.21     | 2.06        | 155                |
| [Cu <sup>II</sup> (imidR)(imidH)DAP] <sup>2+</sup>        | 2.22     | 2.06        | 145                |
| [Cu <sup>I</sup> (imidR)(imidH)DAP] <sup>+</sup> *        |          |             |                    |
| (b)   | 2.22     | 2.05        | 145                |
| (c)   | 2.22     | 2.06        | 150                |
| (d)   | 2.22     | 2.05        | 145                |

\* Refers to Figure 30; only 5-10% of available copper is detected as Cu<sup>II</sup>.

a)  $a_{||}$  = hyperfine splitting constant (the separation between the first two absorption peaks of the spectrum at the low end of the magnetic field).

deoxy and oxy forms of the Cu(I) compounds represent small amounts of oxidized Cu(II) impurities since EPR spectra for both deoxy and oxy derivatives are very similar with no increase in signal intensity or multiplicity (for example, see Figure 30). Thus the deoxy and oxy forms of the dioxygen-active Cu(I) complexes B, D, and F, like the parent  $[\text{Cu}^{\text{I}}(\text{imidH})_2\text{DAP}]^+$  deoxy and oxy forms,<sup>34</sup> are essentially EPR silent at 100 K. Then the proposed  $[\text{LCu}^{\text{II}}-\text{O}_2^{2-}-\text{Cu}^{\text{II}}\text{L}]$  structural unit appears to electronically mimic the EPR silent behavior of oxyhemocyanin,<sup>10</sup> where the Cu(II) centers are fully spin-coupled with  $-J \geq 550 \text{ cm}^{-1}$ .<sup>11</sup>

### Magnetochemical Studies

Variable temperature magnetic susceptibility measurements (80-250 K) on the oxygenated solution of the  $[\text{Cu}^{\text{I}}(\text{imidH})_2\text{DAP}]^+$  complex have determined the approximate spin-coupling constant ( $-J$  value) for this model system. The magnetochemical data are recorded in Tables 9-11. The deoxy- $[\text{Cu}^{\text{I}}(\text{imidH})_2\text{DAP}]^+$  sample, under argon gas, exhibits normal Curie behavior indicating the presence of paramagnetic Cu(II) impurity. This impurity, observed also in the deoxy- $[\text{Cu}^{\text{I}}(\text{imidH})_2\text{DAP}]^+$  EPR spectrum, provides a constant amount of paramagnetism to the overall magnetic moment of the Cu(I) samples but does not affect the determination of the antiferromagnetic coupling constant. The variable temperature magnetic susceptibility data for the oxy- $[\text{Cu}(\text{imidH})_2\text{DAP}]^{n+}$ ,  $[\text{Zn}^{\text{II}}(\text{imidH})_2\text{DAP}]^{2+}$  under dioxygen atmosphere, and  $[\text{Zn}^{\text{II}}(\text{imidH})_2\text{DAP}]^{2+}$  under argon gas have also been obtained. Using the molar susceptibilities of the two Zn(II) preparations (constant over the full temperature range) as diamagnetic blanks and the molar susceptibility of the

Table 9

Magnetochemical Data on Deoxygenated-  
 $[\text{Cu}(\text{imidH})_2\text{DAP}](\text{BF}_4)$  Solution at 0.1 M Copper in  $\text{Me}_2\text{SO}$

| $T, (\text{K})$ | $T^{-1}, (\text{K}^{-1})$ | $\chi_M' \times 10^{-3}, (\text{cgsu})^*$ | $\mu_{\text{eff}}, (\mu_B)$ |
|-----------------|---------------------------|---|-----------------------------|
| 83.0            | 0.0120                    | 1.75                                      | 1.08                        |
| 85.0            | 0.0118                    | 1.57                                      | 1.03                        |
| 87.4            | 0.0114                    | 1.57                                      | 1.05                        |
| 89.5            | 0.0112                    | 1.53                                      | 1.05                        |
| 92.4            | 0.0108                    | 1.56                                      | 1.08                        |
| 99.0            | 0.0101                    | 1.57                                      | 1.12                        |
| 105.0           | 0.0095                    | 1.55                                      | 1.14                        |
| 115.0           | 0.0087                    | 1.57                                      | 1.20                        |
| 121.6           | 0.0082                    | 1.51                                      | 1.21                        |
| 131.5           | 0.0076                    | 1.48                                      | 1.25                        |
| 141.0           | 0.0071                    | 1.43                                      | 1.27                        |
| 155.0           | 0.0065                    | 1.35                                      | 1.30                        |
| 179.0           | 0.0056                    | 1.25                                      | 1.34                        |
| 191.6           | 0.0052                    | 1.23                                      | 1.37                        |
| 210.0           | 0.0048                    | 1.06                                      | 1.33                        |

\*  $\chi_{M,\text{dia}}' = +0.04250$  cgsu  $\{[\text{Zn}(\text{imidH})_2\text{DAP}](\text{BF}_4)_2$  solution under argon}.

Table 10  
Magnetochemical Data on Oxygenated-  
[Cu(imidH)<sub>2</sub>DAP](BF<sub>4</sub>) Solution at 0.1 M Copper in Me<sub>2</sub>SO

| $T, (K)$ | $T^{-1}, (K^{-1})$ | $\chi_M'' \times 10^{-3}, (cgsu)^*$ | $\mu_{eff}, (\mu_B)$ |
|----------|--------------------|-------------------------------------|----------------------|
| 82.4     | 0.0121             | 3.69                                | 1.56                 |
| 87.4     | 0.0114             | 3.32                                | 1.52                 |
| 91.0     | 0.0110             | 3.39                                | 1.57                 |
| 97.0     | 0.0103             | 3.56                                | 1.66                 |
| 103.7    | 0.0096             | 3.65                                | 1.74                 |
| 112.0    | 0.0089             | 3.55                                | 1.78                 |
| 120.5    | 0.0083             | 3.39                                | 1.81                 |
| 130.2    | 0.0077             | 3.31                                | 1.86                 |
| 141.4    | 0.0071             | 3.15                                | 1.89                 |
| 153.9    | 0.0065             | 2.97                                | 1.91                 |
| 166.9    | 0.0060             | 2.63                                | 1.88                 |
| 182.0    | 0.0055             | 2.29                                | 1.83                 |
| 199.5    | 0.0050             | 1.96                                | 1.77                 |
| 220.2    | 0.0045             | 1.71                                | 1.73                 |
| 250.0    | 0.0040             | 1.23                                | 1.57                 |

\*  $\chi_M''_{dia} = -0.0414$  cgsu {[Zn(imidH)<sub>2</sub>DAP](BF<sub>4</sub>)<sub>2</sub> solution, saturated on dioxygen}.

Table 11

Magnetochemical "Difference" Data on Oxygenated-  
[Cu(imidH)<sub>2</sub>DAP](BF<sub>4</sub>) Solution at 0.1 M Copper in Me<sub>2</sub>SO

| T, (K) | T <sup>-1</sup> , K <sup>-1</sup> ) | $\chi_M \times 10^{-3}$ , (cgsu) <sup>*</sup> | $\mu_{eff}$ , ( $\mu_B$ ) |
|--------|-------------------------------------|---|---------------------------|
| 82.4   | 0.0121                              | 2.11  | 1.18                      |
| 87.0   | 0.0115                              | 1.82  | 1.13                      |
| 87.4   | 0.0114                              | 1.75  | 1.11                      |
| 91.0   | 0.0110                              | 1.82  | 1.15                      |
| 97.0   | 0.0103                              | 1.99  | 1.24                      |
| 103.7  | 0.0096                              | 2.10  | 1.32                      |
| 112.0  | 0.0089                              | 1.98  | 1.33                      |
| 120.5  | 0.0083                              | 1.88  | 1.35                      |
| 130.2  | 0.0077                              | 1.79  | 1.37                      |
| 141.4  | 0.0071                              | 1.67  | 1.38                      |
| 153.9  | 0.0065                              | 1.56  | 1.39                      |
| 166.9  | 0.0060                              | 1.29  | 1.31                      |
| 182.0  | 0.0055                              | 1.04  | 1.23                      |
| 199.5  | 0.0050                              | 0.82  | 1.14                      |
| 220.2  | 0.0045                              | 0.71  | 1.12                      |
| 250.0  | 0.0040                              | 0.36  | 0.85                      |

\*  $\chi_M = \chi_M'' - \chi_M'$

deoxy-[Cu<sup>I</sup>(imidH)<sub>2</sub>DAP]<sup>+</sup> sample to serve as a blank for any oxidized Cu(II) impurities present, the "difference" molar susceptibility for the oxy-[Cu(imidH)<sub>2</sub>DAP]<sup>n+</sup> is calculated:

$$\chi_M, \text{ difference} = \{ \chi_{M, \text{oxy-[Cu(imidH)}_2\text{DAP]}^{n+}} - \chi_{M, [\text{Zn}^{\text{II}}(\text{imidH})_2\text{DAP}]^{2+} \text{ in dioxygen}} \} - \{ \chi_{M, \text{deoxy-[Cu}^{\text{I}}(\text{imidH})_2\text{DAP]}^+} - \chi_{M, [\text{Zn}^{\text{II}}(\text{imidH})_2\text{DAP}]^{2+} \text{ in argon}} \}.$$

Roughly, the Néel temperature ( $T_N$ ) is the point on the  $\chi_M$  vs.  $T^{-1}$  plot where a sharp change in slope is noted, indicating antiferromagnetically coupling.<sup>69</sup> As depicted in Figure 31, the  $T_N$  is about 105 K. Two Cu(II) centers undergoing antiferromagnetic coupling represent the classic model for a two  $S=1/2$  spin interaction, where  $H = -2J\mathbf{S}_1 \cdot \mathbf{S}_2$  and  $2J$  is the splitting between singlet and triplet energy levels.<sup>47</sup> The approximate coupling constant value ( $-J$ ) is expressed:<sup>69</sup>

$$-J(\text{cm}^{-1}) \approx 2/3 T_N(\text{K})$$

From this relationship, a  $-J$  value for oxy-[Cu(imidH)<sub>2</sub>DAP]<sup>n+</sup> is then estimated to be 70 cm<sup>-1</sup>. Thus this study provides further evidence that in the oxy-[Cu(imidH)<sub>2</sub>DAP]<sup>n+</sup> derivative, two Cu(II) centers may be linked by a  $\mu$ -peroxo bridge and are antiferromagnetically coupled.

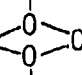
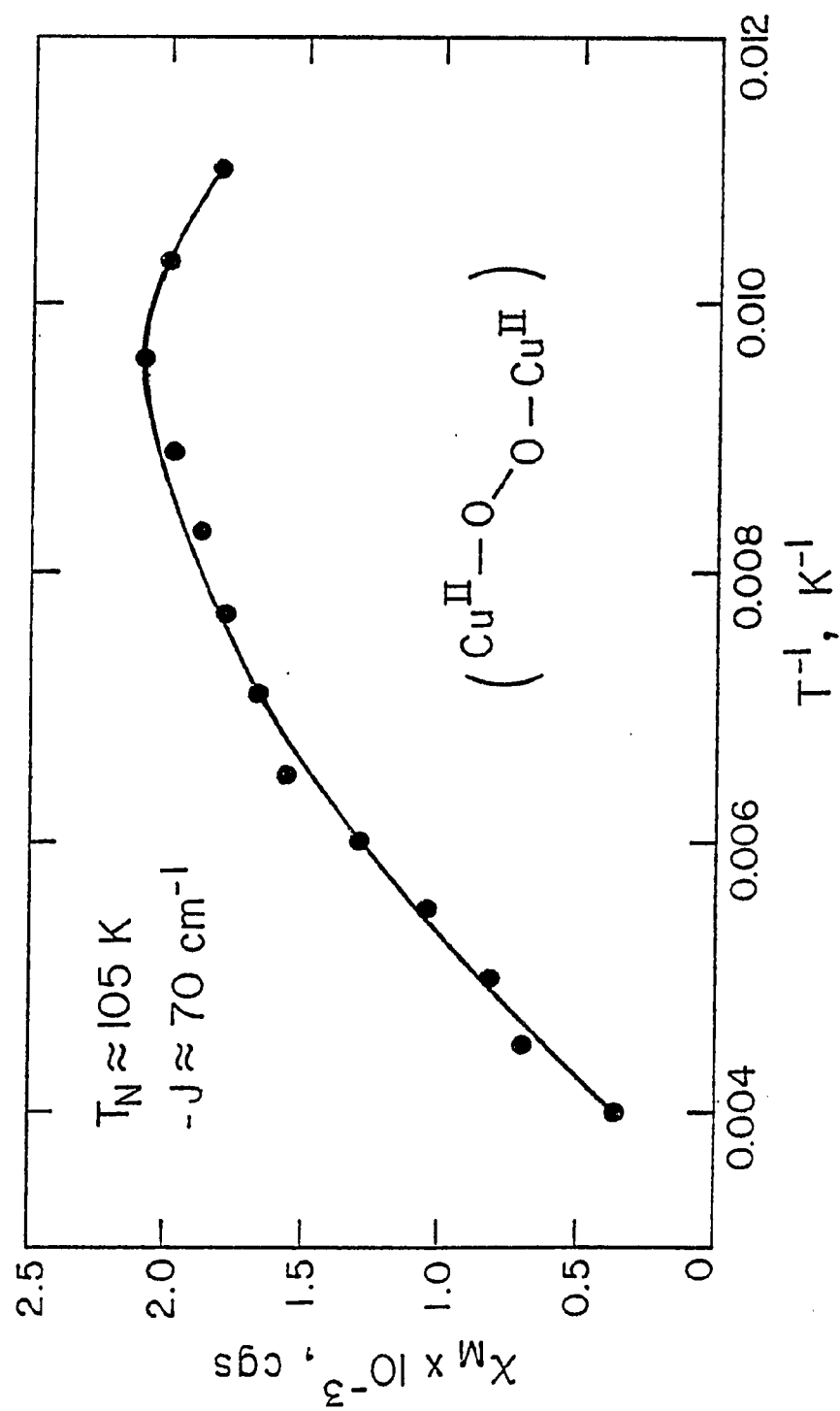
While there is no precedent in the literature for the size of  $-J$  for a metal dimer bridged by a  $\mu$ -peroxo linkage, this experimentally determined  $-J$  value is in line with a binuclear copper complex having two one-atom bridges, i.e., the dimeric [bis(pyridine-N-oxide)]copper(II)-nitrate has a  unit with  $-2J = 10\text{-}100 \text{ cm}^{-1}$ .<sup>70</sup> The magnitude of  $-J$  depends greatly on the geometrical relationship between the

Figure 31

$\chi_M$  vs. Temperature<sup>-1</sup> "Difference" Plot for the  
 Oxygenated-[Cu(imidH)<sub>2</sub>DAP](BF<sub>4</sub>) Solution in Me<sub>2</sub>SO at 0.1 M in Copper



orbitals on the metals with unpaired electron density and the ligand orbitals through which magnetic exchange is fostered. Since this relationship is most probably different for the oxy-Hcyn derivative compared to the oxygenated- $[\text{Cu}(\text{imidH})_2\text{DAP}]^{n+}$  species, a quantitative comparison between  $-J$  for the protein and the model copper-dioxygen compound cannot be made. However, these magnetochemical results qualitatively indicate that the copper centers in the oxy form of  $[\text{Cu}(\text{imidH})_2\text{DAP}]^+$  may be antiferromagnetically coupled through a  $\mu$ -peroxo like bridge, as depicted for oxyhemocyanin.

#### Resonance Raman Results

While EPR spectroscopic and magnetochemical techniques have been used to explore the nature of metal-ligand interactions, direct information about these interactions has been obtained from the assignment of the vibrational modes observed by infrared or Raman spectroscopy.<sup>8</sup> For example, the various mechanisms for a metal-dioxygen bonding scheme have been previously examined by the application of Fourier-transform infrared spectroscopy toward biological and synthetic metal-dioxygen complexes. Vibrational stretching frequencies ( $\nu_{\text{O-O}}$ ) for the uncomplexed dioxygen ligand in its various oxidation states have been determined:<sup>21</sup>  $\text{O}_2$ ,  $1556 \text{ cm}^{-1}$ ;  $\text{O}_2^-$  (superoxide),  $1145 \text{ cm}^{-1}$ ; and  $\text{O}_2^{2-}$  (peroxide),  $770 \text{ cm}^{-1}$ . Comparison between these tabulated values and the  $\nu_{\text{O-O}}$  (identified by the isotope shift in this  $\nu_{\text{O-O}}$  upon substitution of  $^{18}\text{O}_2$  for  $^{16}\text{O}_2$ ) observed for several oxygenated systems has led to the identification of the metal- $\text{O}_2$  bonding scheme in oxyhemoglobin ( $\text{HbO}_2$ ) and the oxy-"picket fence porphyrin" complexes.<sup>71</sup> As models for



the  $\text{HbO}_2$  active site structure, these synthetic iron porphyrins give  $\nu_{\text{O-O(st)}} = 1160 \text{ cm}^{-1}$ , near that for the free superoxide ion ( $1145 \text{ cm}^{-1}$ ) and ca.  $50 \text{ cm}^{-1}$  difference from  $1107 \text{ cm}^{-1}$  for  $\text{HbO}_2$ .<sup>72</sup> Thus these results suggest (and x-ray structural data confirm)<sup>20,21</sup> that the dioxygen molecule as a superoxide-like ligand is bound end-on to the iron center in both oxyhemoglobin and the oxy-picket fence porphyrins.

Although infrared spectroscopy has been used successfully in the study of a few metalloproteins, the enormous absorption of water in the IR spectrum has greatly hampered the IR examination of most biological systems.<sup>73</sup> Likewise, Raman spectroscopy has been marginally useful in these endeavors due to the low intensity of the Raman peaks. However, resonance enhancement of these Raman bands has been found to occur when the scattering molecules are excited with a laser beam of wavelength near an allowed electronic absorption band.<sup>74</sup> Hence the Raman spectrum has been intensified and resonance Raman (RR) spectroscopy has become a sensitive structural probe for metalloproteins with intense chromophores.<sup>75</sup> Recently, RR studies of several dioxygen-active proteins (e.g.,  $\text{HbO}_2$ ,<sup>76</sup> oxyhemerythrin,<sup>73</sup> and oxyhemocyanin)<sup>8,12,13</sup> and synthetic model compounds [e.g.,  $[\text{Co}(\text{salen})_2\text{L}]_2\text{O}_2$ <sup>77</sup> and oxy-picket fence porphyrins]<sup>78</sup> have successfully determined the bond order of the dioxygen ligand and hence the metal- $\text{O}_2$  bonding scheme. In the case of oxyhemocyanin, resonance Raman spectroscopy has been used by Loehr, et al.,<sup>8,12,13</sup> to define the mechanism of the copper-dioxygen interaction within the protein's active site unit, as well as identify the oxidation state of the copper ions. The oxyHcyn derivative has an intense absorption band at 345 nm ( $\epsilon$   $10,000 \text{ M}^{-1} \text{ cm}^{-1}$ ) and weaker bands

around 570 nm ( $\epsilon$  500  $\text{M}^{-1} \text{cm}^{-1}$ ). Laser excitation in the visible region has produced resonance enhancement of a Raman peak at  $744 \text{ cm}^{-1}$ , and based on an  $^{18}\text{O}_2$  isotope shift to  $704 \text{ cm}^{-1}$ , this band has been assigned to a  $\nu_{\text{O-O}}(\text{st})$  mode. This vibrational frequency is characteristic for the peroxide ( $\text{O}_2^{2-}$ ) anion and thus the mode of dioxygen-copper binding at oxyHcyn's active site may be represented as  $[\text{Cu}^{\text{II}}-\text{O}_2^{2-}-\text{Cu}^{\text{II}}]$ . As in the infrared study comparing  $\nu_{\text{O-O}}$  for  $\text{HbO}_2$  and the model oxy-picket fence porphyrins, resonance Raman techniques have been employed in this work to probe the oxygenated  $[\text{Cu}(\text{imidH})_2\text{DAP}]^{n+}$  species for an  $\nu_{\text{O-O}}$  that may be exhibited in this complex's resonance Raman spectrum. In order for this synthetic copper(I) compound to model the active site structure of oxyHcyn, with respect to the  $\text{Cu}-\text{O}_2$  bonding scheme, a  $\nu_{\text{O-O}}(\text{st})$  should be observed in the  $700\text{--}800 \text{ cm}^{-1}$  region of the resonance Raman spectrum.

The following RR spectroscopic studies have been conducted in the laboratories of Professor Thomas M. Loehr at the Oregon Graduate Center and Professor William H. Woodruff at the University of Texas using visible and ultraviolet wavelengths of excitation, respectively. Raman spectra for the deoxy and oxy forms of the  $[\text{Cu}(\text{imidH})_2\text{DAP}]^+$  species, the analogous Cu(II) complex, and the dioxygen-inactive  $[\text{Cu}(\text{PY})_2\text{DAP}]^+$  compound have been obtained by laser excitation of the visible wavelength region of the compounds' absorption spectra (see Figure 32). The signal to noise ratio observed in these visible wavelength excitation experiments is lower than expected for Raman signals undergoing selective resonance enhancement vide infra. Using the 514.4 nm wavelength of an argon laser for excitation, the Raman spectra shown in Figure 33, with the band positions listed in Table 12, were obtained

Figure 32

Electronic Absorption Spectra for the Copper Complexes

- a)  $[\text{Cu}^{\text{I}}(\text{py})_2\text{DAP}]^+$  in  $\text{CH}_3\text{CN}$  at 0.5 mM Copper.
- b) A)  $[\text{Cu}^{\text{I}}(\text{imidH})_2\text{DAP}]^+$  in  $\text{CH}_3\text{CN}$  at 0.5 mM Copper.
- B) Solution A after oxygenation under 1 atm for 5 minutes with absorption of 0.5 moles of  $\text{O}_2$  per Cu.
- C) Solution B after deoxygenation under reduced pressure.
- D) Solution B after a second oxy/deoxy cycle.
- E) Solution B after a third oxy/deoxy cycle.
- F)  $[\text{Cu}^{\text{II}}(\text{imidH})_2\text{DAP}]^{2+}$  in  $\text{CH}_3\text{CN}$  at 0.5 mM Copper.

(Taken from reference 37).

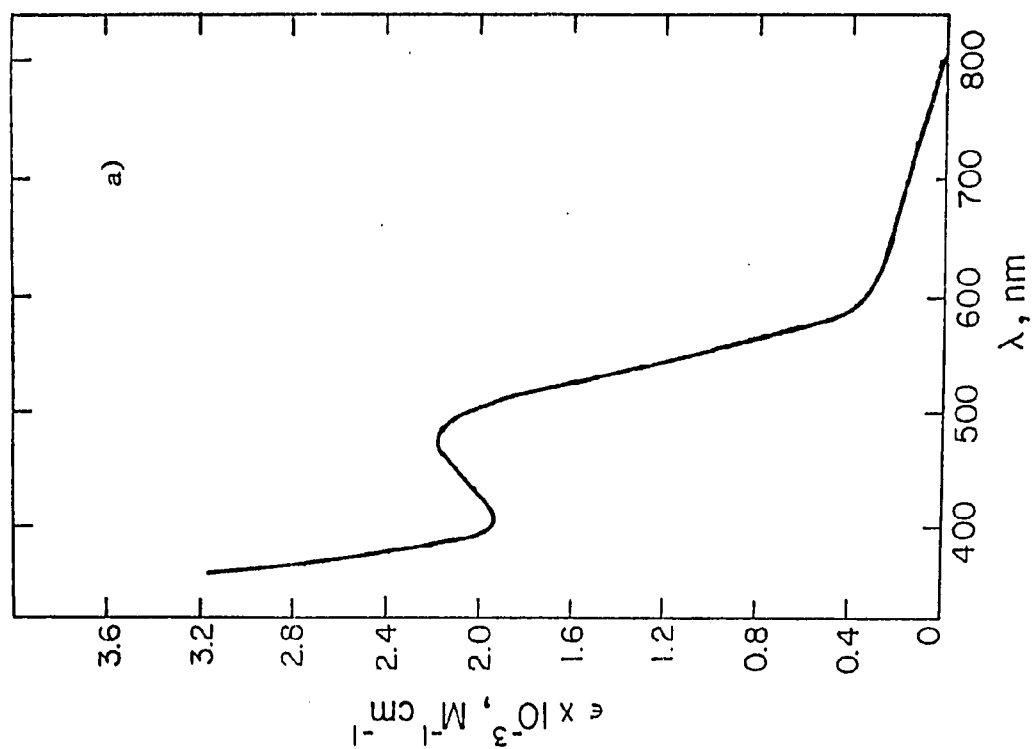
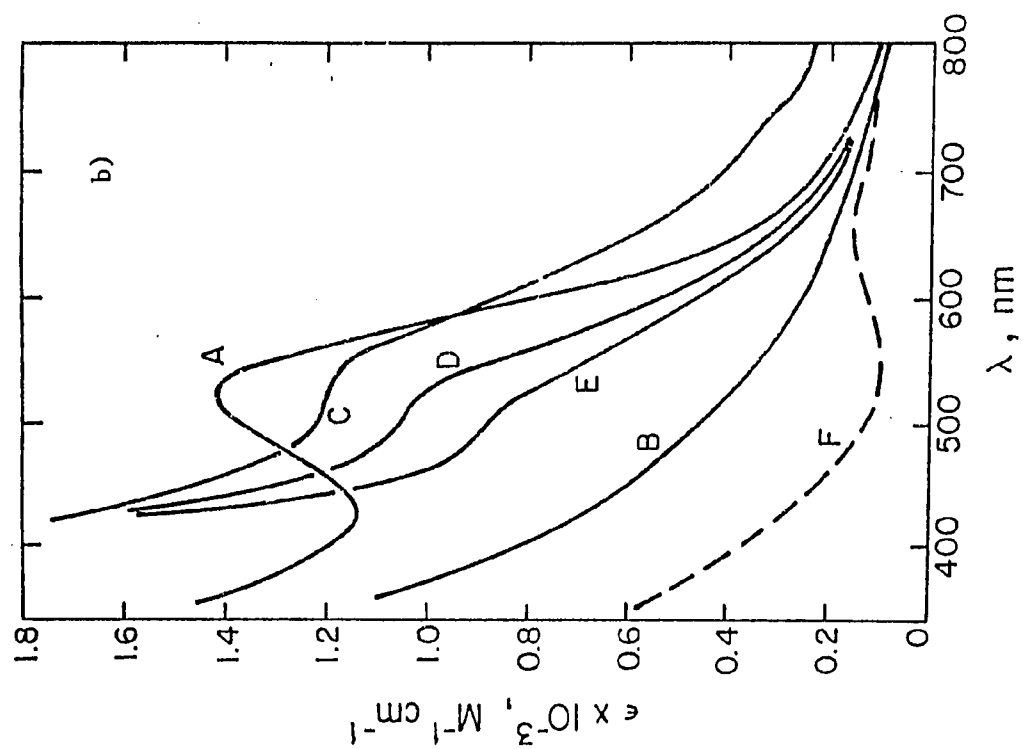
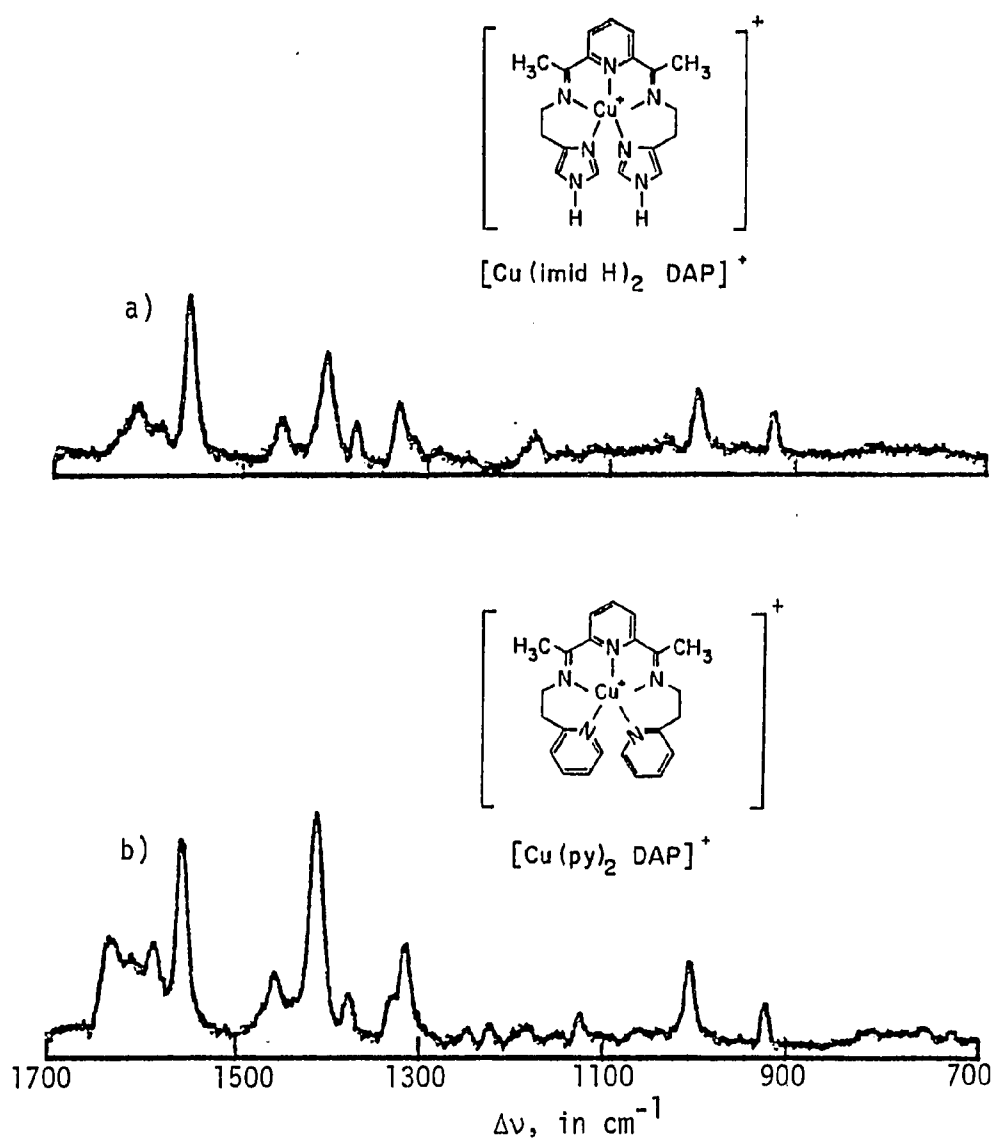


Figure 33

Raman Spectra of  $[\text{Cu}^{\text{I}}(\text{imidH})_2\text{DAP}]^+$  and  $[\text{Cu}^{\text{I}}(\text{py})_2\text{DAP}]^+$  Taken at 77 K with 0.1 M Copper in  $\text{CH}_3\text{CN}$ , Using a 514.5 nm Excitation Wavelength



\* (Solvent Peaks)

Table 12

Raman Spectral Data for the Cu(I) Complexes Using an  
Excitation Wavelength of 514.5 nm

| Signal Position $\Delta\nu_r$ , in $\text{cm}^{-1}$             |  |
|---|--|
| $[\text{Cu}^{\text{I}}(\text{imidH})_2\text{DAP}](\text{BF}_4)$ | $[\text{Cu}^{\text{I}}(\text{py})_2\text{DAP}](\text{BF}_4)$ |
| 1002(m)   | 726(w)   |
| 1181(w)   | 753(w)   |
| 1330(m)   | 811(w)   |
| 1409(s)   | 1002(s)  |
| 1467(m)   | 1123(w)  |
| 1557(s)   | 1150(w)  |
| 1588(m)   | 1182(w)  |
| 1613(m)   | 1223(w)  |
|   | 1247(w)  |
|   | 1314(s)  |
|   | 1327(m)  |
|   | 1409(s)  |
|   | 1513(w)  |
|   | 1557(s)  |
|   | 1588(s)  |
|   | 1611(s)  |
|   | 1635(s)  |

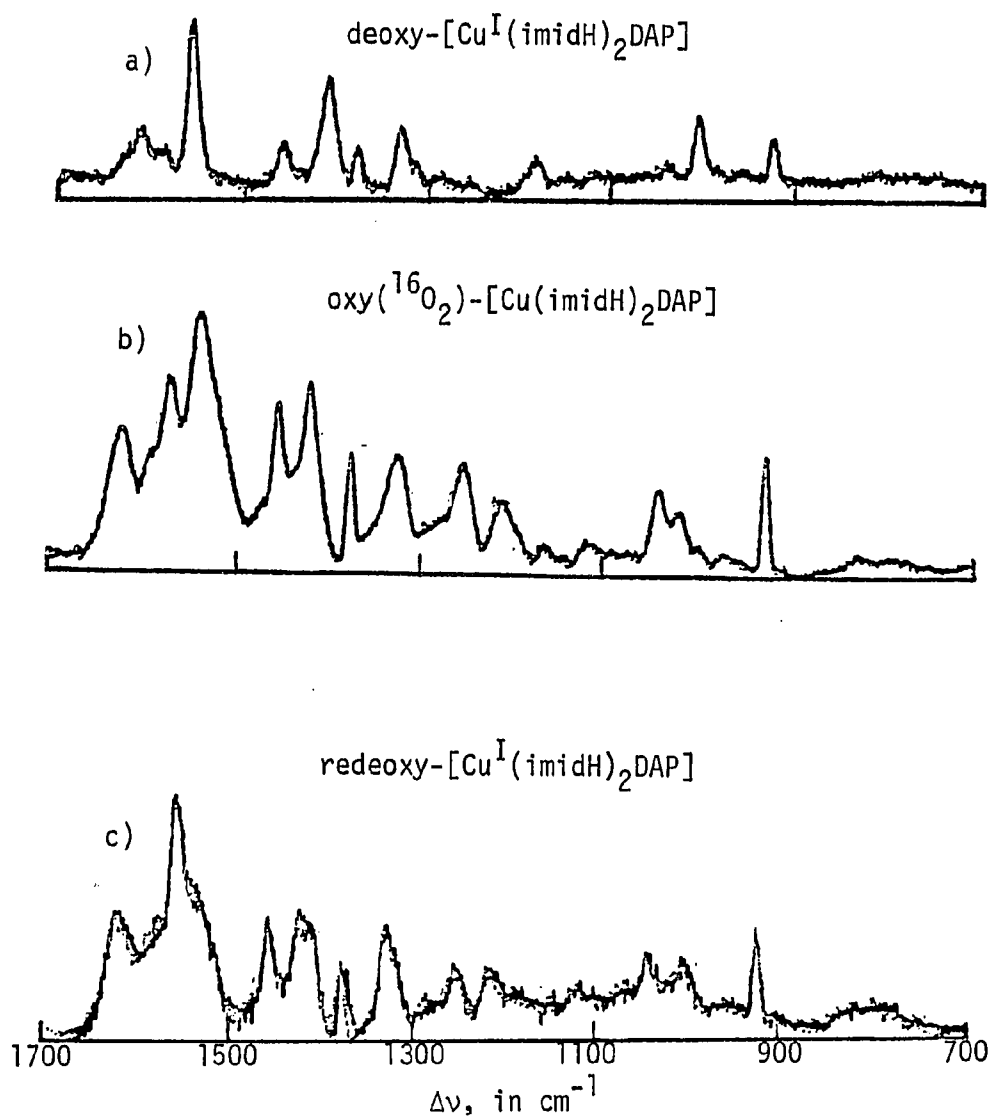
(s) = strong; (m) = medium; (w) = weak.

for  $[\text{Cu}(\text{imidH})_2\text{DAP}]^+$  and  $[\text{Cu}(\text{py})_2\text{DAP}]^+$  at 77 K in frozen, degassed solutions of  $\text{CH}_3\text{CN}$ . Raman peaks are observed at band positions of  $1000\text{--}1650\text{ cm}^{-1}$  from the  $\text{Ar}^+$  laser 514.5 nm plasma line. These positions are typical for excitation of metal-ligand charge transfer transitions. Comparing the Raman spectra for the two Cu(I) complexes, one observes that the  $[\text{Cu}(\text{py})_2\text{DAP}]^+$  derivative offers greater multiplicity in the Raman spectral peaks. This result is probably due to the presence of the additional pyridine moieties in the ligand structure, which contribute to a more complex Raman spectrum than in the case of the  $[\text{Cu}(\text{imidH})_2\text{DAP}]^+$  species.

Since these RR spectroscopic techniques were undertaken to characterize possible O-O stretching frequencies, the cycling between the deoxy, oxy, and redeoxy forms of the  $[\text{Cu}(\text{imidH})_2\text{DAP}]^+$  complex has been exhaustively monitored. Figure 34 and Table 13 depict the results of such a study. Clearly, the RR spectrum for the deoxy- $[\text{Cu}(\text{imidH})_2\text{DAP}]^+$  cation is not identical to that of the oxy- $[\text{Cu}(\text{imidH})_2\text{DAP}]^{n+}$  (oxygenated with dry, prepurified  $^{16}\text{O}_2$  gas). Unfortunately, no Raman-active  $\nu_{\text{O-O(st)}}$  could be identified in Figure 34. The region of interest for an  $\text{O}_2^{2-}$  (peroxide-like) stretching frequency would be approximately  $700\text{--}800\text{ cm}^{-1}$  as the  $\nu_{\text{O-O(st)}}$  for the  $\text{O}_2^{2-}$  in oxyHcyn is  $744\text{ cm}^{-1}$ . However, this region of the Raman spectrum shows no absorption bands. When the green oxygenated material is purged with prepurified nitrogen gas, the light red redeoxy- $[\text{Cu}(\text{imidH})_2\text{DAP}]^+$  solution forms. The Raman spectrum of a frozen aliquot of this redeoxy-Cu(I) species contains peaks from both the deoxy and oxy- $[\text{Cu}(\text{imidH})_2\text{DAP}]^{n+}$  derivatives. In particular, the signal at  $1409\text{ cm}^{-1}$  in Figure 34-a) is absent in

Figure 34

Raman Spectra Taken at 77 K with 0.1 M Copper in  $\text{CH}_3\text{CN}$ ,  
Using 514.5 nm (for a) and 457.9 nm (for b and c) Excitation Wavelengths



\* (Solvent Peaks)



Table 13

| Raman Spectral Data for the Deoxy, Oxy, and Redeoxy<br>Forms of the $[\text{Cu}^{\text{I}}(\text{imidH})_2\text{DAP}](\text{BF}_4)$ Complex |   |
|---|---|
| Signal Position $\Delta\nu_r \text{ cm}^{-1}$   |   |
| Deoxy- $[\text{Cu}^{\text{I}}(\text{imidH})_2\text{DAP}]$   | Redeoxy- $[\text{Cu}^{\text{I}}(\text{imidH})_2\text{DAP}]$ |
| 514.5 nm Excitation   | 457.9 nm Excitation   |
| 1002(m)   | 819(w)  |
| 1181(w)   | 1002(m)   |
| 1330(m)   | 1011(m)   |
| 1409(s)   | 1068(w)   |
| 1467(m)   | 1117(m)   |
| 1557(s)   | 1148(w)   |
| 1588(m)   | 1186(w)   |
| 1613(m)   | 1215(m)   |
| Oxy( $^{16}\text{O}_2$ )- $[\text{Cu}(\text{imidH})_2\text{DAP}]$   | 1253(m)   |
| 457.9 nm Excitation   | 1284(w)   |
| 821(w)  | 1316(sh)  |
| 1013(w)   | 1329(s)   |
| 1116(w)   | 1413(s)   |
| 1163(w)   | 1538(sh)  |
| 1212(m)   | 1557(s)   |
| 1254(m)   | 1610(sh)  |
| 1275(m)   | 1622(s)   |
| 1321(s)   | (s) = strong  |
| 1540(s)   | (m) = medium  |
| 1573(s)   | (w) = weak  |
| 1623(s)   | (sh) = shoulder   |

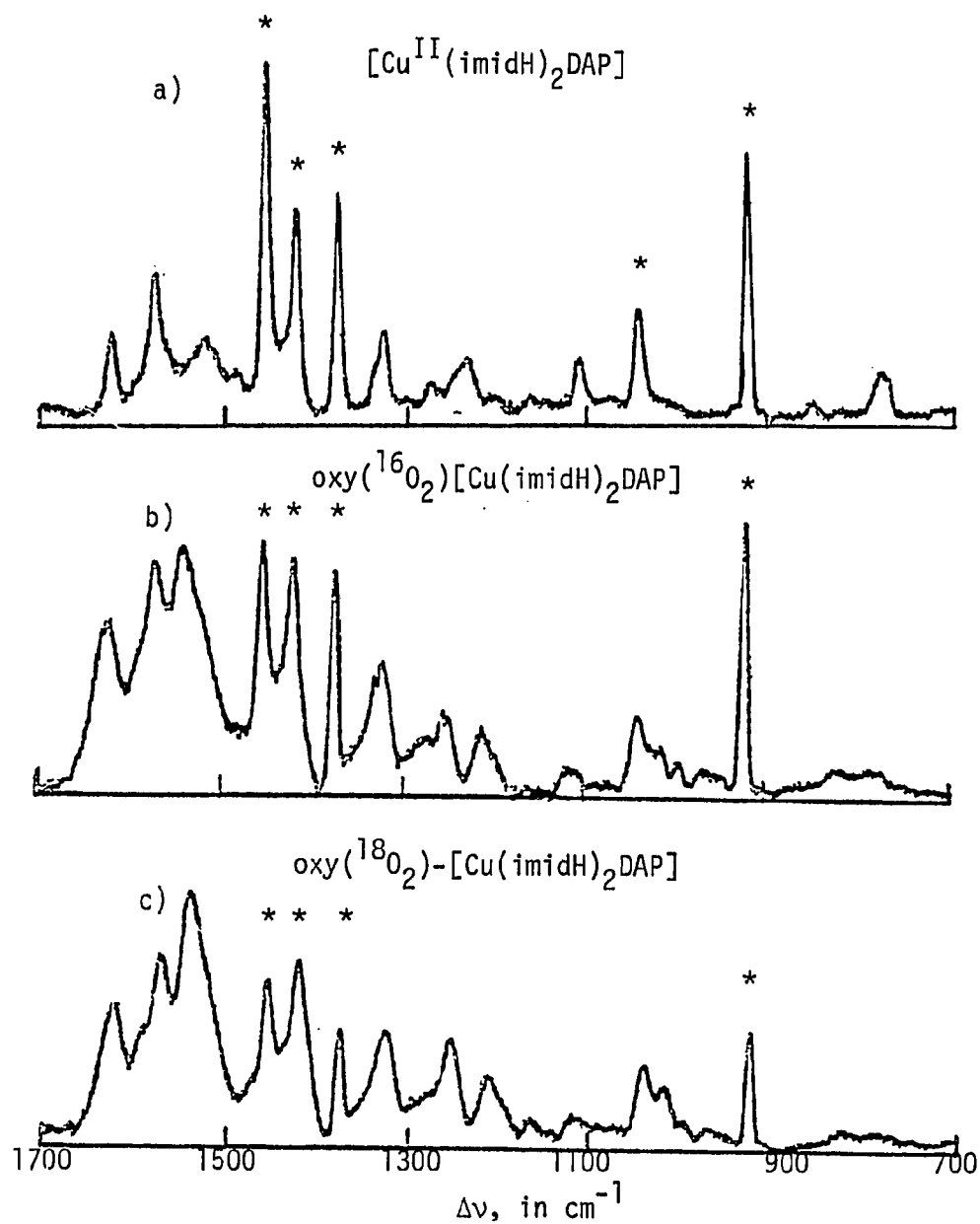
Figure 34-b) and is definitely present in Figure 34-c). Also in the Raman spectrum of the redeoxy material are signals present in the spectrum of the oxy derivative, i.e., the  $1215\text{ cm}^{-1}$  and  $1253\text{ cm}^{-1}$  peaks. Thus, the resonance Raman data show only partial reversibility of the dioxygen cyclization process. The data obtained from the electronic spectral study of the oxygenation reaction also confirm this observation.<sup>37</sup>

In addition to oxygenation by  $^{16}\text{O}_2$  gas, the  $[\text{Cu}(\text{imidH})_2\text{DAP}]^+$  species was treated with  $^{18}\text{O}_2$  gas. Figure 35 and Table 14 illustrate the Raman spectral data obtained from the  $^{16}\text{O}_2$  and  $^{18}\text{O}_2$  derivatives of oxygenated- $[\text{Cu}(\text{imidH})_2\text{DAP}]^{n+}$ , as well as for the  $[\text{Cu}^{\text{II}}(\text{imidH})_2\text{DAP}]^{2+}$  complex. Since the  $^{16}\text{O}_2$ - and  $^{18}\text{O}_2$ - oxy forms of  $[\text{Cu}(\text{imidH})_2\text{DAP}]^{n+}$  exhibit essentially identical Raman spectral bands, no isotope effect is observed. However, the analogous Cu(II) compound's Raman spectrum differs substantially. Most noticeably, the intensity and multiplicity of signals in the  $1300\text{--}1700\text{ cm}^{-1}$  range for the  $^{16}\text{O}_2$ - and  $^{18}\text{O}_2$ -copper derivatives are very dissimilar to that of the oxidized  $[\text{Cu}^{\text{II}}(\text{imidH})_2\text{DAP}]^{2+}$  compound. Thus, the oxygenated- $[\text{Cu}(\text{imidH})_2\text{DAP}]^{n+}$  is definitely not the oxidized  $[\text{Cu}^{\text{II}}(\text{imidH})_2\text{DAP}]^{2+}$  complex.

While the RR experiments involving laser excitation into the visible wavelengths of absorption have yielded some information concerning the oxygenation of the  $[\text{Cu}^{\text{I}}(\text{imidH})_2\text{DAP}]^+$  species, the UV excitation RR study has offered more insight into the copper-dioxygen reaction. In collaboration with Professor Woodruff's laboratory, RR spectra have been obtained at room temperature for the oxy( $^{16}\text{O}_2$ )- $[\text{Cu}(\text{imidH})_2\text{DAP}]^{n+}$ ,  $[\text{Cu}^{\text{II}}(\text{imidH})_2\text{DAP}]^{2+}$ , and  $[\text{Cu}^{\text{II}}(\text{imidH})(\text{py})\text{DAP}]^{2+}$  acetonitrile solutions.

Figure 35

Raman Spectra Taken at 77 K with 0.1 M Copper in  $\text{CH}_3\text{CN}$ ,  
 Using 514.5 nm (for a and c) and 457.9 nm (for b) Excitation Wavelengths



\* (Solvent Peaks)

Raman Spectral Data for the Oxidized and  
Oxygenated Forms of the  $[\text{Cu}(\text{imidH})_2\text{DAP}](\text{BF}_4)$  Complex

| Signal Position $\Delta\nu_r$ , in $\text{cm}^{-1}$                   |   |
|---|---|
| $[\text{Cu}^{\text{II}}(\text{imidH})_2\text{DAP}]$                   | $\text{Oxy}({}^{16}\text{O}_2)-[\text{Cu}(\text{imidH})_2\text{DAP}]$ |
| 514.5 nm Excitation   | 457.9 nm Excitation   |
| 822(w)  | 821(w)  |
| 1015(m)   | 1013(w)   |
| 1116(w)   | 1116(w)   |
| 1164(w)   | 1163(w)   |
| 1212(m)   | 1212(m)   |
| 1253(m)   | 1254(m)   |
| 1325(m)   | 1275(m)   |
| 1542(s)   | 1321(s)   |
| 1575(s)   | 1540(s)   |
| 1626(s)   | 1573(s)   |
| $\text{Oxy}({}^{18}\text{O}_2)-[\text{Cu}(\text{imidH})_2\text{DAP}]$ | 1623(s)   |
| 514.5 nm Excitation   |   |
| 822(w)  | 1253(m)   |
| 1015(m)   | 1325(m)   |
| 1116(w)   | 1542(s)   |
| 1164(w)   | 1575(s)   |
| 1212(m)   | 1626(s)   |
| (s) = strong  |   |
| (m) = medium  |   |
| (w) = weak  |   |

Laser excitation wavelengths of 363.8 nm, 406.7 nm, and 413.1 nm were used. The resonance Raman spectral data gathered are listed in Tables 15 and 16. Comparison between the Raman spectral information obtained for the  $[\text{Cu}^{\text{II}}(\text{imidH})_2\text{DAP}]^{2+}$  species in the visible and UV excitation experiments reveals several points of interest. Some RR signals appearing in the visible excitation Raman spectrum are not present when the UV laser lines are used for excitation. Thus resonance enhancement of the Raman peaks is observed in the UV excitation spectrum. While the resonance condition could be due to visible wavelength electronic transitions, the Raman bands found upon visible laser excitation are fairly weak in intensity considering the high concentration of solute (0.1 M). These lines are probably non-resonating Raman lines. The resonance enhancement of Raman lines most likely originates from the UV electronic transitions, with the source of these transitions being vibrating "ring modes" of the ligand. The fact that the signal intensities relative to each other differ as the various UV excitation lines are employed is further support for this UV-based selective enhancement phenomenon (see Table 15).

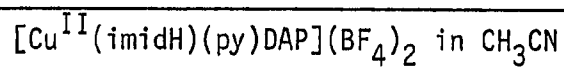
No RR spectrum of the deoxy- $[\text{Cu}^{\text{I}}(\text{imidH})_2\text{DAP}]^+$  species was obtained though several concentrations of copper complex and various UV laser lines of excitation were used. As this compound exhibits a fairly sizeable molar extinction coefficient in the region of excitation lines (ca.  $1500 \text{ M}^{-1} \text{ cm}^{-1}$ ), it probably absorbs too much of this laser line energy to allow for any resonance enhancement of the Raman lines. In other words, "self-absorption" by the Cu(I) complex precludes the collection of a RR spectrum. The oxy( $^{16}\text{O}_2$ )- $[\text{Cu}(\text{imidH})_2\text{DAP}]^{n+}$  deriva-

## Resonance Raman Spectral Data of the Copper Complexes Taken at 295 K

| $[\text{Cu}^{\text{II}}(\text{imidH})_2\text{DAP}](\text{BF}_4)_2$ in $\text{CH}_3\text{CN}$                      |                          |         |          |
|---|--------------------------|---------|----------|
| Excitation Wavelength, nm   | 413.1                    | 406.7   | 363.8    |
| Solute Concentration, $\text{M}$  | 0.0132                   | 0.0132  | 0.0136   |
| Signal Position $\Delta\nu_r$ , $\text{cm}^{-1}$  | 794(w)                   |         |          |
|   | 1072(w)                  |         |          |
|   | 1103(w)                  | 1104(w) |          |
|   | 1115(m)                  | 1115(m) |          |
|   | 1160(w)                  | 1163(w) |          |
|   | 1213(w)                  | 1214(w) |          |
|   | 1250(s)                  | 1251(s) |          |
|   | 1258(s)                  | 1257(s) | 1256(w)  |
|   | 1307(s)                  | 1308(s) | 1309(w)  |
|   | 1322(w)                  | 1324(w) | 1323(m)  |
|   | 1332(w)                  | 1340(w) |          |
|   | 1472(m)                  | 1472(m) |          |
|   | 1573(m)                  | 1574(m) | 1576(m)  |
|   | 1580(m)                  | 1580(m) | 1590(sh) |
|   | 1600(w)                  | 1603(w) |          |
|   | 1622(w)                  | 1621(w) | 1621(m)  |
| $\text{Oxy}(^{16}\text{O}_2)-[\text{Cu}(\text{imidH})_2\text{DAP}]$ , in $\text{CH}_3\text{CN}$ at 4.35 mM Copper |                          |         |          |
| Excitation Wavelength   | 363.8 nm                 |         |          |
| Signal Position $\Delta\nu_r$   | 1332(w) $\text{cm}^{-1}$ |         |          |
|   | 1572(m)                  |         |          |
|   | 1595(m)                  |         |          |
|   | 1620(w)                  |         |          |

Table 16

Resonance Raman Spectral Data Taken at 295 K for




---

|                               |                          |
|-------------------------------|--------------------------|
| Excitation Wavelength         | 406.7 nm                 |
| Solute Concentration          | 0.091 M                  |
| Signal Position $\Delta\nu_r$ | 1104(w) $\text{cm}^{-1}$ |
|                               | 1120(m)                  |
|                               | 1162(w)                  |
|                               | 1188(w)                  |
|                               | 1216(w)                  |
|                               | 1248(s)                  |
|                               | 1256(s)                  |
|                               | 1314(s)                  |
|                               | 1332(m)                  |
|                               | 1352(w)                  |
|                               | 1472(m)                  |
|                               | 1580(s)                  |
|                               | 1600(w)                  |

---

(s) = strong

(m) = medium

(w) = weak

tive yields an acceptable RR spectrum as catalogued in Table 15. As in the visible excitation study, the UV excitation experiment does not show the  $\nu_{O-O(st)}$ . Apparently, no significant ligand ( $\pi$  system) structural changes occur during the copper-dioxygen reaction since the 1300-1600  $\text{cm}^{-1}$  region of the RR spectrum is virtually identical, with respect to band position, for both the  $[\text{Cu}^{\text{II}}(\text{imidH})_2\text{DAP}]^{2+}$  and  $\text{oxy}(^{16}\text{O}_2)-[\text{Cu}(\text{imidH})_2\text{DAP}]^{n+}$  derivatives. In addition, most of the resonance enhancement results from the 300 nm transition of the  $[\text{Cu}^{\text{II}}(\text{imidH})_2\text{DAP}]^{2+}$  complex's absorption spectrum. Since the  $\text{oxy}(^{16}\text{O}_2)-[\text{Cu}(\text{imidH})_2\text{DAP}]^{n+}$  derivative has no such electronic spectral characteristic, it likewise has a more sparse RR spectrum. Comparison of this 1300-1600  $\text{cm}^{-1}$  region for these two copper samples reveals noticeable signal intensity differences. Thus the complex yielding the "Cu(II) RR" spectrum is not the complex which gives the "oxy-Cu RR" spectral data.

The  $[\text{Cu}^{\text{II}}(\text{imidH})(\text{py})\text{DAP}]^{2+}$  and  $[\text{Cu}^{\text{I}}(\text{imidH})(\text{py})\text{DAP}]^+$  compounds also have been studied for comparative purposes. Unfortunately, the deoxy- $[\text{Cu}^{\text{I}}(\text{imidH})(\text{py})\text{DAP}]^+$  and  $\text{oxy}(^{16}\text{O}_2)-[\text{Cu}(\text{imidH})(\text{py})\text{DAP}]^{n+}$  species were found to luminesce when placed in the UV laser line path. The more intense fluorescence spectrum masked the weak Raman-active scattering lines.<sup>79</sup> A RR spectrum has been obtained for the analogous Cu(II) complex. These spectral data are listed in Table 16 and are similar to that of the  $[\text{Cu}^{\text{II}}(\text{imidH})_2\text{DAP}]^{2+}$  species with slight signal shifts due to the slightly different ligand structures.

While the RR spectra obtained in this study are acceptable, the signal to noise ratio is less than that usually recorded for simple



metal complexes having  $\epsilon \geq 1000 \text{ M}^{-1} \text{ cm}^{-1}$  and for samples with large solute concentrations of 0.1 M. Aside from the problem of the "self-absorption" phenomenon, these copper complexes may not give sizeable RR spectral bands due to their fundamental electronic structure. The differences in the ground and excited state structures affect the intensity of the Raman spectrum. Consider the simple single state resonance enhancement expression as defined as follows:<sup>80</sup>

$$\text{Intensity} \propto \frac{\nu_o^4 \epsilon^2}{[(\nu_e - \nu_o)^2 + \Gamma^2]^2}$$

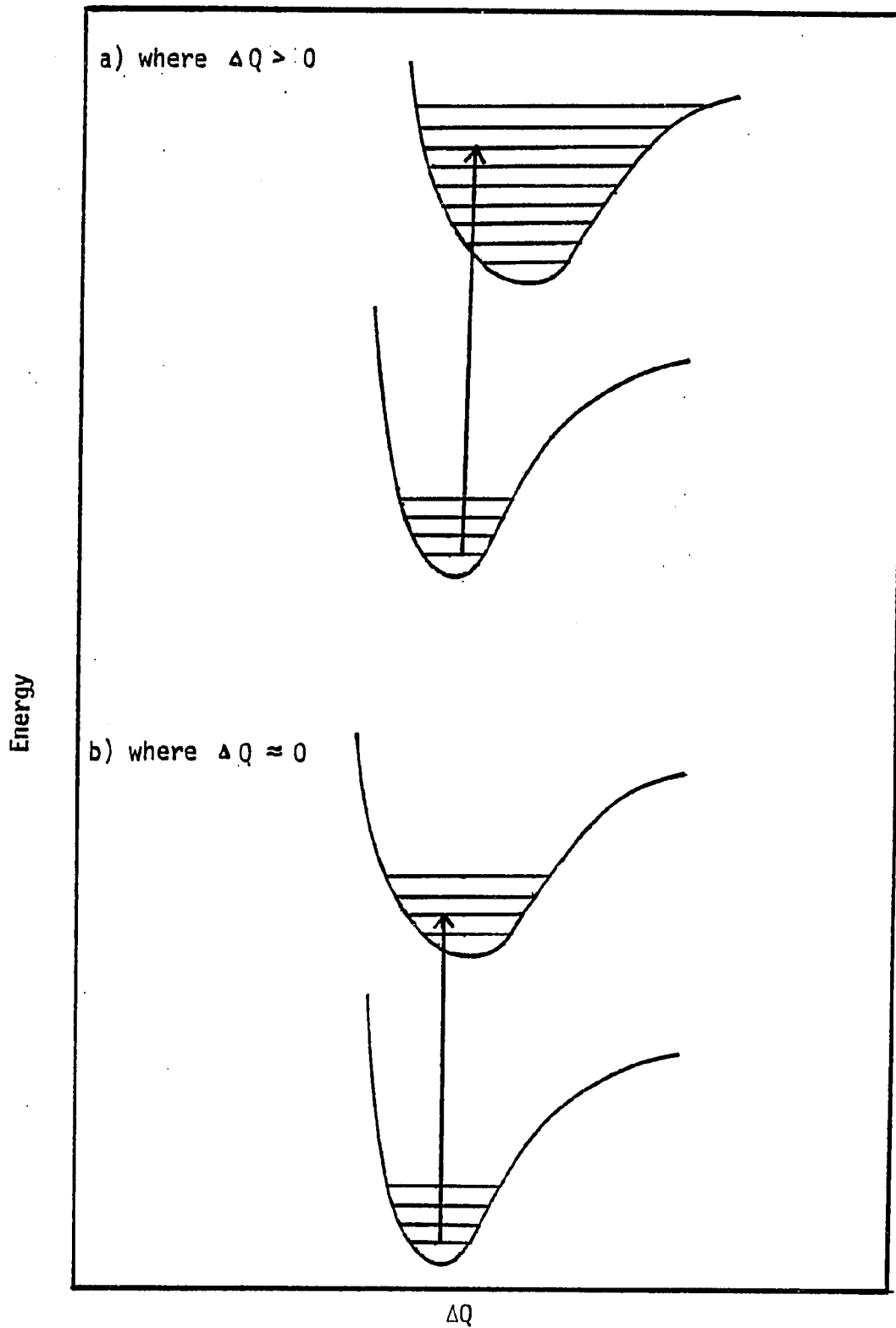
where  $\nu_o$  = laser frequency of excitation

$\nu_e$  = frequency of resonant electronic transition

$\epsilon$  = Franck-Condon factors

$\Gamma$  = damping factor

Since the intensity is directly proportional to  $\epsilon$ , factors affecting the magnitude of  $\epsilon$  will likewise affect the intensity of RR spectral peaks. Consider a potential energy well diagram (Figure 36) where the excited electronic state well is displaced from the ground state well, i.e., a large difference in nuclear coordinates ( $\Delta Q$ ) exists, leading to large Franck-Condon factors. This distortion leads to large vibrational contribution toward the ground  $\rightarrow$  excited state electronic transition and thus large resonance enhancement of the Raman peaks. Typically, small unconjugated  $\pi$  systems exhibit this property by  $\pi \rightarrow \pi^*$  electronic transitions and sizeable RR spectra are obtained.

Potential Energy Well Diagrams

In contrast, the intensity of resonance enhancement is lowered as  $\epsilon$  decreases. When the excited and ground state structures are not greatly distorted from one another, *i.e.*, the energy wells are aligned horizontally with respect to each other along the nuclear coordinate axis ( $\Delta Q \approx 0$ ), the Franck-Condon factors are low and the ground  $\rightarrow$  excited state electronic transition has very little vibrational character. Therefore, the RR spectral bands would be weak. Highly conjugated systems, such as polycyclic aromatic hydrocarbons, exhibit  $n \rightarrow \pi^*$  electronic transitions and low intensity RR bands. Concerning the copper complexes examined in this work, the electronic structure of the copper ion and coordinated pyridine and imidazole moieties may be largely delocalized. Hence, the  $\Delta Q$  for the overall electronic structural change would be very small and the Franck-Condon factors minimal. Thus any RR spectral bands would be of low intensity.<sup>81</sup>

### Conclusions

Through the systematic variation of ligand structure, a family of dioxygen-active copper(I) complexes has been synthesized. The analogous Cu(II) compounds have been examined by electrochemical techniques and a correlation has been proposed: the more positive the  $E_{1/2}$  for the  $\text{Cu(II)} \rightleftharpoons \text{Cu(I)}$  couple, the greater the stability of the Cu(I) species, generated at the electrode surface, and the lower the reactivity of the Cu(I) center toward dioxygen in a reversible manner. These copper(I) complexes have also been studied in order to examine the role, if any, of the imidazole proton in the reversible oxygenation of the parent  $[\text{Cu}^{\text{I}}(\text{imidH})_2\text{DAP}]^+$  compound. The  $[\text{Cu}^{\text{I}}(\text{imidR})_2\text{DAP}]^+$  reacts with dioxygen

(1 mole  $O_2$ :2 moles Cu) in a similar manner to that of the  $[Cu^I(imidH)_2DAP]^+$  species. Clearly, the oxygenation process for the  $[Cu^I(imidR)_2DAP]^+$  cannot follow the proton involvement mechanism. Possibly, the mechanisms for the oxygenation of these two Cu(I) complexes differ, but it is unlikely given the available experimental data. The spectroscopic, electrochemical, and magnetochemical data presented in this work provide additional support for the proposed  $[LCu^{II}-O_2^{2-}-Cu^{II}L]$  structure of the oxygenated-copper species. Although the resonance Raman experiments have not yet elucidated a  $\nu_{O-O(st)}$  for the oxy- $[Cu(imidH)_2DAP]^{n+}$  compound, these spectroscopic results indicate that the oxygenated- $[Cu(imidH)_2DAP]^{n+}$  species is not the oxidized  $[Cu^{II}(imidH)_2DAP]^{2+}$  derivative. Final proof for these copper(I) complexes as dioxygen carriers, and thus valid models for the active site structure in oxyhemocyanin, lies in the growth of single crystals of an oxygenated-copper species. Hopefully these crystals will be grown and x-ray structural analysis completed in the near future. Also, continued synthesis and study of related dioxygen-active copper(I) compounds will further aid in the understanding of the copper(I)-dioxygen reaction, as well as the structure-function relationship in hemocyanin.

REFERENCES

1. E. Ochiai, in "Bioinorganic Chemistry, An Introduction," Allyn and Bacon, Boston, 1977, chapters 6 and 9.
2. O. Warburg, in "Heavy Metal Prosthetic Groups," Oxford University Press, London, 1949.
3. H. A. Kuiper, R. Toënsma, and E. F. J. van Bruggen, European J. Biochem., 68, 425 (1976); C. Bonaventura, B. Sullivan, J. Bonaventura, and S. Bourne, Biochemistry, 13, 4784 (1974).
4. A. J. M. Schoot Uiterkamp, F.E.B.S. Letters, 20, 93 (1972).
5. K. A. Magnus and W. E. Love, J. Mol. Biol., 116, 171 (1977).
6. N. Shaklai, A. Gafni, and E. Daniel, Biochemistry, 17, 4438 (1978).
7. L. Y. Fager and J. O. Alben, Biochemistry, 11, 4786 (1972).
8. T. B. Freedman, J. S. Loehr, and T. M. Loehr, J. Am. Chem. Soc., 98, 2809 (1976).
9. T. Nakamura and H. S. Mason, Biochem. Biophys. Res. Comm., 3, 297 (1960).
10. J. F. Boas, J. R. Pilbrow, G. J. Troup, C. Moore, and T. D. Smith, J. Chem. Soc. (A), 965 (1969).
11. E. L. Solomon, D. M. Dooley, R. Wang, H. B. Gray, M. Cerdonio, F. Mogno, and G. I. Romani, J. Am. Chem. Soc., 98, 1029 (1976).
12. J. S. Loehr, T. B. Freedman, and T. M. Loehr, Bioch. Biophys. Res. Comm., 56, 510 (1974).
13. T. J. Thamann, J. S. Loehr, and T. M. Loehr, J. Am. Chem. Soc., 99, 4187 (1977).
14. J. A. Larrabee, T. G. Spiro, N. S. Ferris, W. H. Woodruff, W. A. Maltese, and M. S. Kerr, J. Am. Chem. Soc., 99, 1979 (1977).
15. J. A. Larrabee and T. G. Spiro, J. Am. Chem. Soc., 102, 4217 (1980).
16. J. M. Brown, L. Powers, B. Kincaid, J. A. Larrabee, and T. G. Spiro, J. Am. Chem. Soc., 102, 4210 (1980).
17. R. S. Himmelwright, N. C. Eickman, and E. I. Solomon, J. Am. Chem. Soc., 101, 1576 (1979).

18. N. C. Eickman, R. S. Himmelwright, and E. I. Solomon, Proc. Natl. Acad. Sci. U.S.A., 76, 2094 (1979).
19. R. S. Himmelwright, N. C. Eickman, C. D. LuBien, and E. I. Solomon, J. Am. Chem. Soc., 102, 5378 (1980).
20. R. E. Dickerson and I. Geis, in "The Structure and Action of Proteins," W. A. Benjamin, Menlo Park, 1969, ch. 3, pp. 44-59 and references therein.
21. J. P. Collman, R. R. Gagné, C. A. Reed, T. R. Halbert, G. Lang, and W. T. Robinson, J. Am. Chem. Soc., 97, 1427 (1975); J. P. Collman, Acc. Chem. Res., 10, 265 (1977); J. P. Collman, J. I. Brauman, T. P. Collins, B. Iverson, and J. L. Sessler, J. Am. Chem. Soc., 103, 2450 (1981).
22. For a recent review on synthetic Fe-O<sub>2</sub> carriers, see J. W. Buchler, Angew. Chem. Internat. Edn., 17, 407 (1978). In addition, the following reviews cover the known O<sub>2</sub> carriers to date: R. G. Wilkins, in "Bioinorganic Chemistry," Adv. Chem. Ser., 100, 111 (1971); J. S. Valentine, Chem. Rev., 73, 235 (1973); F. Basolo, B. M. Hoffman, and J. A. Ibers, Acc. Chem. Res., 8, 384 (1975); G. McLendon and A. E. Martell, Co-ordination Chem. Rev., 19, 1 (1976); L. Vaska, Acc. Chem. Res., 9, 175 (1976); J. A. McGinnety, in "MTP International Review of Science," Series One, ed. D. W. A. Sharp, University Park Press, Baltimore, 1972, vol. 5; and R. D. Jones, D. A. Summerville, and F. Basolo, Chem. Rev., 79, 139 (1979).
23. R. E. Stenkamp and L. H. Jensen, and J. S. Loehr and T. M. Loehr, in "Advances in Inorganic Biochemistry," G. L. Eichhorn and L. G. Marzilli, Ed., Elsevier/North-Holland, New York, 1979, vol. 1, chs. 8 and 9, pp. 219-252.
24. R. R. Gagné, J. L. Allison, R. S. Gall, and C. A. Koval, J. Am. Chem. Soc., 99, 7170 (1977); R. R. Gagné, J. Am. Chem. Soc., 98, 6709 (1976).
25. P. A. Temussi and A. Vitagliano, J. Am. Chem. Soc., 97, 1572 (1975).
26. E. Ochiai, Inorg. Nuclear Chem. Letters, 9, 987 (1973).
27. M. Pasquali, G. Marini, C. Floriani, A. Gaetani-Manfredotti, and C. Guastini, Inorg. Chem., 19, 2525 (1980).
28. C. E. Kramer, G. Davies, R. B. Davis, and R. W. Slaven, J. Chem. Soc. Chem. Comm., 606 (1975).
29. A. R. Amundsen, J. Whelan, and B. Bosmich, J. Am. Chem. Soc., 99, 6730 (1977).

30. T. K. Eccles, Stanford Synchrotron Radiation Laboratory Report No. 78/01, Stanford University, Stanford, California, 1978.
31. R. R. Gagné, R. S. Gall, G. C. Lisensky, R. E. Marsh, and L. M. Speltz, Inorg. Chem., 18, 771 (1979); R. R. Gagné, J. L. Allison, and D. M. Ingñe, Inorg. Chem., 18, 2767 (1979).
32. J. E. Bulkowski, P. L. Burk, M. Ludman, and J. A. Osborn, J. Chem. Soc. Chem. Comm., 498 (1977); P. L. Burk, J. A. Osborn, M. Youinou, Y. Agnus, R. Louis, and R. Weiss, J. Am. Chem. Soc., 103, 1273 (1981).
33. M. G. Simmons and L. J. Wilson, J. Chem. Soc. Chem. Comm., 634 (1978).
34. M. G. Simmons, Ph.D. dissertation, Department of Chemistry, Rice University, Houston, Texas, 1979.
35. R. J. Sunberg and R. B. Martin, Chem. Rev., 74, 471 (1974); E. Ochiai, J. Inorg. Nucl. Chem., 37, 1503 (1975).
36. M. Kato, H. B. Janassen, and J. C. Fanning, Chem. Rev., 64, 99 (1964); W. E. Hatfield and R. Whyman, in "Transition Metal Chemistry," R. L. Carlin, Ed., vol. 5, Marcel Dekker, New York, 1969.
37. M. G. Simmons, C. L. Merrill, L. J. Wilson, L. A. Bottomley, and K. M. Kadish, J. Chem. Soc. (D), 1827 (1980).
38. L. J. Wilson, C. L. Merrill, M. G. Simmons, J. M. Trantham, L. A. Bottomley, and K. M. Kadish, in "Invertebrate Oxygen Binding Proteins. Structure, Active, and Function," Lamy and Lamy, Ed., Marcel Dekker, New York, 1981.
39. D. F. Shriver, in "The Manipulation of Air-Sensitive Compounds," McGraw-Hill, New York, 1969.
40. B. A. Averill, private communication, 1980.
41. P. Hemmreich and C. Sigwart, Experientia, 19, 488 (1963).
42. J. B. Headridge, in "Electrochemical Techniques for Inorganic Chemist," Academic Press, London, 1969.
43. W. W. Umbreit, R. H. Burris, and J. F. Stauffer, in "Manometric Techniques," 4th edition, Burgess, Minneapolis, 1964.
44. A. G. Zwart, Biochem. Biophys Acta, 9, 104 (1952).
45. M. F. Tweedle and L. J. Wilson, Rev. Sci. Instrum., 49, 1001 (1978).

46. M. F. Tweedle, L. J. Wilson, L. Garcia-Iniguez, G. T. Babcock, and G. Palmer, J. Biol. Chem., 253, 8065 (1978).
47. M. F. Tweedle, Ph.D. dissertation, Department of Chemistry, Rice University, Houston, Texas, 1978.
48. T. M. Loehr, W. E. Keyes, and P. A. Penicus, Anal. Biochem., 96, 456 (1979).
49. B. Sjöberg, A. Graslund, J. S. Loehr, and T. M. Loehr, Biochem. Biophys. Res. Comm., 94, 793 (1980).
50. D. F. Shriver and J. B. R. Dunn, Appl. Spec., 28, 319 (1974).
51. D. T. Sawyer and J. L. Roberts, Jr., in "Experimental Electrochemistry for Chemists," Wiley, New York, 1974, ch. 7, pp. 329-394.
52. J. R. Dyer, in "Applications of Absorption Spectroscopy of Organic Compounds," Prentice-Hall, New Jersey, 1965, ch. 3, pp. 22-57.
53. J. D. Korp, I. Bernal, C. L. Merrill, and L. J. Wilson, J. Chem. Soc. (D), 1951 (1981).
54. K. J. Purcell and J. C. Kotz, in "Inorganic Chemistry," W. B. Saunders, Philadelphia, 1977, chs. 9-13.
55. C. Mealli, C. S. Arcus, J. L. Wilkinson, T. J. Marks, and J. A. Ibers, J. Am. Chem. Soc., 98, 711 (1976).
56. A. Crumbliss and A. T. Paulos, Inorg. Chem., 14, 1529 (1975).
57. D. Van der Helm, A. F. Nicholas, and C. G. Fisher, Acta Crystallogr., Sect. B, 26, 1172 (1970).
58. J. A. Ibers and L. J. Wilson, work in progress.
59. M. G. Burnett, V. McKee, and S. M. Nelson, J. C. S. Chem. Commun., 599 (1980).
60. K. Hofmann, in "Imidazole and Its Derivatives," Interscience, New York, 1953, ch. 8, p. 254.
61. H. H. Wasserman, K. Stiller, and M. B. Floyd, Tet. Letters, 3277 (1968).
62. C. S. Foote, E. R. Peterson, and H. S. Ryang, presented at the Seventh Meeting of the American Society of Photochemists, Monterey, June 1978.
63. T. Matsuura and I. Saito, J. Chem. Soc. Chem. Comm., 693 (1967).



64. L. Weil, S. James, and A. R. Buchert, Arch. Biochem. Biophys., 46, 266 (1953).
65. G. Jori, B. Salvato, and L. Tallandini, in "Structure and Function of Haemocyanin," J. V. Bannister, Ed., Springer-Verlag, Berlin, 1977, pp. 156-163.
66. M. DeLey and R. Lontie, in "Structure and Function of Haemocyanin," J. V. Bannister, Ed., Springer-Verlag, Berlin, 1977, pp. 164-171.
67. J. F. Boas, J. R. Pilbrow, G. J. Troup, C. Moore, and T. D. Smith, J. Chem. Soc. (A), 965 (1969); B. G. Malmström and T. Vanngard, J. Mol. Biol., 2, 118 (1960); B. Bleaney and K. D. Bowers, Proc. Roy. Soc., A, 214, 451 (1952).
68. R. Barbucci, A. Mastroianni, and M. J. M. Campbell, Inorganica Chimica Acta, 27, 109 (1978).
69. E. A. Boudreaux and L. N. Mulay, in "Theory and Applications of Molecular Paramagnetism," Wiley, New York, 1976; A. Earnshaw, in "Introduction to Magnetochemistry," Academic Press, London, 1968.
70. W. E. Hatfield, J. A. Barnes, D. Y. Jeter, R. Whyman, E. R. Jones, Jr., J. Am. Chem. Soc., 92, 4982 (1970).
71. J. P. Collman, J. I. Brauman, T. R. Halbert, and K. S. Suslick, Proc. Natl. Acad. Sci. U.S.A., 73, 3333 (1976).
72. J. C. Maxwell, J. A. Volpe, C. H. Barlow, and W. S. Caughey, Biochem. Biophys. Res. Comm., 58, 166 (1974).
73. D. M. Kurtz, Jr., D. F. Shriver, and I. M. Klotz, Co-ordination Chem. Rev., 24, 145 (1977).
74. R. S. Drago, in "Physical Methods in Chemistry," W. B. Saunders, Philadelphia, 1977, ch. 6, pp. 145-158.
75. T. G. Spiro, Acc. Chem. Res., 7, 339 (1974).
76. T. G. Spiro and T. C. Strekas, Proc. Natl. Acad. Sci. U.S.A., 69, 2622 (1972).
77. E. M. Nour and R. E. Hester, J. Mol. Struct., 62, 77 (1980); M. Suzuki, T. Ishiguro, M. Kozuka, and K. Nakamoto, Inorg. Chem., 20, 1993 (1981).
78. M. A. Walters, T. G. Spiro, K. S. Suslick, and J. P. Collman, J. Am. Chem. Soc., 102, 6857 (1980).
79. N. S. Ferris, private communication, 1980.

80. W. H. Woodruff, R. F. Dallinger, T. M. Antalis, and G. Palmer, Biochemistry, 20, 1332 (1981).
81. W. H. Woodruff, private communication, 1981.

## PART II

$\mu$ -IMIDAZOLATO BINUCLEAR METALLOPORPHYRIN COMPLEXES OF IRON AND  
COPPER AS MODELS FOR THE ACTIVE SITE STRUCTURE IN CYTOCHROME OXIDASE

## INTRODUCTION

Cytochrome oxidase is the respiratory enzyme which catalytically reduces one mole of dioxygen to two moles of water with the release of energy which is stored in the ADP-ATP cycle ( $O_2 + 4H^+ = 4e^- \rightarrow 2H_2O + \text{energy}$ ).<sup>1</sup> The enzyme contains four metal centers (two irons and two coppers) per functional unit. Through various spectroscopic and other studies, it is known that the enzyme contains one isolated iron heme unit (cytochrome a) which is low-spin in both the oxidized and reduced forms and one isolated copper center ( $Cu_D$ ; D for EPR detectable), while at the active or dioxygen binding site there is a high-spin iron heme (cytochrome  $a_3$ ) and a second copper center ( $Cu_U$ ; U for EPR undetectable).<sup>2</sup> In a full temperature magnetochemical study, Tweedle *et al.*,<sup>3</sup> have shown for the fully oxidized or resting form of the enzyme that the iron center of  $cyt.a_3^{3+}$  ( $S=5/2$ ) and  $Cu_U^{2+}$  ( $S=1/2$ ) are strongly coupled antiferromagnetically ( $-J \geq 200 \text{ cm}^{-1}$ ) to give a resultant  $S=2$  ground state for the binuclear active site. The structure of the active site of the resting enzyme is presumably a ligand-bridged binuclear unit,  $[Cyt.a_3^{3+}(B)Cu_U^{2+}]$ , although Seiter and Angelos<sup>4</sup> have suggested an alternative model having uncoupled and unbridged high-spin heme  $a_3^{4+}$  and  $Cu^+$  centers, but the suggestion has not received wide-spread support.<sup>5</sup> Also, the Seiter model seems questionable since it assumes a redox-inactive role for  $Cu^+$  while necessitating a relatively rare situation of an iron(IV) hemoprotein center. While the cytochrome oxidase active site  $[heme a_3-(B)-Cu_U]$  structural unit seems to be a generally accepted concept, the exact nature of the bridging ligand, (B), is presently under active debate. Based on spectroscopic studies

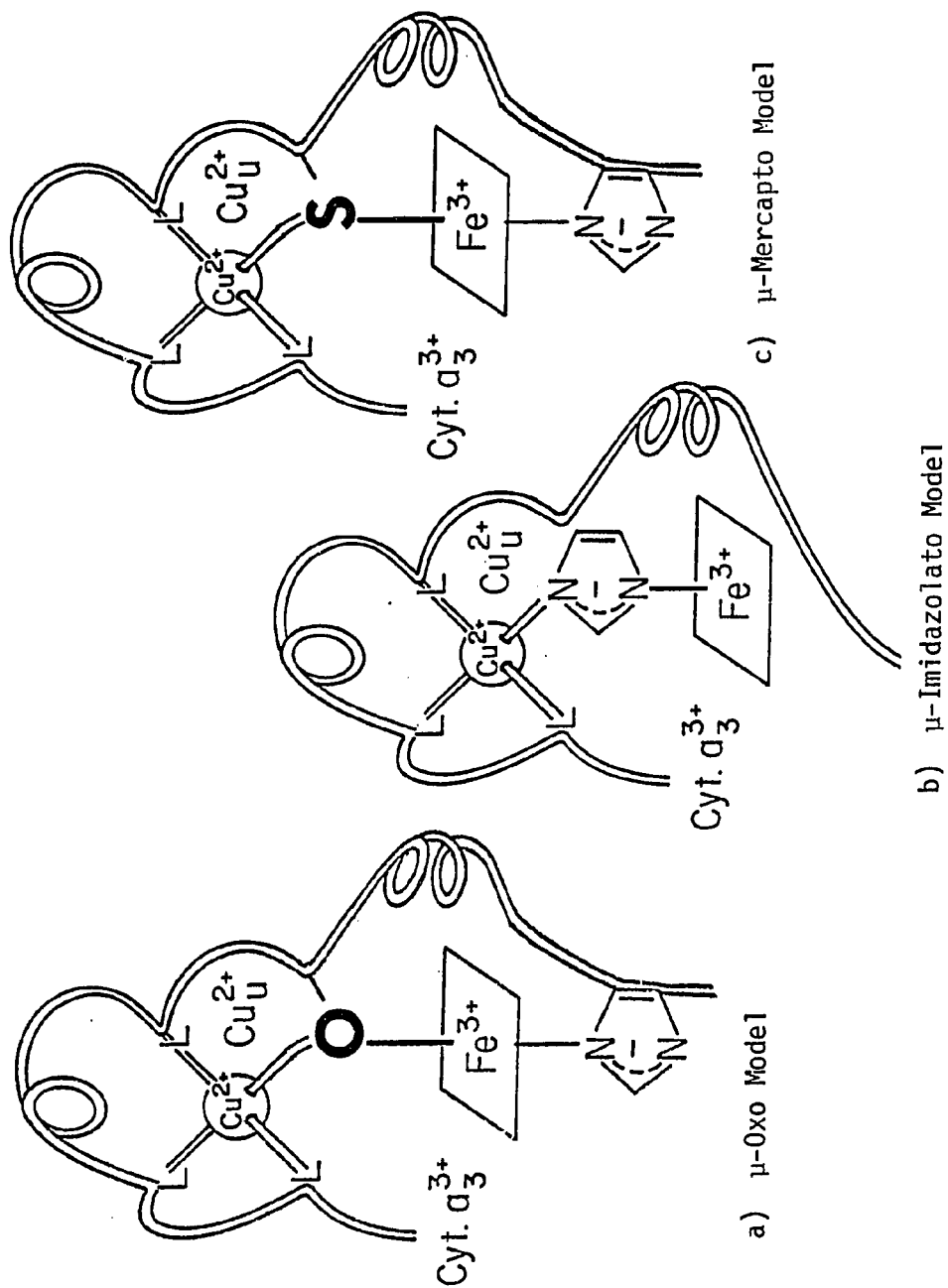
(principally EPR, MCD, EXAFS, and resonance Raman) of cytochrome oxidase, candidates for the bridging ligand include imidazolato from histidine,<sup>3,6</sup> oxo from dioxygen,<sup>7,8</sup> and even mercapto<sup>9,10</sup> from cysteine. These three possibilities are shown collectively in Figure 1.

The  $\mu$ -imidazolato model, first proposed by Palmer *et al.*,<sup>6</sup> incorporates the  $[\text{Fe}^{\text{III}}(\text{imid})\text{Cu}^{\text{II}}]$  unit as the active site structure in resting or oxidized cytochrome oxidase (Figure 1-b). In this proposal, the iron center of heme  $a_3^{3+}$  is linked to the copper(II) center by an imidazolate bridging moiety. Thus in the reduced form of the enzyme, the iron heme  $a_3^{2+}$  would be five coordinate with four N donor atoms from the porphyrin unit and one N from the apical imidazolate ligand. During the catalytic cycle, dioxygen is depicted as binding to the "back side," or sixth coordinating position, of the iron(II) center where it is reduced in a  $4 e^-$  process to two moles of water. To date, circumstantial support for the imidazolate bridging ligand include: (1) EPR measurements on the  $^{15}\text{NO}$ -reduced cytochrome oxidase which indicate that the iron center of heme  $a_3$  has a nitrogen atom as an apical donor atom,<sup>11</sup> (2) x-ray structural data showing that superoxide dismutase (SOD) protein contains a mixed-metal binuclear  $[\text{Cu}^{\text{II}}(\text{imid})\text{Zn}^{\text{II}}]$  site with an imidazolate bridge from histidine,<sup>12,13</sup> and (3) through an  $^{15}\text{N}$ -labeled histidine EPR study by Chan *et al.*,<sup>14</sup> an endogenous imidazole group has been found to axially ligate heme  $a_3$  for the fully reduced cytochrome oxidase.

The  $\mu$ -oxo model, as described by Blumberg,<sup>15</sup> among others,<sup>7,8</sup> is another proposed active site structure for cytochrome oxidase. Employing the  $[\text{Fe}^{\text{III}}\text{--O--Cu}^{\text{II}}]$  structural and catalytic redox model for the

Figure 1

Proposed Models for the Active Site Structure in Cytochrome Oxidase



active site of resting oxidase, a comprehensive and cyclic reaction scheme is constructed to include both the dioxygen binding site of the enzyme and the dioxygen substrate (Figure 2).<sup>7</sup> This  $\mu$ -oxo model seems to be in agreement with the available magnetic and spectroscopic data,<sup>16</sup> including some EXAFS data<sup>17</sup> which suggest an [Fe---Cu] separation of only  $\sim 3 \text{ \AA}$  in resting oxidase, whereas  $\sim 5 \text{ \AA}$  would be required for an imidazolate bridge. However, Beinert and workers<sup>18</sup> have recently used  $^{18}\text{O}_2/^{16}\text{O}_2$  isotope labeling studies to determine whether, or not, a reduced atom of oxygen, from dioxygen, is bound to resting cytochrome oxidase as a  $\mu$ -oxo link between heme  $a_3^{3+}$  and  $\text{Cu}_U^{2+}$ . When water produced by  $^{18}\text{O}_2$ -oxidation of the anaerobically reduced enzyme was compared to that obtained from  $^{16}\text{O}_2$ -oxidation, all the  $^{18}\text{O}_2$  reduced in a single catalytic cycle was accounted for in the form of  $\text{H}_2^{18}\text{O}$  produced. Apparently, neither atom of the reduced dioxygen is employed in the enzyme as a bridge which is stable in the absence of oxidoreductive reactions for several minutes. While this result does not eliminate the possibility of the  $\mu$ -oxo model, it decreases the validity of this proposal.

Alternatively, Powers *et al.*,<sup>9</sup> have discussed the  $\mu$ -mercapto model for the active site structure of cytochrome oxidase (Figure 1-c). Recently obtained EXAFS<sup>9</sup> and resonance Raman data<sup>19</sup> have suggested that the  $\text{Cu}_U^{2+}$  site in the oxidized, or resting, enzyme may be a Type I or blue copper center and as such bound to a sulfur ligand.<sup>20</sup> Furthermore, the heme  $a_3^{3+}$  Fe(III) is found to be six-coordinate and most likely bound to sulfur as well. Based on these EXAFS data, a cyclic mechanism of the dioxygen reduction involving the  $\mu$ -mercapto model has been proposed<sup>9</sup> (see Figure 3). Following the breaking of the Fe-S

Figure 2

Proposed Catalytic Cycle Involving the  $\mu$ -Oxo Model  
for the Active Site Structure in Resting Cytochrome Oxidase

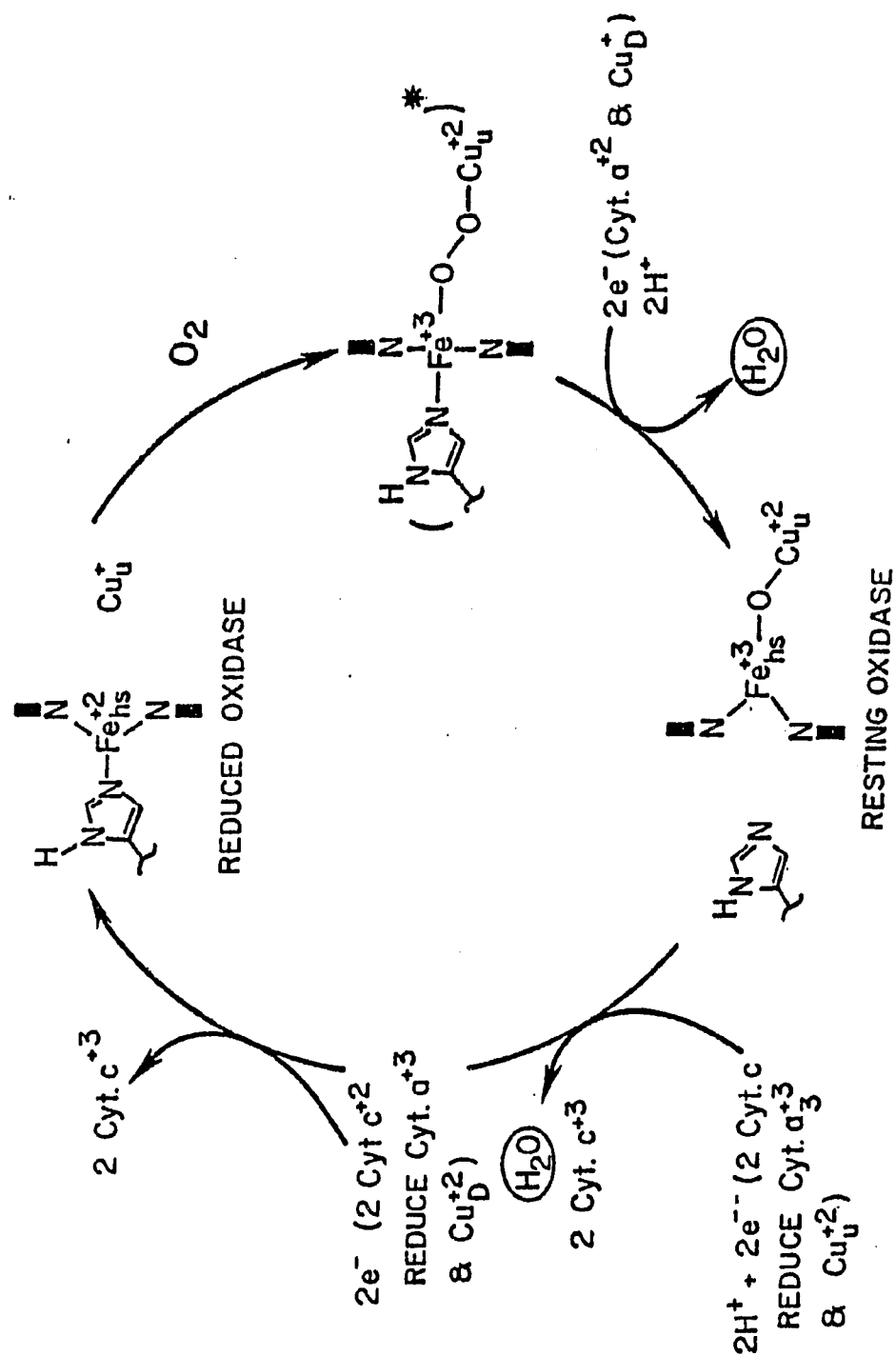
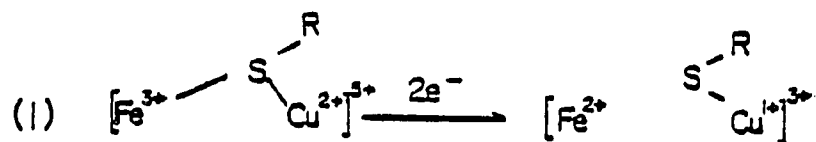


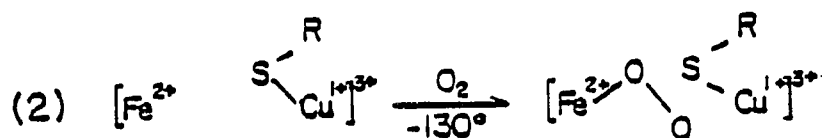


Figure 3

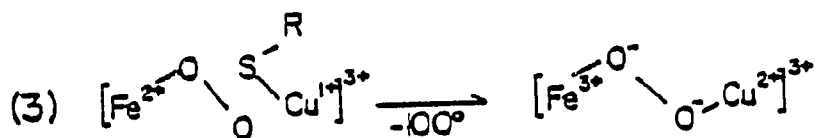
A Proposed Cyclic Mechanism of Oxygen Reduction  
Involving the  $\mu$ -Mercapto Model



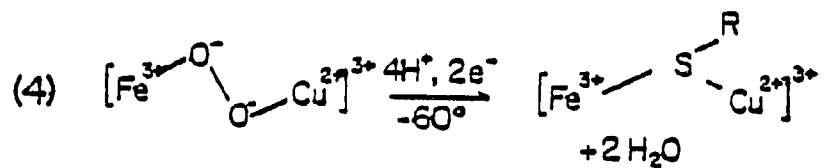
Reduction, bond breaking



Oxycytochrome oxidase



Peroxyoxycytochrome oxidase



Protonation, reduction & bridging

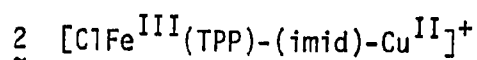
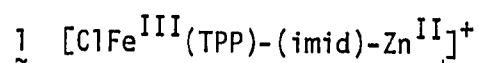
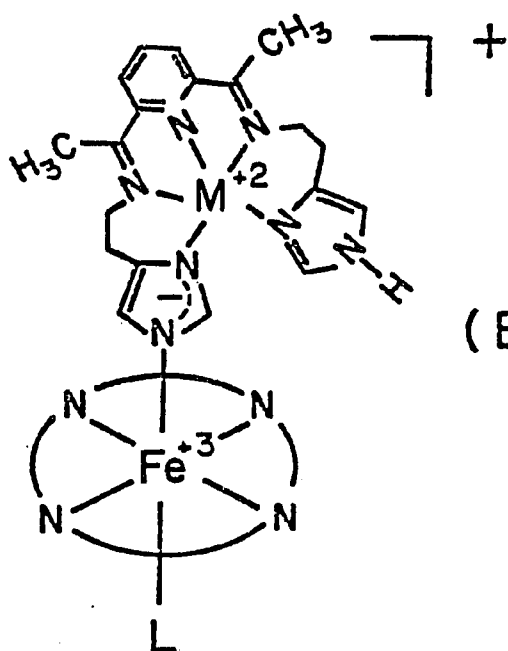
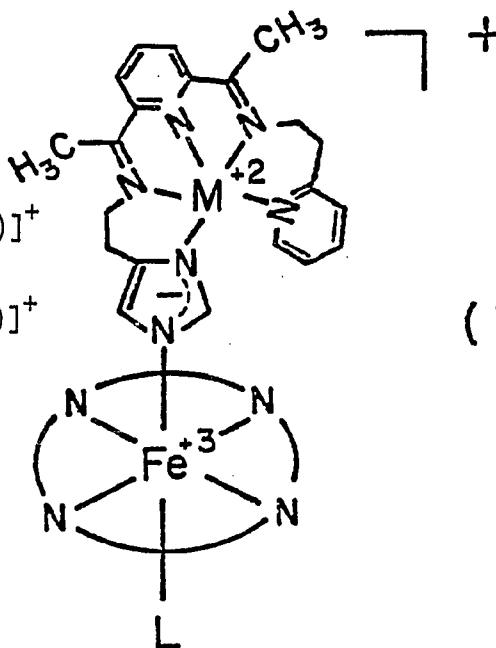
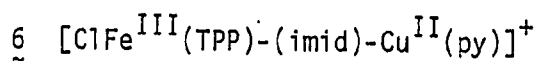
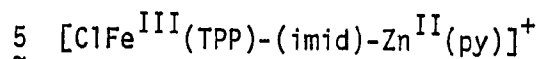
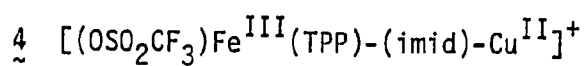
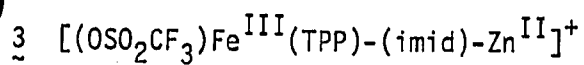
bond, this scheme proceeds to the dioxygen binding step where a  $\mu$ -peroxo iron-copper intermediate is formed. In essence, this mechanism represents a "special case" of the catalytic cycle involving the  $\mu$ -oxo model (see Figure 2). Challenging the  $\mu$ -mercapto model, Brudvig *et al.*,<sup>21</sup> have reported UV electronic spectral data indicating that  $\text{Cu}_U^{2+}$  is not a Type I copper center.

Concerning the observed magnetic behavior of resting cytochrome oxidase, there seems to be little doubt that single atom bridges like oxygen or sulfur can foster antiferromagnetic exchange interactions approaching or exceeding  $200 \text{ cm}^{-1}$ . However, there is less certainty about an imidazolate bridge. Still, there is some magnetochemical evidence to support the  $\mu$ -imidazolate model. The  $[\text{Co}^{\text{II}}(\text{imid})\text{Cu}^{\text{II}}]$  SOD derivative has yielded a  $-J \geq 300 \text{ cm}^{-1}$ <sup>22,23</sup> for this mixed-metal imidazolate-bridged system. This antiferromagnetic coupling constant is as large as that found for the iron(III)-copper(II) exchange interaction in resting cytochrome oxidase, although the binuclear site structure for the two systems differ greatly. The purity of the " $2\text{Co}^{\text{II}}2\text{Cu}^{\text{II}}$ " SOD sample,<sup>23</sup> on which the magnetic susceptibility measurements were taken, has been questioned<sup>24</sup> and, as the result of these queries, preparative procedures have been refined so as to yield higher quality SOD samples.<sup>24</sup> As the SOD magnetochemical results are quite relevant in determining the exact nature of the bridging ligand in the  $[\text{Cyt.a}_3^{3+}-(\text{B})-\text{Cu}_U^{2+}]$  active site of cytochrome oxidase, the variable temperature magnetic susceptibility study of the " $2\text{Co}^{\text{II}}2\text{Cu}^{\text{II}}$ " SOD derivative has been reinvestigated.

In view of the aforementioned data accumulated recently on cytochrome oxidase favoring the  $\mu$ -imidazolato model (as well as the difficulties encountered in preparing and isolating for study  $\mu$ -oxo mixed-metal compounds),<sup>25</sup> several model complexes containing imidazolate-bridged metal centers have been prepared.<sup>26-31</sup> Thus there is no question of the bridging capability of the imidazolate anion. However, the ability of an imidazolate bridge to mediate antiferromagnetic exchange between the bridged metal centers has been questioned repeatedly.<sup>7,29</sup> In fact, past model compounds studied have suggested that, in synthetic systems, imidazolate and other multiatom heterocyclic bridges are incapable of fostering exchange interactions much greater than  $100\text{ cm}^{-1}$ , with most of the  $-J$  values clustered below  $30\text{ cm}^{-1}$ .<sup>7</sup>

In order to further explore the validity of the  $\mu$ -imidazolato model for the active site structure of cytochrome oxidase, six new  $\mu$ -imidazolato mixed-metal  $[\text{LFe}^{\text{III}}(\text{TPP})(\text{imid})\text{M}^{\text{II}}]^+$  and  $[\text{ClFe}^{\text{III}}(\text{imid})\text{M}^{\text{II}}(\text{py})]^+$  compounds (1)-(6) have been synthesized (see Figure 4 where  $(\text{TPP})^{2-}$  = tetraphenylporphyrinato,  $\text{L} = \text{Cl}^-$  and  $(\text{OSO}_2\text{CF}_3)^-$  or "triphlate," and  $\text{M} = \text{Zn}^{2+}$  and  $\text{Cu}^{2+}$ ). While related  $[\text{Fe}^{\text{III}}(\text{imid})\text{Cu}^{\text{II}}]^{n+}$  oxidase model species have been examined in the solution state by Kovacs and workers,<sup>30</sup> and Prosperi et al.,<sup>31</sup> the present work is the first where such species have been isolated, characterized, and studied as analytically pure solids. The solution state chemistry of the new  $\mu$ -imidazolato compounds is complex, involving a (binuclear)  $\rightleftharpoons$  (porphyrin fragment + copper fragment) equilibrium.<sup>32</sup> For this reason, the present work has been confined to the solid state study of these complexes.

Figure 4

The New  $\mu$ -Imidazolato Mixed-Metal Complexes(BF<sub>4</sub>)(BF<sub>4</sub>)

Unfortunately, the complex equilibrium properties of these systems in solution have complicated the attempts to grow crystals for structural verification by x-ray methods. However, the spectroscopic and magnetic behavior of (1)-(6) support their formulation as discrete, binuclear mixed-metal  $\mu$ -imidazolato species in the solid state. Compounds (2), (4), and (6) represent the first such heteronuclear species of  $\text{Fe}^{\text{III}}$  and  $\text{Cu}^{\text{II}}$  to be prepared and isolated as model compounds for the oxidase active site, although Landrum *et al.*,<sup>29</sup> have recently reported a  $\mu$ -imidazolato diporphyrin complex containing  $\text{Mn}^{\text{II}}$  ( $S=5/2$ ) and  $\text{Co}^{\text{II}}$  ( $S=1/2$ ) centers as a spin model for the site. In this  $[\text{Mn}^{\text{II}}(\text{imid})\text{Co}^{\text{II}}]$  compound, antiferromagnetic coupling was found to be weak ( $-J \approx 5 \text{ cm}^{-1}$ ) which led the authors to argue against a  $\mu$ -imidazolato possibility for cytochrome oxidase. The magnetochemical and EPR data presented in this work clearly indicate that the iron(III) and copper(II) centers of the (2) and (6) species are electronically isolated, whereas in  $[(\text{OSO}_2\text{CF}_3)\text{Fe}^{\text{III}}(\text{imid})\text{Cu}^{\text{II}}]^+$  are antiferromagnetically coupled with a  $-J \geq 200 \text{ cm}^{-1}$ . Thus compound (4) is the first synthetic  $\mu$ -imidazolato iron(III)-copper(II) system where strong anti-ferromagnetic exchange interaction between metal centers has been observed. These results, in conjunction with the present magnetic susceptibility study on the " $2\text{Co}^{\text{II}}2\text{Cu}^{\text{II}}$ " SOD derivative, provide additional support for a  $\mu$ -imidazolato structure for the active site of cytochrome oxidase.

## EXPERIMENTAL SECTION

### Materials

All solvents were reagent grade, distilled before use, and stored over molecular sieves: methylene chloride ( $\text{CH}_2\text{Cl}_2$ ) from  $\text{P}_2\text{O}_5$ , acetonitrile ( $\text{CH}_3\text{CN}$ ) from  $\text{KMnO}_4$  and  $\text{Na}_2\text{CO}_3$ , methanol ( $\text{CH}_3\text{OH}$ ) from sodium metal, and tetrahydrofuran (THF) from KOH pellets. Meso-tetraphenylporphine was purchased from Strem Chemicals, Inc.;  $\text{Cu}(\text{BF}_4)_2 \cdot 6\text{H}_2\text{O}$ ,  $\text{Zn}(\text{BF}_4)_2 \cdot 6\text{H}_2\text{O}$ , and anhydrous  $\text{FeCl}_2$  from Alfa Products; [1,2-bis-(dimethylamino)naphthalene] ("proton sponge" = p.s.),  $\text{t-BuO}^-\text{K}^+$ , 2,6-diacetylpyridine (DAP), 2-(2-aminoethyl)pyridine, and silver trifluoromethanesulfonate [ $\text{Ag}(\text{OSO}_2\text{CF}_3)$ ] from Aldrich Chemicals; and histamine, free base, from Sigma Chemical Company.

### Syntheses

To prevent hydrolysis with formation of the  $\mu$ -oxo dimer,  $[\text{Fe}(\text{TPP})]_2\text{O}$ ,<sup>33</sup> the  $[\text{Fe}(\text{TPP})(\text{OSO}_2\text{CF}_3)]$  compound was prepared and recrystallized under an argon atmosphere using Schlenk techniques.<sup>34</sup> The air stable  $[\text{Fe}(\text{TPP})\text{Cl}]$  compound and the chloride and triphlate mixed-metal binuclear complexes,  $[\text{LFe}(\text{TPP})(\text{imid})\text{M}]$ , were synthesized on the open laboratory bench, taking care to eliminate moisture from the reaction mixture. In particular, the presence of water was found to deactivate proton sponge or  $\text{t-BuO}^-\text{K}^+$  base during the preparation of the complexes (1)-(6). Chemical analyses were obtained commercially from Schwarzkopf Microanalytical Laboratory, Inc.

[Fe(TPP)Cl]. Metallation of tetraphenylporphine (TPP) was achieved by the method of Adler *et al.*<sup>35</sup> Two g (3.3 mmol) *meso*-tetraphenylporphine and two g (16.5 mmol) anhydrous FeCl<sub>2</sub> were refluxed in 350 ml reagent grade dimethylformamide (DMF) for 16 h. After evaporation of the solvent, the remaining solids were dried *in vacuo* overnight. The product mixture was washed with CH<sub>2</sub>Cl<sub>2</sub> and filtered, and the filtrates were reduced to dryness by flash evaporation. Next this purple [Fe(TPP)Cl] product was dissolved in a minimum amount (200 ml) of hot THF and precipitated by the addition of 100 ml 6M HCl and enough distilled water for dilution to 800 ml total volume. Following overnight refrigeration, the suspension was filtered and the recrystallized product was collected, washed with water, and dried *in vacuo* overnight.  $\mu_{\text{eff}}(\text{solid}, 298 \text{ K}) = 5.93 \mu_{\text{B}}$ . Anal. calcd. for FeC<sub>44</sub>H<sub>28</sub>N<sub>4</sub>Cl: C, 75.06%; H, 4.00%; N, 7.96%; Fe, 7.93%. Found: C, 75.61%; H, 3.99%; N, 8.03%; Fe, 7.76%.

[Fe(TPP)(OSO<sub>2</sub>CF<sub>3</sub>)]. This compound was prepared by the metathesis of [Fe(TPP)Cl] with Ag(OSO<sub>2</sub>CF<sub>3</sub>) by the method of Reed *et al.*<sup>36</sup> A mixture of [Fe(TPP)Cl] (0.50 g or 0.710 mmol) and Ag(OSO<sub>2</sub>CF<sub>3</sub>) (0.18 g or 0.710 mmol) was dissolved in 30 ml THF, refluxed for about 1/2 h, and then filtered. Reagent grade heptane (45 ml) was added to the filtrates and the purple solution was chilled overnight. Crystals were obtained by filtration and recrystallized from a hot toluene (40 ml) and heptane (100 ml) solvent mixture. The shiny purple crystals were collected, washed with heptane, and dried *in vacuo* overnight.  $\mu_{\text{eff}}(\text{solid}, 298 \text{ K}) = 5.16 \mu_{\text{B}}$ . IR(Nujol mull):  $\nu(\text{OSO}_2\text{CF}_3^-) = 1340 \text{ (s)}, 1240 \text{ (s)}, 1205 \text{ (s)},$

and  $630 \text{ (s) cm}^{-1}$ .<sup>36</sup> Anal. calcd. for  $\text{FeC}_{45}\text{H}_{28}\text{N}_4\text{O}_3\text{SF}_3$ : C, 66.10%; H, 3.45%; N, 6.85%. Found: C, 64.80%; H, 3.69%; N, 6.75%.

$[\text{M}(\text{imidH})_2\text{DAP}](\text{BF}_4)_2$ , where  $\text{M} = \text{Zn}^{2+}$  and  $\text{Cu}^{2+}$ . The zinc(II) and copper(II) complexes were synthesized and characterized by the methods described in Part I of this dissertation, pp. 19 and 22.

$[\text{M}(\text{imidH})(\text{py})\text{DAP}](\text{BF}_4)_2$ , where  $\text{M} = \text{Zn}^{2+}$  and  $\text{Cu}^{2+}$ . The zinc(II) and copper(II) complexes were synthesized and characterized by the methods described in Part I of this dissertation, pp. 21 and 23.

$[\text{ClFe}^{\text{III}}(\text{TPP})(\text{imid})\text{M}^{\text{II}}](\text{BF}_4) \cdot (\text{p.s.H})^+(\text{BF}_4)^-$ , where  $\text{M} = \text{Zn}^{2+}$  [compound (1)] and  $\text{Cu}^{2+}$  [compound 2]. These mixed-metal binuclear complexes were synthesized by the method of Dessens *et al.*<sup>5</sup> A 1:1.2 molar ratio mixture of  $[\text{Fe}(\text{TPP})\text{Cl}]$  (0.2112 g) and  $[\text{M}(\text{imidH})_2\text{DAP}](\text{BF}_4)_2$  (0.2648 g for  $\text{M} = \text{Zn}^{2+}$  and 0.2640 g for  $\text{M} = \text{Cu}^{2+}$ ) was refluxed for 6 h in the presence of one mole equivalent proton sponge (0.096 g) or  $\text{t-BuO}^-\text{K}^+$  (0.050 g) in a dry  $\text{CH}_2\text{Cl}_2/\text{CH}_3\text{CN}$  (10%) solvent mixture. Removal of the solvent, in vacuo, resulted in crystalline product, from which excess  $[\text{M}(\text{imidH})_2\text{DAP}](\text{BF}_4)_2$  was removed by washing with distilled water. Following a heptane wash, the purple-black solids were dried over  $\text{P}_2\text{O}_5$  in vacuo at room temperature for 15 h. The samples prepared using proton sponge were obtained as  $(\text{p.s.H})^+(\text{BF}_4)^-$  occludates, while those synthesized employing  $\text{t-BuO}^-\text{K}^+$  were occludate-free. Strong absorption bands in the infrared spectrum attributed to occluded  $(\text{p.s.H})^+$  were observed at  $825 \text{ cm}^{-1}$  and  $760 \text{ cm}^{-1}$  for compound (1) and at  $820 \text{ cm}^{-1}$  and



755  $\text{cm}^{-1}$  for (2) (see Figure 6-D and 6-E), whereas these marker bands were absent in the preparation using  $\text{t-BuO}^-\text{K}^+$  as base.

For compound (1) prepared with proton sponge as base,  $\mu_{\text{eff}}(\text{solid}, 298 \text{ K}) = 2.67 \mu_{\text{B}}$ . Anal. calcd. for  $\text{FeZnC}_{63}\text{H}_{50}\text{N}_{11}\text{ClBF}_4 \cdot (\text{C}_{14}\text{H}_{19}\text{N}_2)^{+}(\text{BF}_4)^{-}$ : C, 61.38%; H, 4.62%; N, 12.08%; Fe, 3.71%; Zn, 4.34%. Found: C, 61.62%; H, 4.68%; N, 12.67%; Fe, 3.85%; Zn, 4.96%.

For compound (1) prepared with  $\text{t-BuO}^-\text{K}^+$  as base,  $\mu_{\text{eff}}(\text{solid}, 298 \text{ K}) = 3.10 \mu_{\text{B}}$ . Anal. calcd. for  $\text{FeZnC}_{63}\text{H}_{50}\text{N}_{11}\text{ClBF}_4$ : C, 62.82%; H, 4.18%; N, 12.79%; Fe, 4.64%; Zn, 5.43%. Found: C, 62.20%; H, 4.01%; N, 12.62%; Fe, 3.85%; Zn, 5.35%.

For compound (2) prepared with proton sponge as base,  $\mu_{\text{eff}}(\text{solid}, 298 \text{ K}) = 3.39 \mu_{\text{B}}$ . Anal. calcd. for  $\text{FeCuC}_{63}\text{H}_{50}\text{N}_{11}\text{ClBF}_4 \cdot (\text{C}_{14}\text{H}_{19}\text{N}_2)^{+}(\text{BF}_4)^{-}$ : C, 61.45%; H, 4.62%; N, 12.10%; Fe, 3.71%; Cu, 4.22%; Cl, 2.36%. Found: C, 61.08%; H, 4.69%; N, 12.06%; Fe, 3.61%; Cu, 3.82%; Cl, 2.12%.

For compound (2) prepared with  $\text{t-BuO}^-\text{K}^+$  as base,  $\mu_{\text{eff}}(\text{solid}, 298 \text{ K}) = 3.78 \mu_{\text{B}}$ . Anal. calcd. for  $\text{FeCuC}_{63}\text{H}_{50}\text{N}_{11}\text{ClBF}_4$ : C, 62.91%; H, 4.19%; N, 12.81%; Fe, 4.64%; Cu, 5.28%; Cl, 2.95%. Found: C, 62.50%; H, 4.19%; N, 12.05%; Fe, 4.41%; Cu, 4.61%; Cl, 2.39%.

$[(\text{OSO}_2\text{CF}_3)\text{Fe}^{\text{III}}(\text{TPP})(\text{imid})\text{M}^{\text{II}}](\text{BF}_4) \cdot (\text{p.s.H})^+(\text{BF}_4)^{-}$ , where  $\text{M} = \text{Zn}^{2+}$  [compound (3)] and  $\text{Cu}^{2+}$  [compound (4)]. The triphlate iron-zinc and iron-copper binuclear complexes were prepared by first combining the  $[\text{Fe}(\text{TPP})(\text{OSO}_2\text{CF}_3)]$  (0.1226 g) and  $[\text{M}(\text{imidH})_2\text{DAP}](\text{BF}_4)_2$  (0.1324 g for  $\text{M} = \text{Zn}^{2+}$  and 0.1320 g for  $\text{M} = \text{Cu}^{2+}$ ) compounds in a 1:1.2 molar ratio for solution in 150 ml of a  $\text{CH}_2\text{Cl}_2/\text{CH}_3\text{CN}$  (10%) solvent mixture. The

reaction mixture was refluxed for 6 h in the presence of proton sponge (0.048 g) and then reduced to dryness. The purple-grey solid was washed with water and heptane and dried at room temperature in vacuo over  $P_2O_5$  overnight. The final, analytically pure products were obtained as  $(p.s.H)^+(BF_4)^-$  occludates. Absorption peaks in the infrared spectrum attributed to occluded  $(p.s.H)^+$  were observed at  $830\text{ cm}^{-1}$  and  $765\text{ cm}^{-1}$  for compound (3) and at  $825\text{ cm}^{-1}$  and  $760\text{ cm}^{-1}$  for compound (4) (see Figure 6-F and 6-G).

For compound (3) prepared with proton sponge as base,  $\mu_{eff}(\text{solid}, 298\text{ K}) = 3.36\ \mu_B$ . Anal. calcd. for  $FeZnC_{64}H_{50}N_{11}O_3SbF_7 \cdot (C_{14}H_{19}N_2)^+(BF_4)^-$ : C, 57.71%; H, 4.28%; N, 11.22%; Fe, 3.44%; Zn, 4.03%. Found: C, 57.19%; H, 4.89%; N, 10.99%; Fe, 3.40%; Zn, 4.10%.

For compound (4) prepared with proton sponge as base,  $\mu_{eff}(\text{solid}, 298\text{ K}) = 2.19\ \mu_B$ . Anal. calcd. for  $FeCuC_{64}H_{50}N_{11}O_3SbF_7 \cdot (C_{14}H_{19}N_2)^+(BF_4)^-$ : C, 57.78%; H, 4.29%; N, 11.23%; Fe, 3.45%; Cu, 3.92%. Found: C, 57.81%; H, 4.09%; N, 10.85%; Fe, 3.64%; Cu, 3.85%.

$[ClFe^{III}(TPP)(imid)M^{II}(py)](BF_4) \cdot (p.s.H)^+(BF_4)^-$ , where  $M = Zn^{2+}$   
[compound (5)] and  $Cu^{2+}$  [compound (6)]. These compounds were prepared as described above for the other chloride iron-zinc and iron-copper binuclear complexes, with the exception that the  $[M(imidH)(py)DAP](BF_4)_2$  compound was used to supply the imidazolate bridging moiety. In the presence of proton sponge (0.0964 g) or  $t\text{-BuO}^-K^+$  (0.050 g), the  $[Fe(TPP)Cl]$  (0.2112 g) and  $[M(imidH)(py)DAP](BF_4)_2$  (0.2698 g for  $M = Zn^{2+}$  and 0.2690 g for  $M = Cu^{2+}$ ) reactants were dissolved in 150 ml  $CH_2Cl_2/CH_3CN$  (10%) and refluxed for 6 h. The product solution was evaporated and the solids were washed with water and heptane. The

purple crystalline product was dried in vacuo overnight at room temperature over  $P_2O_5$ . The samples prepared using proton sponge were obtained as  $(p.s.H)^+(BF_4)^-$  occludates, while those synthesized employing  $t\text{-BuO}^-K^+$  were occlulate-free. Absorption bands in the infrared spectrum attributed to occluded  $(p.s.H)^+$  were observed at  $820\text{ cm}^{-1}$  and  $760\text{ cm}^{-1}$  for compound (5) and at  $820\text{ cm}^{-1}$  and  $760\text{ cm}^{-1}$  for compound (6) (see Figure 6-H and 6-I), whereas these marker bands were absent in the preparation using  $t\text{-BuO}^-K^+$  as base.

For compound (5) prepared with proton sponge as base,  $\mu_{\text{eff}}(\text{solid}, 298\text{ K}) = 2.69\ \mu_B$ . Anal. calcd. for  $FeZnC_{65}H_{51}N_{10}ClBF_4 \cdot (C_{14}H_{19}N_2)^+(BF_4)^-$ : C, 62.52%; H, 4.65%; N, 11.07%; Fe, 3.68%; Zn, 4.31%; Cl, 2.34%. Found: C, 61.58%; H, 4.74%; N, 11.85%; Fe, 2.96%; Zn, 5.08%; Cl, 2.03%.

For compound (5) prepared with  $t\text{-BuO}^-K^+$  as base,  $\mu_{\text{eff}}(\text{solid}, 298\text{ K}) = 3.04\ \mu_B$ . Anal. calcd. for  $FeZnC_{65}H_{51}N_{10}ClBF_4$ : C, 64.22%; H, 4.23%; N, 11.52%; Fe, 3.39%; Zn, 5.38%. Found: C, 63.45%; H, 4.22%; N, 12.18%; Fe, 3.59%; Zn, 5.84%.

For compound (6) prepared with proton sponge as base,  $\mu_{\text{eff}}(\text{solid}, 298\text{ K}) = 4.51\ \mu_B$ . Anal. calcd. for  $FeCuC_{65}H_{51}N_{10}ClBF_4 \cdot (C_{14}H_{19}N_2)^+(BF_4)^-$ : C, 62.59%; H, 4.65%; N, 11.09%; Fe, 3.68%; Cu, 4.19%; Cl, 2.34%. Found: C, 61.72%; H, 4.62%; N, 11.17%; Fe, 3.32%; Cu, 4.79%; Cl, 1.84%.

For compound (6) prepared with  $t\text{-BuO}^-K^+$  as base,  $\mu_{\text{eff}}(\text{solid}, 298\text{ K}) = 4.68\ \mu_B$ . Anal. calcd. for  $FeCuC_{65}H_{51}N_{10}ClBF_4$ : C, 64.32%; H, 4.24%; N, 11.54%; Fe, 4.60%; Cu, 5.23%. Found: C, 63.40%; H, 4.03%; N, 11.22%; Fe, 4.38%; Cu, 5.25%.

### Physical and Spectroscopic Measurements

Solid state infrared spectra were recorded as Nujol mulls using NaCl plates and a Beckman IR-4230 Spectrophotometer. Mössbauer spectra were obtained using a previously described spectrometer<sup>7</sup> and computer analyzed by the program of Chrisman and Tumolillo.<sup>37</sup> Temperatures were measured by a copper versus constantan thermocouple imbedded into the sample. Sodium nitroprusside (SNP) was used as a reference standard for the isomer shift parameter. Using a Calcomp plotting program, computer-generated plots of the Mössbauer spectra were obtained.

Magnetic susceptibilities of the solids were measured by the Faraday technique using a Cahn model 6600-1 research magnetic susceptibility system and  $\text{Hg}[\text{Co}(\text{NCS})_4]$  as the calibrant. All room temperature measurements were obtained with samples under one atmosphere of helium. Corrections for the ligand and anion diamagnetism in all the complexes were made using the molar susceptibilities calculated from Pascal's Constants:<sup>38</sup>

|   |  |
|---|--|
| $[\text{Fe}(\text{TPP})\text{Cl}]$  | $\chi_{\text{M,dia}} = -238 \times 10^{-6} \text{ cgsu}$ |
| $[\text{Fe}(\text{TPP})(\text{OSO}_2\text{CF}_3)]$  | $\chi_{\text{M,dia}} = -260 \times 10^{-6} \text{ cgsu}$ |
| $[\text{ClFe}(\text{TPP})(\text{imid})\text{Zn}](\text{BF}_4) \cdot (\text{p.s.H})^+(\text{BF}_4)^-$                        | $\chi_{\text{M,dia}} = -690 \times 10^{-6} \text{ cgsu}$ |
| $[\text{ClFe}(\text{TPP})(\text{imid})\text{Cu}](\text{BF}_4) \cdot (\text{p.s.H})^+(\text{BF}_4)^-$                        | $\chi_{\text{M,dia}} = -685 \times 10^{-6} \text{ cgsu}$ |
| $[(\text{OSO}_2\text{CF}_3)\text{Fe}(\text{TPP})(\text{imid})\text{Zn}](\text{BF}_4) \cdot (\text{p.s.H})^+(\text{BF}_4)^-$ | $\chi_{\text{M,dia}} = -705 \times 10^{-6} \text{ cgsu}$ |
| $[(\text{OSO}_2\text{CF}_3)\text{Fe}(\text{TPP})(\text{imid})\text{Cu}](\text{BF}_4) \cdot (\text{p.s.H})^+(\text{BF}_4)^-$ | $\chi_{\text{M,dia}} = -700 \times 10^{-6} \text{ cgsu}$ |
| $[\text{ClFe}(\text{TPP})(\text{imid})\text{Zn}(\text{py})](\text{BF}_4) \cdot (\text{p.s.H})^+(\text{BF}_4)^-$             | $\chi_{\text{M,dia}} = -695 \times 10^{-6} \text{ cgsu}$ |
| $[\text{ClFe}(\text{TPP})(\text{imid})\text{Cu}(\text{py})](\text{BF}_4) \cdot (\text{p.s.H})^+(\text{BF}_4)^-$             | $\chi_{\text{M,dia}} = -690 \times 10^{-6} \text{ cgsu}$ |

For the variable temperature magnetochemical measurements, the cryogenic apparatus consisted of an Air Products Interface model DMX-19 vacuum

shroud, an LT-3-110 B Heli-tran system, and an APD-TL digital temperature readout monitoring an iron-doped gold versus chromel thermocouple.

The solution state magnetic susceptibility studies on the "2Co2Cu" superoxide dismutase protein were also performed on the Cahn 6600-1 Faraday balance, using the cryogenic apparatus described above. The superoxide dismutase protein samples were prepared and supplied by Professor James Fee of the Biophysics Department, the University of Michigan. The metal ion analyses on the "2Co2Cu" SOD sample were determined by atomic absorption and EPR spectroscopy in the Fee laboratory and found to be 3.4 mM in total  $\text{Co}^{\text{II}}$ , 6.1 mM in total  $\text{Cu}^{\text{II}}$ , and 2.7 mM in EPR-detectable  $\text{Cu}^{\text{II}}$ .<sup>39</sup> These protein samples were degassed with argon and studied as received. Using a quartz boat with a gas-tight cap,<sup>40</sup> the samples were sealed under an argon gas atmosphere to avoid contamination of the solution by the intrusion of moist air. Triply distilled water and 1.0 M  $\text{NiCl}_2 \cdot 6\text{H}_2\text{O}$  solution were used as calibrants.<sup>40</sup>

The EPR spectra of the polycrystalline solids were taken at 10 K on a Varian E-line spectrometer. The magnetic field positions were referenced relative to diphenylpicrylhydrazyl (dpph). Using analytically pure ammonium sulfate as a solid support, samples were prepared containing 10% mixed-metal binuclear complex.

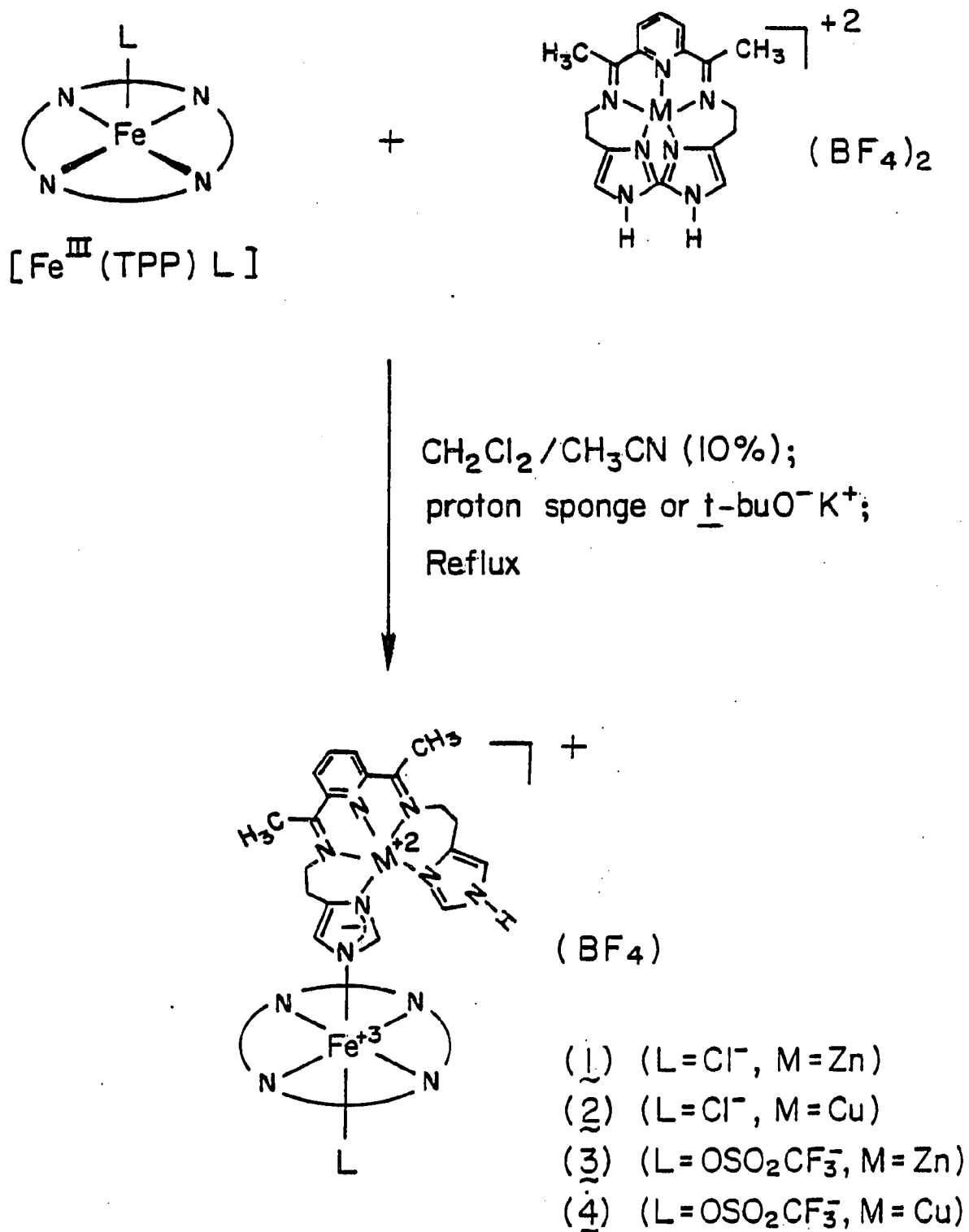
## RESULTS AND DISCUSSION

### Synthesis and Characterization of the Complexes

The synthetic scheme for the  $\mu$ -imidazolato iron(III)-zinc(II) and iron(III)-copper(II) compounds is shown in Figure 5. The  $\mu$ -imidazolato complexes (1)-(4) were prepared by the reaction of one mole  $[\text{Fe}(\text{TPP})\text{L}]$  with 1.2 moles  $[\text{M}^{\text{II}}(\text{imidH})_2\text{DAP}]^{2+}$  <sup>41</sup> in the presence of one mole equivalent of a base such as [1,2-bis-(dimethylamino)naphthalene] (proton sponge) or  $t\text{-BuO}^-\text{K}^+$ . In the presence of excess base and long reaction times, trinuclear or even polynuclear compounds, formulated as  $\{\text{Cu}^{\text{II}}\text{-porphyrin-Cu}^{\text{II}}\}_n$  species, <sup>5</sup> were obtained but not further characterized. No reaction occurred in the absence of base, and the zinc(II) and copper(II) compounds,  $[\text{M}^{\text{II}}(\text{imidH})(\text{py})\text{DAP}]^{2+}$  <sup>42</sup> (with one terminal pyridine group replacing an imidazole moiety), also reacted in the presence, but not the absence, of base to form the binuclear  $[\text{ClFe}^{\text{III}}(\text{TPP})(\text{imid})\text{M}^{\text{II}}(\text{py})]^+$  species (5) and (6). The use of  $[\text{Cu}^{\text{II}}(\text{py})_2\text{DAP}]^{2+}$  in the reaction procedure produced no binuclear or polynuclear product, in keeping with the absence of a coordinating and bridging imidazolate functional group. Compounds (1)-(6) exhibit satisfactory elemental analyses (see Experimental Section) consistent with the 1:1 (Fe:M) structural formulations as shown in Figure 4. The samples prepared using proton sponge were obtained as  $(\text{p.s.H})^+(\text{BF}_4)^-$  occludates, while those synthesized employing  $t\text{-BuO}^-\text{K}^+$  were occludate-free. The absorption of aromatic compounds into the crystal lattice of metalloporphyrins has been reported in the literature, <sup>36</sup> and, thus, the formation of these  $(\text{p.s.H})^+(\text{BF}_4)^-$  occludates was not unexpected. The occludate and

Figure 5

Synthetic Scheme for the  $\mu$ -Imidazolato Mixed-Metal Complexes



occludate-free samples gave essentially identical magnetic and spectroscopic results, although the data presented in this work are for the  $(p.s.H)^+(BF_4)^-$  occludate samples exclusively.

The infrared spectroscopic data presented in Figure 6 indicate the success of the binuclear complex syntheses. While the 1700-4000  $cm^{-1}$  IR spectral range is blank for all of the complexes, the 600-1700  $cm^{-1}$  region contains spectral peaks corresponding to the appropriate functional groups present in the dimers. For example, the C=N imine stretching frequency around 1580-1600  $cm^{-1}$  is observed, as is the broad B-F stretch centered around 1050  $cm^{-1}$ .<sup>43</sup> In the case of the  $[(OSO_2CF_3)-Fe(TPP)(imid)M]^+$  species, absorption peaks at 635  $cm^{-1}$  and 1225  $cm^{-1}$ , characteristic for the  $(OSO_2CF_3)$  moiety,<sup>36</sup> are exhibited in the Figure 6-F) and 6-G) infrared spectra, but are absent in the IR spectra of the chloride mixed-metal compounds. Strong absorption bands in the infrared spectrum attributed to occluded  $(p.s.H)^+$  are found ca. 830  $cm^{-1}$  and 760  $cm^{-1}$  for all the compounds. In no case are there strong bands around 890  $cm^{-1}$  and 870  $cm^{-1}$  which might indicate formation of some  $\mu$ -oxo porphyrin product.<sup>33</sup>

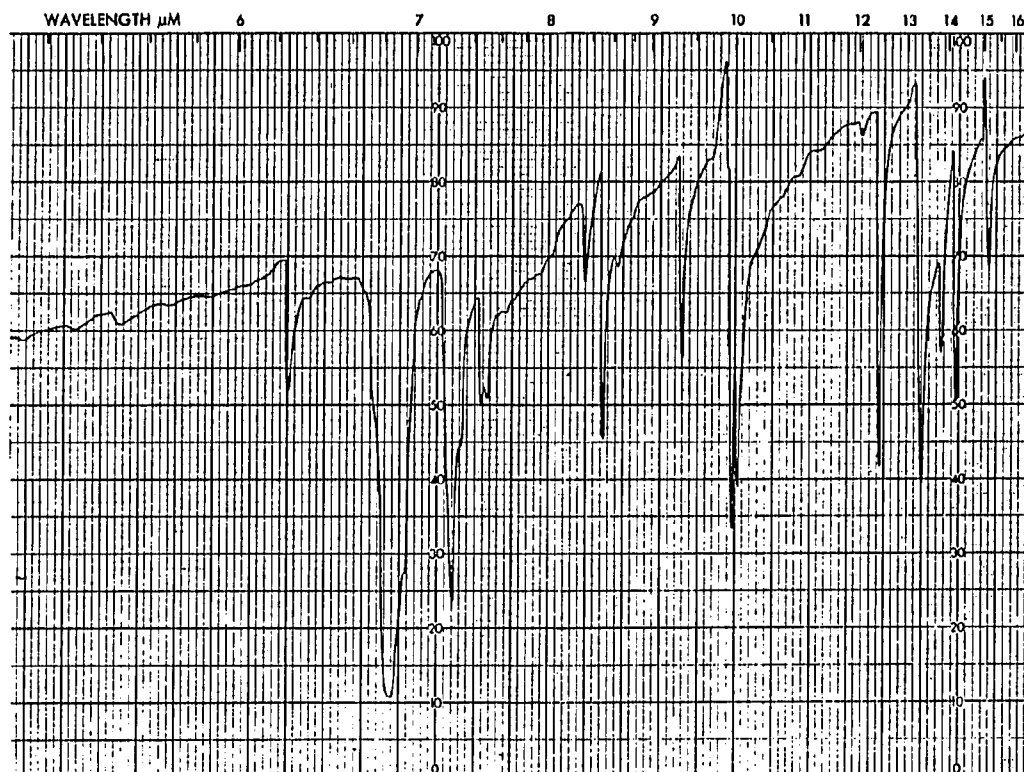
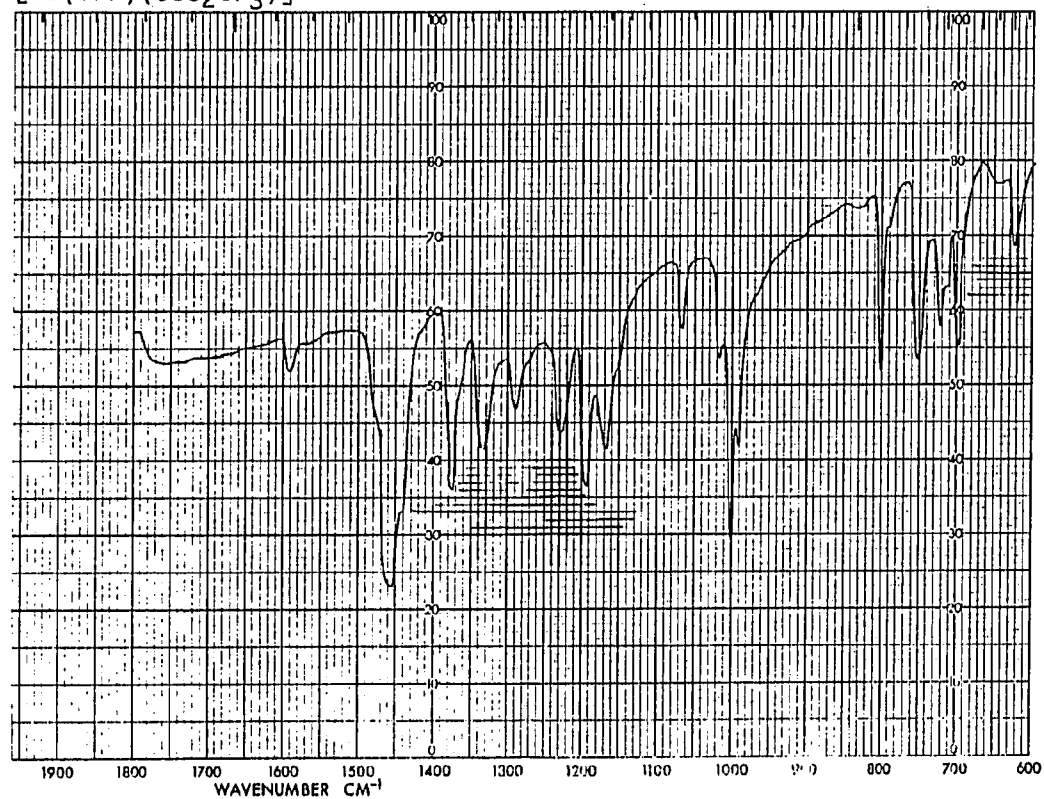
#### Mössbauer Spectroscopic Measurements

The zero-field  $^{57}Fe$  Mössbauer spectra at 100 K have been collected (Figure 7) for the  $[LFe(TPP)(imid)M]^+$  and  $[ClFe(TPP)(imid)Cu(py)]^+$  binuclear complexes, as well as for the chloride and triphlate  $[Fe(TPP)L]$  compounds. Table 1 lists the isomer shift ( $\delta_{SNP}$  in mm/s) and quadrupole splitting ( $\Delta E_Q$  in mm/s) parameters for the mixed-metal complexes, using sodium nitroprusside as a reference standard for the

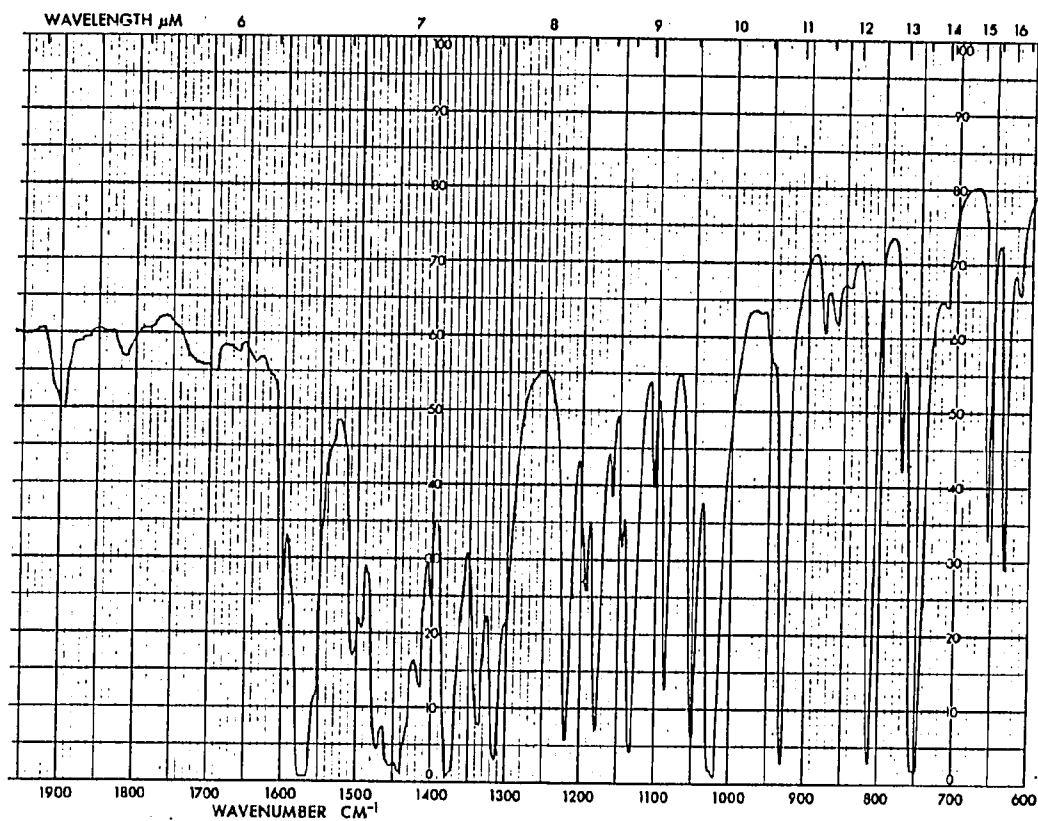


Figure 6  
Nujol Mull Infrared Spectrum of

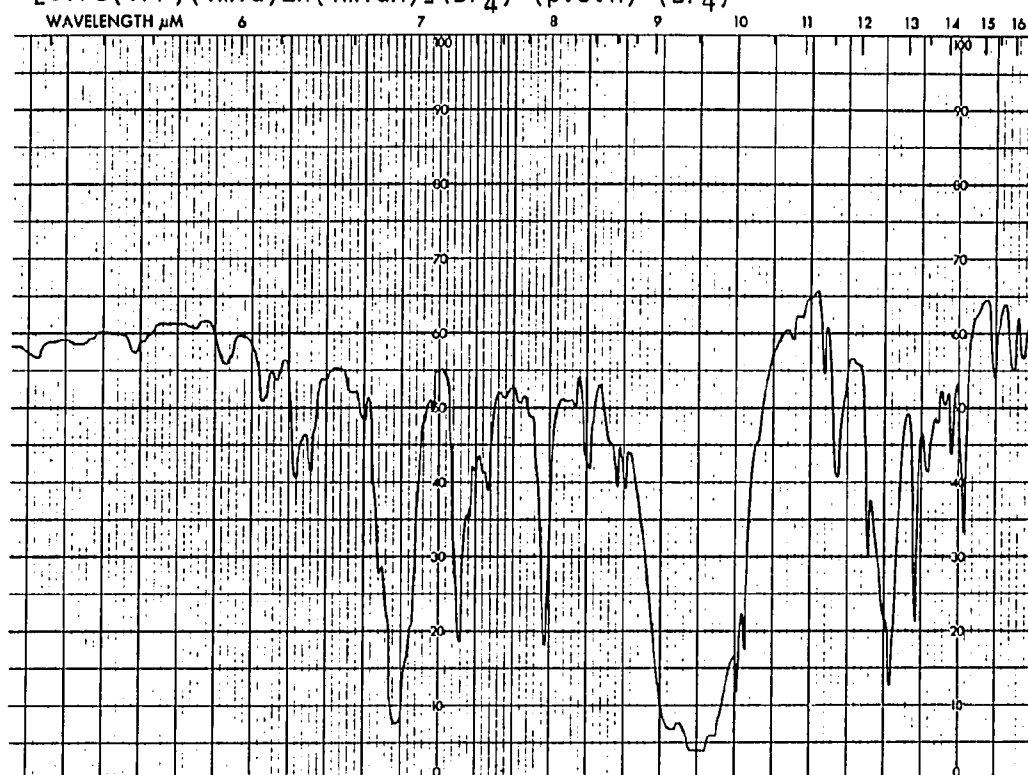
- A)  $[\text{Fe}(\text{TPP})\text{Cl}]$
- B)  $[\text{Fe}(\text{TPP})(\text{OSO}_2\text{CF}_3)]$
- C) [1,2-bis-(dimethylamino)naphthalene] (proton sponge)
- D)  $[\text{ClFe}(\text{TPP})(\text{imid})\text{Zn}(\text{imidH})](\text{BF}_4) \cdot (\text{p.s.H})^+(\text{BF}_4)^-$
- E)  $[\text{ClFe}(\text{TPP})(\text{imid})\text{Cu}(\text{imidH})](\text{BF}_4) \cdot (\text{p.s.H})^+(\text{BF}_4)^-$
- F)  $[(\text{OSO}_2\text{CF}_3)\text{Fe}(\text{TPP})(\text{imid})\text{Zn}(\text{imidH})](\text{BF}_4) \cdot (\text{p.s.H})^+(\text{BF}_4)^-$
- G)  $[(\text{OSO}_2\text{CF}_3)\text{Fe}(\text{TPP})(\text{imid})\text{Cu}(\text{imidH})](\text{BF}_3) \cdot (\text{p.s.H})^+(\text{BF}_4)^-$
- H)  $[\text{ClFe}(\text{TPP})(\text{imid})\text{Zn}(\text{py})](\text{BF}_4) \cdot (\text{p.s.H})^+(\text{BF}_4)^-$
- I)  $[\text{ClFe}(\text{TPP})(\text{imid})\text{Cu}(\text{py})](\text{BF}_4) \cdot (\text{p.s.H})^+(\text{BF}_4)^-$

A)  $[\text{Fe}(\text{TPP})\text{Cl}]$ B)  $[\text{Fe}(\text{TPP})(\text{OSO}_2\text{CF}_3)]$ 

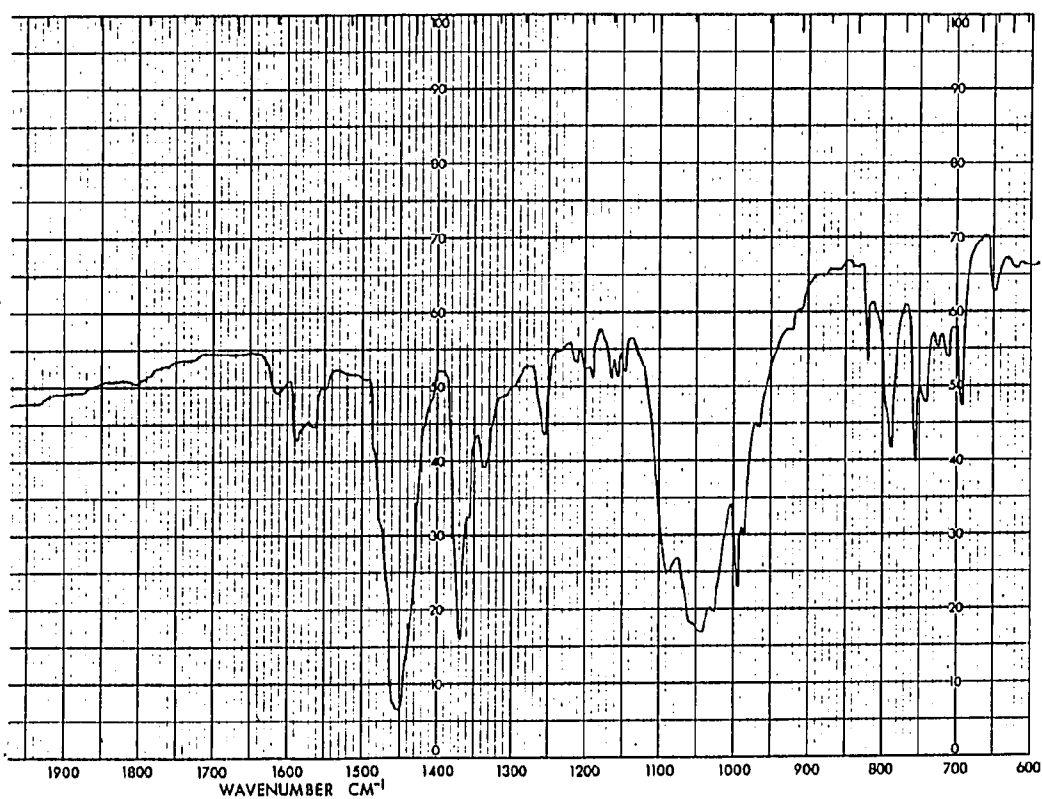
## c) [1,2-bis-(dimethylamino)naphthalene]



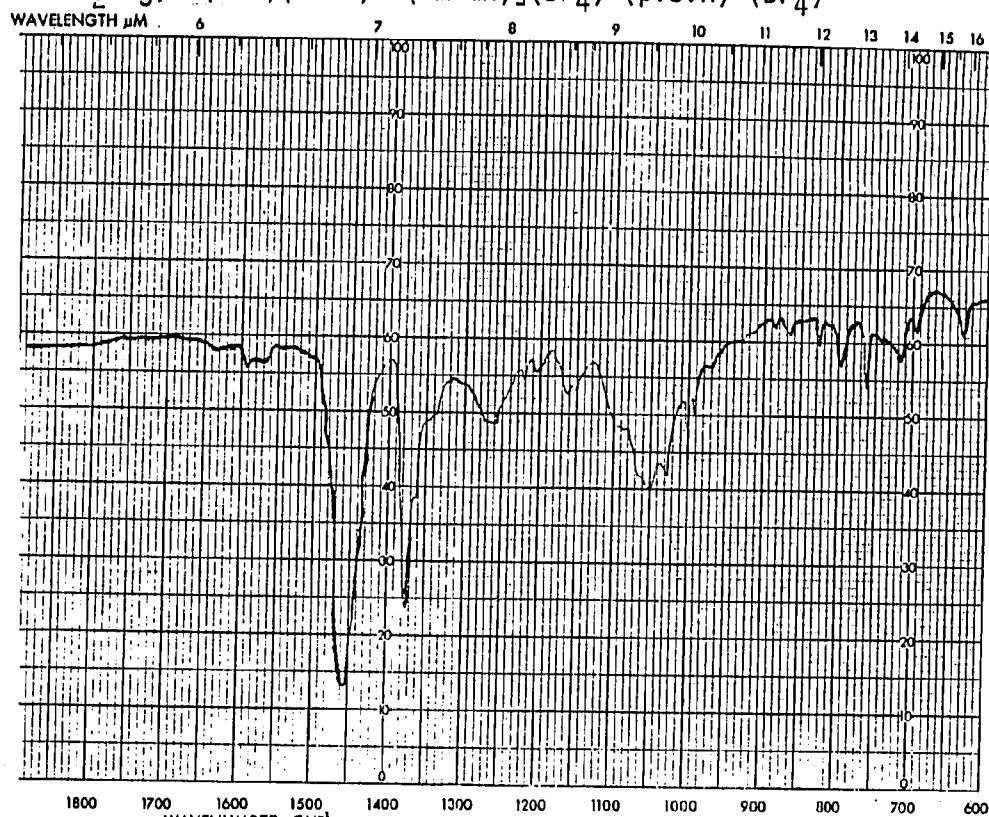
D)  $[\text{ClFe}(\text{TPP})(\text{imid})\text{Zn}(\text{imidH})](\text{BF}_4) \cdot (\text{p.s.H})^+(\text{BF}_4)^-$



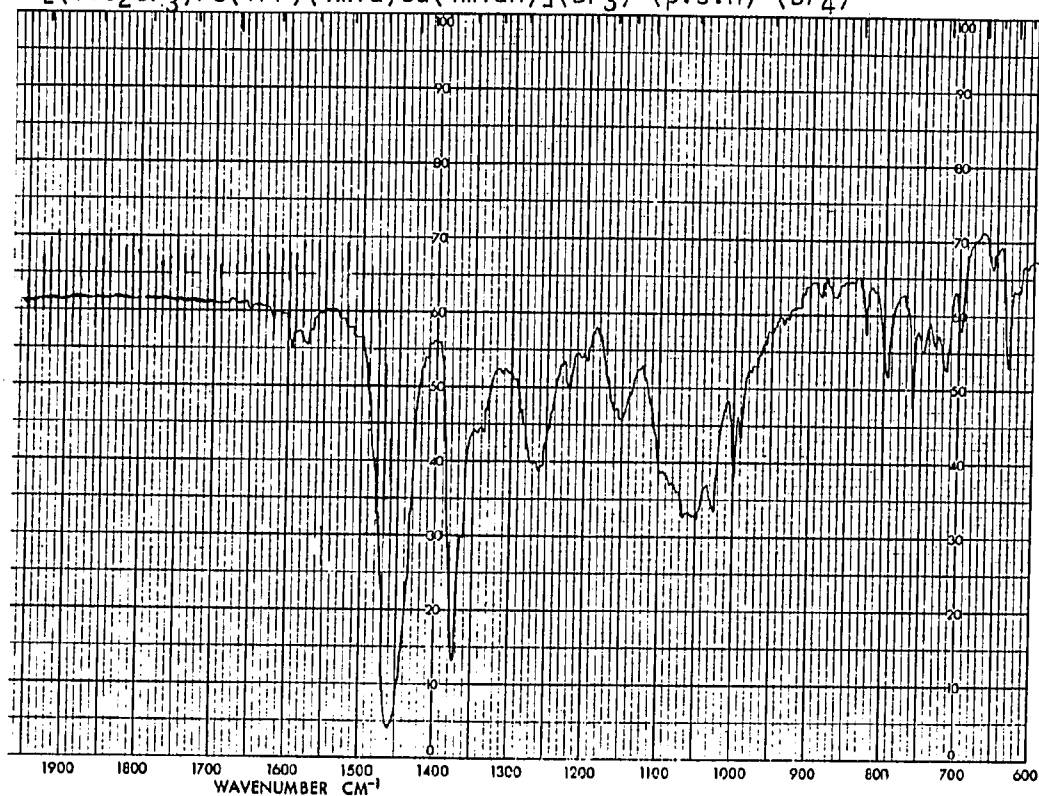
E)  $[\text{ClFe}(\text{TPP})(\text{imid})\text{Cu}(\text{imidH})](\text{BF}_4) \cdot (\text{p.s.H})^+(\text{BF}_4)^-$



F)  $[(\text{OSO}_2\text{CF}_3)\text{Fe}(\text{TPP})(\text{imid})\text{Zn}(\text{imidH})](\text{BF}_4) \cdot (\text{p.s.H})^+(\text{BF}_4)^-$

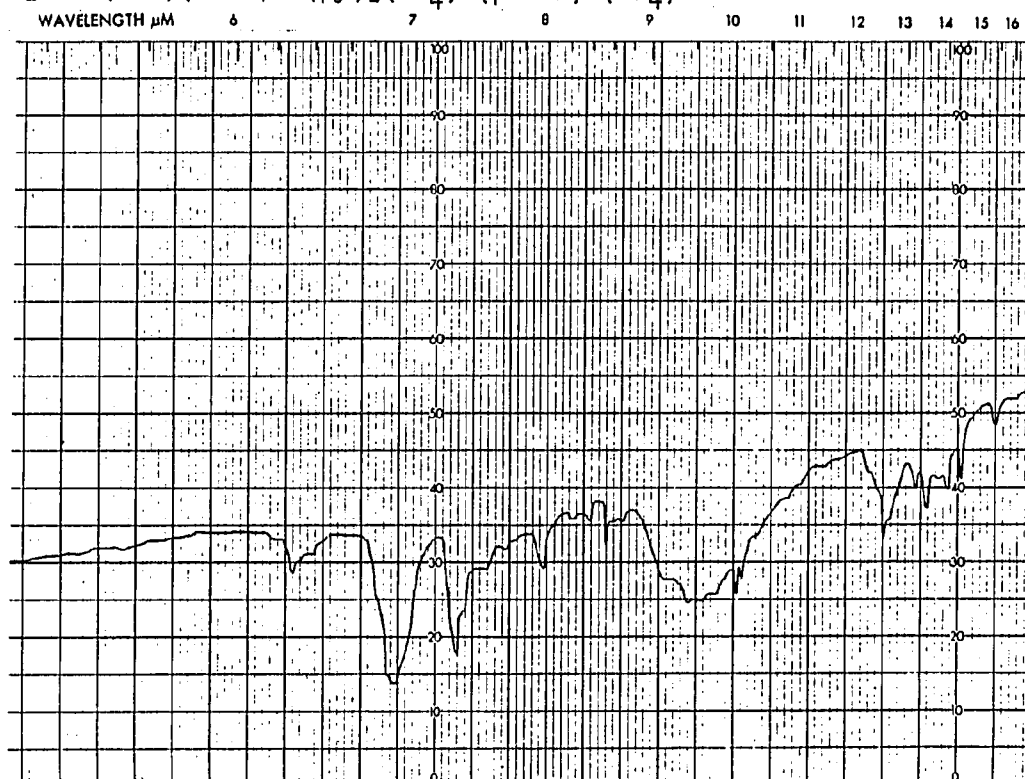


G)  $[(\text{OSO}_2\text{CF}_3)\text{Fe}(\text{TPP})(\text{imid})\text{Cu}(\text{imidH})](\text{BF}_3) \cdot (\text{p.s.H})^+(\text{BF}_4)^-$



H)  $[\text{ClFe}(\text{TPP})(\text{imid})\text{Zn}(\text{py})](\text{BF}_4) \cdot (\text{p.s.H})^+(\text{BF}_4)^-$

171



I)  $[\text{ClFe}(\text{TPP})(\text{imid})\text{Cu}(\text{py})](\text{BF}_4) \cdot (\text{p.s.H})^+(\text{BF}_4)^-$

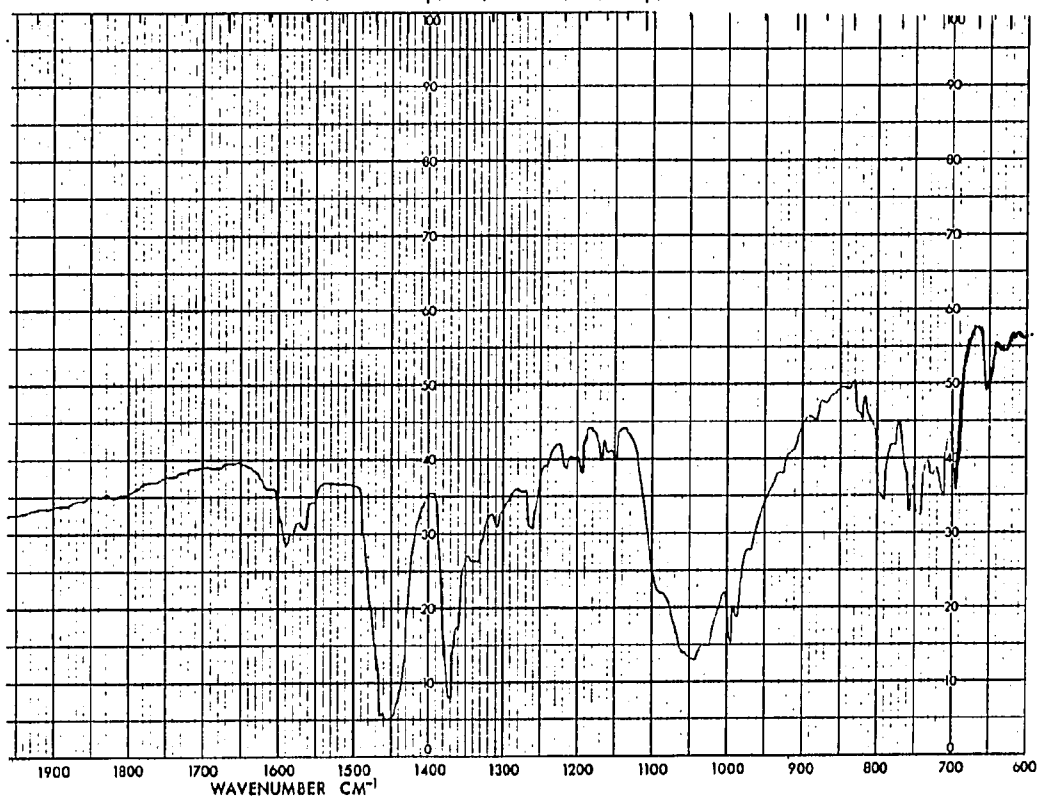
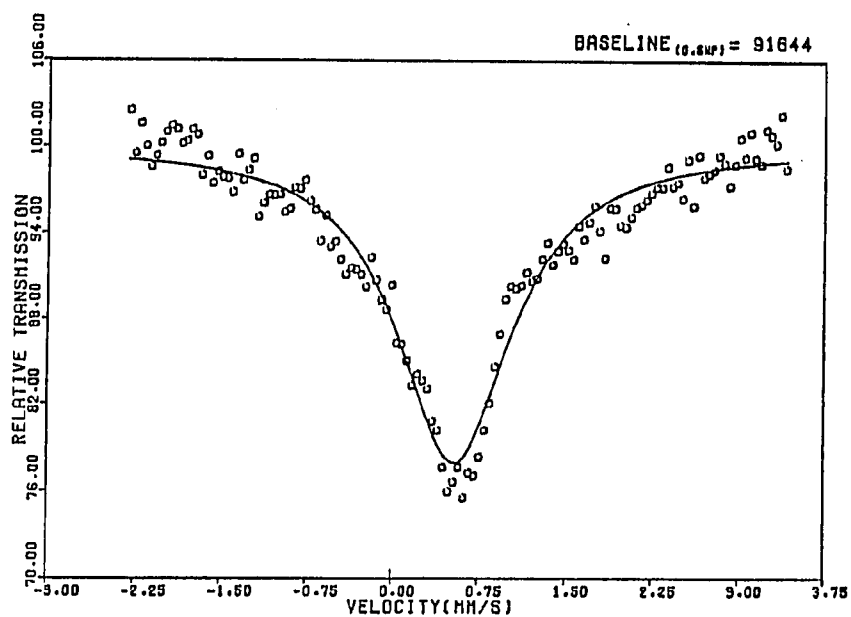
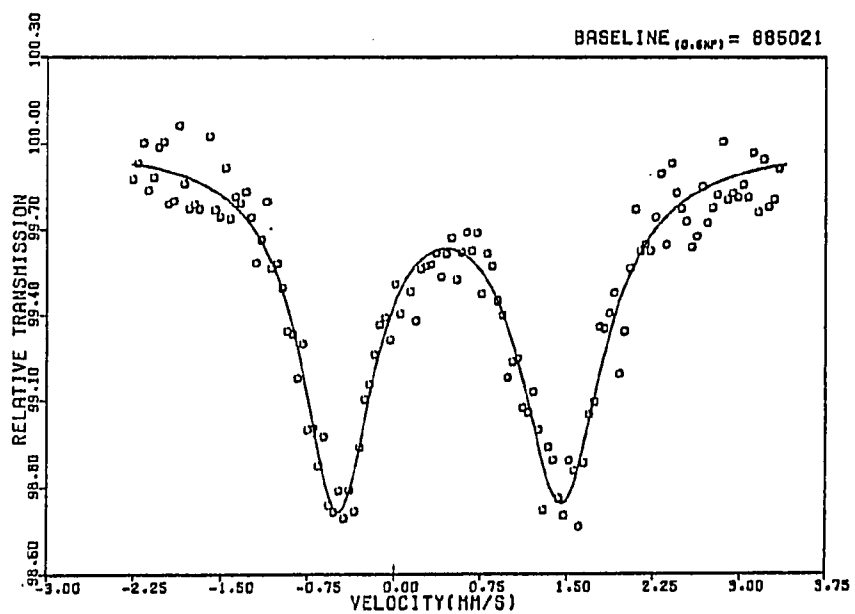
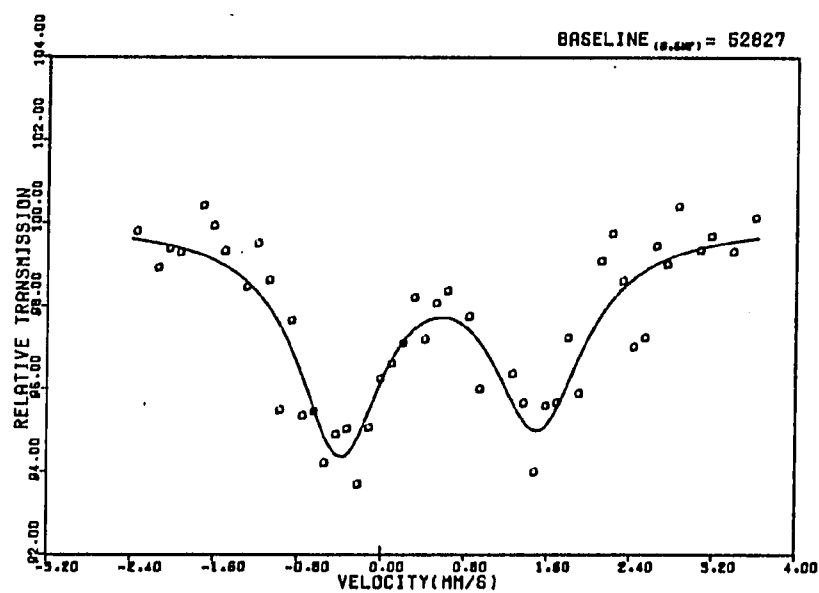
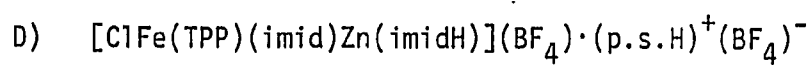
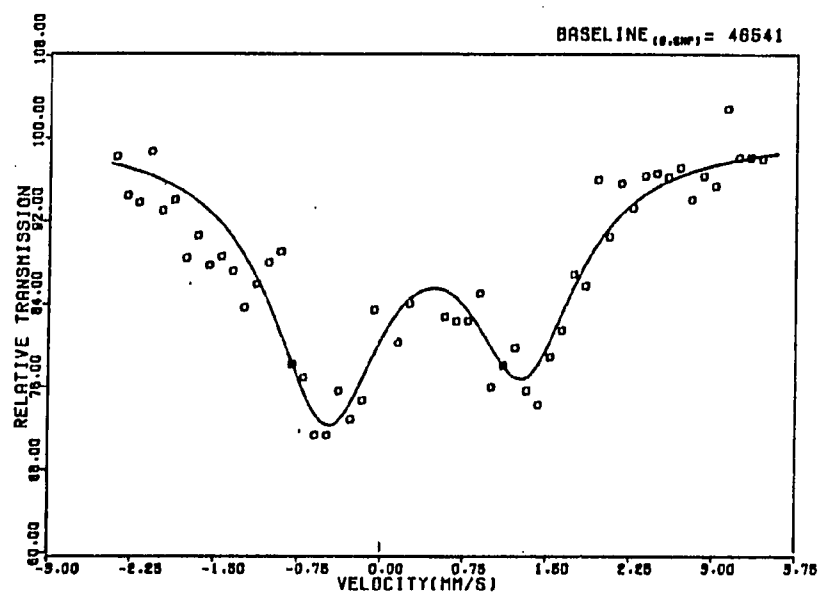
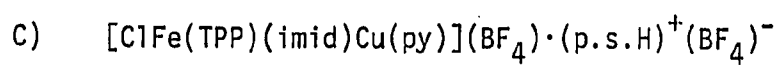


Figure 7Mössbauer Spectrum at 100 K of

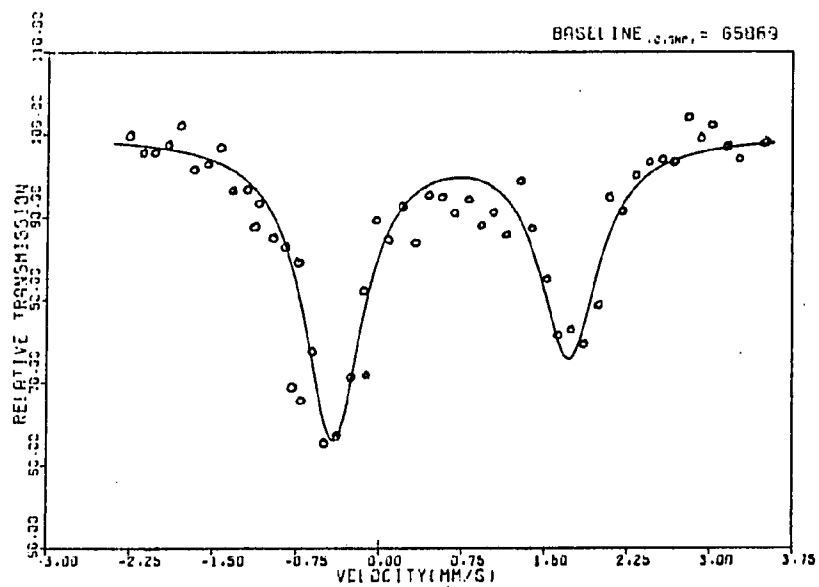
- A)  $[\text{Fe}(\text{TPP})\text{Cl}]$
- B)  $[\text{ClFe}(\text{TPP})(\text{imid})\text{Cu}(\text{imidH})](\text{BF}_4) \cdot (\text{p.s.H})^+(\text{BF}_4)^-$
- C)  $[\text{ClFe}(\text{TPP})(\text{imid})\text{Cu}(\text{py})](\text{BF}_4) \cdot (\text{p.s.H})^+(\text{BF}_4)^-$
- D)  $[\text{ClFe}(\text{TPP})(\text{imid})\text{Zn}(\text{imidH})](\text{BF}_4) \cdot (\text{p.s.H})^+(\text{BF}_4)^-$
- E)  $\text{Fe}(\text{TPP})(\text{OSO}_2\text{CF}_3)]$
- F)  $[(\text{OSO}_2\text{CF}_3)\text{Fe}(\text{TPP})(\text{imid})\text{Cu}(\text{imidH})](\text{BF}_4) \cdot (\text{p.s.H})^+(\text{BF}_4)^-$

A)  $[\text{Fe}(\text{TPP})\text{Cl}]$ B)  $[\text{ClFe}(\text{TPP})(\text{imid})\text{Cu}(\text{imidH})](\text{BF}_4) \cdot (\text{p.s.H})^+(\text{BF}_4)^-$ 





E)  $\text{Fe}(\text{TPP})(\text{OSO}_2\text{CF}_3)]$



F)  $[(\text{OSO}_2\text{CF}_3)\text{Fe}(\text{TPP})(\text{imid})\text{Cu}(\text{imidH})](\text{BF}_4) \cdot (\text{p.s.H})^+(\text{BF}_4)^-$

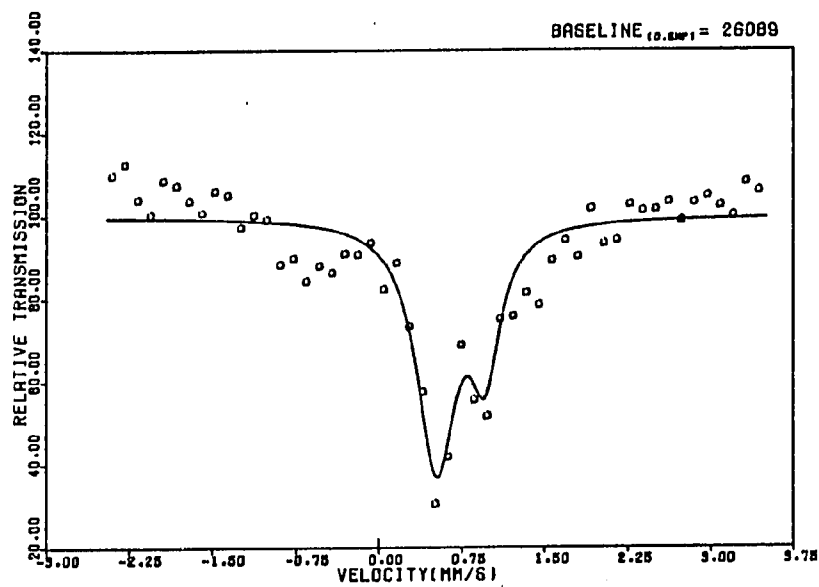


Table 1

Mössbauer Parameters for the  $\mu$ -Imidazolato Complexes at 100 K

| Complex  | Isomer Shift <sup>a)</sup><br>$\delta$ , mm/s | Quadrupole Splitting<br>$\Delta E_Q$ , mm/s |
|--|---|---|
| $[\text{ClFe}^{\text{III}}(\text{TPP})(\text{imid})\text{Zn}^{\text{II}}(\text{imidH})](\text{BF}_4) \cdot \text{p.s.H}^+\text{BF}_4^-$                        | 0.45  | 1.93  |
| $[\text{ClFe}^{\text{III}}(\text{TPP})(\text{imid})\text{Cu}^{\text{II}}(\text{imidH})](\text{BF}_4) \cdot \text{p.s.H}^+\text{BF}_4^-$                        | 0.48  | 1.95  |
| $[\text{ClFe}^{\text{III}}(\text{TPP})(\text{imid})\text{Cu}^{\text{II}}(\text{py})](\text{BF}_4) \cdot \text{p.s.H}^+\text{BF}_4^-$                           | 0.40  | 1.87  |
| $[(\text{OSO}_2\text{CF}_3)\text{Fe}^{\text{III}}(\text{TPP})(\text{imid})\text{Cu}^{\text{II}}(\text{imidH})](\text{BF}_4) \cdot \text{p.s.H}^+\text{BF}_4^-$ | 0.77  | 0.36  |

a) Isomer shift referenced to SNP standard.

isomer shift parameter. The  $^{57}\text{Fe}$  Mössbauer of (1) and (2) indicate essentially identical electronic environments about the iron center, with both compounds exhibiting quadrupole split doublets typical of low-spin  $\text{Fe}^{\text{III}}$  centers. The isomer shift and quadrupole splitting parameters for (1) and (2) are identical within experimental error:  $\delta_{\text{SNP}} = 0.46 (\pm 0.02) \text{ mm/s}$  and  $\Delta E_Q = 1.94 (\pm 0.03) \text{ mm/s}$ . The  $[\text{ClFe}(\text{TPP})(\text{imid})\text{Cu}(\text{py})]^+$  species also gives a Mössbauer spectrum with parameters quite similar to that of compounds (1) and (2), but, unfortunately, compound (5) has not yielded a resolvable Mössbauer spectrum to date.<sup>44</sup>

Concerning the  $[(\text{OSO}_2\text{CF}_3)\text{Fe}(\text{imid})\text{Cu}]^+$  species, the  $^{57}\text{Fe}$  Mössbauer spectrum obtained clearly indicates a change in the electronic environment around the iron(III) center in going from the parent  $[\text{Fe}(\text{TPP})-(\text{OSO}_2\text{CF}_3)]$  to compound (4). As shown in Figure 7, the  $[\text{Fe}(\text{TPP})-(\text{OSO}_2\text{CF}_3)]$  species exhibits a widely spaced quadrupole split doublet ( $\delta_{\text{SNP}} = 0.66 \text{ mm/s}$  and  $\Delta E_Q = 2.13 \text{ mm/s}$ , similar to the Mössbauer parameters obtained by Reed *et al.*<sup>36</sup>), and the  $[(\text{OSO}_2\text{CF}_3)\text{Fe}(\text{imid})\text{Cu}]^+$  species yields a very closely spaced quadrupole split doublet ( $\delta_{\text{SNP}} = 0.77 \text{ mm/s}$  and  $\Delta E_Q = 0.36 \text{ mm/s}$ ). Also comparison between Mössbauer spectra of the chloride compounds (2) and (6) and triphlate complex (4) reveals that the electronic environment about the iron(III) center in (2) and (6) is very different from the iron in (4). Comparison of the Mössbauer spectrum of (4) to that of (3) would be useful but compound (3) has failed to yield a resolvable Mössbauer spectrum even at 100 K and long collection times,<sup>44</sup> so no additional information about

these compounds' electronic structure is available from the Mössbauer spectroscopic technique at this time.

### Magnetochemical and EPR Studies

Variable-temperature (15-300 K) magnetic susceptibility data, listed in Table 2, for the four  $\mu$ -imidazolato species are displayed in Figure 8 as plots of  $\mu_{\text{eff}}(\mu_B)$  vs. temperature(K). The curves shown are merely illustrative and not computer fit to the data. Full temperature magnetochemical data have also been obtained for the  $[\text{ClFe}^{\text{III}}(\text{TPP})\text{-imid})\text{Cu}^{\text{II}}(\text{py})]^+$  species and these data are documented in Table 2. The results for compound (6) essentially parallel that of compound (2), discussed below, with the room temperature magnetic moment of  $4.7 \mu_B^{295\text{K}}$ . For the sake of clarity, the  $\mu_{\text{eff}}$  vs. temperature for (6) has been omitted from Figure 8. Compound (1) has a room temperature magnetic moment of  $2.67 \mu_B^{295\text{K}}$ , a value somewhat high for a simple  $S=1/2$ , low-spin ground state for this six-coordinate  $\text{Fe}^{\text{III}}$  porphyrin center with an axial  $\text{Cl}^-$  and a  $\text{Zn}^{\text{II}}$ -metallated imidazolate ligand. However, the gradual decrease in  $\mu_{\text{eff}}$  down to ca.  $2.15 \mu_B$  at 50 K is basically in agreement with an  $S=1/2$  assignment. Nevertheless, as discussed below, the EPR spectrum of (1) in the polycrystalline state indicates an electronic structure for iron which is not a strict case of a classical  $S=1/2$  system. For compound (2), where an  $S=1/2 \text{ Cu}^{\text{II}}$  center replaces  $\text{Zn}^{\text{II}}$ , the  $\mu_{\text{eff}}$  vs. temperature curve parallels that found for compound (1) but with the additional paramagnetism expected for an  $S=1/2 \text{ Cu}^{\text{II}}$  center having  $\mu_{\text{eff}} = 2.0 \mu_B$ . Thus, comparative full-temperature magnetochemical data for (1) and (2) indicate magnetically

Table 2  
Variable-Temperature (15-300 K) Magnetochemical  
Data for the  $\mu$ -Imidazolato Complexes

| Compound | T(K)  | $\chi_M'$ (cgsu)      | $\mu_{\text{eff}}(\mu_B)$ |
|----------|-------|-----------------------|---------------------------|
| (1)      | 294.5 | $0.30 \times 10^{-2}$ | 2.67                      |
|          | 238.2 | 0.29                  | 2.34                      |
|          | 226.0 | 0.30                  | 2.32                      |
|          | 211.3 | 0.31                  | 2.30                      |
|          | 175.3 | 0.36                  | 2.26                      |
|          | 147.8 | 0.42                  | 2.22                      |
|          | 132.0 | 0.45                  | 2.19                      |
|          | 115.5 | 0.52                  | 2.19                      |
|          | 105.4 | 0.55                  | 2.16                      |
|          | 97.3  | 0.60                  | 2.15                      |
|          | 91.7  | 0.62                  | 2.14                      |
|          | 87.0  | 0.66                  | 2.14                      |
|          | 70.4  | 0.86                  | 2.20                      |
|          | 59.4  | 0.99                  | 2.17                      |
|          | 51.5  | 1.12                  | 2.15                      |
|          | 45.6  | 1.24                  | 2.13                      |
|          | 39.3  | 1.40                  | 2.10                      |
|          | 34.5  | 1.54                  | 2.06                      |
|          | 30.6  | 1.75                  | 2.07                      |

(Table 2 Continued)

| Compound | T(K)  | $\chi_M'$ (cgsu)      | $\mu_{\text{eff}}(\mu_B)$ |
|----------|-------|-----------------------|---------------------------|
|          | 28.9  | 1.75                  | 2.01                      |
|          | 24.7  | 1.98                  | 1.98                      |
|          | 21.6  | 2.20                  | 1.95                      |
|          | 18.6  | 2.48                  | 1.92                      |
| (2)      | 293.8 | $0.42 \times 10^{-2}$ | 3.39                      |
|          | 277.5 | 0.45                  | 3.41                      |
|          | 230.3 | 0.54                  | 3.34                      |
|          | 218.6 | 0.55                  | 3.29                      |
|          | 203.1 | 0.58                  | 3.26                      |
|          | 182.3 | 0.65                  | 3.24                      |
|          | 169.2 | 0.69                  | 3.21                      |
|          | 157.0 | 0.76                  | 3.23                      |
|          | 146.0 | 0.79                  | 3.18                      |
|          | 136.0 | 0.86                  | 3.19                      |
|          | 125.4 | 0.92                  | 3.15                      |
|          | 116.7 | 1.00                  | 3.16                      |
|          | 107.4 | 1.08                  | 3.14                      |
|          | 97.7  | 1.19                  | 3.14                      |
|          | 94.2  | 1.23                  | 3.13                      |
|          | 89.0  | 1.29                  | 3.12                      |

| Compound | T(K)  | $\chi_M^{\sim}$ (cgsu) | $\mu_{\text{eff}}(\mu_B)$ |
|----------|-------|------------------------|---------------------------|
|          | 84.0  | 1.36                   | 3.10                      |
|          | 70.0  | 1.43                   | 3.08                      |
|          | 62.0  | 1.61                   | 3.07                      |
|          | 52.5  | 1.90                   | 3.05                      |
|          | 44.2  | 2.26                   | 3.02                      |
|          | 39.0  | 2.56                   | 3.00                      |
|          | 35.6  | 2.81                   | 2.97                      |
|          | 25.0  | 4.00                   | 2.88                      |
|          | 20.0  | 5.00                   | 2.84                      |
|          | 17.2  | 5.81                   | 2.79                      |
| (3)      | 294.8 | $0.41 \times 10^{-2}$  | 3.36                      |
|          | 254.7 | 0.48                   | 3.36                      |
|          | 222.9 | 0.57                   | 3.37                      |
|          | 196.0 | 0.64                   | 3.34                      |
|          | 179.7 | 0.70                   | 3.33                      |
|          | 162.3 | 0.78                   | 3.33                      |
|          | 142.6 | 0.89                   | 3.31                      |
|          | 130.2 | 0.97                   | 3.29                      |
|          | 122.5 | 1.03                   | 3.28                      |
|          | 112.5 | 1.13                   | 3.28                      |



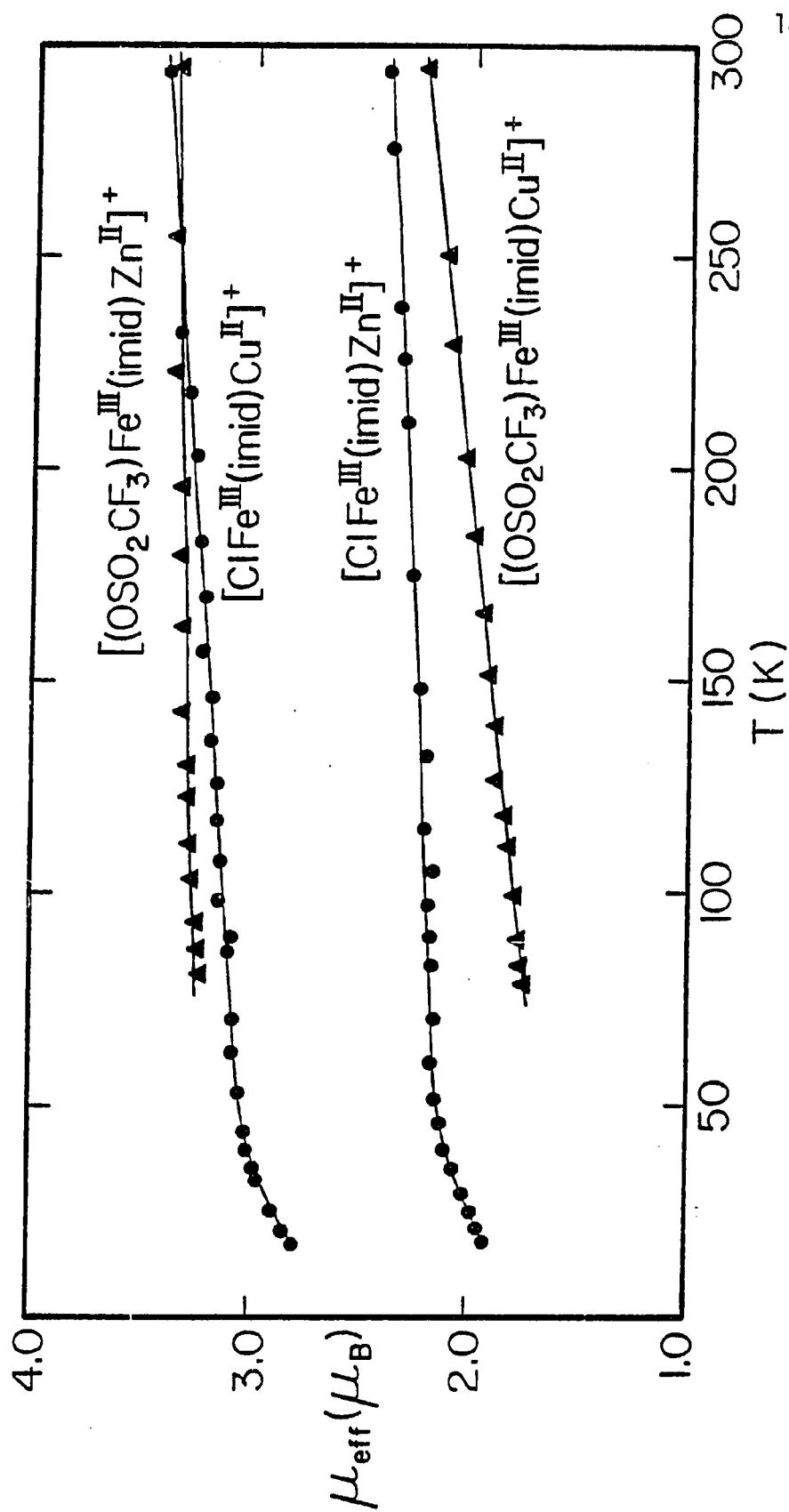
| Compound | T(K)  | $\chi_M'$ (cgsu)      | $\mu_{\text{eff}}(\mu_B)$ |
|----------|-------|-----------------------|---------------------------|
|          | 103.0 | 1.21                  | 3.27                      |
|          | 98.6  | 1.28                  | 3.27                      |
|          | 92.8  | 1.34                  | 3.24                      |
|          | 86.5  | 1.44                  | 3.23                      |
|          | 82.2  | 1.52                  | 3.24                      |
|          | 80.5  | 1.53                  | 3.21                      |
| (4)      | 293.0 | $1.35 \times 10^{-3}$ | 2.19                      |
|          | 251.4 | 1.53                  | 2.12                      |
|          | 229.7 | 1.73                  | 2.11                      |
|          | 203.3 | 1.83                  | 2.03                      |
|          | 184.3 | 1.93                  | 1.97                      |
|          | 166.1 | 2.09                  | 1.93                      |
|          | 151.2 | 2.33                  | 1.92                      |
|          | 139.3 | 2.47                  | 1.88                      |
|          | 126.8 | 2.81                  | 1.89                      |
|          | 117.7 | 2.88                  | 1.84                      |
|          | 111.1 | 3.01                  | 1.82                      |
|          | 101.3 | 3.26                  | 1.79                      |
|          | 99.3  | 3.37                  | 1.80                      |
|          | 89.3  | 3.70                  | 1.77                      |

| Compound | T(K)  | $\chi_M$ (cgsu)       | $\mu_{\text{eff}}$ ( $\mu\text{B}$ ) |
|----------|-------|-----------------------|--------------------------------------|
|          | 86.3  | 3.76                  | 1.76                                 |
|          | 84.5  | 3.75                  | 1.73                                 |
|          | 82.6  | 3.95                  | 1.75                                 |
|          | 80.7  | 4.04                  | 1.75                                 |
| (6)      | 291.0 | $0.94 \times 10^{-2}$ | 4.68                                 |
|          | 236.7 | 1.04                  | 4.44                                 |
|          | 208.9 | 1.16                  | 4.41                                 |
|          | 191.0 | 1.30                  | 4.40                                 |
|          | 175.3 | 1.38                  | 4.40                                 |
|          | 162.5 | 1.49                  | 4.41                                 |
|          | 147.1 | 1.63                  | 4.38                                 |
|          | 128.6 | 1.85                  | 4.37                                 |
|          | 110.3 | 2.17                  | 4.38                                 |
|          | 101.6 | 2.34                  | 4.36                                 |
|          | 94.2  | 2.50                  | 4.34                                 |
|          | 90.7  | 2.59                  | 4.34                                 |
|          | 87.1  | 2.70                  | 4.34                                 |
|          | 85.8  | 2.93                  | 4.49                                 |
|          | 83.2  | 2.82                  | 4.34                                 |
|          | 73.0  | 3.42                  | 4.47                                 |

| Compound | T(K) | $\chi_M$ (cgsu) | $\mu_{\text{eff}}(\mu_B)$ |
|----------|------|-----------------|---------------------------|
|          | 62.0 | 3.93            | 4.42                      |
|          | 52.5 | 4.58            | 4.39                      |
|          | 42.0 | 5.57            | 4.33                      |
|          | 32.2 | 6.97            | 4.24                      |
|          | 21.6 | 10.00           | 4.16                      |

Figure 8

$\mu_{\text{eff}}(\mu_B)$  vs. Temperature (K) Plots for the  $\mu$ -Imidazolato Complexes



isolated  $S=1/2$  centers in (2), with the bridging imidazolate ligand fostering little ( $\lesssim 15 \text{ cm}^{-1}$ ), if any, antiferromagnetic coupling between  $\text{Cu}^{\text{II}}$  and  $\text{Fe}^{\text{III}}$ .

The EPR spectra of (1), (2), and (3) as polycrystalline solids at 10 K are shown in Figure 9. EPR parameters for the EPR active compounds studied in this work are documented in Table 3. The  $g$  factors attributed to the low-spin iron component in (1) and (3) are strikingly similar to the results of a reported experiment by Peisach et al.,<sup>45</sup> where hemin chloride, a low-spin ferric porphyrin, was combined with imidazole and NaOH, presumably producing an imidazolate anion, and its EPR spectrum recorded. The  $g$  factors obtained ( $g_{zz} = 2.78$ ,  $g_{yy} = 2.26$ , and  $g_{xx} = 1.72$ ) are very different from those of hemin chloride plus imidazole with no base added ( $g_{zz} = 3.02$ ,  $g_{yy} = 2.24$ , and  $g_{xx} = 1.51$ ), thereby indicating that an imidazolate anion significantly alters an EPR signal in a characteristic manner.

In Figure 9, compound (1) exhibits a broad, multiple resonance in the  $g \approx 2$  region of the spectrum which is characteristic of a low-spin  $S=1/2$   $\text{Fe}^{\text{III}}$  porphyrin center in tetragonally distorted fields. In this same region, compound (2) displays a similar spectral pattern, but with an additional superimposed component centered around  $g = 2$  that can be assigned to  $\text{Cu}^{\text{II}}$ . Furthermore, both compounds also exhibit a  $g \approx 6$  resonance which is typical of a rhombically split high-spin  $S=5/2$  state. From relative integration of these  $g = 2$  and  $g = 6$  signals, the  $S=1/2$  state in (1) and (2) is present in approximately 80-90% abundance, although integration of EPR signals from solid samples is not an especially reliable measure of relative paramagnet concentrations. The

EPR Spectra at 10 K for the  $\mu$ -Imidazolato  
Complexes in the Polycrystalline State

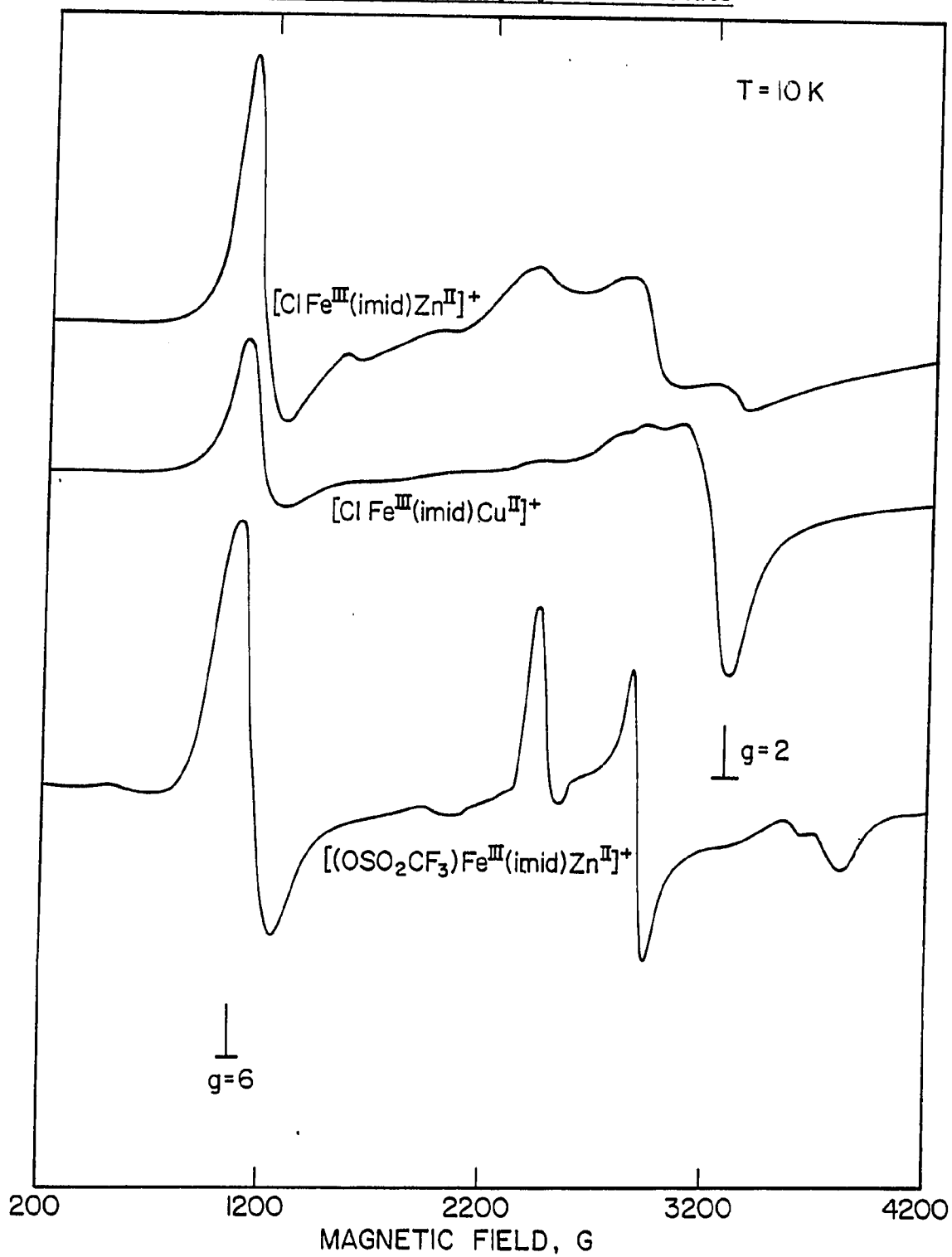


Table 3  
EPR Parameters at 10 K for the  $\mu$ -Imidazolato  
Complexes in the Polycrystalline State

| Compound | g Factors  |  |
|----------|--|--|
|          | <u>Fe</u>  | <u>Cu</u>                                    |
| (1)      | $g_{\perp} = 5.67$<br>$g_{\parallel} = 1.99$ ( $g_{zz} = 2.79$ )<br>$(g_{yy} = 2.26)$<br>$(g_{xx} \approx 1.71)$ |  |
| (2)      | $g_{\perp} = 5.62$<br>$g_{\parallel}$ (not resolved)   | $g_{\perp} = 2.09$<br>$g_{\parallel} = 2.22$ |
| (3)      | $g_{\perp} = 5.62$<br>$g_{\parallel} = 1.99$ ( $g_{zz} = 2.72$ )<br>$(g_{yy} = 2.28)$<br>$(g_{xx} = 1.73)$       |  |

$g \approx 6$  signal could arise from some high-spin impurity in (1) and (2), with the most likely source of such an impurity being that of the  $[\text{Fe}^{\text{III}}(\text{TPP})\text{Cl}]$  precursor. However, the Mössbauer spectra of both (1) and (2) indicate no such impurity [in Figure 7-B) and 7-D), the  $\delta_{\text{SNP}} = 0.41$  mm/s for  $[\text{Fe}^{\text{III}}(\text{TPP})\text{Cl}]$ , shown in Figure 7-A), should be quite apparent]. Also the elemental analyses of (1) and (2) are in agreement with their being analytically pure compounds. Of course, a small amount of  $S=5/2$  impurity could be EPR active and yet escape detection by chemical analyses and Mössbauer spectroscopy, and if present in only ca. 5% it would adequately explain the somewhat high value of  $\mu_{\text{eff}}^{295\text{ K}} = 2.67 \mu_{\text{B}}$  for (1), as compared to the 2.2-2.4  $\mu_{\text{B}}$  range normally found for low-spin  $\text{Fe}^{\text{III}}$ . Since the  $\mu_{\text{eff}}$  vs. temperature plots in Figure 8 are Curie in nature, the observed magnetic behavior is most probably not attributable to a thermally dependent  $(S=1/2) \rightleftharpoons (S=5/2)$  spin-equilibrium process, unless very small thermodynamic parameters are involved. Regardless of whether the  $g \approx 6$  signals in question arise from some  $S=5/2$  impurity, or from a thermally dependent spin-equilibrium process with small thermodynamic parameters, the basic conclusion of this part of the study is unchanged: antiferromagnetic exchange through imidazolate in (2) is at best weak and equal to  $15 \text{ cm}^{-1}$ .

In contrast to the weak exchange interaction found in compound (2), similar magnetic and EPR data on (3) and (4) reveal quite different behavior concerning the ability of imidazolate to foster magnetic coupling between  $\text{Fe}^{\text{III}}$  and  $\text{Cu}^{\text{II}}$ . It is now thought that  $\text{Fe}^{\text{III}}$  in the  $[\text{Fe}^{\text{III}}(\text{TPP})(\text{OSO}_2\text{CF}_3)]$  precursor to (3) and (4) exhibits a quantum-mechanical admixture of  $S=3/2$  and  $S=5/2$  spin states.<sup>36,46-52</sup> However,



this does not necessarily mean that the  $\mu$ -imidazolato binuclear species, derived from  $[\text{Fe}^{\text{III}}(\text{TPP})(\text{OSO}_2\text{CF}_3)]$ , would also reflect this unusual electronic structure; and, indeed, the EPR spectrum for (3) discounts the presence of such a spin-admixture occurring in (3) since the spectrum consists of two distinct signals at  $g = 6,2$  ( $S=5/2$ ) and  $g = 2$  ( $S=1/2$ ) rather than a single unique signal expected for some spin-admixture of  $S=1/2$ ,  $3/2$ , or  $5/2$  states.<sup>53</sup> The variable-temperature magnetochemical data for (3) and (4) are also shown in Figure 8. The room temperature magnetic moment of (3) is  $3.36 \mu_{\text{B}}^{295 \text{ K}}$  which is an unusual value for an  $\text{Fe}^{\text{III}}$  porphyrin compound. Nevertheless, this and the above EPR results can be rationalized by assuming the presence of a simple mixture of two distinct molecular species of spin =  $5/2$  and  $1/2$  coexisting in the same crystalline sample of (3). Until a crystal structure of (3) is forthcoming, any explanations as to the origin of such a spin mixture would be speculative at best. Whatever the explanation, the magnetochemical and EPR results for (3) are reproducible from preparation to preparation. Alternatively, the simultaneous presence of both  $g \approx 6,2$  and  $g \approx 2$  signals could arise from a thermally dependent ( $S=5/2$ )  $\rightleftharpoons$  ( $S=1/2$ ) spin-equilibrium,<sup>54,55</sup> but the reasonably Curie behavior of the  $\mu_{\text{eff}}$  vs. temperature plot for (3) over a 80-300 K range argues against this possibility. By assuming limiting values of  $\mu_{\text{eff}}(S=5/2) = 5.9 \mu_{\text{B}}$  and  $\mu_{\text{eff}}(S=1/2) = 2.3 \mu_{\text{B}}$ , a mixture consisting of ca. 20% ( $S=5/2$ ) and 80% ( $S=1/2$ ) would satisfactorily account for the observed full temperature magnetic properties of (3).

The most significant result of this study concerns compound (4). As seen in Figure 8, this compound, with its  $[\text{Fe}^{\text{III}}(\text{imid})\text{Cu}^{\text{II}}]$  core,

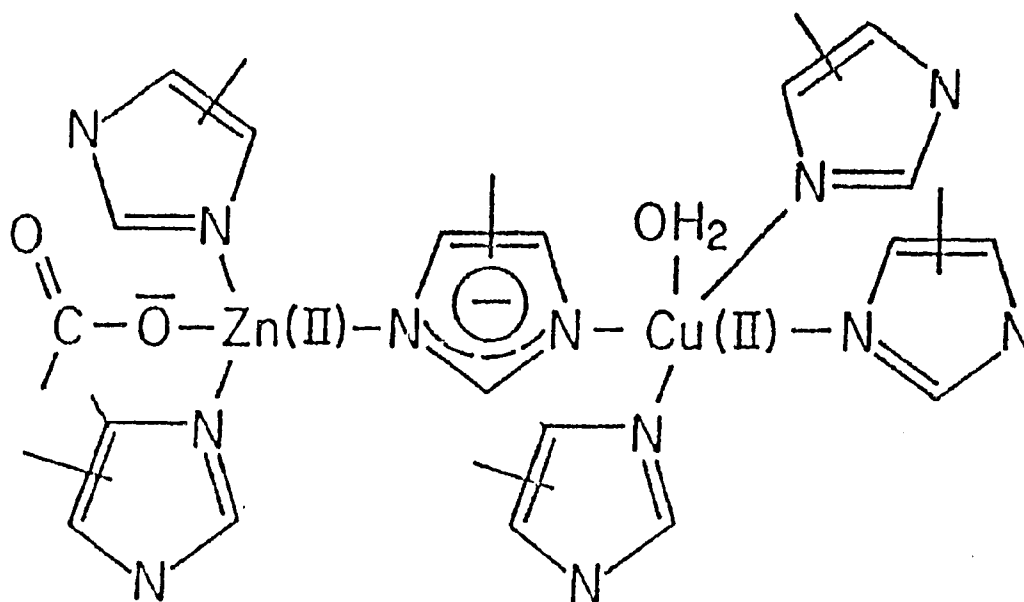
exhibits a magnetic moment of  $2.19 \mu_B^{295 \text{ K}}$  at room temperature which is a value substantially depressed relative to that of compound (3), where  $\mu_{\text{eff}} = 3.36 \mu_B^{295 \text{ K}}$  for a  $[\text{Fe}^{\text{III}}(\text{imid})\text{Zn}^{\text{II}}]$  core. Furthermore, this magnetochemical pattern is generally maintained over the full 80-300 K temperature range studied, with both compounds being nearly Curie in behavior. Probably the most reasonable interpretation of this result (also supported by the EPR data below) is that a strong anti-ferromagnetic coupling interaction is mediated by imidazolate between  $\text{Fe}^{\text{III}}$  and  $\text{Cu}^{\text{II}}$  in (4) to generate a fully spin-coupled ground state with  $-J_{(\text{Fe}^{\text{III}}-\text{Cu}^{\text{II}})} \gtrsim 200 \text{ cm}^{-1}$ . The exact nature of this resultant spin-coupled ground state is open to some interpretation, especially since the electronic structure of  $\text{Fe}^{\text{III}}$  in (3) probably involves a heterogeneous mixture of two spin states,  $S=5/2$  and  $S=1/2$ , in the same crystalline lattice. However, as in (3), assuming an  $[S=1/2(80\%), S=5/2(20\%)] \text{Fe}^{\text{III}}$  mixture in (4), and strong antiferromagnetic coupling between  $S=1/2 \text{ Cu}^{\text{II}}$  and the (80%,20%) mixture in  $\text{Fe}^{\text{III}}$  to produce a resulting  $[S=0(80\%), S=2(20\%)]$  spin-coupled ground state, the calculated room temperature magnetic moment of ca.  $2.2 \mu_B$  is in excellent agreement with the  $2.19 \mu_B^{295 \text{ K}}$  value found experimentally. Furthermore, as expected from this analysis where only even spin states contribute to the ground state, compound (4) should be EPR silent, and, indeed, such is the case.<sup>56</sup> Thus the available magnetic and EPR spectral data for (3) and (4) clearly indicate that an imidazolate bridge is quite capable of mediating strong antiferromagnetic exchange interaction between  $\text{Fe}^{\text{III}}$  and  $\text{Cu}^{\text{II}}$  in a synthetic metalloporphyrin complex.

A Reinvestigation of the Magnetic Properties of the "2Co2Cu"  
Superoxide Dismutase (SOD) Derivative

Copper-zinc superoxide dismutase is a binuclear, heterometallic enzyme with one copper(II) and one zinc(II) site in each of two identical monomeric units. In addition, the x-ray structural analysis<sup>12</sup> of SOD has shown that the copper(II) and zinc(II) centers are linked by an imidazolate bridge from a histidine moiety (see Figure 10).<sup>57</sup> When 50% of the zinc is substituted by cobalt(II), the resulting CoCu derivative is 100% active but the amount of EPR-detectable Cu(II) is just 50% of the total copper present, suggesting a magnetic exchange interaction between cobalt(II) and copper(II) centers.<sup>58</sup> Additional EPR experiments by Rotilio *et al.*,<sup>59</sup> indicate that the Co(II) and Cu(II) centers are strongly coupled antiferromagnetically with a  $-J_{(\text{Co}^{\text{II}}-\text{Cu}^{\text{II}})} \gtrsim 100 \text{ cm}^{-1}$ . Magnetic susceptibility studies by Moss and Fee<sup>22</sup> over the temperature range of 1.4-77 K and on a sample preparation containing ca. 30% uncoupled Co(II) and 50% Cu(II) as Cu(II)-Cu(II) pairs, estimate a lower limit of  $-J_{(\text{Co}^{\text{II}}-\text{Cu}^{\text{II}})} \gtrsim 5 \text{ cm}^{-1}$ . Further magnetochemical studies by Desideri *et al.*,<sup>23</sup> on a different 2Co2Cu SOD preparation indicate normal Curie behavior in the temperature range 30-200 K for this derivative, placing a lower limit for antiferromagnetic coupling between Co(II) and Cu(II) centers at  $-J_{(\text{Co}^{\text{II}}-\text{Cu}^{\text{II}})} \gtrsim 300 \text{ cm}^{-1}$ . Thus this result provides direct evidence that an imidazolate bridging ligand can foster strong magnetic exchange interaction between two metal centers in a protein environment.

Since Desideri's work indirectly supports the  $\mu$ -imidazolato possibility for the cytochrome oxidase active site structure, the validity

Figure 10  
Schematic Drawing of the Active Site of Bovine  
Superoxide Dismutase



of his result becomes an important consideration in the oxidase problem. Because of this, all aspects of the Desideri experiment have been scrutinized; and, in particular, the purity of the 2Co2Cu SOD sample has been questioned.<sup>24</sup> A better sample preparation for this protein derivative has recently been achieved by Fee,<sup>39</sup> on which the following variable temperature (80-200 K) magnetic susceptibility measurements have been obtained. The magnetochemical data, shown in Figure 11 as a  $\chi_M'$  vs.  $T^{-1}$  plot and listed in Table 4, indicate Curie behavior for the 2Co2Cu sample over the temperature range examined. The slope of the  $\chi_M'$  vs.  $T^{-1}$  plot is equal to  $\mu_{\text{eff}}^2$ , the observed magnetic moment squared, and is found to be  $5.25 \mu_B^2$ . A theoretical  $\mu_{\text{eff}}^2$  is calculated, based on the spin states and molar concentrations of the  $\text{Co}^{\text{II}}\text{Cu}^{\text{II}}$  protein unit (3.4 mM) and some adventitious  $\text{Cu}^{\text{II}}$ -EPR detectable (2.7 mM).<sup>39</sup> Comparing the present magnetochemical data with Desideri work, the  $\text{Co}^{\text{II}}\text{Cu}^{\text{II}}$  species is assumed to be an  $S=1$  system, arising from the antiferromagnetic coupling of the  $\text{Co}^{\text{II}}(S=3/2)$  and  $\text{Cu}^{\text{II}}(S=1/2)$  centers, and thus contributes a spin-only  $\mu_{\text{eff,theo.}}^2 = [4S(S+1)] = 8.0 \mu_B^2$  to the sample's total magnetic moment squared. The adventitious  $\text{Cu}^{\text{II}}$ , as an  $S=1/2$  system, has a spin-only  $\mu_{\text{eff,theo.}}^2 = 3.0 \mu_B^2$ . The  $[(\text{mM})(\mu_{\text{eff,theo.}}^2)]$  products for both the  $\text{Co}^{\text{II}}\text{Cu}^{\text{II}}$  and  $\text{Cu}^{\text{II}}$  paramagnetic components are summed and the following equation for the total spin-only magnetic moment squared is established:<sup>60</sup>

$$\mu_{\text{eff,total}}^2 = \frac{[(\text{mM}_{\text{Cu}^{\text{II}}})(\mu_{\text{eff,Cu}^{\text{II}}}^2) + (\text{mM}_{\text{Co}^{\text{II}}\text{Cu}^{\text{II}}})(\mu_{\text{eff,Co}^{\text{II}}\text{Cu}^{\text{II}}}^2)](\mu_{\text{eff,CoCu}}^2)}{[(\text{mM}_{\text{Co}^{\text{II}}\text{Cu}^{\text{II}}})(\mu_{\text{eff,Co}^{\text{II}}\text{Cu}^{\text{II}}}^2)]}$$

Figure 11  
 $\chi_M'$  vs.  $\text{Temperature}^{-1}$  Plot for the "2Co2Cu" Superoxide Dismutase Sample

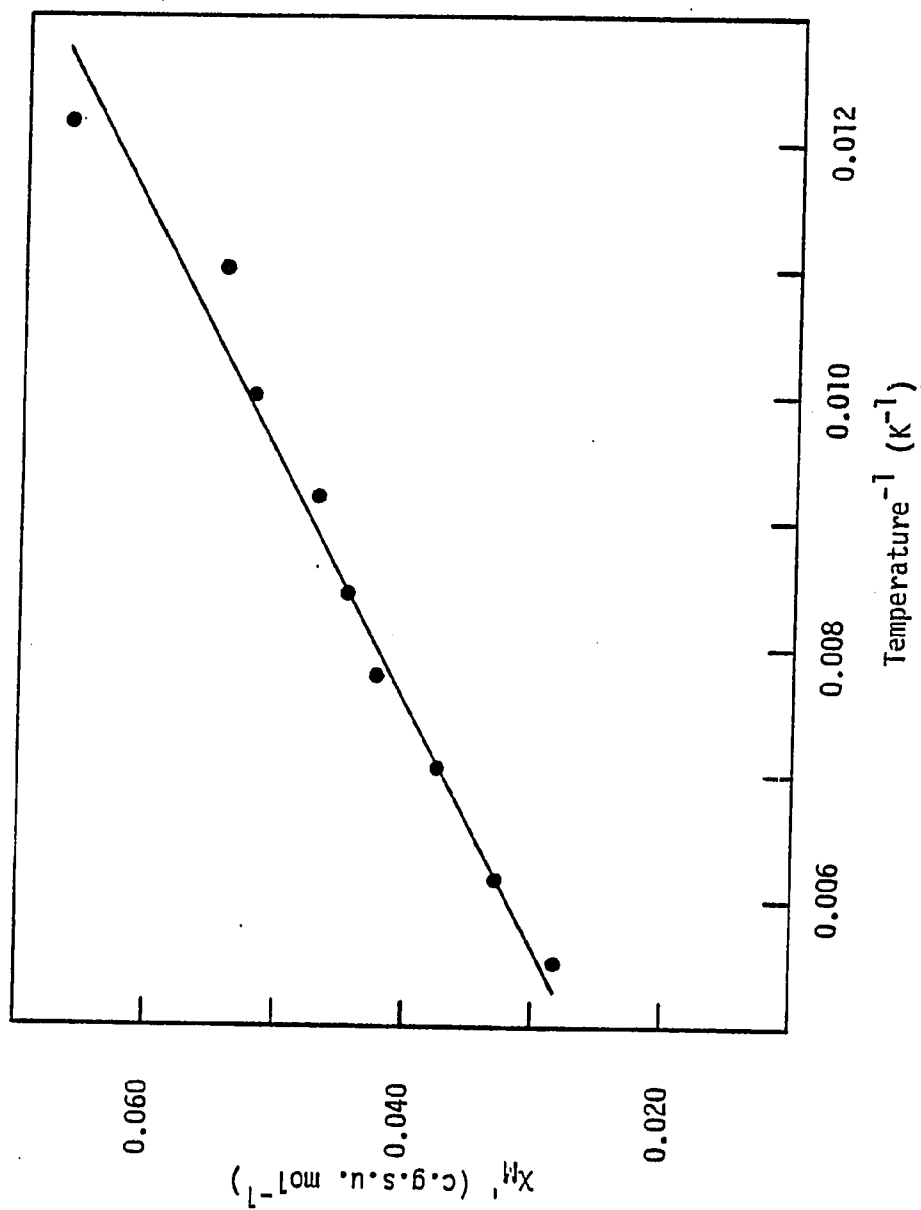


Table 4Magnetic Susceptibility Data for "2Co2Cu" Superoxide Dismutase Sample

| Temperature (K) | Inverse Temperature ( $K^{-1}$ ) | $\chi_M'$ (c.g.s. $mol^{-1}$ ) |
|-----------------|----------------------------------|--------------------------------|
| 82.3            | 0.0122                           | 0.0671                         |
| 90.7            | 0.0110                           | 0.0541                         |
| 99.8            | 0.0100                           | 0.0518                         |
| 108.7           | 0.0092                           | 0.0471                         |
| 118.6           | 0.0084                           | 0.0447                         |
| 128.6           | 0.0078                           | 0.0424                         |
| 140.8           | 0.0070                           | 0.0376                         |
| 162.0           | 0.0062                           | 0.0329                         |
| 181.5           | 0.0055                           | 0.0282                         |

For the particular 2Co2Cu SOD sample studied in this work, the total spin-only  $\mu_{\text{eff,theo.}}^2$  is calculated to be  $10.4 \mu_B^2$ . Alternatively, if the  $\text{Co}^{\text{II}}\text{Cu}^{\text{II}}$  protein unit is assumed to be a totally uncoupled system, i.e., magnetically isolated  $\text{Co}^{\text{II}}$  ( $S=3/2$ ) and  $\text{Cu}^{\text{II}}$  ( $S=1/2$ ) centers, similar calculations lead to a total spin-only  $\mu_{\text{eff,theo.}}^2 = 17.4 \mu_B^2$ . Considering the  $\mu_{\text{eff,theo.}}^2$  and experimental  $\mu_{\text{eff}}^2$  values, the electronic structure of  $[\text{Co}^{\text{II}}(\text{imid})\text{Cu}^{\text{II}}]$  in the 2Co2Cu SOD sample most probably involves the antiferromagnetic coupling of the  $\text{Co}(\text{II})$  and  $\text{Cu}(\text{II})$  centers. However, the experimentally determined  $\mu_{\text{eff}}^2$  value is about half the  $\text{Co}^{\text{II}}\text{Cu}^{\text{II}}$  "coupled"  $\mu_{\text{eff,theo.}}^2$  value. The explanation for this discrepancy is not apparent at this time, although complications in sample preparation and determination of metal concentrations by EPR could contribute to this disagreement.<sup>39</sup> Nevertheless, these magnetochemical data on the 2Co2Cu SOD sample prepared by Fee qualitatively confirm Desideri's claim that strong antiferromagnetic coupling  $[-J(\text{Co}^{\text{II}}-\text{Cu}^{\text{II}}) \geq 300 \text{ cm}^{-1}]$  across imidazolate exists in the 2Co2Cu superoxide dismutase derivative.<sup>23</sup>

### Conclusions

The active site structure in cytochrome oxidase, and, in particular, the nature of the bridging ligand in the  $[\text{Cyt.a}_3^{3+}-(\text{B})-\text{Cu}_U^{2+}]$  structural unit of resting oxidase have been examined by a modeling approach. The  $\mu$ -mercapto<sup>9</sup> and  $\mu$ -oxo<sup>7</sup> models for this active site structure have been proposed in the recent wake of EXAFS<sup>9</sup> and resonance Raman<sup>19</sup> data and the acknowledged ability of these one-atom bridges to foster strong antiferromagnetic coupling between two metal centers, as observed



between  $\text{Fe}^{\text{III}}$  and  $\text{Cu}^{\text{II}}$  in the resting enzyme. Conversely, the  $\mu$ -imidazolato model, first proposed by Palmer<sup>6</sup> in 1976, has seemingly been losing favor since a number of synthetic  $\mu$ -imidazolato binuclear compounds reported in the literature have not exhibited strong magnetic exchange interaction between two metal centers. Yet an  $^{18}\text{O}_2$ -labeled turnover experiment by Beinert<sup>18</sup> and Chan's  $^{15}\text{N}$ -histidine EPR study<sup>14</sup> of reduced oxidase do tend to favor the  $\mu$ -imidazolato possibility at the expense of the  $\mu$ -oxo proposal. In addition, the  $2\text{Co}2\text{Cu}$  superoxide dismutase magnetochemical study presented in this work qualitatively confirms Desideri's finding<sup>23</sup> that  $\text{Co}(\text{II})$  and  $\text{Cu}(\text{II})$ , bridged by an imidazolate moiety, do indeed exhibit strong antiferromagnetic coupling with  $-J_{(\text{Co}^{\text{II}}-\text{Cu}^{\text{II}})} \gtrsim 300 \text{ cm}^{-1}$ . This result indicates that an imidazolate bridge is capable of mediating strong magnetic exchange between metal centers in a protein environment. While the active site structure and even the metal centers and spin states differ in superoxide dismutase and cytochrome oxidase, indirect support for the  $\mu$ -imidazolato model in oxidase is provided by this study.

Finally, the comparative magnetic and EPR spectral data for  $[(\text{OSO}_2\text{CF}_3)\text{Fe}^{\text{III}}(\text{TPP})(\text{imid})\text{Zn}^{\text{II}}]^+$  and  $[(\text{OSO}_2\text{CF}_3)\text{Fe}^{\text{III}}(\text{TPP})(\text{imid})\text{Cu}^{\text{II}}]^+$  indicate that an imidazolate bridging ligand can mediate strong anti-ferromagnetic exchange between  $\text{Fe}^{\text{III}}$  and  $\text{Cu}^{\text{II}}$  in a synthetic metalloporphyrin complex. While the magnitude of this exchange interaction  $[-J_{(\text{Fe}^{\text{III}}-\text{Cu}^{\text{II}})} \gtrsim 200 \text{ cm}^{-1}]$  may be as strong as that operating in resting oxidase, this result obviously does not prove the existence of an imidazolate bridge at the active site in oxidase, especially since the  $[\text{ClFe}^{\text{III}}(\text{TPP})(\text{imid})\text{Cu}^{\text{II}}]^+$  analogue displays a comparatively weak inter-

action, with  $-J_{(\text{Fe}^{\text{III}}-\text{Cu}^{\text{II}})} \lesssim 15 \text{ cm}^{-1}$ . Rather, the result serves to rekindle this suggestion as a viable possibility. Further modeling studies using the present species and other  $\mu$ -imidazolato mixed-metal complexes should elaborate on this possibility by clarifying what electronic/structural conditions promote magnetic coupling across imidazolate bridges.

# REFERENCES AND NOTES

1. See for example: A. L. Lehninger, "The Mitochondrion," W. A. Benjamin, New York, 1973.
2. B. G. Malmström, "Metal Ion Activation of Dioxygen," T. G. Spiro, Ed., J. Wiley, New York, 1980, ch. 5, p. 181.
3. M. F. Tweedle, L. J. Wilson, L. Garcia-Iniguez, G. T. Babcock, and G. Palmer, J. Biol. Chem., 253, 8065 (1978). Also see: T. H. Moss, E. Shapiro, T. E. King, H. Beinert, and C. R. Hartzell, J. Biol. Chem., 253, 8072 (1978).
4. C. H. A. Seiter and S. G. Angelos, Proc. Natl. Acad. Sci. U. S. A., 77, 1806 (1980).
5. S. E. Dessens, C. L. Merrill, R. J. Saxton, R. L. Ilaria, J. W. Lindsey, and L. J. Wilson, J. Am. Chem. Soc., in press, 1982.
6. G. Palmer, G. T. Babcock, and L. E. Vickery, Proc. Natl. Acad. Sci. U.S.A., 73, 2006 (1973).
7. R. H. Petty, B. R. Welch, L. J. Wilson, L. A. Bottomley, and K. M. Kadish, J. Am. Chem. Soc., 102, 611 (1980).
8. C. A. Reed and J. T. Landrum, FEBS Letters, 106, 265 (1979).
9. B. Chance and L. Powers, Biophys. Journal, 33, 95a (1981); L. Powers, B. Chance, Y. Ching, and P. Angiolillo, Biophys. Journal, 33, 95a (1981); L. Powers, B. Chance, Y. Ching, and P. Angiolillo, Biophys. Journal, 34, 465 (1981).
10. T. Antalís, Ph.D. dissertation, Biochemistry Department, Rice University, Houston, Texas, 1981.
11. M. F. J. Blokzijl-Homan and B. F. van Gelder, Biochem. Biophys. Acta, 234, 493 (1971).
12. J. S. Richardson, K. A. Thomas, B. H. Rubin, and D. C. Richardson, Proc. Natl. Acad. Sci. U.S.A., 72, 1349 (1975).
13. J. A. Fee and R. G. Briggs, Biochem. Biophys. Acta, 400, 439 (1975).
14. T. H. Stevens and S. I. Chan, J. Biol. Chem., 256, 1069 (1980).
15. W. Blumberg, The Japanese-American Seminar on Cytochrome Oxidase, Kobe, Japan, 1978, paper 27.

16. G. Palmer, T. Antalis, G. T. Babcock, L. Garcia-Iniguez, M. F. Tweedle, L. J. Wilson, and L. E. Vickery, "Mechanisms of Oxidizing Enzymes," T. P. Singer and R. Ondarza, Ed., Elsevier North Holland Press, Amsterdam, 1978, p. 222, and references cited therein.
17. W. E. Blumberg and J. Peisach, Biophys. Journal, 25, 34a (1979).
18. R. W. Shaw, J. E. Rife, M. H. O'Leary, and H. Beinert, J. Biol. Chem., 256, 1105 (1981).
19. W. H. Woodruff, R. F. Dallinger, T. M. Antalis, and G. Palmer, Biochemistry, 20, 1332 (1981).
20. R. Malkin and B. G. Malmström, Adv. in Enzymology, 33, 177 (1970); H. Beinert, Coord. Chem. Reviews, 23, 119 (1977).
21. G. W. Brudvig and S. I. Chan, FEBS Letters, 106, 139 (1979).
22. T. H. Moss and J. A. Fee, Biochem. Biophys. Res. Comm., 66, 799 (1975).
23. A. Desideri, M. Cerdonio, F. Mogno, S. Vitale, L. Calabrese, D. Cocco, and G. Rotilio, FEBS Letters, 89, 83 (1978).
24. J. A. Fee, private communication. The Desideri preparation is thought to have contained enormous amounts of adventitious EPR-detectable Cu(II). The presence of this extra paramagnet in the Co(II)Cu(II) derivative would complicate the interpretation of the magnetochemical data obtained from such a sample.
25. P. D. W. Boyd and T. D. Smith, Inorg. Chem., 10, 2041 (1971); D. H. O'Keefe, C. H. Barlow, W. S. Caughey, G. A. Smythe, W. H. Fuchsman, T. H. Moss, and H. R. Lilienthal, Bioinorg. Chem., 5, 125 (1975); D. Chin, A. L. Balch, and G. N. LaMar, J. Am. Chem. Soc., 102, 1446 (1980).
26. G. Kolks, C. R. Frihart, H. N. Rabinowitz, and S. J. Lippard, J. Am. Chem. Soc., 98, 5720 (1976).
27. J. T. Landrum, C. A. Reed, K. Hatano, and W. R. Scheidt, J. Am. Chem. Soc., 100, 3232 (1978).
28. M. S. Haddad, E. N. Duesler, and D. N. Hendrickson, Inorg. Chem., 18, 141 (1979).
29. J. T. Landrum, D. Grimmet, K. J. Haller, W. R. Scheidt, and C. A. Reed, J. Am. Chem. Soc., 103, 2640 (1981).
30. D. Kovacs and R. E. Shepherd, J. Inorg. Biochem., 10, 67 (1979).

31. T. Prosperi and A. A. G. Tomlison, Chem. Comm. (J.C.S.), 18, 141 (1979).
32. H. Goff, C. L. Merrill, and L. J. Wilson, unpublished results. Initial  $^1\text{H}$  n.m.r. studies of the  $[\text{ClFe}^{\text{III}}(\text{TPP})(\text{imid})\text{M}^{\text{II}}]^+$  and  $[\text{ClFe}^{\text{III}}(\text{TPP})(\text{imid})\text{M}^{\text{II}}(\text{py})]^+$  binuclear compounds in  $\text{CD}_2\text{Cl}_2$  indicate that the major iron species in solution exists in the low-spin ( $S=1/2$ ) state, presumably as the iron-metal binuclear, although in equilibrium with a high-spin ( $S=5/2$ ) iron porphyrin and a  $\text{Cu}^{\text{II}}$  or  $\text{Zn}^{\text{II}}$  fragment. The addition of the  $\text{Cu}^{\text{II}}$  or  $\text{Zn}^{\text{II}}$  compound to  $[\text{Fe}(\text{TPP})\text{Cl}]$  in the absence of proton sponge base yields no changes in the  $^1\text{H}$  n.m.r. spectrum of  $[\text{Fe}(\text{TPP})\text{Cl}]$ , and thus no dimer and/or polymer formation is evidenced. Relevant to the modeling of the cytochrome oxidase active site structure, some copper-iron spin-spin relaxation is observed for the binuclears, but antiferromagnetic coupling is small. Unfortunately, these studies do not prove that the imidazolate bridge between the metal centers is intact in solution, although the likelihood of this appears great. Further work is indicated, and in particular the binuclear  $[(\text{OSO}_2\text{CF}_3)\text{Fe}^{\text{III}}(\text{TPP})(\text{imid})\text{M}^{\text{II}}]^+$  compound will be investigated in the near future.
33. I. A. Cohen, J. Am. Chem. Soc., 91, 1980 (1969); E. B. Fleischer and T. S. Srivastava, J. Am. Chem. Soc., 91, 2403 (1969).
34. D. F. Shriver, "The Manipulation of Air-sensitive Compounds," McGraw-Hill Book Co., New York, 1969.
35. A. D. Adler, F. Kampas, and J. Kim, J. Inorg. Nucl. Chem., 32, 2443 (1970).
36. C. A. Reed, T. Mashkio, S. P. Bentley, M. E. Kastner, W. R. Scheidt, K. Spartalain, and G. Lang, J. Am. Chem. Soc., 101, 2948 (1979).
37. B. L. Chrisman and T. A. Tumolillo, Comput. Phys. Commun., 2, 322 (1975).
38. R. S. Drago, "Physical Methods in Chemistry," W. B. Saunders Company, Philadelphia, 1977, ch. 11, p. 413.
39. James Fee, private communication.
40. M. F. Tweedle and L. J. Wilson, Rev. Sci. Instrum., 49, 1001 (1978).
41. M. G. Simmons, C. L. Merrill, L. J. Wilson, L. A. Bottomley, and K. M. Kadish, J. Chem. Soc. Dalton, 1827 (1980).

42. L. J. Wilson, C. L. Merrill, M. G. Simmons, J. M. Trantham, L. A. Bottomley, and K. M. Kadish, "Invertebrate Oxygen Binding Proteins. Structure, Active Site and Function," Lamy and Lamy, Ed., Marcel Dekker, Inc., New York, 1981
43. J. R. Dyer, "Applications of Absorption Spectroscopy of Organic Compounds," Prentice-Hall, Inc., Englewood Cliffs, 1965, ch. 3.
44. The signal obtained after 72 hours for compound (5) was very broad ( $hwhh \approx 1$  mm/s), probably with two unresolvable components resembling the widely spaced quadrupole split doublet obtained for compound (1). In the case of compound (3), the signal collected after 72 hours was likewise quite broad, with three or more unresolvable components. This being the case, it is a considerably different spectrum than that obtained for compound (4) in Figure 7-F).
45. J. Peisach, W. E. Blumberg, and A. Adler, Ann. N. Y. Acad. Sci., 206, 310 (1973).
46. H. Goff and E. Shimomura, J. Am. Chem. Soc., 102, 31 (1980).
47. H. Kobayashi, Y. Kaizu, and K. Eguchi, Adv. Chem. Ser., 191, 327 (1980).
48. H. Masuda, T. Taga, K. Osaki, H. Sugimoto, Z. Yoshida, and H. Ogoshi, Inorg. Chem., 19, 950 (1980).
49. H. Ogoshi, H. Sugimoto, and Z. Yoshida, Biochim. Biophys. Acta, 621, 19 (1980).
50. M. E. Kastner, W. R. Scheidt, T. Mashiko, and C. A. Reed, J. Am. Chem. Soc., 100, 666 (1978).
51. D. A. Summerville, I. A. Cohen, K. Hatano, and W. R. Scheidt, Inorg. Chem., 17, 2906 (1978).
52. D. H. Dolphin, J. R. Sams, and T. B. Tsin, Inorg. Chem., 16, 711 (1977).
53. M. M. Maltempo, J. Chem. Phys., 61, 2540 (1974).
54. See for example: E. K. Barefield, D. H. Busch, and S. M. Nelson, Q. Rev. Chem. Soc., 22, 457 (1968).
55. E. V. Dose, M. A. Hoselton, N. Sutin, M. F. Tweedle, and L. J. Wilson, J. Am. Chem. Soc., 100, 1141 (1978).

56. In fact, compound (4) displays very weak signals in both the  $g \approx 6$  and  $g \approx 2$  regions, but these signals account for 0.4% of the  $\text{Fe}^{\text{III}}$  and  $\text{Cu}^{\text{II}}$  present, when integrated against signals from solid samples of  $[\text{Fe}^{\text{III}}(\text{TPP})(\text{OSO}_2\text{CF}_3)]$  and  $[\text{Cu}^{\text{II}}(\text{imidH})_2\text{DAP}](\text{BF}_4)_2$ . Being so weak, these signals are best attributed to very small amounts of  $\text{Fe}^{\text{III}}$  and  $\text{Cu}^{\text{II}}$  impurities in the sample and not to the  $[\text{Fe}^{\text{III}}(\text{imid})\text{Cu}^{\text{II}}]$  core of compound (4). Furthermore, dipolar relaxation broadening, by the so-called Leigh Effect [J. S. Leigh, Jr., *J. Chem. Phys.*, 52, 2608 (1970)] is not likely to be responsible for the EPR quietness of (4), since the magnetic susceptibility data are also consistent with strong antiferromagnetic coupling in the compound.
57. J. A. Fee, "Metal Ions in Biology," H. Sigel, Ed., Marcel Dekker, Inc., New York, Vol. 13, in press.
58. L. Calabrese, G. Rotilio, and B. Mondovi, *Biochim. Biophys. Acta*, 263, 827 (1972).  
~~~
59. G. Rotilio, L. Calabrese, B. Mondovi, and W. E. Blumberg, *J. Biol. Chem.*, 249, 3157 (1974).  
~~~
60. G. Palmer, private communication.